Adam Mickiewicz University in Poznań
Faculty of Chemistry

**mgr inż. Mateusz Pawlaczyk**

# Synthesis and application of functional hybrid and polymeric materials in chemical analysis

## Otrzymywanie i zastosowanie w analizie chemicznej funkcjonalnych układów hybrydowych i polimerowych

A doctoral dissertation submitted in the form of a thematically coherent series of scientific articles published in scientific journals, prepared in the field of Science, in the discipline of Chemical science.

Supervision: Prof. dr hab. Grzegorz Schroeder
Co-supervision: Dr hab. Michał Cegłowski

**Poznań, 2021**

# ACKNOWLEDGEMENTS

The very first person I would like to thank is my supervisor, **Prof. dr hab. Grzegorz Schroeder**, who has always been encouraging, supportive, advisory, and understanding during my PhD studies.

Thank you for all the imparted knowledge; for invaluable help and uncountable advice and discussions at the steps of laboratory work, publishing, and presenting the results; for giving the opportunity of being creative and self-responsible for the scientific steps taken; and also, for permanent kindness and appreciation.

Nonetheless, I think that no words can adequately express my gratefulness.

I would also like to thank my co-supervisor, **Dr hab. Michał Cegłowski**, for a friendly work atmosphere, and for being advisory and helpful during the preparation of scientific articles and the dissertation.

The following doctoral dissertation would not be presented without the support of my research group, especially my lab-mate, **Maria**, with who I spent four productive and memorable years. Thank you for your instant support, help in scientific and administrational problems, and accompanying in PhD student duties.

I am also very grateful to all my friends, especially **Aleksandra**, for being maximally supportive, motivating, comforting, and understanding through the whole ups and downs here in the Faculty.

I would like also to express my sincere gratitude to **my family**, especially my Mother, Sister, and Aunt, for the constant support, motivation, inducing self-confidence, and continuous faith in my academic and scientific activities.

Finally, I would like to thank **ChemInter Project** (grant no. POWR.03.02.00-00-I026/16) especially for the chance of doing my PhD studies in this project and financial support.

# Table of contents

# Résumé

## PERSONAL DATA

| | |
|---|---|
| Name and surname | Mateusz Pawlaczyk |
| Date of birth | 26th October 1994 |
| Place of birth | Łódź |

## EDUCATION

| | |
|---|---|
| Since 10. 2017 | Adam Mickiewicz University in Poznań, Faculty of Chemistry<br>PhD Studies, Chemistry<br>*Synthesis and application of functional hybrid and polymeric materials in chemical analysis* |
| 03. 2016 – 07. 2017 | Technical University of Łódź, Faculty of Chemistry<br>Master of Science, Chemistry (Modern Organic Synthesis and Analysis)<br>*Mapping of B21-B30 fragment of human insulin* |
| 10. 2012 – 02. 2016 | Technical University of Łódź, Faculty of Chemistry<br>Bachelor of Engineering, Chemistry (Organic Synthesis)<br>*Synthesis and studies on properties of amyloidogenic analogues of B12-B17 human insulin fragment modified by an incorporation of* N-*methylated amino acids residues* |

## TRAINING

1) Two monthly (09. 2015 and 09. 2016) specialization practices in Screening Lab of Medical Biology Institute of Polish Academy of Science under the supervision of Assoc. Prof. Agnieszka Olejniczak. The practices involved investigation of lipophilicity of novel compounds and synthesis, purification, and analysis of novel carboranyl (boron-carbon clusters) derivatives exhibiting potential bioactivity;
2) Training on the operation, calibration, and maintenance of LibertyBlue™ CEM peptide synthesizer;
3) Training on the analysis of particles' size with dynamic laser scattering (DLS) method using Litesizer™500 Anton Paar apparatus.

## ACHIEVEMENTS

1) The authorship and co-authorship in 14 scientific papers presented as regular articles in international journals or post-conference proceedings;
2) Osman Achmatowicz Award for the best Engineering thesis in Chemistry;
3) An Award for the best proceeding paper 6th International Conference on Nanomaterials, Nanodevices, Fabrication, and Characterization (ICNNFC 2021);
4) Recipient of Rector's and pro-quality scholarships during whole PhD studies duration.

# The list of published articles

## The articles published in international journals

1) **M. Pawlaczyk**, J. Kurczewska, G. Schroeder, Nanomaterials Modification by Dendrimers – A review, World Journal of Research and Review 6(5) (2018), 14-30; IF = 0; MNiSW = 0
   ISSN: 2455-3956
2) **M. Pawlaczyk**, G. Schroeder, Adsorption studies of Cu(II) ions on dendrimer-grafted silica-based materials, Journal of Molecular Liquids 281 (2019), 176-185; IF = 6.165; MNiSW = 100
   DOI: 10.1016/j.molliq.2019.02.043
3) **M. Pawlaczyk**, S. Pasieczna-Patkowska, J. Ryczkowski, G. Schroeder, Photoacoustic infrared spectroscopic studies of silica surface functionalized by dendrimers, Vibrational Spectroscopy 103 (2019), 102943; IF = 2.507; MNiSW = 40
   DOI: 10.1016/j.vibspec.2019.102943
4) **M. Pawlaczyk**, G. Schroeder, Efficient Removal of Ni(II) and Co(II) Ions from Aqueous Solutions Using Silica-based Hybrid Materials Functionalized with PAMAM Dendrimers, Solvent Extraction and Ion Exchange 38(5) (2020), 496-521; IF = 2.513; MNiSW = 70
   DOI: 10.1080/07366299.2020.1766742
5) **M. Pawlaczyk**, S. Pasieczna-Patkowska, G. Schroeder, Photoacoustic Spectroscopy of Surface-Functionalized $Fe_3O_4$-$SiO_2$ Nanoparticles, Applied Spectroscopy 74(6) (2020), 712-719; IF = 2.388; MNiSW = 70
   DOI: 10.1177/0003702820913647
6) **M. Pawlaczyk**, G. Schroeder, Dendrimer-Functionalized Hybrid Materials Based on Silica as Novel Carriers of Bioactive Acids, Molecules 25(11) (2020), 2660-2680; IF = 4.411; MNiSW = 100
   DOI: 10.3390/molecules25112660
7) M. Guć, M. Cegłowski, **M. Pawlaczyk**, J. Kurczewska, E. Reszke, G. Schroeder, Application of FAPA mass spectrometry for analysis of fragrance ingredients used in cosmetics, Measurement 168(15) (2020), 108326; IF = 3.927; MNiSW = 200
   DOI: 10.1016/j.measurement.2020.108326
8) **M. Pawlaczyk**, G. Schroeder, Dual-Polymeric Resin Based on Poly(methyl vinyl ether-*alt*-maleic anhydride) and PAMAM Dendrimer as a Versatile Supramolecular Adsorbent, ACS Applied Polymer Materials 3(2) (2021), 956-967; IF = 4.089; MNiSW = 20
   DOI: 10.1021/acsapm.0c01254

9) **M. Pawlaczyk**, G. Schroeder, Deferoxamine-Modified Hybrid Materials for Direct Chelation of Fe(III) Ions from Aqueous Solutions and Indication of the Competitiveness of In Vitro Complexing toward a Biological System, ACS Omega 6(23) (2021), 15168-15181; IF = 3.512; MNiSW = 70
DOI: 10.1021/acsomega.1c01411
10) **Pawlaczyk**, M. Guć, G. Schroeder, Adsorption and selectivity studies of direct and magnetite-cored molecularly imprinted polymers (MIPs and magMIPs) towards chosen chalcones investigated with various analytical methods, RSC Advances 11(41) (2021), 25334-25347; IF = 3.361; MNiSW = 100
DOI: 10.1039/D1RA03391C
11) **M. Pawlaczyk**, R. Frański, M. Cegłowski, G. Schroeder, Mass spectrometric investigation of organo-functionalized magnetic nanoparticles binding properties toward chalcones, Materials 14(16) (2021), 4705-4720; IF = 3.623; MNiSW = 140
DOI: 10.3390/ma14164705

## The post-conference proceeding paper and monographs

1) M. Świontek, P. Król, **M. Pawlaczyk**, J. Frączyk, Z.J. Kamiński, B. Kolesińska, Analogues of insulin hot spots containing Aib residues as a potential inhibitors of insulin aggregation process, Proc. 34th European Peptide Symposium (2016), 169
ISBN: 9781510852488
2) M. Świontek, **M. Pawlaczyk**, J. Frączyk, Z.J. Kamiński, B. Kolesińska, Nowe rdzenie amyloidogenne insuliny. Poszukiwanie inhibitorów procesu agregacji insuliny. Nowe inhibitory procesu agregacji insuliny, Na pograniczu chemii i biologii, *Wydawnictwo Naukowe UAM*, Poznań (2017), 161-171
3) **M. Pawlaczyk**, G. Schroeder, Hybrydowe nanomateriały magnetyczne, *Cursiva*, Kostrzyn (2017)
ISBN: 978-83-62108-39-8
4) **M. Pawlaczyk**, M. Guć, G. Schroeder, Silica-dendrimer nanohybrid materials as adsorbents for heavy metal ions in aqueous solutions, Proceedings of the 4th World Congress on Recent Advances in Nanotechnology (RAN'19), 2019
DOI: 10.11159/icnnfc19.123
5) M. Guć, **M. Pawlaczyk**, G. Schroeder, A molecularly imprinted polymer coated-nanocomposite of magnetic nanoparticles for organic compounds recognition, Proceedings of the 4th World Congress on Recent Advances in Nanotechnology (RAN'19), 2019
DOI: 10.11159/icnnfc19.126
6) **M. Pawlaczyk**, M. Guć, Synteza materiałów hybrydowych $SiO_2$-PAMAM i określenie ich właściwości adsorpcyjnych wobec jonów Cu(II), Ni(II) oraz Co(II), Na pograniczu Chemii i Biologii, *Wydawnictwo Naukowe UAM*, Poznań (2020), 135-154

7) M. Guć, **M. Pawlaczyk**, Analiza niskocząsteczkowych związków organicznych z wykorzystaniem magnetycznych polimerów z odciekiem molekularnym oraz techniki FAPA-MS, Na pograniczu Chemii i Biologii, *Wydawnictwo Naukowe UAM*, Poznań (2020), 155-170

8) **M. Pawlaczyk**, G. Schroeder, Investigation of the metal cations adsorption selectivity using nanocavities-rich polyamine-cross-linked PMVEAMA, Proceedings of the 6th World Congress on Recent Advances in Nanotechnology (RAN'21), 2021
DOI: 10.11159/icnnfc21.lx.103

# The list of conferences

| ORAL PRESENTATIONS | | |
|---|---|---|
| **International** | **M. Pawlaczyk**, G. Schroeder<br>"Investigation of the Metal Cations Adsorption Selectivity Using Nanocavities-Rich Polyamine-Cross-Linked PMVEAMA" | 6th International Conference on Nanomaterials, Nanodevices, Fabrication and Characterization (ICNNFC'2021), Lisbon, 14-16.06.2021 |
| **Domestic** | M. Guć**, M. Pawlaczyk**, G. Schroeder<br>„Polimery z odciskiem molekularnym oraz materiały hybrydowe funkcjonalizowane kwasem borowym" | Seminarium „Postępy w chemii boru", Radziejowice, 26-28.04.2019 |
| | **M. Pawlaczyk**, M. Guć, G. Schroeder<br>„Materiały hybrydowe sfunkcjonalizowane dendrymerami jako efektywne materiały adsorpcyjne"<br><br>M. Guć**, M. Pawlaczyk**, G. Schroeder<br>„Zastosowanie magnetycznych polimerów z odciskiem molekularnym do oznaczania organicznych związków chemicznych metodą spektrometrii mas" | 62. Zjazd Naukowy PTChem, Warszawa, 2-6.09.2019 |
| | **M. Pawlaczyk**, M. Guć, G. Schroeder<br>„Synteza materiałów hybrydowych $SiO_2$-PAMAM i określenie ich właściwości adsorpcyjnych wobec jonów Cu(II), Ni(II) oraz Co(II)"<br><br>M. Guć**, M. Pawlaczyk**, G. Schroeder<br>„Analiza niskocząsteczkowych związków organicznych z wykorzystaniem magnetycznych polimerów z odciskiem molekularnym oraz techniki FAPA-MS" | XVII Ogólnopolskie Seminarium dla Doktorantów i Studentów „Na pograniczu chemii i biologii", Jastrzębia Góra, 12-15.05.2019 |
| | **M. Pawlaczyk**, M. Guć, G. Schroeder<br>„Krzemionka funkcjonalizowana dendrymerami poli(amidoaminowymi) (PAMAM) jako nowatorski adsorbent jonów metali ciężkich"<br><br>M. Guć**, M. Pawlaczyk**, G. Schroeder<br>„Polimery wdrukowane molekularnie do ilościowego oznaczania organicznych związków chemicznych z zastosowaniem spektrometrii mas z jonizacją w warunkach otoczenia (FAPA-MS, ang. Flowing Atmospheric-Pressure Afterglow Mass Spectrometry)" | X Poznańska Konferencja Naukowa „Chemia – Nauka i Przemysł", Poznań, 30.11.2018 |
| | **M. Pawlaczyk**, M. Guć, J. Kurczewska, G. Schroeder<br>„Nanomateriały funkcjonalizowane dendrymerami" | 61. Zjazd Naukowy PTChem, Kraków, 17-21.09.2018 |

| POSTER PRESENTATIONS | | |
|---|---|---|
| **International** | **M. Pawlaczyk**, G. Schroeder<br>"Modification of Magnetite Nanoparticles with Triazine-Based Dendrons and their Application as Drug-Transporting Systems" | Nanotech France 2021, Paris, 23-25.06.2021 |
| | M. Gołdyn, **M. Pawlaczyk**, E. Bartoszak-Adamska<br>"Purine alkaloid systems with 2,6-dihydroxybenzoic acid as a coformer – X-ray structural analysis and solubility studies" | Joint Polish-German Crystallographic Meeting, Wrocław, 24-27.02.2020 |
| | **M. Pawlaczyk**, M. Guć, G. Schroeder<br>"Silica-dendrimer nanohybrid materials as adsorbents for heavy metal ions in aqueous solutions"<br><br>M. Guć**, M. Pawlaczyk**, G. Schroeder<br>"A molecularly imprinted polymer coated-nanocomposite of magnetic nanoparticles for organic compounds recognition" | 4th International Conference on Nanomaterials, Nanodevices, Fabrication and Characterization, Rome, 14-16.04.2019 |
| | **M. Pawlaczyk**, M. Guć, G. Schroeder<br>"Silica-based PAMAM dendrimer-grafted materials as adsorbents for Cu(II) ions"<br><br>M. Guć**, M. Pawlaczyk**, G. Schroeder<br>"Analysis of estrogens in samples using the molecularly imprinted polymers (MIP) or magnetic molecularly imprinted polymers (mag-MIP) with FAPA-MS" | 13th International Seminar "Biomolecules – Identification and Functions", Kraków, 19-20.10.2018 |
| | **M. Pawlaczyk**, M. Guć, G. Schroeder<br>"Preparation of hybrid deferoxamine/ nanoparticles for removal of metal ions"<br><br>M. Guć**, M. Pawlaczyk**, G. Schroeder<br>"Synthesis and application of molecularly imprinted polymers (MIP) and magnetic molecularly imprinted polymers (mag-MIP) to selective analysis of hormones" | Chemistry Beyond Nature, Poznań, 21-22.06.2018 |

| POSTER PRESENTATIONS | | |
|---|---|---|
| **Domestic** | **M. Pawlaczyk**, M. Guć, G. Schroeder<br>„Określenie zdolności sorpcyjnych materiałów hybrydowych $SiO_2$-PAMAM wobec kwasu foliowego jako modelowego związku wykazującego aktywność biologiczną”<br><br>M. Guć**, M. Pawlaczyk**, G. Schroeder<br>„Analiza niesteroidowych leków przeciwzapalnych metodą FAPA- MS z wykorzystaniem komercyjnie dostępnych polimerów z odciskiem molekularnym” | 62. Zjazd Naukowy PTChem, Warszawa, 2-6.09.2019 |
| | **M. Pawlaczyk**, G. Schroeder<br>“Silica-based hybrid materials modified with PAMAM dendrimers as efficient adsorbents of heavy metal ions” | VII Łódzkie Sympozjum Doktorantów Chemii, Łódź, 9-10.05.2019 |
| | M. Guć**, M. Pawlaczyk**, J. Kurczewska, M. Cegłowski, G. Schroeder<br>„Polimery z odciskiem molekularnym do ilościowego oznaczania organicznych związków chemicznych z zastosowaniem spektrometrii mas z jonizacją w warunkach otoczenia (FAPA-MS)” | 61. Zjazd Naukowy PTChem, Kraków, 17-21.09.2018 |
| | **M. Pawlaczyk**, M. Guć, G. Schroeder<br>„Nowa klasa zmiataczy molekularnych – krzemionka modyfikowana dendrymerem poli(amidoaminowym) (PAMAM)”<br><br>M. Guć**, M. Pawlaczyk**, G. Schroeder<br>„Zastosowanie polimerów molekularnie wdrukowanych w analizie kwercetyny technikami FAPA-MS i ESI-MS” | NanoBioMateriały – teoria i praktyka, Toruń, 6-8.06.2018 |

# The list of abbreviations used

| | |
|---|---|
| bis-MPA | bis(hydroxymethyl)propionic acid dendrimer |
| DETA | diethylenetriamine |
| DFO | deferoxamine |
| EDA | ethylenediamine |
| EDX-SEM | energy dispersive X-ray scanning electron microscopy |
| ESI-MS | electrospray ionization mass spectrometry |
| FT-IR | Fourier-transform infrared spectroscopy |
| IUPAC | International Union of Pure and Applied Chemistry |
| MRI | magnetic resonance imagining |
| MS | mass spectrometry |
| NSAID | Nonsteroidal anti-inflammatory drug |
| PAMAM | poly(amidoamine) dendrimer |
| PBS | phosphate-buffered saline |
| PEG | polyethylene glycol |
| PET | positron emission tomography |
| PMVEAMA | poly(methyl vinyl ether-*alt*-maleic anhydride) |
| PPI | poly(propylene imine) dendrimer |
| PPIX | protoporphyrin IX |
| $q_m$ | maximal adsorption capacity [mg $g^{-1}$] |
| SEC | size-exclusion chromatography |
| SEM | scanning electron microscopy |
| SERS | surface enhanced Raman spectroscopy |
| SPE | solid-phase extraction |
| TETA | triethylenetetramine |
| TG | thermogravimetric analysis |
| TREN | tris(2-aminoethyl)amine |
| TRI-OXA | 4,7,10-trioxa-1,13-tridecanediamine |
| XRF | X-ray fluorescence |

# 1

# Literature overview

Materials chemistry is one of the most dynamically explored fields of nowadays science. This growth is driven by the direct or indirect utilization and application of various materials, in order to sustain life expectations and demands. Such criteria are met by a group of materials called "hybrid materials", which are defined by IUPAC as *"Materials composed of an intimate mixture of inorganic components, organic components, or both types of components"*.[1-2] Although, the concept of inorganic-organic hybrid materials appeared only in the second half of the 20$^{th}$ century, such non-defined hybrids have been commonly used already in Ancient history.[3] Classic examples of the materials obtained by an unconscious combination of inorganic and organic components, leading to a new hybrid material, were paints and dyes. Easily accessible pigments, such as an orange-brownish rust powder ($Fe_2O_3$), an intensive yellow carotenoid called crocin contained in saffron, or crocus, a reddish-purple secretion of sea snails, a blue indigo dye derived from a flowering plant, or carbon black mixed with a painting medium – most usually various aluminosilicate clays – and secreted organic binders (saliva, blood, fat, or urine) led to effective, permanent, low-cost, and easy-obtainable paintings used even in the 19$^{th}$ century.[4] Other examples may include the use of mixtures of amylopectin-rich rice gruel with clay, sand, or calcium carbonate for urban constructions, or stable and plastic kaolin-urea mixtures applied in the manufacturing of ceramics in Ancient China. However, today's science sets more complex and mankind-directed requirements connected with globalization, such as environmental protection, sustainable development, energy and data storage, etc. But why are hybrid materials so interesting from the scientific point of view? There is a lot of factors affecting their tremendous popularity, such as (i) a variety of available and/or known inorganic and organic components; (ii) creation of new physicochemical properties of materials with simultaneous preservation of components' properties; (iii) a wide range of their applicability in analytical

and applied chemistry, optics, or electronics; (iv) an easiness in their production, even at large-scale; and (v) a variety of synthetic approaches.[5-6]

General classification of hybrid materials includes Type I materials, which hybridization is based on weak physical and/or non-covalent attractions between inorganic and organic components (e.g. encapsulation/entrapping process or embedding within a matrix stabilized by π-π stacking, van der Waals or electrostatic interactions, or hydrogen bonds), while Type II materials are stabilized by strong covalent bonds.[7] It is worthy to highlight at this point that, from the synthetic point of view, a combination of polymeric support and organic receptor leads to dual-polymeric materials, which might be classified as hybrid materials. However, a countless amount of hybrid materials' compositions and their multiple applications make the general summary impossible. Therefore, this summary will focus on the types of supports and functionalizing organic domains reported in the articles included in my doctoral dissertation.

## The role of supporting materials

The main role of supports used for the creation of novel functional materials is primarily affording the desired physical properties. However, the choice of a particular support leads to several beneficial properties, especially an easiness of the functionalization, biocompatibility, or chemical stability. These features are exhibited by inorganic platforms, such as silica ($SiO_2$), titania ($TiO_2$), magnetite nanoparticles ($Fe_3O_4$), quantum dots, zeolites, and carbon or halloysite nanotubes. Nevertheless, satisfactory physicochemical or biological characteristics, e.g. water dispersibility, cytocompatibility, or cytoadhesiveness, of several bio-derived and synthetic polymers, lead to their recent propagation as functional materials' components.

The high applicability of silica in various branches of material chemistry is strictly related to its high melting point (~ 1700°C), accessibility in natural deposits, a simple protocol for the obtaining of amorphous or ordered silica particles of a controlled porosity and size, and well-described modification approach through hydrolytic co-condensation using functional silanes.[8,9] Other frequently used inorganic platforms are magnetite nanoparticles. Among their main advantages is high magnetic susceptibility affording easy and fast separation or 3D direction,

a variety of cheap synthetic approaches leading to nanosized particles, *in vitro* and *in vivo* cytocompatibility, and high durability.[10-12] However, not only inorganic particles are preferably chosen as platforms of functional materials. Although moderate attention has been paid to the alternating synthetic copolymer of methyl vinyl ether and maleic anhydride (PMVEAMA), its biocompatibility, low toxicity, biodegradability, the presence of pendant anhydride domains undergoing an easy functionalization, and biologically beneficial mucoadhesiveness have been evidenced in the literature.[13-15] Therefore, these three materials have been chosen as preferred supports for the obtaining of functional materials.

## Dendrimers as functionalizing organic receptors

The term "dendrimer" has been used for the very first time in a scientific article in 1985 by Tomalia, who presented a method for obtaining a new class of monodisperse poly(amidoamine) dendritic macromolecules.[16] Although a quite similar approach for the synthesis of poly-armed molecules had been already published in 1978 by the group of Vögtle,[17] the report of Tomalia is now treated as a focal point of significant interest in dendrimers chemistry.

In order to explain and justify the fame of dendrimers, we need to answer the question: what are their structural features, and thus application areas? Dendrimers, also named as tree-like molecules, and previously as arborols or cascade molecules, are highly branched, mono-dispersed, and multivalent macromolecules of well-defined three-dimensional architecture.[18-19] They consist of polyfunctional core molecule surrounded by branched arms (dendrons). The branching level, identified as a dendrimers' generation, determines the molecular size, the number of internal and terminal functional groups, and the presence of internal cavities/voids – free spaces between subsequent branches. Owing to the described structural features, dendrimers may find multiple applications in analytical chemistry, drug and gene delivery, or catalysis.[20-27] Up to now, a variety of types of dendrimers have been proposed and characterized, including: poly(amidoamine) (PAMAM); poly(propylene imine) (PPI); polypeptide (especially based on poly-L-lysine); polyester (especially based on 2,2-bis-(hydroxymethyl)propionic acid (bis-MPA)); triazine; Fréchet-type (poly(arylalkyl

ether)-based); polyether; cyclotriphosphazane-based; carbosilane; and polyphenylene dendrimers.

However, due to the type of functional internal amide groups and terminal amine groups, synthetic approaches, and ability to interact with various analytes illustrated in Figure 1, PAMAM dendrimers gained the most significant attention in their application in either free or support-immobilized forms. A synthetic strategy of poly(amidoamine) dendrimers involves two main approaches: divergent and convergent methods,[28] which are based on the repetitive coupling of building units to a core molecule, and coupling of pre-synthesized branches to a core molecule, respectively.

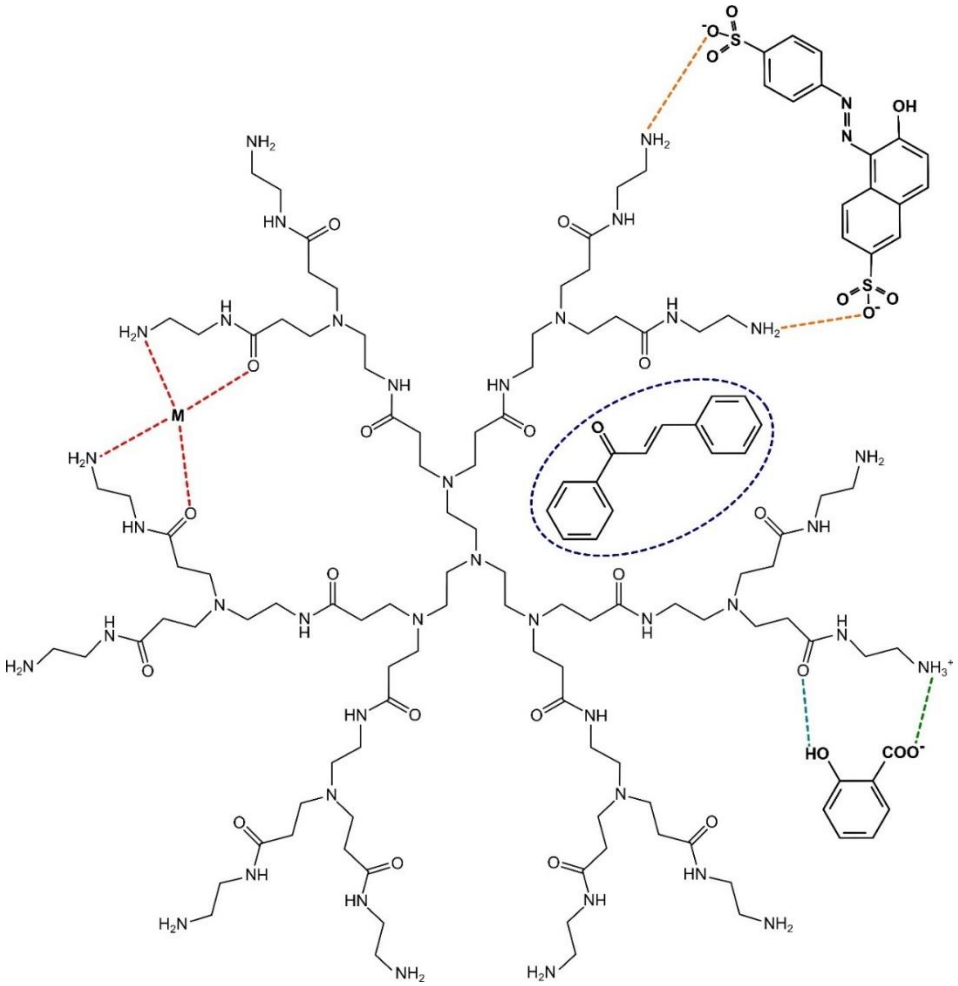


**Figure 1.** The structure of a classic PAMAM dendrimer containing ethylenediamine (EDA) as a terminal amine component, and its possible interaction mechanisms: chelation of metal cations (red); ion-dipole interactions (orange); proton exchange leading to electrostatic interactions (green); hydrogen bonding (sea blue); and supramolecular inclusion (navy blue).

Free PAMAM dendrimers exhibit several analytical and biological applications, which are strictly correlated with their structural features, such as the possibility of interactions with other chemicals through different types of bonding, the ability of supramolecular inclusion of various molecules into dendritic cavities, water-solubility, or permeation through membranes.[29] However, it has been postulated that highly branched PAMAM dendrimers of a higher generation containing numerous terminal $-NH_2$ groups can lead to inconvenient interactions with negatively charged membranes' domains or blood constituents.[30,31] Therefore, poly(amidoamine) dendrimers and their PEGylated, acylated, or lauroylated derivatives shielding aggressively positive charge, were successfully used for a delivery of drugs, nucleic acids, or contrasting agents,[32-40] an enhancement of poorly water-soluble drugs,[41-44] and optical sensing or binding of analytes.[45-50] The successful and promising studies over the application of free and functionalized PAMAM dendrimers in biological chemistry led to the designing of functional materials with immobilized dendritic domains, applicable in various fields. Such materials might be obtained by following two different synthetic approaches: (1) 'grafting to' method, which involves immobilization of a pre-synthesized dendrimer on the surface of a material through a reactive linker; and (2) 'grafting from' method, based on the synthesis of dendrons on a surface-modified material with a particular functional group - usually an amine group. The first approach leads to the formation of a system containing fully-dendritic domains on the surface, while the latter leads to a system grafted with quasi-dendritic structures, in which the material particle is a dendritic core (Figure 2). Nonetheless, both types of materials contain branched and basic amido-amine-rich molecular receptors, which are able to form chemical complexes with (i) metal cations through chelation mechanism; (ii) acidic molecules by a proton exchange leading to an acid-base system; or (iii) negatively charged species through dipole-ion interaction. Moreover, the formation of host/guest supramolecular structure, in which pendant PAMAM residue plays a role of the host, is also an alternative route of dendrimer-grafted material interactions with analytes.

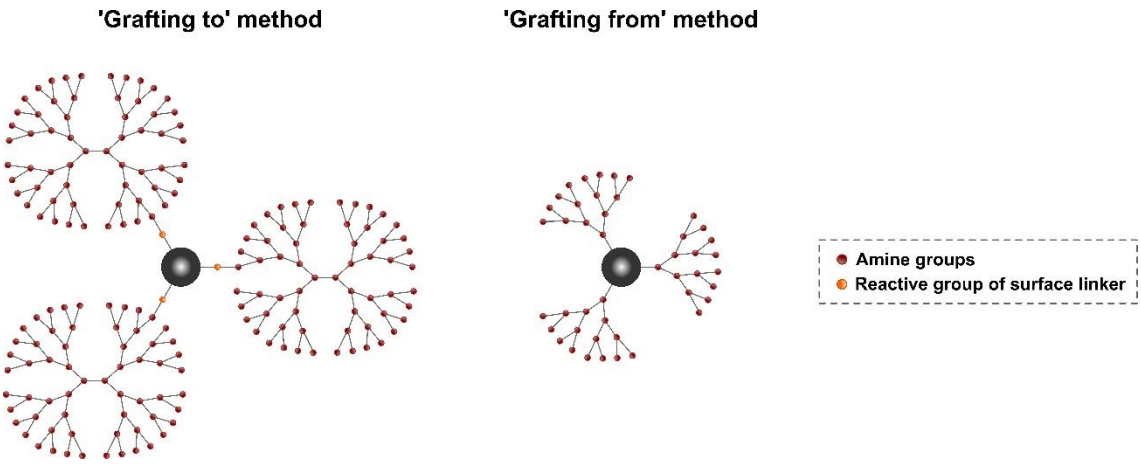


**Figure 2.** The schematic representation of the materials functionalized with generation 3 PAMAM dendrimers or dendrons, obtained following the 'grafting to' and 'grafting from' approaches, respectively.

One of the first researches aiming at the synthesis of materials containing PAMAM dendrons, and their application as toxic metal ions scavengers, was performed by Qu et al. in 2006.[51] The conducted studies involved the adsorption of a series of metal cations from their aqueous solutions on the silica-based adsorbents grafted with amine- or ester-terminated PAMAM dendrons. Consequently, several materials grafted with PAMAM dendrimers or their conjugates with 5-sulfosalicylic acid or methyl isothiocyanate were further used in the chelation of Pb(II), Pd(II), Co(II), Au(III), Hg(II), Ag(I), Fe(III), or Cu(II) from their aqueous or ethanolic solutions.[52-62] The effectiveness of the silica-PAMAM in remediation of toxic metal cations has triggered an implementation of SBA-15 or MCM-41 types of mesoporous silica, titania, carbon nanotubes, halloysite nanotubes, or magnetite nanoparticles as supports for metal cation scavenging systems.[63-72] Moreover, owing to the multiple terminal groups in the structure of PAMAM dendrimers, several materials grafted with such molecular receptors were also investigated for their efficiency in the removal of various acidic or anionic species, especially anionic dyes (malachite green, methyl orange, reactive blue, Congo red, etc.) and phenol compounds.[73-77] The formation of complexes between dendritic-functionalized materials and metal cations has also prompted the use of such materials as matrices for metal-containing catalysts. After the complexation of metal cations by a surface dendrimer, the material is treated with a reducing agent (most often $NaBH_4$), leading to metallodendrimer-functionalized particles. The main advantage of these

materials is preventing metal nanoparticles from agglomeration, leaching, and passivation, and a uniform structure of dispersing matrix leading to regularly and well-defined located metal nanoparticles, which jointly provide highly efficient, easily recyclable, and eco-friendly catalysts of various organic reactions. For instance, SBA-15 mesoporous silica functionalized with hydroxyl-terminated PAMAM dendrimer complexed with Fe(III) ions showed very good catalytic activity accelerating the formation of C–C bonds between chosen ketones and indoles following Michael addition, $Fe_3O_4$ nanoparticles functionalized with PAMAM-Co(II) complex were studied for the catalysis of Mizoroki-Heck cross-coupling between aryl halides and alkyl acrylates, or magnetic graphene oxide grafted with PAMAM dendrimer allowed for solvent-free and fast Knoevenagel condensation between malononitrile and various aryl aldehydes.[78-81] Also, materials functionalized with dendrimers may play the role of a platform for the immobilization of enzymes, leading to an improved stability of biocatalysts and their enhanced reusability.[82-84]

Another, highly important application of dendrimer-functionalized materials is the delivery of bioactive compounds or nucleic acids. Several studies including adsorption and subsequent *in vitro* release of drugs in pseudophysiological conditions showed that silica particles, carbon, titania and alumina nanotubes, or $Fe_3O_4$-based materials grafted with PAMAM dendrimer domain are effective in the delivery of e.g.: methotrexate and doxorubicin – anticancer agents; anthocyanin – a potential antioxidant; silibinin – a drug used in hepatic diseases; ibuprofen, ketoprofen, and diclofenac – non-steroidal anti-inflammatory drugs; clofibric acid – an anticholesteremic agent; carvedilol – a drug used un hypertension treatment; or deferasirox – a drug used to reduce iron overload.[85-90] The effective release of the drugs to aqueous releasing media has also prompted an *in vitro* investigation of (PAMAM-grafted materials)-drug cytotoxicity towards several cancer cells lines. For instance, nano$SiO_2$-PAMAM-anthocyanin showed satisfactory apoptotic activity towards Nauro-2A brain neuroblastoma cell lines, mesoporous silica-PAMAM-doxorubicin towards UMUC3 human urothelial carcinoma cell lines, or $Fe_3O_4$-citric acid-PAMAM-curcumin towards MCF-7 human breast adenocarcinoma.[91-93] Biomedical application of the mentioned hybrid materials is not limited to the delivery of synthetic or naturally-derived pharmaceuticals,

but also may be connected with their implementation in gene therapy – the transfer of cargo nucleic acid (various types of RNA or DNA) through cell membranes.[94-98]

## Deferoxamine as a functionalizing organic domain

Deferoxamine, also known as desferrioxamine or DFO, is a trihydroxamic acid, which was discovered as a metabolite of the soil bacterium *Streptomyces pilosus* in the late 1950s.[99] Almost 40 years later, in 1988, Bergeron and Pegram presented the very first and relatively efficient multi-step synthesis of DFO.[100] A presence of three hydroxamic acid domains strictly determines its chelating properties especially towards trivalent metal cations (Figure 3). Among all metal cations, deferoxamine-Fe(III) complex shows the highest stability constant, reaching log$\beta$ values of 30.6 and 41.6 for [ML] and $[MHL]^+$ (M – the metal ions, Fe(III); L – the ligand, deferoxamine) complexes, respectively,[101] which contributed to its clinical application in the treatment of chronic or sudden iron overload.[102] Pure deferoxamine has also been proved for beneficial effects in the treatment of various hepatic diseases, neurodegenerative disorders triggered by iron dysregulations, and for inhibition of K562 leukemia cells' viability.[103-106]

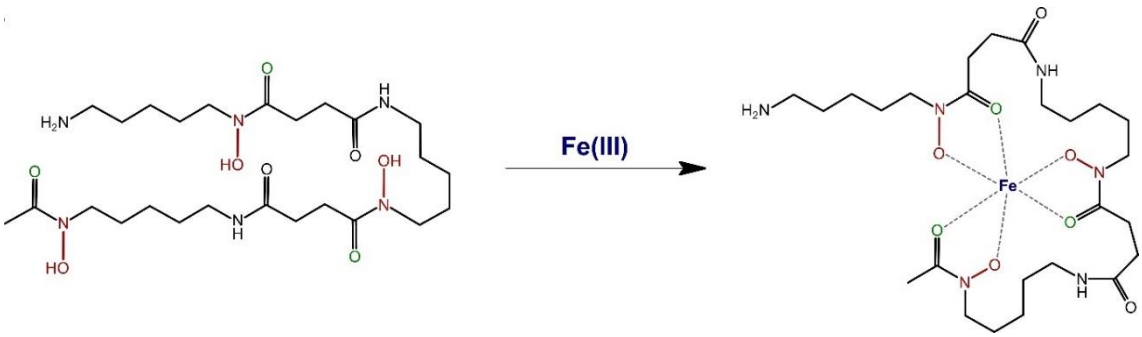


**Figure 3.** The formation of deferoxamine complex with Fe(III) ion.

Although deferoxamine is not the most extensively applied surface functionalizing agent, there are several examples of DFO-grafted platforms investigated for the detection and/or quantification of trivalent cations. For instance, materials based on silver nanoparticles were successfully applied for sensing of Fe(III) ions using surface-enhanced Raman scattering (SERS) method[107-108] or silica chips modified with DFO were used for quantification of the picomolar concentration of ferric ions in subarctic Pacific seawater samples using IR spectroscopy.[109] Other materials based on silica, agarose beads, carbon

material, or common filtration paper were also investigated for sorptive properties towards various metal cations, including Fe(III), Cr(VI), V(V), or Cu(II).[110-113] Also, such materials may be applied for chelation of $^{89}Zr$ isotope, making them bifunctional systems for simultaneous drug delivery and positron emission tomography (PET) imagining.[114,115]

## Applications of hybrid materials in chemical analysis

Among the most demanded application fields of hybrid materials are analytical chemistry, environmental protection, and biomedicine. These application directions can be fulfilled by the implementation of systems containing the two above-described types of organic functionalizing domains – PAMAM dendrimers and deferoxamine. Namely, the materials containing surface poly(amidoamine) dendritic supramolecular receptor might be applied as either (i) pre-concentration systems allowing for quantitative or qualitative analysis of non-detectable trace amounts of analytes; (ii) efficient materials for remediation of chemicals exhibiting human toxicity; (iii) platforms for directed and controlled transport of therapeutics, drugs, and nucleic acids, also often enriched with ability of imagining using magnetic resonance imagining (MRI); (iv) solids applied in solid-phase extraction (SPE) for separation or purification step; or (v) deposits for size-exclusion chromatography (SEC). Furthermore, the materials containing a specific chelating domain of deferoxamine also meet the applicability criteria by high affinity to metal cations, especially Fe(III), which leads to their use as efficient metal sensors, scavengers dedicated to toxic metal ions pollution, or biocompatible materials enabling simultaneous targeted biodistribution and visualization by their complexation with specific isotopes.

## References


(1) J. Alemán, A.V. Chadwick, J. He, M. Hess, K. Horie, R.G. Jones, P. Kratochvíl, I. Meisel, I. Mita, G. Moad, S. Penczek, R.F.T. Stepto, Definitions of terms relating to the structure and processing of sols, gels, networks, and inorganic–organic hybrid materials, Pure Appl. Chem. 79 (2007), 1801-1829.

(2) G. Kickelbick, Hybrid Materials – Past, Present and Future, Hybrid Mater. 1 (2014), 39–51.

(3) M. Faustini, L. Nicole, E. Ruiz-Hitzky, C. Sanchez, History of Organic–Inorganic Hybrid Materials: Prehistory, Art, Science, and Advanced Applications, Adv. Funct. Mater. 28 (2018), 1704158.

(4) P. Gómez-Romero, C. Sanchez, Hybrid materials. Functional properties. From Maya Blue to 21st century materials, New J. Chem. 29 (2005), 57-58.

(5) A. Kayan, Inorganic-organic hybrid materials and their adsorbent properties, Adv. Compos. Hybrid Mater. 2 (2019), 34–45.

(6) K. Lu, Hybrid materials – a review on co-dispersion, processing, patterning, and properties, Int. Mater. Rev. 65 (2020), 463-501.

(7) Y.E. Silina, K.V. Gernaey, D. Semenova, I. Iatsunskyi, Application of Organic-Inorganic Hybrids in Chemical Analysis, Bio- and Environmental Monitoring, Appl. Sci. 10 (2020), 1458-1479.

(8) A. Rimola, D. Costa, M. Sodupe, J.F. Lambert, P. Ugliengo, Silica Surface Features and Their Role in the Adsorption of Biomolecules: Computational Modeling and Experiments, Chem. Rev. 113 (2013), 4216–4313.

(9) G. Busca, Catalytic materials based on silica and alumina: Structural features and generation of surface acidity, Progress Mater. Sci. 104 (2019), 215-249.

(10) A.G. Niculescu, C. Chircov, A.M. Grumezescu, Magnetite nanoparticles: Synthesis methods – A comparative review, Methods (2021), https://doi.org/10.1016/j.ymeth.2021.04.018.

(11) K. Myklie, P. Nowak, P. Rybczyński, M. Ziegler-Borowska, Polymer-Coated Magnetite Nanoparticles for Protein Immobilization, Materials 14 (2021), 248-287.

(12) F. Yazdani, M. Seddigh, Magnetite nanoparticles synthesized by co-precipitation method: The effects of various iron anions on specifications, Mater. Chem. Phys. 184 (2016), 318-323.

(13) A. Mira, C.R. Mateo, R. Mallavia, A. Falco, Poly(methyl vinyl ether-alt-maleic acid) and ethyl monoester as building polymers for drug-loadable electrospun nanofibers, Sci. Rep. 7 (2017), 1-13.

(14) J. Varshosaza, M. Minaiyanb, L. Dayyan, Poly(methyl vinyl ether-co-maleic acid) for enhancement of solubility, oral bioavailability and anti-osteoporotic effects of raloxifene hydrochloride, Eur. J. Pharm. Sci. 112 (2018), 195-206.

(15) N. Zhou, X. Ma, K.V. Bernaerts, P. Ren, W. Hu, T. Zhang, Expansion of Ovarian Cancer Stem-like Cells in Poly(ethylene glycol)-Cross-Linked Poly(methyl vinyl ether-*alt*-maleic acid) and Alginate Double-Network Hydrogels, ACS Biomater. Sci. Eng. 6 (2020), 3310-3326.

(16) D.A. Tomalia, H. Baker, J. Dewald, M. Hall, G. Kallos, S. Martin, J. Roeck, J. Ryder, P. Smith, A New Class of Polymers: Starburst-Dendritic Macromolecules, Polymer Journal 17 (1985), 117-132.

(17) E. Bubleier, W. Wehner, F. Vögtle, Cascade and Nonskid-Chain-Like Syntheses of Molecular Cavity Topologies, Synthesis 2 (1978), 155-158.

(18) A.M. Caminade, D. Yan, D.K. Smith, Dendrimers and hyperbranched polymers, Chem. Soc. Rev. 44 (2015), 3870-3873.

(19) E.N. Augustus, E.T. Allen, A. Nimibofa, W. Donbebe, A Review of Synthesis, Characterization and Applications of Functionalized Dendrimers, Am. J. Polym. Sci. 7 (2017), 8-14.

(20) Z. Mhlwatika, B.A. Aderibigbe, Application of Dendrimers for the Treatment of Infectious Diseases, Molecules 23 (2018), 2205-2236.

(21) L. Palmerston Mendes, J. Pan, V.P. Torchilin, Dendrimers as Nanocarriers for Nucleic Acid and Drug Delivery in Cancer Therapy, Molecules 22 (2017), 1401-1421.

(22) A.M. Caminade, J.P. Majoral, Which Dendrimer to Attain the Desired Properties? Focus on Phosphorhydrazone Dendrimers, Molecules 23 (2018), 622-633.

(23) M. Sajida, M.K. Nazala, Ihsanullaha, N. Baigb, A.M. Osman, Removal of heavy metals and organic pollutants from water using dendritic polymers based adsorbents: A critical review, Sep. Pur. Technol. 191 (2018), 400-423.

(24) F. Najafi, M. Salami-Kalajahi, H. Roghani-Mamaqani, A review on synthesis and applications of dendrimers, J. Iran. Chem. Soc. 18 (2021), 503-517.

(25) D. Astruc, F. Chardac, Dendritic Catalysts and Dendrimers in Catalysis, Chem. Rev. 101 (2001), 2991-3023.

(26) P. Kesharwani, K. Jain, N.K. Jain, Dendrimer as nanocarrier for drug delivery, Progress Polym. Sci. 39 (2014), 268-307.

(27) S. Nigam, D. Bahadur, Dendrimer-conjugated iron oxide nanoparticles as stimuli-responsive drug carriers for thermally-activated chemotherapy of cancer, Colloids Surf. B Biointerf. 155 (2017), 182-192.

(28) Z. Lyu, L. Ding, A.Y.T. Huang, C.L. Kao, L. Peng, Poly(amidoamine) dendrimers: covalent and supramolecular synthesis, Mater. Today Chem. 13 (2019), 34-48.

(29) L.J. Fox, R.M. Richardson, W.H. Briscoe, PAMAM dendrimer – cell membrane interactions, Adv. Colloid Interf. Sci. 257 (2018), 1-18.

(30) C.F. Jones, R.A. Campbell, A.E. Brooks, S. Assemi, S. Tadjiki, G. Thiagarajan, C. Mulcock, A.S. Weyrich, B.D. Brooks, H. Ghandehari, D.W. Grainger, Cationic PAMAM Dendrimers Aggressively Initiate Blood Clot Formation, ACS Nano 6 (2012), 9900-9910.

(31) M., Ehsan, A.N. Kharat, M. Adeli, Polyamidoamine and polyglycerol; their linear, dendritic and linear–dendritic architectures as anticancer drug delivery systems, J. Mater. Chem. B 3 (2015) 3896-3921.

(32) A. Zarebkohan, F. Najafi, H.R. Moghimi, M. Hemmati, M.R. Deevband, B. Kazemi, Synthesis and characterization of a PAMAM dendrimer nanocarrier 4 functionalized by SRL peptide for targeted gene delivery to the brain, Eur. J. Pharm. Sci. 78 (2015), 19-30.

(33) M.R. Carvalho, R.L. Reis, J.M. Oliveira, Dendrimer nanoparticles for colorectal cancer applications, J. Mater. Chem. B 8 (2020), 1128-1138.

(34) M. Marcinkowska, E. Sobierajska, M. Stanczyk, A. Janaszewska, A. Chworos, B. Klajnert-Maculewicz, Conjugate of PAMAM Dendrimer, Doxorubicin and Monoclonal Antibody-Trastuzumab: The New Approach of a Well-Known Strategy, Polymers 10 (2018), 187-197.

(35) C. Yan, J. Gu, Y. Lv, W. Shi, H. Jing, Improved intestinal absorption of water-soluble drugs by acetylation of G2 PAMAM dendrimer nanocomplexes in rat, Drug Deliv. Transl. Res. 7 (2017), 408-415.

(36) F. Abedi-Gaballu, G. Dehghan, M. Ghaffari, R. Yekta, S. Abbaspour-Ravasjani, B. Baradaran, J.E.N. Dolatabadi, M.R. Hamblin, PAMAM dendrimers as efficient drug and gene delivery nanosystems for cancer therapy, Appl. Mater. Today 12 (2018), 177-190.

(37) P. Kesharwani, S. Banerjee, U. Gupta, M.C.I.M. Amin, S. Padhye, F.H. Sarkar, A.K. Iyer, PAMAM dendrimers as promising nanocarriers for RNAi therapeutics, Mater. Today 18 (2015), 565-572.

(38) J. Li, H. Liang, J. Liu, Z. Wang, Poly (amidoamine) (PAMAM) dendrimer mediated delivery of drug and pDNA/siRNA for cancer therapy, Int. J. Pharm 546 (2018), 215-225.

(39) S.L. Mekuria, T.A. Debele, H.C. Tsai, Encapsulation of Gadolinium Oxide Nanoparticle ($Gd_2O_3$) Contrasting Agents in PAMAM Dendrimer Templates for Enhanced Magnetic Resonance Imaging In Vivo, ACS Appl. Mater. Sci. 9 (2017), 6782-6795.

(40) D. Liu, C. Wang, J. Yang, Y. An, R. Yang, G. Teng. CRGDK-Functionalized PAMAM-Based Drug-Delivery System with High Permeability, ACS Omega 5 (2020), 9316-9323.

(41) Y.K. Katare, R.P. Daya, C. Sookram Gray, R.E. Luckham, J. Bhandari, A.S. Chauhan, R.K. Mishra, Brain Targeting of a Water Insoluble Antipsychotic Drug Haloperidol via the Intranasal Route Using PAMAM Dendrimer, Mol. Pharmaceutics 12 (2015), 3380-3388.

(42) D. Luong, P. Kesharwani, B.A. Killinger, A. Moszczynska, F.H. Sarkar, S. Padhye, A.K. Rishi, A.K. Iyer, Solubility enhancement and targeted delivery of a potent anticancer flavonoid analogue to cancer cells using ligand decorated dendrimer nano-architectures, J. Colloid Interf. Sci. 484 (2016), 33-43.

(43) D.M. Shadrack, H.S. Swai, J.J.E. Munissi, E.B. Mubofu, S.S. Nyandoro, Polyamidoamine Dendrimers for Enhanced Solubility of Small Molecules and Other Desirable Properties for Site Specific Delivery: Insights from Experimental and Computational Studies, Molecules 23 (2018), 1419-1438.

(44) J. Lu, N. Li, Y. Gao, N. Li, Y. Guo, H. Liu, X. Chen, C. Zhu, Z. Dong, A. Yamamoto, The Effect of Absorption-Enhancement and the Mechanism of the PAMAM Dendrimer on Poorly Absorbable Drugs, Molecules 23 (2018), 2001-2016.

(45) I. Sohail, I.A. Bhatti, A. Ashar, F.M. Sarim, M. Mohsin, R. Naveed, M. Yasir, M. Iqbal, A. Nazir, Polyamidoamine (PAMAM) dendrimers synthesis, characterization and adsorptive removal of nickel ions from aqueous solution, J. Mater. Res. Technol. 9 (2020), 498-506.

(46) E. Soršak, J. Volmajer Valh, Š. Korent Urekb, A. Lobnik, Application of PAMAM dendrimers in optical sensing, Analyst 140 (2015), 976-989.

(47) E.B. Bahadir, M.K. Sezgintürk, Poly(amidoamine) (PAMAM): An emerging material for electrochemical bio(sensing) applications, Talanta 148 (2016), 427-438.

(48) C. Deraedt, G. Melaet, W.T. Ralston, R. Ye, G.A. Somorjai, Platinum and Other Transition Metal Nanoclusters (Pd, Rh) Stabilized by PAMAM Dendrimer as Excellent Heterogeneous Catalysts: Application to the Methylcyclopentane (MCP) Hydrogenative Isomerization, Nano Lett. 17 (2017), 1853-1862.

(49) P. Ilaiyaraja, A.K. Singha Deb, D. Ponraju, B. Venkatraman, Xanthate functionalized PAMAM dendrimer (XFPD) chelating ligand 2 for treatment of radioactive liquid wastes, J. Environ. Chem. Eng. 3 (2015), 1047-1054.

(50) A.M.A. Adam, T.A. Altalhi, S.M. El-Megharbel, H.A. Saad, M.S. Refat, Using a Modified Polyamidoamine Fluorescent Dendrimer for Capturing Environment Polluting Metal Ions Zn2+, Cd2+, and Hg2+: Synthesis and Characterizations, Crystals 11 (2021), 92-111.

(51) R. Qu, Y. Niu, C. Sun, C. Ji, C. Wang, G. Cheng, Syntheses, characterization, and adsorption properties for metal ions of silica-gel functionalized by ester- and amino-terminated dendrimer-like polyamidoamine polymer, Micropor. Mesopor. Mater. 97 (2006), 58-65.

(52) R. Qu, Y. Niu, J. Liu, C. Sun, Y. Zhang, H. Chen, C. Ji, Adsorption and desorption behaviors of Pd(II) on silica-gel functionalized with ester- and amino-terminated dendrimer-like polyamidoamine polymers, React. Funct. Polym. 68 (2008), 1272-1280.

(53) Y. Niu, R. Qu, C. Sun, C. Wang, H. Chen, C. Ji, Y. Zhang, X. Shao, F. Bu, Adsorption of Pb(II) from aqueous solution by silica-gel supported hyperbranched polyamidoamine dendrimers, J. Haz. Mater. 244-245 (2013), 276– 286.

(54) R. Qu, X. Ma, M. Wang, C. Sun, X. Sun, S. Sun, Y. Zhang, P. Yin, Homogeneous preparation of polyamidoamine grafted silica gels and their adsorption properties as Au3+ adsorbents, J. Industr. Eng. Chem. 20 (2014), 4382-4392.

(55) Y. Zhang, R. Qu, T. Xu, Y. Zhang, C. Sun, C. Ji, Y. Wang, Fabrication of Triethylenetetramine Terminal Hyperbranched Dendrimer-Like Polymer Modified Silica Gel and Its Prominent Recovery Toward Au (III), Front. Chem. 7 (2019), 577-589.

(56) Y. Zhang, R. Qu, C. Sun, C. Ji, H. Chen, P. Yin, Improved synthesis of silica-gel-based dendrimer-like highly branched polymer as the Au(III) adsorbents, Chem. Eng. J. 270 (2015), 110-121.

(57) X. Wu, L. Luo, Z. Chen, K. Liang, Syntheses, characterization and adsorption properties for Pb2+ of silica-gel functionalized by dendrimer-like polyamidoamine and 5-sulfosalicylic acid, Appl. Surf. Sci. 364 (2016), 86-95.

(58) R. Qu, C. Sun, F. Ma, Z. Cui, Y. Zhang, X. Sun, C. Ji, C. Wang, P. Yin, Adsorption kinetics and equilibrium of copper from ethanol fuel on silica-gel functionalized with amino-terminated dendrimer-like polyamidoamine polymers, Fuel 92 (2012), 204-210.

(59) Y. Niu, J. Yang, R. Qu, Y. Gao, N. Du, H. Chen, C. Sun, W. Wang, Synthesis of Silica-Gel-Supported Sulfur-Capped PAMAM Dendrimers for Efficient Hg(II) Adsorption: Experimental and DFT Study, Ind. Eng. Chem. Res. 55 (2016), 3679-3688.

(60) X. Song, Y. Niu, Z. Qiu, Z. Zhang, Y. Zhou, J. Zhao, H. Chen, Adsorption of Hg(II) and Ag(I) from fuel ethanol by silica gel supported sulfur-containing PAMAM dendrimers: Kinetics, equilibrium and thermodynamics, Fuel 206 (2017), 80-88.

(61) X. Song, Y. Niu, P. Zhang, C. Zhang, Z. Zhang, Y. Zhu, R. Qu, Removal of Co(II) from fuel ethanol by silica-gel supported PAMAM dendrimers: Combined experimental and theoretical study, Fuel 199 (2017), 91-101.

(62) R. Qu, C. Sun, F. Ma, Y. Zhang, C. Ji, P. Yin, Removal of Fe(III) from ethanol solution by silica-gel supported dendrimer-like polyamidoamine polymers, Fuel 219 (2018), 205–213.

(63) Y. Jiang, Q. Gao, H. Yu, Y. Chen, F. Deng, Intensively competitive adsorption for heavy metal ions by PAMAM-SBA-15 and EDTA-PAMAM-SBA-15 inorganic-organic hybrid materials, Micropor. Mesopor. Mater. 103 (2007), 316-324.

(64) W. Xiao, B. Yan, H. Zeng, Q. Liu, Dendrimer functionalized graphene oxide for selenium removal, Carbon 105 (2016), 655-664.

(65) M.A. Barakat, M.H. Ramadan, M.A. Alghamdi, S.S. Algarny, H.L. Woodcock, J.N. Kuhn, Remediation of Cu(II), Ni(II) and Cr(III) ions from simulated wastewater by dendrimer/titania composites, J. Environ. Manag. 117 (2013), 50-57.

(66) M.A. Barakat, M.H. Ramadan, J.N. Kuhn, H.L. Woodcock, Equilibrium and kinetics of Pb2+ adsorption from aqueous solution by dendrimer/titania composites, Desalin. Water Treat. 52 (2014), 5869-5875.

(67) A. Maleki, B. Hayati, F. Najafi, F. Gharibi, S.W. Joo, Heavy metal adsorption from industrial wastewater by PAMAM/TiO2 nanohybrid: Preparation, characterization and adsorption studies, J. Mol. Liq. 224 (2016), 95-104.

(68) B. Hayati, A. Maleki, F. Najafi, H. Daraei, F. Gharibi, G. McKay, Super high removal capacities of heavy metals (Pb2+and Cu2+) using CNT dendrimer, J. Haz. Mater. 336 (2017), 146-157.

(69) B. Hayati, A. Maleki, F. Najafi, H. Daraei, F. Gharibi, G. McKay, Synthesis and characterization of PAMAM/CNT nanocomposite as a super-capacity adsorbent for heavy metal (Ni2+, Zn2+, As3+, Co2+) removal from wastewater, J. Mol. Liq. 224 (2016), 1032-1040.

(70) M.H. Kanani-Jazi, S. Akbari, M.H. Kish, Efficient removal of Cr (VI) from aqueous solution by halloysite/poly(amidoamine) dendritic nano-hybrid materials: kinetic, isotherm and thermodynamic studies, Adv. Powder Technol. 31 (2020), 4018-4030.

(71) L. Luan, B. Tang, Y. Liu, A. Wang, B. Zhang, W. Xu, Y. Niu, Selective capture of Hg(II) and Ag(I) from water by sulfur-functionalized polyamidoamine dendrimer/magnetic Fe3O4 hybrid materials, Separ. Purif. Technol. 257 (2021), 117902.

(72) K. Lakshmi, R. Rangasamy, Synthetic modification of silica coated magnetite cored PAMAM dendrimer to enrich branched Amine groups and peripheral carboxyl groups for environmental remediation, J. Mol. Struct. 1224 (2021), 129081.

(73) S.A. Hassan, A.S. Darwish, H.M. Gobara, N.E.A. Abed-elsatar, S.R. Fouda, Interaction profiles in poly (amidoamine) dendrimer/montmorillonite or rice straw ash hybrids-immobilized magnetite nanoparticles governing their removal efficiencies of various pollutants in wastewater, J. Mol. Liq. 230 (2017), 353-369.

(74) P. Wang, Q. Ma, D. Hu, L. Wang, Removal of Reactive Blue 21 onto magnetic chitosan microparticles functionalized with polyamidoamine dendrimers, React. Funct. Polym. 91-92 (2015), 43-50.

(75) M.B. Wazir, M. Daud, F. Ali, M.A. Al-Harthi, Dendrimer assisted dye-removal: A critical review of adsorption and catalytic degradation for wastewater treatment, J. Mol. Liq. 315 (2020), 113775.

(76) B. Hayati, N.M. Mahmoodi, A. Maleki, Dendrimer-titania nanocomposite: synthesis and dye-removal capacity, Res. Chem. Intermed. 41 (2015), 3743-3757.

(77) V. Khatibikamal, H.A. Panahi, A. Torabian, M. Baghdadi, Optimized poly(amidoamine) coated magnetic nanoparticles as adsorbent for the removal of nonylphenol from water, Microchem. J. 145 (2019), 508-516.

(78) R. Patala, J.H. Noh, R. Meijboom, Determination of maximum loading capacity of polyamidoamine (PAMAM) dendrimers and evaluation of $Cu^{55}$ dendrimer encapsulated nanoparticles for catalytic activity, Int. J. Chem. Kinet. 50 (2018), 693-704.

(79) R. Ye, F.F. Faucher, G.A. Somorjai, Supported iron catalysts for Michael addition reactions, Mol. Catal. 447 (2018), 65-71.

(80) M. Arghan, N. Koukabi, E. Kolvari, Cobalt supported on dendronized magnetic nanoparticles: A new highly efficient and recyclable catalyst for the Mizoroki–Heck cross-coupling reaction, Appl. Organometal. Chem. 33 (2019), e4823.

(81) B. Maleki, F. Taheri, R. Tayebee, F. Adibian, Dendrimer-Functionalized Magnetic Graphene Oxide for Knoevenagel Condensation, Org. Prep. Proced. Int. 53 (2021), 284-290.

(82) P. Zhao, L. Tian, X. Li, Z. Ali, B. Zhang, H. Zhang, Q. Zhang, Effect of the Structure and Length of Flexible Chains on Dendrimers Grafted Fe3O4@SiO2/PAMAM Magnetic Nanocarriers for Lipase Immobilization, ACS Sustainable Chem. Eng. 4 (2016), 6382-6390.

(83) M. Li, H. Shen, Z. Zhou, W. He, P. Su, J. Song, Y. Yang, Controllable and high-performance immobilized enzyme reactor: DNA-directed immobilization of multienzyme in polyamidoamine dendrimer-functionalized capillaries, Electrophoresis 0 (2020), 1-10.

(84) S. Peiman, R. Baharfar, B. Maleki, Immobilization of trypsin onto polyamidoamine dendrimer functionalized iron oxide nanoparticles and its catalytic behavior towards spirooxindole-pyran derivatives in aqueous media, Mater. Today Comm. 26 (2021), 101759.

(85) C.C. Torres, C.H. Campos, C. Diáz, V.A. Jiménez, F. Vidal, J.L. Guzmán, J.B. Alderete, PAMAM-grafted $TiO_2$ nanotubes as novel versatile materials for drug delivery applications, Mat. Sci. Eng. C 65 (2016), 164-171.

(86) C.H. Campos, C. Diáz, J.L. Guzmán, J.B. Alderete, C.C. Torres, V.A. Jiménez, PAMAM-Conjugated Alumina Nanotubes as Novel Noncytotoxic Nanocarriers with Enhanced Drug Loading and Releasing Performances, Macromol. Chem. Phys. 217 (2016), 1712-1722.

(87) S. Chandra, G. Noronha, S. Dietrich, H. Lang, D. Bahadur, Dendrimer-magnetic nanoparticles as multiple stimuli responsive and enzymatic drug delivery vehicle, J. Magn. Magn. Mater. 380 (2015), 7-12.

(88) R. Lotfi, B. Hayati, S. Rahimi, A.A. Shekarchi, N.M. Mahmoodi, A. Bagheri, Synthesis and characterization of PAMAM/SiO2 nanohybrid as a new promising adsorbent for pharmaceuticals, Microchem. J. 146 (2019), 1150-1159.

(89) X. Zheng, T. Wang, H. Jiang, Y. Li, T. Jiang, J. Zhang, S. Wang, Incorporation of Carvedilol into PAMAM-functionalized MWNTs as a sustained drug delivery system for enhanced dissolution and drug-loading capacity, Asian J. Pharm. Sci. 8 (2013), 278-286.

(90) A.S. Taleghani, P. Ebrahimnejad, A. Heydarinasab, A. Akbarzadeh, Adsorption and controlled release of iron-chelating drug from the amino-terminated PAMAM/ordered mesoporous silica hybrid materials, J. Drug Deliv. Sci. Technol. 56 (2020), 101579.

(91) O. Yesil-Celiktas, C. Pala, E.O. Cetin-Uyanikgil, C. Sevimli-Gur, Synthesis of silica-PAMAM dendrimer nanoparticles as promising carriers in *Neuro blastoma* cells, Anal. Biochem. 519 (2017), 1-7.

(92) B. Wang, K. Zhang, J. Wang, R. Zhao, Q. Zhang, X. Kong, Poly(amidoamine)-modified mesoporous silica nanoparticles as amucoadhesive drug delivery system for potential bladder cancer therapy, Colloids Surf. B Bionterf. 189 (2020), 110832.

(93) H. Nosrati, M. Adibtabar, A. Sharafi, H. Danafar, M.H. Kheiri, PAMAM-modified citric acid-coated magnetic nanoparticles as pH sensitive biocompatible carrier against human breast cancer cells, Drug Dev. Ind. Pharm. 44 (2018), 1377-1384.

(94) Y. Gu, Y. Guo, C. Wang, J. Xu, J. Wu, T.B. Kirk, D. Ma, W. Xue, A polyamidoamne dendrimer functionalized graphene oxide for DOX and MMP-9 shRNA plasmid co-delivery, Mat. Sci. Eng. C 70 (2017), 572-585.

(95) Z. Long, Y.P. Wu, H.Y Gao, Y.F. Li‡ R.R. He, M. Liu, Functionalization of Halloysite Nanotubes via Grafting of Dendrimer for Efficient Intracellular Delivery of siRNA, Bioconjugate Chem. 29 (2018), 2606-2618.

(96) C.H. Edwards, C.R. Christie, A. Masotti, A. Celluzzi, A. Caporali, E.M. Campbell, Dendrimer-coated carbon nanotubes deliver dsRNA and increase the efficacy of gene knockdown in the red four beetle *Tribolium castaneum*, Sci. Rep. 10 (2020), 12422.

(97) A. Masotti, M.R. Miller, A. Celluzzi, L. Rose, F. Micciulla, P.W.F. Hadoke, S. Bellucci, A. Caporali, Regulation of angiogenesis through the efficient delivery of microRNAsinto endothelial cells using polyamine-coated carbon nanotubes, Nanomed. Nanotechnol. Biol. Med. 12 (2016), 1511-1522.

(98) A. Celluzzi, A. Paolini, V. D'Oria, R. Risoluti, S. Materazzi, M. Pezzullo, S. Casciardi, S. Sennato, F. Bordi, A. Masotti, Biophysical and biological contributions of polyamine-coated carbon nanotubes and bidimensional buckypapers in the delivery of miRNAs to human cells, Int. J. Nanomed. 13 (2018), 1-18.

(99) R. Codd, T. Richardson-Sanchez, T.J. Telfer, M.P. Gotsbacher, Advances in the Chemical Biology of Desferrioxamine B, ACS Chem. Biol. 13 (2018), 11-25.

(100) R.J. Begeron, J.J. Pegram, An Efficient Total Synthesis of Desferrioxamine B, J. Org. Chem. 53 (1988), 3131-3134.

(101) D. Belotti, M. Remelli, Deferoxamine B: A Natural, Excellent and Versatile Metal Chelator, Molecules 26 (2021), 3255-3275.

(102) Y. Li, H. Yang, W. Ni, Y. Gu, Effects of deferoxamine on blood-brain barrier disruption after subarachnoid hemorrhage, PLoS ONE 12 (2017), e0172784.

(103) S.F. Darwish, W.M. El-Bakly, E.M. El-Naga, A.S. Awad, E. El-Demerdash, Antifibrotic mechanism of deferoxamine in concanavalin A induced-liver fibrosis: Impact on interferon therapy, Biochem. Pharmacol. 98 (2015), 231-242.

(104) G. Rassu, A. Salis, E.P. Porcu, P. Giunchedi, M. Roldo, E. Gavini, Composite chitosan/alginate hydrogel for controlled release of deferoxamine: A system to potentially treat iron dysregulation diseases, Carbohydrate Polym. 136 (2016), 1338-1347.

(105) Y. Yang, Y. Xu, A. Su, D. Yang, X. Zhang, Effects of Deferoxamine on Leukemia In Vitro and Its Related Mechanism, Medical Sci. Monit. 24 (2018), 6735-6741.

(106) L.R. Hanson, J.M. Fine, D.B. Renner, A.L. Svitak, R.B. Burns, T.M. Nguyen, N.J. Tuttle, D.L. Marti, S.S. Panter, W.H. Frey II, Intranasal delivery of deferoxamine reduces spatial memory loss in APP/PS1 mice, Drug Deliv. and Transl. Res. 2 (2012), 160–168.

(107) F. Yan, Y.K. Shrestha, C.L. Spurgeon, Determination of ferric ions using surface-enhanced Raman scattering based on desferrioxamine-functionalized silver nanoparticles, Chem. Commun. 49 (2013), 7962-7964.

(108) P. Galinetto, A. Taglietti, L. Pasotti, P. Pallavicini, G. Dacarro, E. Giulotto, M.S. Grandi, Sers Activity of Silver Nanoparticles Functionalized With a Desferrioxamine B Derived Ligand For Fe(III) Binding and Sensing, J. Appl. Spectroscopy 82 (2016), 1052-1059.

(109) E.G. Roy, C. Jiang, M.L. Wells, C. Tripp, Determining Subnanomolar Iron Concentrations in Oceanic Seawater Using a Siderophore-Modified Film Analyzed by Infrared Spectroscopy, Anal. Chem. 80 (2008), 4689-4695.

(110) A. Rasheed, A.A. Costa Carvalho, G.G. Arantes de Carvalho, T. Ghous, C.S. Nomura, B.P. Esposito, Chromium removal from aqueous solutions using new silica gel conjugates of desferrioxamine or diethylenetriaminepentaacetic acid, Env. Sci. Pollution Res. 27 (2020), 15635-15644.

(111) M.L. Godino-Salido, A. Santiago-Medina, R. López-Garzón, M.D. Gutiérrez-Valero, P. Arranz-Mascarós, M.D. López de la Torre, M. Domingo-García, F.J. López-Garzón, Preparation and characterization of trihydroxamic acid functionalized carbon materials for the removal of Cu(II) ions from aqueous solution, Appl. Surf. Sci. 387 (2016), 128-138.

(112) G. Alberti, G. Emma, R. Colleoni, M. Pesavento, V.M. Nurchi, R. Biesuz, Novel DFO-functionalized mesoporous silica for iron sensing. Part 2. Experimental detection of free iron concentration (pFe) in urine Samales, Analyst 139 (2014), 3940-3948.

(113) G. Alberti, F. Quattrini, R. Colleoni, V.M. Nurchi, R. Biesuz, Deferoxamine–paper for iron(III) and vanadium(V) sensing, Chem. Papers 69 (2015), 1024-1032.

(114) F. Gao, C. Ieritano, K.T. Chen, G.M. Dias, J. Rousseau, F. Bénard, Y. Seimbille, Two bifunctional desferrioxamine chelators for bioorthogonal labeling of biovectors with zirconium-89, Org. Biomol. Chem. 16 (2018), 5102-5106.

(115) J.Y. Park, S. Park, T.S. Lee, Y.H. Hwang, J.Y. Kim, W.J. Kan, J. Key, Biodegradable micro-sized discoidal polymeric particles for lung-targeted delivery system, Biomaterials 218 (2019), 119331.

# 2

# Purpose and goals

The contemporary world demands the implementation of efficient methods for environmental protection. The most threatening pollutants of industrial as well as environmental waters are toxic metal ions, which may cause several diseases or organism's dysfunctions after long-term accumulation in tissues, and synthetic organic dyes, exhibiting significant human toxicity and non-biodegradability. Another highly important issue is connected with the creation of materials suitable for the effective delivery of therapeutics or the ones finding biomedical applications in the treatment of sudden or chronic diseases.

Accordingly, the main aim of the following dissertation was to investigate the efficiency of the proposed PAMAM- and deferoxamine-grafted hybrid materials in both mentioned analytical directions – remediation of toxic compounds and delivery of bioactive molecules. Since the studied materials contained different supports and grafting agents, the undertaken scientific problems also answered the question: how do the support and the grafting agent influence the effectiveness and applicability of hybrid materials?

The choice of poly(amidoamine) dendrimers as molecular receptors was driven by its interaction versatility, i.e. ability of simultaneous metal ions chelation, formation of hydrogen bonds, and electrostatic interactions. Therefore, the materials based on silica and poly(methyl vinyl ether-*alt*-maleic anhydride) (PMVEAMA) grafted with the dendrimers containing different terminal amine components, were studied for their sorptive properties towards toxic metal cations and organic dyes, which are presented in appended articles **A1**, **A2**, and **A4**. Moreover, the highly basic character of the introduced receptors was also a reason for an investigation of the ability of the materials to transport model acidic drugs, which is presented in articles **A3** and **A4**. It is also important to highlight, that the undertaken research problems involved an investigation of the applicability of the materials functionalized with the pre-synthesized supramolecular compounds,

using ‘grating to’ methodology, which allowed for the retaining of the fully-dendritic structure of the surface receptors.

The second type of the chosen grafting agents was deferoxamine, which is reported as a siderophore – an agent exhibiting extremely high chelating properties towards Fe(III) ions and moderate effectiveness towards other trivalent metal cations. The choice of such chelating domain was directly driven by a lack of reported deferoxamine-modified efficient Fe-sorbents in the literature. Therefore, I have focused my studies on the immobilization of deferoxamine residue on three different supports: pre-synthesized magnetite nanoparticles, amorphous silica particles, and PMVEAMA, and the description of their binding effectiveness towards Fe(III) ions, which was presented in article **A5**. Moreover, the presented research problems refer also to an investigation of factors influencing the sorption efficiency.

The presented doctoral dissertation is based on the following scientific articles:

Appendix A1 **M. Pawlaczyk**, G. Schroeder, Adsorption studies of Cu(II) ions on dendrimer-grafted silica-based materials, Journal of Molecular Liquids 281 (2019), 176-185; IF = 6.165; MNiSW = 100; DOI: 10.1016/j.molliq.2019.02.043

Appendix A2 **M. Pawlaczyk**, G. Schroeder, Efficient Removal of Ni(II) and Co(II) Ions from Aqueous Solutions Using Silica-based Hybrid Materials Functionalized with PAMAM Dendrimers, Solvent Extraction and Ion Exchange 38(5) (2020), 496-521; IF = 2.513; MNiSW = 70; DOI: 10.1080/07366299.2020.1766742

Appendix A3 **M. Pawlaczyk**, G. Schroeder, Dendrimer-Functionalized Hybrid Materials Based on Silica as Novel Carriers of Bioactive Acids, Molecules 25(11) (2020), 2660-2680; IF = 4.411; MNiSW = 100**;** DOI: 10.3390/molecules25112660

Appendix A4 **M. Pawlaczyk**, G. Schroeder, Dual-Polymeric Resin Based on Poly(methyl vinyl ether-alt-maleic anhydride) and PAMAM Dendrimer as a Versatile Supramolecular Adsorbent, ACS Applied Polymer Materials 3(2) (2021), 956-967; IF = 4.089; MNiSW = 20; DOI: 10.1021/acsapm.0c01254

Appendix A5 **M. Pawlaczyk**, G. Schroeder, Deferoxamine-Modified Hybrid Materials for Direct Chelation of Fe(III) Ions from Aqueous Solutions and Indication of the Competitiveness of In Vitro Complexing toward a Biological System, ACS Omega 6(23) (2021), 15168-15181; IF = 3.512; MNiSW = 70; DOI: 10.1021/acsomega.1c01411

# 3

# Discussion of the research

## Silica-based materials functionalized with different poly(amidoamine) dendrimers

The chelating properties of poly(amidoamine) dendrimers led to the design and synthesis of four dendrimers containing ethylenediamine (EDA), tris(2-aminoethyl)amine (TREN), triethylenetetramine (TETA), or 4,7,10-trioxa-1,13-tridecanediamine (TRI-OXA) as terminal amine components, their immobilization on commercially available silica microparticles functionalized with isocyanate groups, and the final application of the obtained hybrid materials as adsorbents dedicated to Cu(II) ions. The described studies are presented in article **A1**, entitled "*Adsorption studies of Cu(II) ions on dendrimer-grafted silica-based materials*". The designed dendrimers were synthesized following the divergent approach, which was based on branching of the amine core (TREN) with methyl acrylate, and subsequent amidation of polyester intermediate with four chosen structurally different amines. The products were characterized with $^{1}$H- and $^{13}$C-NMR spectroscopy, and MS analysis performed in electrospray ionization mode (ESI-MS), which showed several dendrimers' fragmentation ions, which is related to the polyamide character of the products.[116] The synthetic strategy for the obtaining of the designed dendrimers is illustrated in Figure 1 in **A1**, while the structures of the final dendrimers, hereinafter labelled as EDA, TREN, TETA, and TRI-OXA, according to the terminal amine used, are illustrated in Figure 4.

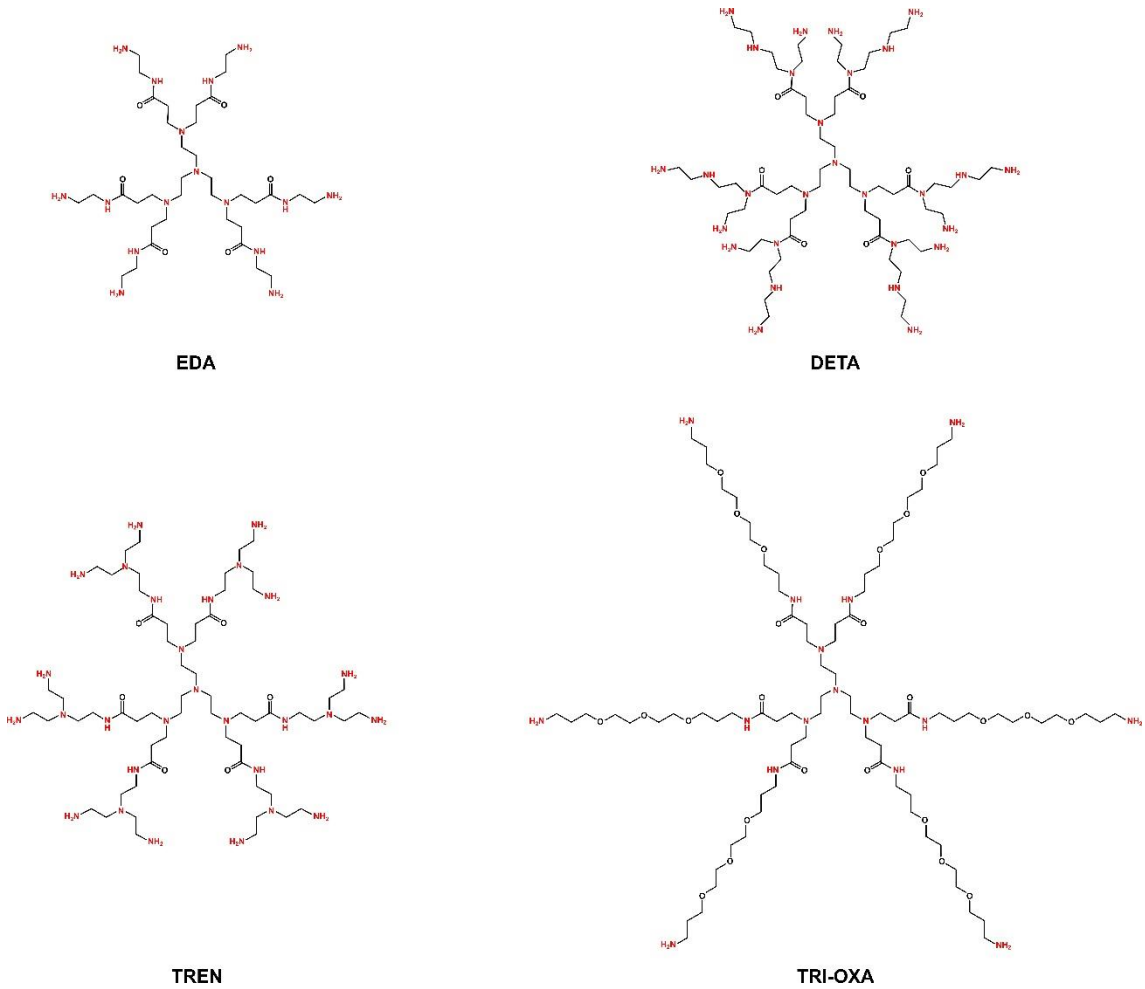


**Figure 4.** The structures of the synthesized poly(amidoamine) (PAMAM) dendrimers with four different amino-terminal components; red – amine groups.

The calculated grafting performance of EDA, TREN, TETA, and TRI-OXA dendrimers were 0.310, 0.155, 0.152, and 0.078 mmol $g^{-1}$, respectively, indicating an influence of the length and structural features of the terminal amine used on the immobilization efficiency. The highest grafting value was achieved for EDA dendrimer, which contained the shortest amine, resulting in the most compact character of the receptor, in contrary to TRI-OXA dendrimer with the lowest grafting level, containing the longest linear amine. An additional factor, which limits, and thus determines the dendrimers' grafting level is the fixed loading of surface reactive groups (isocyanate domains) on the surface of the commercial silica particles, which equaled 1.33 mmol $g^{-1}$. However, the relatively low values of PAMAM grafting efficiency give multiple times higher values of the introduced amine and amide groups. The FT-IR-characterized materials were subsequently studied for adsorptive properties towards Cu(II), which included performing

initially adsorption isotherms. The amounts of the ions adsorbed from a series of Cu(II) solutions of different concentrations, prepared in a buffer solution of pH 5.4, at adsorption equilibria allowed for the calculation of several adsorption parameters and assessment of the isothermal model of the adsorption processes. For all the materials, the adsorption followed the Langmuir model, which is consistent with its assumption, that an adsorbate forms a monolayer on the surface of a material. The maximal adsorption capacities of the materials ($q_m$) were calculated, ranging between 19.8 and 104.6 mg $g^{-1}$, with the highest value for the material grafted with EDA dendrimer. This is related to the highest loading of the chelating receptor on the surface of the material. On the other hand, the lowest adsorptive performance was ascribed for material containing TRI-OXA dendrimer, while moderately satisfactory, but comparable, sorptive capacities of 62.9 and 70.6 mg $g^{-1}$ were calculated for the materials containing TREN and TETA dendrimers, respectively. Furthermore, kinetic and thermodynamic studies of Cu(II) ions adsorption on all the materials were performed. They resulted in several kinetic parameters presented in Table 4 and Table 5 in **A1**, such as adsorption rate constants and the time needed for the half-adsorption ($t_{1/2}$). Moreover, the adsorption experiments conducted at three different temperatures allowed for a calculation of several thermodynamic parameters such as adsorption enthalpy, entropy, and free Gibb's energy, which values are collected in Table 6 in **A1**. The calculated positive values of the enthalpy of the described processes indicated that the adsorption of Cu(II) ions on the PAMAM-grafted hybrid materials is an endothermic process, and thus intensifies with the temperature increase.

Furthermore, the materials containing surface PAMAM dendrimer residues were tested for the adsorption of other d-block metal cations. The article **A2**, entitled "*Efficient Removal of Ni(II) and Co(II) Ions from Aqueous Solutions Using Silica-based Hybrid Materials Functionalized with PAMAM Dendrimers*" focuses on the description of the efficiency of the materials in the binding of toxic Ni(II) and Co(II) ions from their aqueous samples. The initial stage of the comprehensive studies aimed at the choice of the aqueous environment, in which the adsorption of the ions is the most effective. The conducted experiments aiming at the indication of the adsorption capacity pH-dependence, presented as Figure 3 in **A2**, showed that the sorption efficiency is significantly reduced in highly acidic conditions (pH < 4).

Such an observation is connected with the increased protonation of the terminal and internal amine and amide groups of PAMAM dendrimer, which causes increased repulsion between chelating receptor and cationic species. The highest adsorption effectiveness was observed for AcOH/AcONa buffer of pH 5.4, which therefore was chosen as a standard solvent for Ni(II) and Co(II) salts. All the materials functionalized with four structurally different poly(amidoamine) dendrimers were further studied, including isothermal, kinetic, and thermodynamic experiments. The first, which were performed in order to describe the binding potential of the materials at the adsorption equilibrium, showed again that the ions' adsorption follows the Langmuir model, on which basis the values of $q_m$ were calculated. The highest adsorption capacity values were calculated for the materials containing EDA and TRI-OXA pendant dendritic residues, reaching Ni(II) ions capacity of 93.6 and 116.6 mg $g^{-1}$, and Co(II) ions capacity of 99.1 and 101.1 mg $g^{-1}$, respectively. The higher sorption potential of TRI-OXA-functionalized material towards Ni(II) and Co(II) ions than Cu(II) ions might be connected with slightly larger ionic radii of these two cations, in relation to previously studied Cu(II) ions, resulting in easier tethering within large cavities of the dendritic receptor. Furthermore, the kinetics of the ions adsorption process was investigated, of which parameters are collected in Table 3 in **A2**. The calculated values are the amount of time needed for the adsorption of half of the maximal capacity of the sorbents $t_{1/2}$ ranged between 2.12 and 3.89 h for adsorption of Ni(II) ions and between 2.81 and 5.35 h for Co(II) ions, proving the effectiveness of the materials. Moreover, on the basis of the adsorption studies conducted at three different temperatures, the thermodynamic coefficients have been calculated. The calculated positive values of $\Delta H$ indicate the endoenergeticity of the adsorption processes and the positive values of $\Delta S$ show that a driving force of the adsorption is increased randomness at the material-solution interface connected with solvation effects. Moreover, the decreasing $\Delta G$ values with the temperature increase, indicate the thermal intensification of the adsorption of the cations. All the above-described experiments were conducted in the samples containing only one ionic type, which aimed at the description of the effectiveness of the materials towards the particular metal cation. However, to fully characterized the sorptive potential of the PAMAM-grafted silicas, the selectivity studies using a binary system containing both Ni(II) and Co(II)

ions were performed. The selectivity was monitored using two analytical techniques: UV-Vis spectroscopy and X-Ray fluorescence spectroscopy (XRF). Table 5 in **A2** presents a comparison of $\alpha_{Co}^{Ni}$ separation factors calculated for the obtained materials using the first analytical technique, and the percentages of nickel and cobalt ions adsorbed from their mixture. The different affinity of Ni(II) and Co(II) ions to PAMAM-grafted materials is primarily related to the slight differences between their hydrated radii.[117] Moreover, since the pendant dendritic residues are highly basic, the difference in the electronegativity of both cations might also lead to the adsorption selectiveness. Taking these two factors into account, the adsorption process should be directed towards more electronegative nickel ions, described with a smaller hydrated radius. Indeed, the obtained silica-based materials grafted with different poly(amidoamine) dendrimers were described with separation factors higher than 1, ranging between 1.05 and 3.19, and thus showing the higher selectivity towards Ni(II) ions. Nevertheless, the highest Ni/Co selectivity coefficients are demonstrated for the materials containing TREN and TETA dendritic types, which might be explained by the more branched character of these dendrimers, in relation to EDA and TRI-OXA domains. Therefore, the competitive diffusion of both cations is related to the steric hindrance, hindering the diffusion of "bigger" Co(II) ions into the interior of the dendrimers in comparison to Ni(II) ions. Nevertheless, all the materials exhibit satisfactory binding efficiency towards d-block metal cations, which depends on the structure of the used dendritic grafting agent.

The proven adsorptive efficiency of the PAMAM-grafted materials towards metal cations has contributed to a further exploration of the binding properties of the materials towards acidic molecules exhibiting bioactivity. Article **A3**, which is entitled "*Dendrimer-Functionalized Hybrid Materials Based on Silica as Novel Carriers of Bioactive Acids*" presents an investigation of binding and further *in vitro* release of the chosen acidic biomolecules by the dendrimer-grafted silica materials. A series of four hybrid materials were obtained by the incorporation of previously presented four poly(amidoamine) dendrimers (EDA, TREN, TETA, and TRI-OXA) to the surface of commercially available silica particles functionalized with glycidoxy linker. The grafting of PAMAM domains followed the epoxide ring-opening triggered by the nucleophilic attack of the dendrimer terminal amine group, leading

to silica-PAMAM materials. Since the nucleophile-sensitive glycidoxy group was chosen as a functionalizable linker, the reactions must have been carried out in non-nucleophilic solvent able of PAMAM dendrimers solubilization, which was DMF. The successful introduction of dendritic domains on the support surface was proved by FT-IR spectroscopy by the appearance of new signals corresponding to the stretching of amide N-H and C=O groups. Moreover, the materials were further characterized with scanning electron microscopy (SEM), thermogravimetric (TG) analysis, showing the 10 to 16% samples mass loss connected with the decomposition of organic residue, and elemental analysis, which allowed for the calculation of the PAMAM loading ranging between 0.054 and 0.113 mmol $g^{-1}$. The grafting efficiencies of the dendrimer onto silica particles containing glycidoxy linker were lower than those calculated for the materials functionalized through isocyanate group, which is connected with the higher affinity and sensitivity of −N=C=O groups towards an attack of nucleophiles. The assumed potential of PAMAM-grafted materials of interacting with acidic components was initially proved by the performed ESI-MS analyses of the mixtures of exemplary TREN dendrimer with three chosen acidic biomolecules: salicylic acid (NSAID), nicotinic acid (vitamin $B_3$), and folic acid (vitamin $B_9$), which are presented in Figure S3 (Supplementary Information; article **A3**). Additionally, folic acid is a close analog of methotrexate, a broadly used anticancer drug, therefore a description of its affinity towards potential drug carriers relates to the sorptive behavior of a real chemo-therapeutic. The spectra of the mixtures of TREN dendrimer with monocarboxylic salicylic or nicotinic acid showed only mono-positive or mono-negative signals in the corresponding spectra, which are related to the transfer of a single proton from the acidic molecule to the dendrimer. On the other hand, the spectrum of the mixture of TREN dendrimer with dicarboxylic folic acid showed predominantly di-positive and di-negative signals in their spectra, proving the transfer of two protons from folic acid to the dendrimer. Such an observation indicates that PAMAM dendrimers are able to create an ionic pair with various acidic drugs, forming stable PAMAM-drug complexes, which might be successfully applied to other therapeutics containing acidic domains. Furthermore, PAMAM dendrimers immobilized on the surface of supports retain their chemical properties, and thus, the obtained silica-based hybrid materials were subsequently studied for adsorption efficiency

towards the chosen three acidic bioactive compounds. The isothermal parameters presented in Table 1 in **A3** show that the adsorption of the drug follows the Freundlich isothermal model, proved by the comparison of correlation coefficients ($R^2$ and $\chi^2$), which are consistent with the ability of the drugs to form intermolecular interactions, especially through π-π stacking, enhancing the formation of an adsorbate polylayer on the surface of the materials. Nonetheless, the moderate linear fit to the Langmuir model led to the calculation of adsorption capacities $q_m$ values, which allowed for the presentation of the efficiency of the drugs' adsorption (from the highest to the lowest) in the following series: folic acid > salicylic acid > nicotinic acid. The ability for the binding relies on their specific structural features and might be enhanced or decreased by the interactions with basic domains of the dendrimers. In general, the highest affinity towards the PAMAM-grafted materials was ascribed for folic acid, which is a consequence of the presence of two carboxylic groups supporting the interactions with the supramolecular receptors on the surface of the materials, and strongly expanded backbone affording intermolecular interactions. The values of maximal adsorption capacities $q_m$ of folic acid calculated for all the hybrid materials were high and varied between 202.43 and 274.72 mg $g^{-1}$. Although, salicylic and nicotinic acid are relatively small molecules, which might be trapped within dendritic cavities, the presence of only a single −COOH group results in a lower affinity towards the supramolecular receptors, which is proved by significantly lower adsorption capacities. The reason for the higher adsorption performance of salicylic acid than of nicotinic acid can be found in the formation of hydrogen bonds between hydroxyl group present in the molecule and PAMAM residue. When it comes to a description of the influence of the surface dendritic structure on the adsorptive properties, the most determining factor is the grafting efficiency. The highest values of maximal adsorption capacities were calculated for the material containing EDA surface dendrimer, leading to the values of 274.71, 157.48, and 20.11 mg $g^{-1}$ for folic, salicylic, and nicotinic acid, respectively. The presence of TREN dendrimer increased the adsorptive properties of the material, while the most branched TETA dendrimer and the longest TRI-OXA dendrimer decreased the adsorption of the drugs. The studied hybrid materials were also subjected to the thermodynamic studies of the drugs' adsorption, conducted at 301, 313, and 328 K. On the basis of

sorption performance at equilibria, thermodynamic parameters were calculated, which are presented in Table 2 in **A3**. Since the investigated interactions between the PAMAM-functionalized materials and the acidic biomolecules are based on the electrostatic interactions, the values of standard enthalpy $\Delta H$ are slightly positive, especially for the experiments involving folic acid with two exhalable protons. Moreover, the calculated Gibbs' free energy $\Delta G$ values, which are in good relation to the adsorption efficiency, decrease with the temperature increase, indicating that the temperature is an adsorption-enhancing factor. The last step of the described studies, referring to the article title, aimed at the monitoring of the release of the drugs from material-drug complexes. *In vitro* studies involved incubation of the materials with adsorbed drug molecules in three different aqueous media: HCl/KCl buffer of pH 2.0, AcOH/AcONa buffer of pH 5.4, and phosphate-buffered saline (PBS) of pH 7.4. The choice of such different releasing solutions was driven by their pH values referring to the conditions of gastric juice, skin, and plasma/saliva, respectively. The release profiles (cumulative drug release *vs.* time) presented in Figure 6 in **A3** highlight several factors influencing the transport of the drugs, for example, the release conditions or the structure of the drug. The structural features of the drugs, such as a number of carboxylic groups and the presence of hydrogen bond donors or acceptors affect the non-covalent stabilization of PAMAM-drug complex. Furthermore, the possibility of intermolecular interactions of the drug molecules through e.g. π−π stacking leads to the formation of a polylayer of the adsorbate, which facilitates the release of the "outer" layer of the drug to a releasing solution. Moreover, since the formed material-drug complexes are mostly stabilized by electrostatic interactions, pH of the releasing medium is of the greatest importance. As it is visualized in the release profiles, the most acidic environment (pH 2.0) leads to the highest release percentages, which is related to the extensive disruption of electrostatic interactions between the surface of the cationized PAMAM dendrimer and anionized drug residue. In these conditions, the overall percentages of the drugs released varied between 37.22 and 99.83%. On the contrary, release experiments handled in PBS buffer of pH 7.4 were much less efficient, reaching the release percentages between 5.45 and 49.28%. In this case, a key role might be ascribed to the desorption of molecules from an external surface of the polylayer of the drug

bound to the materials. Moreover, when comparing the release profiles of particular drugs, it may be concluded that folic acid has the lowest desorption affinity, as a result of the H-bonds formation. Accordingly, values of folic acid maximal release at pH 2.0 were the lowest and varied between 35.42 to 54.90%. On the other hand, salicylic and nicotinic acids were much weaker stabilized than folic acid, as their release from materials containing EDA and TREN dendrimers ranged even between 86.88 and 99.83% in pH 2.0. Moreover, the release of the drugs from the material-drug complexes may be affected by the supramolecular inclusion of "small" molecules of the drugs within the dendritic cavities. Such entrapment was described for the materials grafted with TETA and TRI-OXA dendrimers, containing structurally wide and easily accessible internal cavities, resulting in the lower drug release percentages of nicotinic and salicylic acid. Thus, the presented materials were successfully applied for the binding of the chosen model bioactive molecules, and their further release in different aqueous pseudophysiological media, indicating their potential application as drug-transporting systems.

## The dual-polymeric material based on the synthetic polymer modified with the PAMAM dendrimer

The confirmed enhanced binding properties of silica-based materials functionalized with PAMAM receptors towards toxic metal ions and acidic bioactive compounds have triggered the implementation of the dendrimer to a synthetic alternative copolymer of methyl vinyl ether and maleic anhydride (poly(methyl vinyl ether-*alt*-maleic anhydride); PMVEAMA). The incorporation of a dendrimer to the polymeric support led to the creation of a dual-polymeric material, which was intended to exhibit versatile sorptive properties. Therefore, the adsorption effectiveness was studied using acidic bioactive molecules (salicylic, nicotinic, and folic acid), toxic anionic dyes (Congo Red and Sunset Yellow FCF), and riboflavin, which can be classified as both biomolecule and organic dye. The results of the performed studies are presented in article **A4**, entitled "*Dual-Polymeric Resin Based on Poly(methyl vinyl ether-alt-maleic anhydride) and PAMAM Dendrimer as a Versatile Supramolecular Adsorbent*". The study began with the synthesis of a new PAMAM dendrimer containing diethylenetriamine as both core and terminal amine component (hereinafter labeled as DETA) and was followed by the synthesis of

the demanded dual-polymeric material, according to the scheme presented in Figure 5.

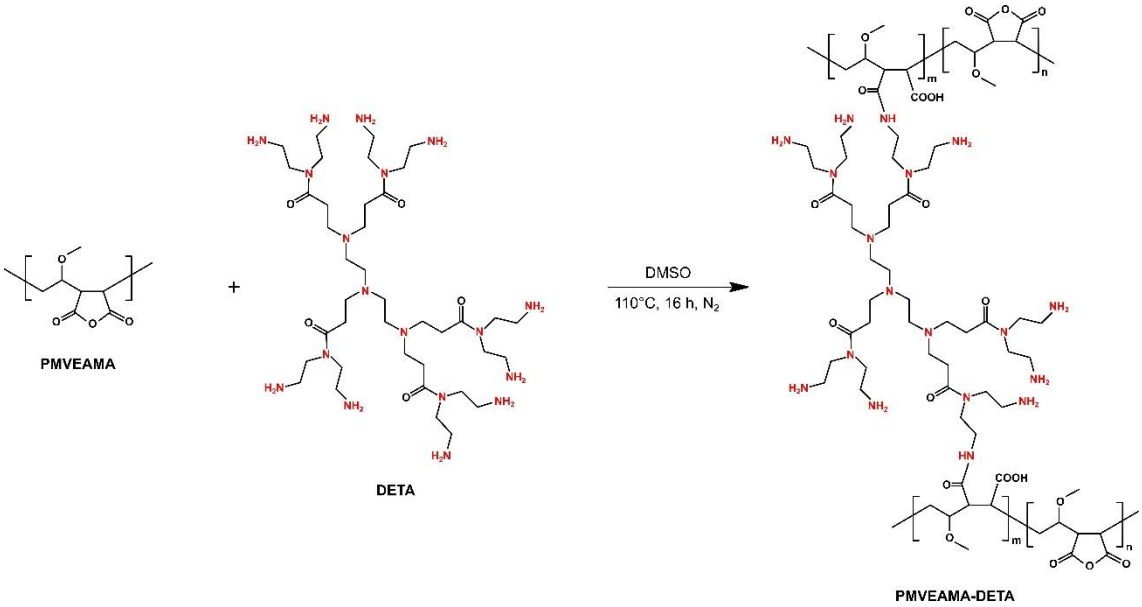


**Figure 5.** The synthetic protocol for obtaining the dual-polymeric material; *m* and *n* relate to the amount of modified and unmodified anhydride domains, respectively; red – amine groups.

Although a maleic anhydride ring opens under the nucleophilic attack of a single free amine group, the presence of multiple terminal $-NH_2$ groups in DETA dendrimer influenced the formation of cross-linking product, i.e. interconnected subsequent polymeric chains with polyamine agent. Such a phenomenon has been already implemented in several studies aiming at the creation of porous materials for analytical and biomedical applications.[118,119] However, even if the cross-linking process takes place, the final material is not supposed to lose its binding ability, due to the presence of multiple unaltered free amine groups.

The obtained material precipitated with $Et_2O$ was characterized with several techniques, involving FT-IR spectroscopy, SEM imagining, TG measurements, which proved the formation of a cross-linking product by the appearance of a single oxidation step in the TG curve, and elemental analysis, allowing the calculation of the grafting level of 0.702 mmol $g^{-1}$. The grafting value was consistent with the value calculated on the basis of an acidimetric titration of the material, which was 0.687 mmol $g^{-1}$. A significantly enhanced functionalization level of PMVEAMA with the dendrimer, in a relation to the grafting of silica particles with PAMAM

dendrimers described in articles **A1**-**A3**, is attributed to unlimited access to reactive anhydride domains across the whole length of polymeric chains. The sorptive effectiveness of the dual-polymeric material was investigated with various sorption experiments, which were started with adsorption isothermal studies. The adsorption of all the analytes followed the Freundlich isothermal model since the nature of the chosen adsorbates allows for their intermolecular interactions through π-π stacking or hydrogen bonds. The calculated maximal adsorption capacity values reached 310.6 and 367.7 mg $g^{-1}$ for Sunset Yellow FCF and Congo Red dyes, and 304.9, 134.2, and 91.6 mg $g^{-1}$ for folic, salicylic, and nicotinic acid, respectively. The lowest sorption affinity was described for riboflavin ($q_m$ = 26.5 mg $g^{-1}$), which was driven by the lack of carboxylic domains in its structure, responsible for the strong binding to the host molecule. Additionally, the influence of the temperature on the equilibrium state of the analytes' adsorption on PMVEAMA-DETA has been determined. The thermodynamic parameters, which are collected in Table 2 in **A4** show that the adsorption of acidic drugs is an exothermic process, while the adsorption of anionic dyes or neutral riboflavin exhibits endothermal character. Since the described adsorption processes are spontaneous ($\Delta G < 0$), the thermal effects of the process are related to the driving forces of the binding processes. In the case of the adsorption of the anionic dyes, the binding process is based on non-covalent ion-dipole interactions or hydrogen bonding, and therefore the process is controlled by solvation effects. It results in the high value of the entropy of the process – indicating that it is driven by increased randomness at the solid-liquid interface – and thus the value of the enthalpy is elevated, which contributes to the endothermal effect of the process. On the other hand, the binding of acidic dyes on the surface of the PAMAM-grafted material is afforded by a proton exchange between the analyte and the material, in the formation of a new bond. Such processes are not controlled by solvation effects (low $\Delta S$ values), and thus the spontaneity of the process is afforded by very low or negative $\Delta H$. In the described adsorption of folic, salicylic, and nicotinic acid, $\Delta H$ values range between -5.5 and -3.3 kJ $mol^{-1}$, indicating the slightly exothermic character of the process. Nevertheless, the adsorption of all the analytes was described as positively influenced by the temperature increase. Up to this point, the performed isothermal and thermodynamic studies involved the application of

all the chosen analytes, in order to fully characterize the material affinity towards the biomolecules and the organic dyes. However, the studies intended to exhibit PMVEAMA-DETA applicability as either a reusable scavenger of organic dyes or a platform for the transport of drugs, and thus the further studies were divided into two corresponding sections.

Firstly, the kinetic and reusability experiments dedicated to Congo Red, Sunset Yellow FCF, and riboflavin were performed. The most informative parameter describing the intensity and rate of the adsorption of the dyes is the half-adsorption time $t_{1/2}$, which values are presented in Table S4 (Supplementary Information; article **A4**). Extremely low values calculated for Congo Red and Sunset Yellow FCF of 0.02 and 0.19 h, respectively, proved the high affinity of the dyes towards PAMAM pendant residue of the material, which is related to two carboxylate domains in their structure stabilizing the attractive interactions material-dye. A lower half-adsorption time of 1.83 h was described for riboflavin, which is connected with the stabilization of the material-riboflavin complex only through hydrogen bonds. Moreover, the synthesized dual-polymeric material has been also subjected to reusability tests involving 5 cycles of adsorption/desorption processes towards the dyes, using a solution of HCl – a strong acid – as a desorbing agent. After the successful first adsorption step, in which the binding percentages ranged between 65.23 and 85.72%, the material treated with the acidic desorbing medium exhibited increased adsorption efficiency towards the dyes by approximately 10%. Such phenomenon is explainable by two facts: (i) the protonation of free terminal $-NH_2$ groups of DETA dendrimer, which results in intensified attractive interactions with anionic dyes; and (ii) the acidic hydrolysis of maleic anhydride rings, which had not been modified during the functionalization process, resulting in the appearance of additional hydrogen bond donors and acceptors (−COOH groups). The further adsorption/desorption cycles led to a slight decrease of the adsorption capability of the material, by 2.64, 4.91, and 9.49% for Congo Red, Sunset Yellow FCF, and riboflavin, respectively. The presented results undoubtedly prove the efficiency and reusability of PMVEAMA-DETA for the scavenging of toxic organic dyes.

On the other hand, the effectiveness of the materials as a potential drug-transporting system was investigated with the use of four model bioactive acids

(salicylic, nicotinic, and folic acid) and riboflavin, which play a role of vitamin $B_2$ in human organisms. The drug-loaded samples of the dual-polymeric material were incubated in three different aqueous media, which intended to mimic the conditions of physiological fluids, i.e. buffer solutions of pH 2.4, 5.4, and 7.4 (Figure 7, article **A4**). The highest drugs release percentages were established for the most acidic release medium of pH 2.4, ranging between 43.19 and 94.90%, which is consistent with the analogous drug release studies presented in the previous article **A3**. The release performance can be presented in the following series: salicylic acid > nicotinic acid > riboflavin > folic acid, which is directly related to the intensity and the type of interactions stabilizing the complexes of the material with the biocompounds. Nevertheless, the cumulative drug release described for less acidic conditions also led to satisfactory results, which jointly with the cytocompatibility of the polymer used, reported in the literature, indicate the usefulness of the dual-polymeric material as a drug transporting platform.

## The hybrid materials functionalized with Fe-chelating domain – deferoxamine

The above-presented PAMAM dendrimers exhibit universal chelating properties towards metal cations, which were connected with the presence of unspecific amide and amine groups. However, several organic receptors present binding affinity directed towards a group of ions of a particular valence, which are usually determined by a number of donor groups of ligands. Among such organic compounds, deferoxamine (DFO) can be described as a specific chelator of Fe(III) ions, which is related to its classification as a trihydroxamic acid (containing 3 –C(O)–N–OH structural motifs). Therefore, immobilization of DFO on a surface of either inorganic support or polymeric chains might result in high-performance adsorptive materials dedicated to ferric ions. Such an attempt is presented in article **A5**, entitled "*Deferoxamine-Modified Hybrid Materials for Direct Chelation of Fe(III) Ions from Aqueous Solutions and Indication of the Competitiveness of In Vitro Complexing toward a Biological System*", which presents an investigation of the adsorptive potential of DFO-functionalized materials based on $SiO_2$, magnetic $Fe_3O_4$ nanoparticles, and PMVEAMA. The studies involved the preparation of five materials, which included DFO-grafting on commercially available silica through

isocyanate or maleimide linker, on pre-synthesized magnetite nanoparticles functionalized with isocyanate- or maleimide-silyl linker, and on poly(methyl vinyl ether-*alt*-maleic anhydride) through the anhydride domain. Accordingly, the materials are hereinafter labeled as $SiO_2$-NCO-DFO, $SiO_2$-maleimide-DFO, $Fe_3O_4$-NCO-DFO, $Fe_3O_4$-maleimide-DFO, and PMVEAMA-DFO, respectively, which structures are presented in Figure 6, while the protocols of their synthesis are illustrated in Figure S1 (Supplementary Information, article **A5**). It should be also indicated that silica particles and the polymer were directly functionalized with the receptor, while $Fe_3O_4$ nanoparticles were encapsulated with a silica layer following the Stöber method[120] prior to further functionalization with isocyanate- or maleimide-silyl derivative and deferoxamine, in order to enhance the stability of the materials, protect magnetite core, and avoid leaching of the iron ions.[121] Moreover, the introduced silica layer allows for easy functionalization of the obtained $Fe_3O_4/SiO_2$ system.

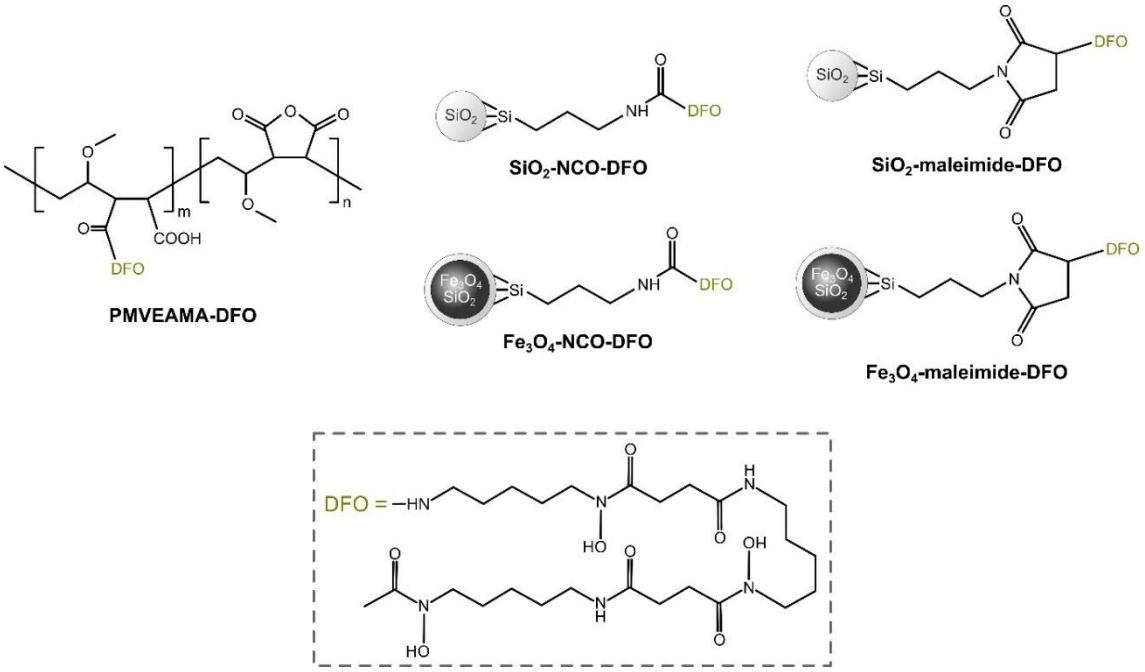


**Figure 6.** The structures of the synthesized deferoxamine-functionalized adsorbents; *m* and *n* in material PMVEAMA-DFO correspond to modified and unaltered anhydride domains, respectively.

The obtained hybrid materials were characterized with several techniques, including FT-IR spectroscopy, thermogravimetric measurements, elemental analysis, SEM imagining, and XRD analysis dedicated only to magnetite-cored

materials. The Fe-binding potential of the presented materials was investigated with four basic adsorption studies. An optimal binding pH value was specified from the pH range of 1 to 5, using buffer solutions and distilled water as solvents. The highest adsorption performance was described for the solution of pH 2.45, which corresponds to the solution of pure Fe(III) ions in distilled water, and thus further adsorptive experiments were handled in the given conditions. The subsequently performed isothermal studies proved that the adsorption of ferric ions on the DFO-functionalized materials follows the Langmuir isotherm model. The fitting of experimental data to the isothermal model allowed for the calculation of several parameters describing the adsorbents' efficiency towards Fe(III) ions. An especially informative $q_m$ parameter varied between 87.41 and 140.65 mg $g^{-1}$, which shows the high effectiveness of the synthesized Fe-scavengers. Interestingly, both silica- and magnetite-based materials functionalized with DFO domain through maleimide linker exhibited higher $q_m$ values than these materials grafted through isocyanate linker. This phenomenon might be related to the possibility of ferric ions entrapment within maleimide cyclic domain, enhancing the final adsorptive properties of the materials. The chosen Fe-complexed materials containing silica particles and the polymer used as the supports were also subjected to the elemental mapping of iron in the samples using energy-dispersive X-ray scanning electron microscopy (EDX-SEM) (Fig 3 F-H, article **A5**), visualizing the amount and the intensity of Fe(III) adsorption, which is consistent with the ascribed materials adsorptive potential. In order to assess the rate of Fe(III) ions adsorption on the adsorbents, kinetic studies were employed. Accordingly, values of the half-adsorption time $t_{1/2}$ were calculated, which varied between 4.98 and 10.30 h, reaching the lowest values for PMVEAMA- and magnetite-based materials, which indicate their high effectiveness. Such a conclusion is also evidenced by the highest values of their initial adsorption rates $k_i$. The adsorption studies included experiments at different temperatures in order to describe thermodynamic parameters, which are presented in Table 4 in article **A5**. The spontaneity of the described process ($\Delta G < 0$) is mostly related to elevated values of the Fe-binding process entropy, which varied between 54.23 and 107.74 J $mol^{-1}$ $K^{-1}$, indicating that the adsorption of Fe(III) ions on the synthesized materials is driven by increased randomness at the solution-adsorbent interface, as a result of solvation effects.

The last part of the performed basic adsorption experiments involved incubation of $SiO_2$-NCO-DFO and $SiO_2$-maleimide-DFO materials in three different mixtures of Fe/Al, Fe/Cr, and Fe/Al/Cr systems, in order to assess the selectivity of the materials towards Fe(III) in the presence of other trivalent metal cations as coexisting ions. The selectivity was investigated by XRF studies of the material-ions complexes, which excluded the use of $Fe_3O_4$-based materials since this technique would present the Fe signal corresponding to a sum of ferric ions adsorbed on the material, and of the material itself. Nevertheless, the silica-based materials showed high selectivity, reaching 91.4-97.4 % adsorption of Fe(III) ions. The calculated low percentages of Cr(III) or Al(III) ions content in the material-ions complexes might be a result of their chelation by DFO domains remained free after their saturation by Fe(III) ions. The proven effectiveness of the materials has prompted the use of exemplary $Fe_3O_4$-NCO-DFO in the competitive binding of Fe(III) ions complexed protoporphyrin IX (PPIX), which intended to mimic the biological complex of hemin – an analogue of heme B, the constituent of oxygen-transporting hemoglobin. The study involved a preparation of PPIX-Fe(III) complex and observation of changes in its ESI-MS spectra after incubation with pure deferoxamine or $Fe_3O_4$-based functional material (Figure 8, article **A5**). The spectrum of a mixture of PPIX-Fe(III) and pure DFO already showed a full transfer of Fe(III) ions to deferoxamine domain, and thus high competitiveness, which is proved by the appearance of signals at $m/z$ 563.5 and 585.5, corresponding to free PPIX and its sodium adduct, and the signals at $m/z$ 561.5 and 614.4 related to free excessive DFO domain and its complex with Fe(III) ions, respectively. The suspected full transfer of ferric ions from PPIX complex to the material, after their 1-minute incubation, is evidenced by the presence of the most intense signal at $m/z$ 614.4 referring to [DFO-2H+Fe], and no signals corresponding to PPIX-Fe complex. It should be pointed out that this ESI-MS signal in the spectrum of the post-experiment solute is caused by the nanosized character of the material and the short time of its separation, which triggered the access of the material into the ionization source, and thus the analysis of pendant DFO-receptor groups on the surface of the material. The same trend was observed for similar experiments held in different buffer solutions in pH range of 3 to 8, which proves the efficiency of the material towards *in vitro* competitive binding in various conditions.

## References


(116) M.A. Kaczorowska, H.J. Cooper, Electron Capture Dissociation, Electron Detachment Dissociation, and Collision-Induced Dissociation of Polyamidoamine (PAMAM) Dendrimer Ions with Amino, Amidoethanol, and Sodium Carboxylate Surface Groups, J. Am. Soc. Mass. Spectr. 19 (2008), 1312-1319.

(117) J. Raya, S. Jana, S.K. Bhanja, T. Tripathy, Efficient Removal of Co(II), Ni(II), and Zn(II) Metal Ions from Binary and Ternary Solutions Using a pH Responsive Bifunctional Graft Copolymer, Colloid Polym. Sci. 296 (2018), 1275-1291.

(118) C. Zhang, P.C. Zhu, L. Tan, J.M. Liu, B. Tan, X.L. Yang, H.B. Xu, Triptycene-Based Hyper-Cross-Linked Polymer Sponge for Gas Storage and Water Treatment, Macromolecules 48 (2015), 8509-8514.

(119) K. Imato, A. Takahara, H. Otsuka, Self-Healing of a Cross-Linked Polymer with Dynamic Covalent Linkages at Mild Temperature and Evaluation at Macroscopic and Molecular Levels, Macromolecules 48 (2015), 5632-5639.

(120) Z. Lu, J. Dai, X. Song, G. Wang, W. Yang, Facile synthesis of $Fe_3O_4/SiO_2$ composite nanoparticles from primary silica particles, Colloids Surf. A Physicochem. Eng. Aspects 317 (2008), 450–456.

(121) I. Al Kawni, R. Garcia, S. Youssef, M. Abboud, J. Podlecki, R. Habch, Stabilization and encapsulation of magnetite nanoparticles, Mater. Res. Express 3 (2016) 125024.

# 4

# Summary of the research

The following thesis entitles "*Synthesis and application of functional hybrid and polymeric materials in chemical analysis*" aimed at the use of various poly(amidoamine) dendrimers and deferoxamine as the grafting agents towards the chosen inorganic and polymeric supports, which were silica microparticles, magnetite nanoparticles, and poly(methyl vinyl ether-*alt*-maleic anhydride). The binding character of the organic receptors used has determined the applicability of the prepared materials as the scavengers dedicated to toxic compounds and as the platforms for drug delivery.

Since the literature shows an implementation of various hybrid materials functionalized predominantly with EDA-containing dendrimers or PAMAM dendrons obtained using the 'grafting to' synthetic approach, the following thesis focused on the immobilization of fully-dendritic PAMAM domains containing structurally different terminal amine components: ethylenediamine, tris(2-aminoethyl)amine, diethylenetriamine, triethylenetetramine, or 4,7,10-trioxa-1,13-tridecanediamine. The characterized PAMAM-grafted hybrid and polymeric materials were investigated for their adsorptive properties towards three groups of analytes: toxic metal ions (Cu(II), Ni(II), and Co(II) cations), organic dyes (Congo Red, Sunset Yellow FCF), and bioactive molecules (salicylic, nicotinic, and folic acid, and riboflavin). The main scientific problem aimed at the interpretation of an influence of the grafting agent used on the adsorptive potential of the materials, which was especially driven by the different structures and branching character of the immobilized PAMAM dendrimers.

The investigation of the adsorptive potential of the silica-based materials grafted with PAMAM dendrimers towards Cu(II) ions was presented in article **A1**. The studies involved performing comprehensive adsorption studies, in order to fully characterize the binding features of the materials. Furthermore, article **A2** focused on the investigation of the binding efficiency of the silica-based materials towards other toxic metal cations, which were Ni(II) and Co(II) ions, involving the direct

adsorption of the ions from single-component solutions and the selectivity studies using the two-component system. All of the conducted experiments led to the satisfactory results of the metal cations scavenging, reaching maximal adsorption capacity even of 116.6 mg $g^{-1}$. The amine-rich character of the implemented PAMAM dendrimers has also led to the application of the silica-PAMAM hybrid materials as drug-transporting platforms, which was presented in article **A3**. The studies aimed at the description of the adsorptive potential of the materials towards three model acidic bioactive molecules: folic, salicylic, and nicotinic acid. The obtained material-drug complexes were also subjected to *in vitro* release studies performed in different pseudophysiological aqueous media of different pH values. All the studies confirmed the influence of the structure of the terminal amine component of the dendrimer, and thus the dendrimer itself, on the sorptive properties of the hybrid materials. Therefore, the application potential of designed hybrid materials towards a particular analyte can be tuned by the structure of dendrimers, leading to functional materials of enhanced binding properties, higher selectiveness, or enhanced pro-longed drug delivery potential.

The sorptive performance of materials containing a pendant PAMAM residue was also investigated for the dual-polymeric material consisting of the polymeric support of PMVEAMA and DETA-containing PAMAM dendrimer (PMVEAMA-DETA), which is presented in article **A4**. The sorbent was studied for the adsorption and reusability potential towards toxic organic dyes, and drug delivery potential. The studies resulted in highly satisfactory binding efficiency towards Congo Red, Sunset Yellow FCF, and riboflacin. Also, the material was described as reusable, which was evidenced by only a slight decrease in the binding performance even after 5 cycles of adsorption/desorption of the dyes. Since the material contained the amine-rich PAMAM domain, it was tested for the delivery of model bioactive molecules: folic, salicylic, and nicotinic acid, and riboflavin. The release performance in biomimicking media was influenced by the structures of the drugs, which indicates a possibility of tuning of PAMAM-drug interactions extent by a change of the structure of the dendrimer. Nevertheless, the high values of cumulative drugs release, especially in acidic conditions, and the documented cytocompatibility and mucoadhesiveness of the polymeric support may lead to the implementation of drug delivery platforms for *in vivo* application.

The second kind of the chosen organic receptors was a trihydroxamic acid – deferoxamine – exhibiting chelating properties towards trivalent metal cations, especially Fe(III) ions. The organic domain was grafted on three different types of supports: silica particles, magnetic $Fe_3O_4$ nanoparticles, and the polymeric chains of PMVEAMA. The resulted hybrid and polymeric materials were accordingly tested for their ability of Fe(III) ions scavenging, which are described in article **A5**. The different values of adsorption capacity for all the synthesized hybrids were directly influenced by the types of the linkers used for the anchoring of deferoxamine, which determines the DFO-grafting level. Nevertheless, all of the materials exhibited satisfactory binding efficiency towards Fe(III) ions, which varied between 87.41 and 140.65 mg $g^{-1}$. Moreover, the performed experiments showed the proper selectivity of the exemplary silica-based materials towards ferric ions in the presence of other trivalent coexisting ions. However, the choice of the support might influence not only the grafting level, but also other additional properties of the final material, which may facilitate their use in the analysis. For instance, the obtained magnetite-cored systems allowed for their easy separation using an external magnetic field, which allowed for the simplified examination of their competitive Fe-complexing ability using a biological complex of hemin. The exemplary $Fe_3O_4$-containing material exhibited fast and full *in vitro* transfer of ferric ions from the biological complex to the material. Such a result might influence in *in vivo* application of DFO-grafted materials containing nanosized, biocompatible, and magnetically susceptible $Fe_3O_4$ core, in the sudden burst release of Fe(III) ions or in their chronic overload in human organisms.

To summarize, all of the studies showed an assumed influence of the supramolecular receptor on the materials' binding potential, which therefore might be a key point for further exploration of applications of this kind of materials in different branches of analytical chemistry, which might be:

- Removal/scavenging of toxic entities;
- Pre-concentrating of unanalyzable amounts of chemicals;
- Transport of drugs, therapeutics, and other bioactive molecules;
- Directed or selective solid-phase extraction systems.

# Abstract

The ongoing globalization prompts the implementation of new materials, which either inhibit negative results of human activity, increase positive effects towards human health and life quality, or facilitate sustainable development. For the last few decades, significant attention has been paid to (i) hybrid materials, which are generally defined as two-component materials consisting of inorganic support, which is grafted with a functional organic receptor (inorganic-organic hybrids); and (ii) functional polymeric materials consisting of polymer chains functionalized with an organic receptor. Such materials exhibit combined physicochemical properties of both components, which further results in the development of new functionalities related to the domains used.

Among numerous, almost uncountable, organic domains treated as potential grafting agents, poly(amidoamine) (PAMAM) dendrimers and a trihydroxamic acid – deferoxamine (DFO) exhibit interesting chemical properties from the analytical point of view. Therefore, the following doctoral dissertation focuses on their implementation as grafting agents dedicated to three types of supports, in order to obtain functional hybrid and polymeric materials for analytical applications. PAMAM dendrimers are highly interesting structures, which is related to their multifunctionality as a result of (i) branched character inducing the presence of internal cavities; and (ii) the presence of multiple functional amide and amine groups, affording various interaction pathways with analytes, which makes them a group of versatile supramolecular receptors. The given structural features result in the possible entrapment of small molecules within the dendritic matrix, and non-covalent interactions with analytes through electrostatic, ion-dipole, and dipole-dipole interactions, hydrogen bonding, or chelation. Therefore, PAMAM-grafted hybrid materials may find applications in e.g. analytical chemistry, environmental protection, biomedicine, or catalysis. On the other hand, clinically used deferoxamine plays a role of siderophore – a scavenger of Fe(III) ions – which is related to the presence of three hydroxamic acid domains in its structure, determining the high stability of deferoxamine-Fe(III) complex ($\log\beta_{\text{DFO-Fe(III)}} = 30.6$). Therefore, functional materials containing pendant deferoxamine residue on their surface may be successfully used not only as tools for enhanced adsorption,

quantification, or sensing of ferric ions, but also as platforms for targeted complexation of Fe(III) ions excess in organisms.

The presented characteristic chemical features of the two kinds of organic receptors led to their immobilization on the chosen inorganic supports, which were silica and magnetite nanoparticles, and on the polymeric chain of poly(methyl vinyl ether-*alt*-maleic anhydride) (PMVEAMA), which was one of the goals of the following doctoral dissertation. Nevertheless, the main scientific problems, which were intended to be answered during the performed, and herein presented studies, are connected with the description of an influence of the grafting agent structure and the support used, on the final sorptive properties of the hybrid materials. The studies are presented in a series of five scientific articles **A1**-**A5**, which are included in the following dissertation.

The performed studies focused on three segments, while each of them involved a sufficient materials' characterization with FT-IR spectroscopy, TG analysis, SEM imagining, or elemental analysis – when required, and subsequent investigation of their adsorptive potential towards the specifically chosen analytes.

The first scientific goal aimed at the synthesis of four PAMAM dendrimers, which differed in the structure of an amine terminal component used, i.e. contained ethylenediamine, tris(2-aminoethyl)amine, triethylenetetramine, or 4,7,10-trioxa-1,13-tridecanediamine (hereinafter labeled as EDA, TREN, TETA, and TRI-OXA, respectively). The dendrimers were characterized with ESI-MS, $^{1}$H-NMR, and $^{13}$C-NMR analyses prior to their immobilization on the surface of amorphous silica containing pendant isocyanate or glycidoxy functional linkers. The obtained hybrid materials $SiO_2$-EDA, $SiO_2$-TREN, $SiO_2$-TETA, and $SiO_2$-TRI-OXA were studied for adsorptive properties towards Cu(II), Ni(II), and Co(II) ions as pollutants, and folic, salicylic, and nicotinic acids as model bioactive acidic compounds. The experiments showed that the structure of the terminal amine component of the dendrimers, and thus the structure of the dendrimers themselves, has an impact on the binding potential of the hybrid materials, and also on the drug-transporting ability evidenced by *in vitro* release studies.

The next scientific problem concerned an investigation of the sorptive potential of the dual-polymeric material consisting of PMVEAMA as the support, and the synthesized PAMAM type dendrimer containing diethylenetriamine as the amine terminal component (hereinafter labeled as DETA) as the grafting agent. Even though the polynucleophilic character of the dendrimer has triggered the formation of cross-linking product, the material showed high adsorptive properties towards the chosen organic dyes (Congo red, Sunset Yellow FCF, riboflavin) and drugs (folic, salicylic, and nicotinic acid, and riboflavin). The obtained polymeric adsorbent is applicable as a reusable binding material since, after several cycles of the adsorption/desorption of the dyes, only a slight decrease in the adsorption efficiency was observed. Moreover, PMVEAMA-DETA was also proved for an *in vitro* drug delivery potential, which combined with the reported cytocompatibility of the support may lead to efficient *in vivo* applicability of the platform for the transport of therapeutics. The last scientific problem focused on the application of DFO-functionalized materials based on silica particles, magnetite nanoparticles, and PMVEAMA for effective adsorption of Fe(III) ions. Each of the materials exhibited satisfactory efficiency in the remediation of ferric ions from their aqueous solutions. The studies showed that the support and the type of the linker used for immobilization of the receptor have an impact on the sorptive performance of the materials. Furthermore, exemplary materials were also proved for: selectiveness towards Fe(III) in the presence of co-existing trivalent Cr(III) and Al(III) ions; fast and full *in vitro* transfer of Fe(III) ions from the biological complex of hemin to the magnetic DFO-modified material; and retained stability and magnetic susceptibility in human serum.

All the results may lead to the creation of new devices finding versatile application in analytical chemistry (sensing materials; pre-concentration tools), biomedicine (targeted platforms for delivery of drugs, therapeutics, antibodies, nucleic acids, etc.; materials for improved magnetic imagining or radiolabeling; *in vivo* scavengers of excessive non-transferrin bound ferric ions), or environmental protection (adsorbents of toxic entities).

# Streszczenie

Stale postępująca globalizacja jest jedną z głównych przyczyn projektowania oraz implementacji nowych materiałów, których nadrzędnym zadaniem jest hamowanie negatywnych skutków ludzkiej działalności, poprawianie jakości życia i zdrowia lub wspieranie zrównoważonego rozwoju. W ciągu ostatnich dekad znaczącą uwagę skupiły na sobie (i) materiały hybrydowe, które definiowane są jako materiały dwukomponentowe składające się z nieorganicznego nośnika zawierającego na swojej powierzchni organiczny receptor molekularny (hybrydy nieorganiczno-organiczne); oraz (ii) funkcjonalne materiały polimerowe składające się łańcucha polimerowego i zakotwiczonego na nim organicznego receptora. Materiały tego rodzaju charakteryzują się sumarycznymi właściwościami fizykochemicznymi obu komponentów, co skutkuje nadaniem materiałowi nowych cech funkcjonalnych.

Wśród prawie niepoliczalnej grupie związków organicznych, które mogą zostać wykorzystane jako potencjalne domeny funkcjonalizujące, wyróżnić można dendrymery poli(amidoaminowe) (PAMAM) oraz deferoksaminę należącą do grupy kwasów trihydroksamowych, które wykazują interesujące, z punktu widzenia chemii analitycznej, właściwości chemiczne. Tym samym, tematyka przedstawionej rozprawy doktorskiej skupia się na wykorzystaniu wskazanych receptorów organicznych jako czynników funkcjonalizujących wobec trzech rodzajów materiałów nośnikowych, prowadząc do otrzymania nowych funkcjonalnych materiałów hybrydowych i polimerowych znajdujących zastosowanie w szeroko pojętej analityce chemicznej. Zastosowanie dendrymerów PAMAM jest ściśle związane z ich polifunkcjonalnością, tj. (i) rozgałęzioną strukturą, która determinuje pojawianie się wewnętrznych wnęk pomiędzy ramionami dendrymerów; oraz (ii) obecnością wielu grup amidowych oraz aminowych, zapewniających różnorodne ścieżki oddziaływania z analitami, co łącznie zapewnia ich uniwersalność jako receptory supramolekularne. Wymienione cechy strukturalne dendrymerów PAMAM powodują, że mogą one oddziaływać z wybranymi analitami poprzez fizyczne uwięzienie małych cząsteczek w matrycy dendrymeru oraz poprzez oddziaływania niekowalencyjne, takie jak oddziaływania elektrostatyczne, oddziaływania typu jon-dipol i dipol-dipol, wiązania wodorowe, a także poprzez chelatowanie. Dzięki temu materiały zawierające na swojej powierzchni domeny

PAMAM mogą znaleźć zastosowanie w m.in. chemii analitycznej, ochronie środowiska, biomedycynie lub katalizie. Z kolei, dotychczas stosowana prawie wyłącznie klinicznie deferoksamina (DFO) skategoryzowana może być jako siderofor – cząsteczka wiążąca jony Fe(III) – co jest związane z obecnością trzech grup kwasu hydroksamowego w jej strukturze, wpływającą na silną stabilizację kompleksu deferoksamina-Fe(III) ($\log\beta_{\text{DFO-Fe(III)}}$ = 30.6). Tym samym, materiały zawierające na swej powierzchni domenę DFO mogą być zastosowane nie tylko jako materiały do zintensyfikowanej adsorpcji, oznaczenia lub detekcji jonów Fe(III), ale również jako platformy do ukierunkowanego wiązania nadmiaru tychże jonów w organizmach.

Przedstawione właściwości chemiczne dwóch rodzajów receptorów organicznych przyczyniły się do ich immobilizacji na wybranych nośnikach nieorganicznych, którymi była krzemionka oraz nanocząstki magnetytu, oraz na kopolimerze eteru metylowo winylowego i bezwodnika maleinowego (PMVEAMA), co było jednym z celów przedstawionej pracy doktorskiej. Niemniej jednak, główne problemy naukowe, które zostały zaadresowano w ramach przeprowadzonych i przedstawionych badań, skupiały się na określeniu wpływu zarówno czynnika funkcjonalizującego, jak i użytego nośnika na właściwości sorpcyjne otrzymanych materiałów hybrydowych. Badania te zostały opublikowane w serii pięciu artykułów **A1**-**A5**, które stanowią podstawę przedstawionej rozprawy doktorskiej.

Badania podzielone zostały na trzy etapy, z których każdy obejmował syntezę i charakterystykę materiałów z wykorzystaniem spektroskopii FT-IR, analizy TG, obrazowania SEM lub analizy elementarnej – kiedy wymagane – oraz określenie ich zdolności adsorpcyjnych wobec wybranych analitów.

Pierwszy celem naukowym była synteza czterech dendrymerów PAMAM różniących się użytym terminalnym komponentem aminowym, tj. zawierające etylenodiaminę, tris(2-aminoetylo)aminę, trietylenotetraminę lub 4,7,10-trioksa-1,13-tridekanodiaminę (nazwane odpowiednio EDA, TREN, TETA oraz TRI-OXA). Dendrymery zostały scharakteryzowane technikami ESI-MS, $^{1}$H-NMR, and $^{13}$C-NMR, a następnie zakotwiczone na powierzchni amorficznej krzemionki zawierającej powierzchniowe grupy izocyjanianowe lub ugrupowania glicydoksy. Otrzymane

materiały $SiO_2$-EDA, $SiO_2$-TREN, $SiO_2$-TETA oraz $SiO_2$-TRI-OXA zostały przebadane pod względem ich właściwości adsorpcyjnych wobec jonów Cu(II), Ni(II) oraz Co(II), jako jonów metali toksycznych oraz wobec kwasu foliowego, salicylowego oraz nikotynowego, jako modelowych cząsteczek kwasowych o udokumentowanej bioaktywności. Przeprowadzone eksperymenty pokazały, że struktura użytej aminy, a tym samym struktura dendrymeru, ma wpływ zarówno na zdolność adsorpcyjną wobec wybranych adsorbatów, jak również na zdolność do transportu biomolekuł zbadaną w trybie *in vitro*.

Kolejny problem badawczy skupiał się na określeniu potencjału sorpcyjnego dwupolimerowego materiału składającego się z polimerowego nośnika PMVEAMA oraz dendrymeru typu PAMAM zawierającego dietylenoaminę jako komponent aminowy (nazywany dalej dendrymerem DETA), jako receptor molekularny. Pomimo poli-nukleofilowego charakteru dendrymeru, który przyczynił się do powstania usieciowanej struktury polimerowej (*ang.* cross-linking), otrzymany materiał wykazywał wysoką zdolność adsorpcyjną wobec wybranych barwników organicznych (czerwień Congo, żółcień pomarańczowa FCF, ryboflawina) oraz związków bioaktywnych (kwas foliowy, kwas salicylowy, kwas nikotynowy). Uzyskany adsorbent polimerowy może być zastosowany do wielokrotnego wiązania barwników z roztworu, ponieważ zaobserwowano jedynie nieznaczny spadek zdolności sorpcyjnej po kilku cyklach adsorpcji/desorpcji. PMVEAMA-DETA został również określony jako potencjalny nośnik leków, wykazując zadowalające wyniki uwalniania leków w trybie *in vitro*, co w połączeniu z udokumentowaną cytokompatybilnością nośnika polimerowego może prowadzić do jego wykorzystania jako platformy do transportu *in vivo* terapeutyków.

Trzecim, a zarazem ostatnim, problemem naukowym podjętym w przedstawionej rozprawie doktorskiej było zastosowanie materiałów funkcjonalnych opartych na cząstkach krzemionki, nanocząstkach magnetytu oraz PMVEAMA zawierających deferoksaminę, jako adsorbentów wobec jonów Fe(III). Każdy z otrzymanych materiałów wykazywał zadowalającą wydajność w wiązaniu jonów z roztworów wodnych. Badania wykazały, że stopień wiązania jonów jest zależny od rodzaju użytego nośnika, a przede wszystkim typu linkera, który determinuje stopień immobilizacji receptora na powierzchni materiałów. Ponadto,

wybrane materiały zostały również poddane badaniom, których rezultatem było potwierdzenie: selektywności materiałów wobec jonów Fe(III) w obecności innych trójwartościowych jonów, tj. Cr(III) oraz Al(III); szybki, całkowity transfer jonów Fe(III) z kompleksu biologicznego (heminy) do materiału opartego na nanocząstkach $Fe_3O_4$; zachowana stabilność oraz podatność magnetyczna materiałów opartych na nanocząstkach magnetytu w ludzkim serum.

Wszystkie przedstawione wyniki badań mogą prowadzić do wytworzenia multiaplikacyjnych materiałów funkcjonalnych w obrębie chemii analitycznej (materiały do detekcji, oznaczania lub wstępnego zatężania analitów z rozcieńczonych roztworów – *ang*. pre-concentration), biomedycynie (platformy dostarczające m.in. leki, terapeutyki, kwasy nukleinowe oraz przeciwciała; materiały wspomagające obrazowanie; materiały do wiązania nadmiarowych wolnych jonów Fe(III) w organizmie w trybie *in vivo*) oraz ochronie środowiska (adsorbenty wobec toksycznych indywiduów chemicznych).

# Appendix A – the published articles

**Appendix A1** **M. Pawlaczyk**, G. Schroeder, Adsorption studies of Cu(II) ions on dendrimer-grafted silica-based materials, Journal of Molecular Liquids 281 (2019), 176-185;
DOI: 10.1016/j.molliq.2019.02.043

**Appendix A2** **M. Pawlaczyk**, G. Schroeder, Efficient Removal of Ni(II) and Co(II) Ions from Aqueous Solutions Using Silica-based Hybrid Materials Functionalized with PAMAM Dendrimers, Solvent Extraction and Ion Exchange 38(5) (2020), 496-521;
DOI: 10.1080/07366299.2020.1766742

**Appendix A3** **M. Pawlaczyk**, G. Schroeder, Dendrimer-Functionalized Hybrid Materials Based on Silica as Novel Carriers of Bioactive Acids, Molecules 25(11) (2020), 2660-2680;
DOI: 10.3390/molecules25112660

**Appendix A4** **M. Pawlaczyk**, G. Schroeder, Dual-Polymeric Resin Based on Poly(methyl vinyl ether-alt-maleic anhydride) and PAMAM Dendrimer as a Versatile Supramolecular Adsorbent, ACS Applied Polymer Materials 3(2) (2021), 956-967;
DOI: 10.1021/acsapm.0c01254

**Appendix A5** **M. Pawlaczyk**, G. Schroeder, Deferoxamine-Modified Hybrid Materials for Direct Chelation of Fe(III) Ions from Aqueous Solutions and Indication of the Competitiveness of In Vitro Complexing toward a Biological System, ACS Omega 6(23) (2021), 15168-15181;
DOI: 10.1021/acsomega.1c01411

**Appendix A1**

Journal of Molecular Liquids 281 (2019) 176–185

Contents lists available at ScienceDirect

Journal of Molecular Liquids

journal homepage: www.elsevier.com/locate/molliq

# Adsorption studies of Cu(II) ions on dendrimer-grafted silica-based materials

Mateusz Pawlaczyk *, Grzegorz Schroeder

*Faculty of Chemistry, Adam Mickiewicz University in Poznan, Umultowska 89b, 61-614 Poznan, Poland*

ARTICLE INFO

*Article history:*
Received 4 December 2018
Received in revised form 5 February 2019
Accepted 9 February 2019
Available online 17 February 2019

*Keywords:*
PAMAM dendrimers
Silica particles
Hybrid materials
$Cu^{2+}$ adsorption

ABSTRACT

Globally observed increase in water contamination has prompted the search for novel, efficient adsorbents, in particular those capable of adsorbing heavy metals. A group of novel hybrid materials composed of silica-gel functionalized with dendritic structures was synthesized. Firstly, four poly(amidoamine) dendrimers (PAMAM) were synthesized in a two-step synthesis: (1) Michael addition between amine core – tris(2-aminoethyl)amine - and methyl acrylate; (2) amidation with the use of four structurally diverse amines: ethylenediamine, triethylenetetramine, tris(2-aminoethyl)amine and 4,7,10-trioxa-1,13-tridecanediamine. Obtained dendrimers were characterized with NMR and MS analysis, and subsequently used as grafting agents dedicated to isocyanate-functionalized silica particles. The obtained hybrid materials ($SiO_2$-dendrimers) were subjected to IR spectroscopic study and tested for their adsorptive properties towards $Cu^{2+}$ ions. Adsorption studies included obtaining of adsorption isotherms and kinetic and thermodynamic studies, using spectrophotometric measurements. Adsorption capacity values of the materials fluctuated between 19.8 and 104.6 mg $g^{-1}$. Also, other coefficients, such as adsorption rate constants, standard enthalpies or standard Gibbs free energies, describing chelating ability of adsorbents were considerably various for different materials. According to the results, incorporation of structurally diverse amines as amino-terminal components of dendritic structure had a significant influence on adsorptive properties of silica-dendrimer hybrid materials.



## 1. Introduction

In recent years, silica-gel has gained much attention not only as a widely used support exhibiting satisfactory mechanical and thermal stability, but also as inorganic platform for hybrid materials, which may find effective applications in many fields, as e.g. drug and gene delivery systems, novel catalysts or adsorbents of toxic compounds and metal ions [1–6].

Hybrid materials are inorganic-organic species consisting of inorganic platform surface modified with organic structures, including various carboxylic acids, surfactants, carbohydrate and protein domains or dendrimers [7]. Dendrimers are very attractive macromolecules, which may find widespread use as functionalizing agents, because of their highly-branched, repetitive, symmetric and regular structure, monodispersity and high biocompatibility [8]. One of the most powerful type of dendrimers are poly(amidoamine) ones (PAMAM), which consist of an amine core surrounded by amidoamine branches. Because of the amino-rich structure of PAMAM dendrimers, they can be applied as grafting agents for obtaining hybrid materials, further used not only as adsorbents towards heavy metal ions and organic dyes, but also as effective platforms for bioactive molecules delivery or gene transfection [9–12]. However, overall physicochemical properties of hybrid materials depend on the dendritic structure (amine core, branches and amino-termini of dendrimer), and also

on the material synthetic route. It is worth mentioning that comprehensive dendritic character of functionalizing agent on hybrid material is retained only while following the 'grafting to' approach, involving ready-made poly(amidoamine) dendrimer interacting with surface group of bare or pre-treated inorganic platform. Additionally, pretreating, such as introducing of linker, may also contribute to decrease in grafting tension, making the functionalizing agent more labile, thus exhibiting higher effectiveness for designed application. Unfortunately, both manipulations in the synthetic route are not widely-used [13–16].

Nevertheless, modification of silica-gel surface with poly(amidoamine) dendrimers and dendrimer-like structures has been extensively explored, especially for preparation of supports finding application in environment protection, such as heavy metal ions adsorbents. The key advantage of such materials is high binding affinity towards metal ions, provided by the presence of numerous amide and amine groups, which generate internal and external binding sites, which hinders the adsorbate elution. Thus, silica-based PAMAM-grafted materials may find application in scavenging, separation, extraction and preconcentration of metal ions from water or organic solutions [17,18].

* Corresponding author.
*E-mail address:* mateusz.pawlaczyk@amu.edu.pl (M. Pawlaczyk).

https://doi.org/10.1016/j.molliq.2019.02.043
0167-7322/

However, the most important coefficient, describing and validating potential adsorptive material, maximal adsorption capacity $q_m$, depends on many factors, which is a driving force for conducting new, innovative studies.

For instance, Qu et al. have focused their attention on the synthesis and characterization of ester- and amino-terminated poly(amidoamine) dendrimer-like structures grafted onto silica surface, designed as potential adsorbent for base metal ions ($Cu^{2+}$, $Ni^{2+}$, $Zn^{2+}$, $Hg^{2+}$) and noble metal ions ($Au^{3+}$, $Pd^{2+}$, $Pt^{4+}$, $Ag^{+}$) [19,20]. Similar experiments have been carried out by a few research groups, for different dendrimer generations (size and volume), kind of adsorbed metal ions and water solution pH [21,22]. The hybrid adsorptive efficiency was the highest for dendrimer generation G2.0 and G3.0, providing the highest number of amide and amine chelating groups and also enough steric hindrance to let the ions diffuse inside dendritic structure. Adsorption capacity of hybrid material also depends on the size and anionic/cationic character of desired ion, e.g. $Pt^{4+}$ ion usually appears as $PtCl_6^{2-}$ anion in water solution, thus solution pH determining protonation of dendrimer's terminal amine groups may cause either repulsive or attractive effect between the adsorbent surface and the metal ions. Nevertheless, $SiO_2$-PAMAM materials exhibit high adsorption capacities, reaching e.g. 2.45 mmol/g for $SiO_2$-G2.0 PAMAM towards $AuCl_4^-$, even in ethanol solutions, which makes them desirable synthetic targets for designing and preparing novel, efficient and eco-friendly adsorbents [23–25].

The aim of our study was to synthesize novel hybrid materials based on surface modification of silica-gel with four poly(amidoamine) dendrimers composed of tris(2-aminoethyl)amine as dendrimer core and various amine termini. We proposed the synthesis of dendrimers and simultaneous functionalization of silica-gel surface, in order to maintain fully dendritic character of the functionalizing agent, unlike in the most of literature reports in the field. The obtained materials were investigated for their adsorptive properties towards $Cu^{2+}$ ions in water solutions, depending on the used amino-terminal component, including obtaining of adsorption isotherms, but also kinetic and thermodynamic studies of adsorption processes were conducted.

## 2. Materials and methods

### 2.1. Materials and chemicals

All used reagents were commercially available products. The silica-gel functionalized with surface isocyanate groups ($SiO_2$-NCO) were obtained from SiliCycle Inc. (Quebec, QC, Canada), characterized with particle size ranging between 40 and 63 μm, specific surface area: 482 $m^2$/g, pore diameter: 59 Å, pore volume: 0.71 mL/g, molecular loading: 1.33 mmol/g and surface coverage: 3.12 μmol/$m^2$. Methyl acrylate, tris (2-aminoethyl)amine, ethylenediamine, triethylenetetramine, 4,7,10-trioxa-1,13-tridecanediamine and copper (II) perchlorate hexahydrate $Cu(ClO_4)_2 \times 6H_2O$ were purchased from Sigma-Aldrich (St. Louis, MO, USA) and used without any further purification. Methanol of the purity grade p.a. was obtained from STANLAB (Lublin, Poland). Diethyl ether, isopropanol and methylene chloride of the purity grade p.a. were purchased from POCH (Gliwice, Poland).

### 2.2. Instruments

The $^1H$ and $^{13}C$ NMR spectra of dendrimers were recorded on Varian VNMR-S 400 MHz spectrometer (Palo Alto, CA, USA). Positive ESI-MS spectra were recorded on amaZon SL ion trap Bruker mass spectrometer (Bremen, Germany), using electrospray ion source (ESI) in infusion mode. Sample solutions were introduced at a flow rate 5 μL $min^{-1}$ into the ionization source, using a syringe pump. Analysis were performed in so-called "enhanced resolution mode", i.e. mass range: 50–2200 $m/z$ and scanning rate: 8100 $m/z$ per second. Capillary voltage was determined at −4.5 kV and − 500 V for endplate offset. The source and desolvation temperatures were set at 80 and 250 °C, respectively. Helium was used as the cone gas at flow rate of 50 L $h^{-1}$ and nitrogen was used as the desolvating gas at flow rate of

800 L $h^{-1}$. FT-IR spectra of obtained hybrid materials were recorded on a Bruker IFS 66/s spectrometer (Billerica, MA, USA) at the wavelength ranging between 400 and 4000 $cm^{-1}$ with resolution set at 2 $cm^{-1}$, using 1.5 mg of samples in KBr pellets. Concentration of $Cu^{2+}$ in samples was determined by spectrophotometric method, using Agilent 8453 UV–Vis spectrophotometer.

### 2.3. Synthesis of poly(amidoamine) (PAMAM) dendrimers (**2**)–(**5**)

The procedure of poly(amidoamine) dendrimers synthesis is illustrated in Fig. 1, on the example of obtaining of PAMAM dendrimer with ethylenediamine amino-terminus. A three-necked flask was charged with methyl acrylate (70.52 g, 0.820 mol) solution in 50 mL of methanol. The stirred solution was cooled in ice-water bath in anhydrous atmosphere to 0 °C upon stirring and then tris(2-aminoethyl) amine (10 g, 0.068 mol) solution in 50 mL of methanol was added dropwise within 2 h, maintaining 0 °C temperature of the mixture. Afterwards, ice-water bath was removed and the mixture was allowed to warm to room temperature and was stirred for seven days. The resulting mixture was subjected to evaporation to remove excess of solvent and unreacted methyl acrylate, yielding intermediate ester product (**1**): ESI-MS: $m/z$: 663.56 $[M + H^+]^+$.

Ester intermediate (**1**) was the starting material for the synthesis of desired poly(amidoamine) dendrimers. The general procedure for obtaining dendrimers **3**–**5** was the same as that used earlier for obtaining and characterization of dendrimer **2** containing ethylenediamine terminus [15]. To a stirred anhydrous solution of appropriate amine: triethylenetetramine (27.74 g, 0.190 mol), tris(2-aminoethyl)amine (27.74 g, 0.190 mol) or 4,7,10-trioxa-1,13-tridecanediamine (41.80 g, 0.190 mol) in 50 mL methanol, cooled in ice-water bath to 0 °C, ester intermediate (**1**) (10 g, 0.015 mol) solution in methanol (30 mL) was added dropwise within 2 h maintaining 0 °C temperature of mixture. Then, the resulting mixture was allowed to warm to room temperature and was stirred for seven days, leading to formation of products **3**, **4** and **5**, respectively (Fig. 2). Afterwards, the excess of solvent was removed under reduced pressure and dendrimers were extracted with cold diethyl ether, obtaining pure products.

Dendrimer **2**: $^1H$ NMR ($CDCl_3$, 400 MHz), $\delta$: 2.21 (12H, m, $CH_2$), 2.38–2.73 (48H, m: overlapping $CH_2$, $NH_2$), 3.05 (12H, m, $CH_2$), 8.07 (6H, bs, CONH); ESI-MS: $m/z$: 831.72 $[M + H]^+$.

Dendrimer **3**: $^1H$ NMR ($CD_3OD$, 400 MHz), $\delta$: 2.40–2.55 (24H, m, $CH_2$), 2.62–2.77 (60H, m, $CH_2$), 2.82 (12H, t, $CH_2$), 3.32 (12H, t, $CH_2$); $^{13}C$ NMR ($CD_3OD$, 400 MHz), $\delta$: 35.5, 41.5, 42.5, 50.2, 51.7, 53.2, 54.6, 58.8, 177.6; ESI-MS: $m/z$: 1346.97 $[M + H]^+$.

Dendrimer **4**: $^1H$ NMR ($CD_3OD$, 400 MHz), $\delta$: 2.39–2.53 (24H, m, $CH_2$), 2.64 (24H, t, $CH_2$) 2.65 (36H, dt, $CH_2$), 2.79–2.86 (12H, m, $CH_2$), 3.32 (12H, t, $CH_2$); $^{13}C$ NMR ($CD_3OD$, 400 MHz), $\delta$: 35.4, 39.6, 40.6, 54.0, 55.4, 58.7, 177.3; ESI-MS: $m/z$: 1055.95 $[M + H]^+$, 909.78 $[M + H]^+$, 528.56 $[M + 2H]^{2+}$, 455.47 $[M + 2H]^{2+}$, 352.85 $[M + 3H]^{3+}$, 304.12 $[M + 3H]^{3+}$.

Dendrimer **5**: $^1H$ NMR ($CD_3OD$, 400 MHz), $\delta$: 1.74 (12H, kw, $CH_2$), 1.79 (12H, kw, $CH_2$) 2.43 (12H, t, $CH_2$), 2.65 (12H, m, $CH_2$), 2.70 (12H, t, $CH_2$), 2.82 (12H, t, $CH_2$), 3.26 (12H, t, $CH_2$), 3.58 (12H, t, $CH_2$), 3.61 (12H, t, $CH_2$), 3.64–3.74 (48H, m, $CH_2$); $^{13}C$ NMR ($CD_3OD$, 400 MHz), $\delta$: 31.2, 34.2, 35.5, 39.2, 40.5, 51.6, 52.1, 71.2, 71.7, 72.1, 72.4, 177.2; ESI-MS: $m/z$: 1572.01 $[M + H]^+$, 787.01 $[M + 2H]^{2+}$, 525.20 $[M + 3H]^{3+}$, 449.22 $[M + 4H]^{4+}$, 394.17 $[M + 4H]^{4+}$.

### 2.4. Synthesis of hybrid materials $SiO_2$-dendrimer

To an anhydrous solution of dendrimer: (**2**) (4.48 g, 5.4 mmol), (**3**) (7.27 g, 5.4 mmol), (**4**) (7.27 g, 5.4 mmol) or (**5**) (9.67 g, 5.4 mmol) in 30 mL of methanol, cooled in dry ice-isopropanol bath to −50 °C, 6 g

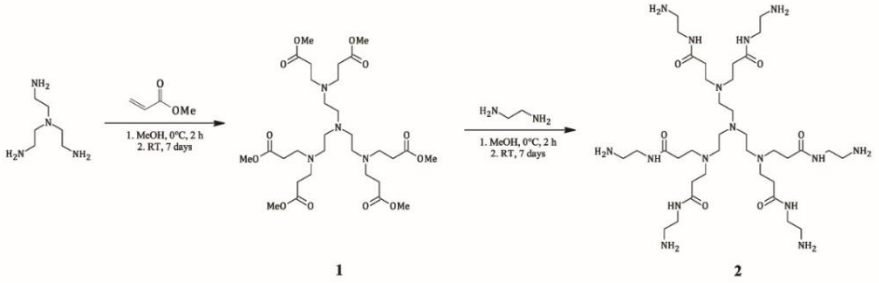


1 2

**Fig. 1.** A scheme of the synthesis of PAMAM dendrimers with tris(2-aminoethyl)amine as the amine core via ester intermediate (**1**), on the example of synthesis of PAMAM dendrimer with ethylenediamine as terminal amino-component (**2**).

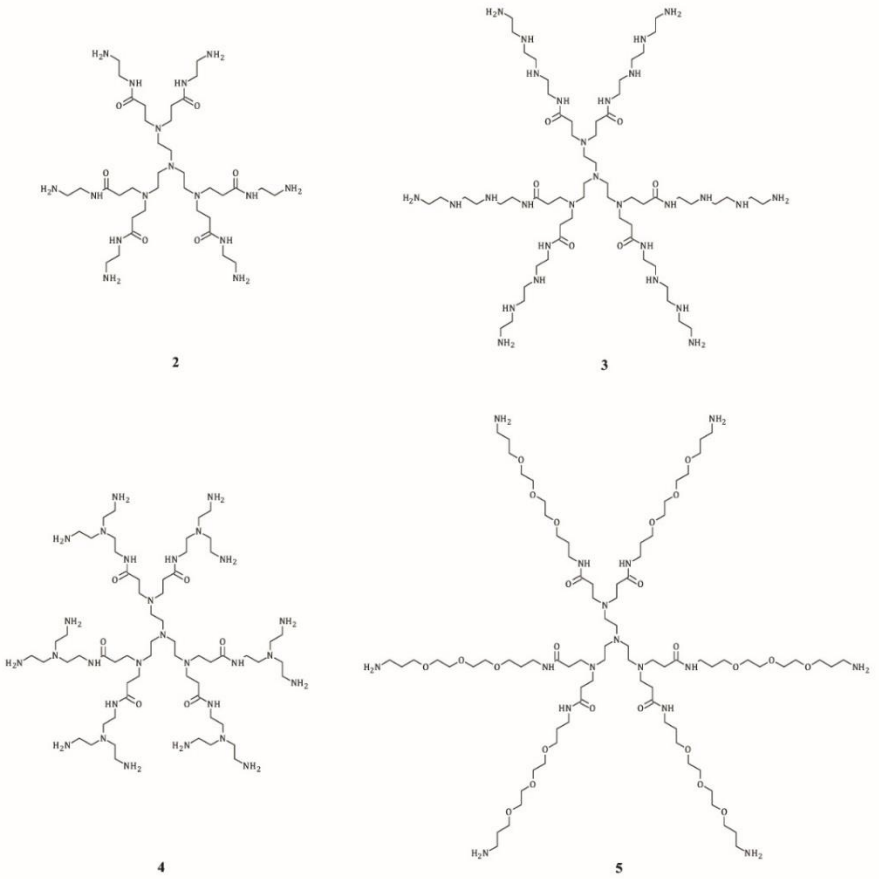

2 3

4 5

**Fig. 2.** Structural patterns of PAMAM dendrimers with tris(2-aminoethyl)amine as the amine core and different terminal amino-components: ethylenediamine (**2**), triethylenetetramine (**3**), tris(2-aminoethyl)amine (**4**) and 4,7,10-trioxa-1,13-tridecanediamine (**5**).

of silica-gel functionalized with surface isocyanate groups was added slowly, not to let temperature rise. Then, the reaction mixture was stirred at −50 °C for 3 h. Afterwards, the mixture was allowed to warm to room temperature and was stirred overnight. The solid product was washed three times with methanol (10 mL) and twice with methylene chloride (10 mL), then dried at room temperature under vacuum, yielding light yellow powders (Fig. 3).

### 2.5. Determination of amino groups on poly(amidoamine) dendrimer-grafted silica

Loading of dendrimers onto the silica surface was examined with the following general procedure: 20 mg of silica-based materials were stirred with 20 mL of 0.01 M HCl aqueous solution at room temperature for 2 h. Then, the solution was filtered off and titrated with 0.005 M NaOH aqueous solution, using phenolphthalein as indicator. Titration experiments were repeated three times for each hybrid material $SiO_2$-dendrimer.

### 2.6. Copper (II) ions adsorption experiments

Studies of $Cu^{2+}$ adsorption on synthesized materials were performed, using copper perchlorate salt $Cu(ClO_4)_2$ as metal ions source. Obtaining each isotherm was preceded by the general procedure: 10 mL of copper (II) perchlorate solution at six different concentrations (0.1, 0.5, 1, 2, 5, 10 mM), buffered to pH 5.4 at acetic acid/sodium acetate buffer, were poured onto 10 mg of each $SiO_2$-dendrimer material. The mixtures were stirred for 24 h at room temperature, reaching equilibrium state. The concentrations of metal ions before and after the equilibrium state were measured, using UV–Vis spectrophotometric studies. The amounts of $Cu^{2+}$ adsorbed on the materials studied were calculated by the following equation:

$$q_{eq} = \frac{(c_0 - c_{eq}) \cdot V}{m}$$

where: $q_{eq}$ – is the amount of metal adsorbed [mg $g^{-1}$]; $c_0$ and $c_{eq}$ – the initial and equilibrium concentrations of copper ions, respectively [mg $L^{-1}$]; $V$ – the volume of added aqueous solution (10 mL) and $m$ is the mass of sample [mg].

Kinetics studies were performed according to the general procedure: 20 mL of 5 mM copper perchlorate aqueous solution, buffered in acetic buffer at pH 5.4, were added to 20 mg sample of obtained hybrid materials and the contents were stirred at room temperature. Samples of copper solution were collected at time intervals and their concentrations were established using UV–Vis spectrophotometric measurements. The amount of metal adsorbed on the hybrid materials in each contact time was established using the equation given below:

$$q_t = \frac{(c_0 - c_t) \cdot V}{m}$$

where: $q_t$ – is the amount of metal adsorbed at the time $t$ [mg $g^{-1}$]; $c_0$ and $c_t$ – the starting concentration of copper ions and after time $t$, respectively [mg $L^{-1}$]; $V$ – the volume of added aqueous solution (20 mL) and $m$ is the mass of sample [mg].

For thermodynamics studies, general procedure was as follows: 10 mL of 5 mM $Cu(ClO_4)_2$ aqueous solution, buffered at pH 5.4 with acetic buffer, were poured to the set of three 10 mg samples of synthesized materials and stirred for 24 h at three different temperatures: 301 ± 1 K, 313 ± 1 K and 328 ± 1 K. Determination of copper content was followed by the procedure described for obtaining of isotherms.

## 3. Results and discussion

### 3.1. Synthesis and characterization of hybrid materials $SiO_2$-dendrimer

The group of adsorbents dedicated to cooper ions binding was synthesized in two main steps. The first step was the synthesis of four poly(amidoamine) dendrimers, consisting of tris(2-aminoethyl)amine as the amine core and four various amines as amino-termini. The synthesis included two simple reactions: Michael reaction between tris (2-aminoethyl)amine and methyl acrylate, using 2.1-fold excess of methyl acrylate and subsequent nucleophilic carbonyl substitution (amidation) with particular amines. Both reactions were carried out in standard conditions, giving satisfactory yields: at first at lowered temperature (0 °C), and then at room temperature for several days, while there are a few reports recommending the use of high temperature or microwave irradiation as accelerating factors [19,26,27]. Moreover, the optimum reaction conditions were chosen as the most effective, avoiding side reactions as cross-linking or retro-Michael reaction [28]. The obtained PAMAM dendrimers were characterized with electrospray ionization mass spectrometry analysis (ESI-MS) in positive ion mode (Fig. A. 4a–4c; SI), excluding characterization of dendrimer **2**, which has been already reported in the literature [15].

Each spectrum showed molecular peaks $[PAMAM+H]^+$, however for dendrimers **3**, **4** and **5** their abundance was very low, while the peaks corresponding to various fragmentation ions ($[PAMAM - x\ amine + n\ H]^{n+}$ and $[PAMAM - x\ CH_2CH_2C(O)\text{-amine} + n\ H]^{n+}$, $x = 1; 2; 3$) showed much higher intensities. What is more, for dendrimer

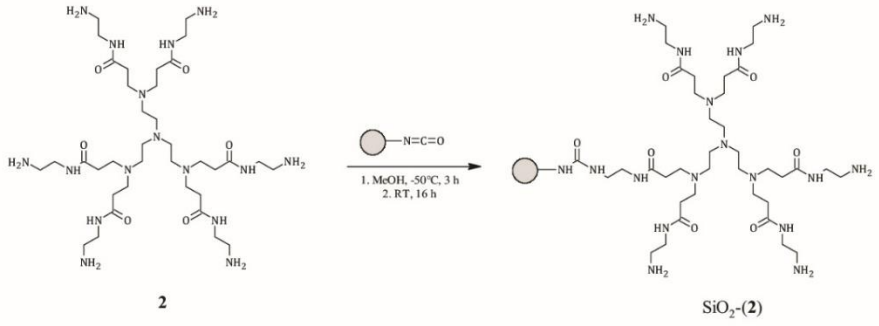


**Fig. 3.** Synthetic route for PAMAM dendrimer-grafted silica surface, on the example of the reaction between PAMAM dendrimer **2** and silica functionalized with isocyanate surface groups.

containing triethylenetetramine as amino-terminal component (**3**), the peaks assigned to the fragmentation ions of each triethylenetetramine part, were observed. The trend in detecting fragmentation ions in ESI-MS spectra of PAMAM dendrimers has already been highlighted in literature [15]. Moreover, the $^{1}$H NMR (Fig. A. 2a–2c; SI) and $^{13}$C NMR (Fig. A. 3a–3c; SI) spectra of dendrimers **3**, **4** and **5** confirmed the structures of the synthesized dendrimers. No peaks corresponding to primary or secondary amine group protons were detected in the $^{1}$H NMR spectra, which was the consequence of choosing deuterated methanol as a solvent for PAMAM dendrimers [29].

The synthesized dendrimers constituted building blocks for obtaining hybrid materials, which was achieved by addition reaction between the isocyanate groups on the surface of functionalized silica-gel and the terminal amino groups of poly(amidoamine) dendrimers. The reactions were carried out for 2 h at a maximum temperature of −50 °C, in order to prevent addition of solvent molecules (methanol) to silica-isocyanate. Afterwards, the reaction mixtures were stirred at room temperature to suppress the unreacted –NCO groups on silica surface.

The amounts of amino terminal groups on materials surface (Table 1), which define the loading of dendritic structures on silica-gel platforms, were determined using a simple alkacymetric titration [30]. According to the experimental data, the highest loading was obtained for $SiO_2$-(**2**), reaching 0.310 mmol/g and the lowest of 0.078 mmol/g for $SiO_2$-(**5**). The $SiO_2$-(**2**) material contains ethylenediamine, which is the smallest and the least branched amine used, as the terminal component of dendrimer **2**. Thus, dendrimer **2** makes the least steric hindrance, which was related to the highest loading of silica with this dendrimer.

In contrast, dendrimer **5**, containing the longest amine, that is 4,7,10-trioxa-1,13-tridecanediamine, was characterized by the lowest loading on silica.

The synthesized materials were also characterized with FT-IR spectroscopy, the relevant spectra are collected in Fig. 4. They show several absorption bands, which evidence successful grafting of dendritic structures on silica surface. The bands at 1637 and 1570 $cm^{-1}$ are assigned to the C—O stretching vibration in the amide carbonyl group C(O)-NH, and the N-H bending vibration in the amine and amide groups. Each spectrum also shows the bands assigned to the asymmetric stretching vibration of –$CH_2$– groups at 2942 $cm^{-1}$, however they have relatively low intensity, in consistence with the low loading of PAMAM dendrimers on the silica surface. The broad absorption peak at approximately 3477 $cm^{-1}$ corresponds to the vibration of remaining silanol groups on silica surface, and it might overlap with that of the stretching vibration of primary amine groups. Very strong peaks were observed at 464, 800 and 1095 $cm^{-1}$, which are assigned to the bending, symmetric stretching and asymmetric stretching vibrations of Si-O-Si bonds in silica network, respectively [22]. No spectrum showed the peak that would evidence the presence of free terminal ester group, which indicates the maximally successful functionalization of silica surface with PAMAM dendrimers. It should be added that the possibility of structural disturbances of the dendrimers on the silica surface is negligible in view of drastic difference between the nanometric size of the functionalizing agents molecules [31] and micrometric size silica particles. Hence, microscopic images would not expose any structural defects of dendritic structures anchored to silica platform. Furthermore, the synthesized and characterized dendrimers were used as grafting agents for hybrid materials' synthesis conducted with 'grafting-to' approach, which fully excluded possible structural defects of functionalizing agent.

**Table 1**
The amounts of dendrimers grafted onto silica surface (loading).

| Hybrid material | Loading [mmol/ g] |
|---|---|
| $SiO_2$-(**2**) | 0.310 |
| $SiO_2$-(**3**) | 0.152 |
| $SiO_2$-(**4**) | 0.155 |
| $SiO_2$-(**5**) | 0.078 |

### *3.2. Investigation of the hybrid materials adsorption properties towards $Cu^{2+}$*

A new class of adsorbents designed for removal of heavy metal ions from aqueous solutions were obtained. Silica-based materials were grafted with various poly(amidoamine) dendrimers, which exhibit strong chelating affinity towards metal ions thanks to the presence of numerous amine and amide groups. However, structural variety of used dendrimers amino-components may also have a further impact on chelating properties of synthesized hybrid materials. Thus, adsorption experiments, including determination of adsorption isotherms, as well as kinetics and thermodynamics, are vital to conclude about the structural requirements for affording best adsorptive properties of designed materials.

#### *3.2.1. Adsorption isotherms*

Determination of adsorption isotherms at equilibrium state gives important parameters, referring to sorption mechanism between adsorbent and analyte as well as to optimization of metal ions uptake from aqueous solutions [32]. The isotherms obtained for experiments of $Cu^{2+}$ ions adsorption on the synthesized silica-materials grafted with various PAMAM dendrimers are depicted in Fig. 5. So far, several mathematical isotherm models describing pollutants adsorption from their solutions have been proposed [33], however the most frequently used are Langmuir and Freundlich models.

The Langmuir model assumes the homogeneity of adsorbent surface and formation of adsorbate monolayer, which is connected with the same values of binding sites energies. This model also excludes intermolecular effects of the adsorbate [34]. For discussed experiments of copper (II) ions binding onto hybrid materials the Langmuir isotherm (Fig. A. 5a.; SI) can be described as its extensively used linear plot:

$$\frac{c_{eq}}{q_{eq}} = \frac{c_{eq}}{q_m} + \frac{1}{q_m K_L}$$

where: $c_{eq}$ – is the concentration of $Cu^{2+}$ ions in aqueous solution in equilibrium state [mg $L^{-1}$]; $q_{eq}$ and $q_m$ – the equilibrium and maximum amount of copper bound to adsorbent, respectively [mg $g^{-1}$]; $K_L$ – the Langmuir constant associated with adsorption energy [L $mg^{-1}$]. According to the linear plot of Langmuir isotherm, very important parameters of adsorption process, such as maximum adsorption capacity $q_m$ and Langmuir binding constant $K_L$ were defined from slope and intercept of linear regression (Table 2). Moreover, on the basis of Langmuir isotherm, the dimensionless separation $R_L$ factor, which determines the value of isotherm fitting, was calculated from the equation:

$$R_L = \frac{1}{1 + K_L c_{max}}$$

where: $K_L$ – is the Langmuir constant [L $mg^{-1}$]; $c_{max}$ – the maximal initial concentration of $Cu^{2+}$ ions, used for isothermal analysis [mg $L^{-1}$]. Values of $R_L$ factor for all used hybrid materials for copper (II) ions adsorption are collected in Table 2. Interpretation of $R_L$ factor is based on the theory which assumes that Langmuir isotherm is: unfavorable ($R_L > 1$), favorable ($0 < R_L < 1$), linear ($R_L = 1$) or irreversible ($R_L = 0$) [35]. For all materials the separation factors were determined and their values indicated favorability of the adsorption process.

For the Freundlich isotherm model, it is postulated that the adsorbate molecules are able to interact with each other, contributing to formation of the adsorbate multilayer, which may also be a result of the

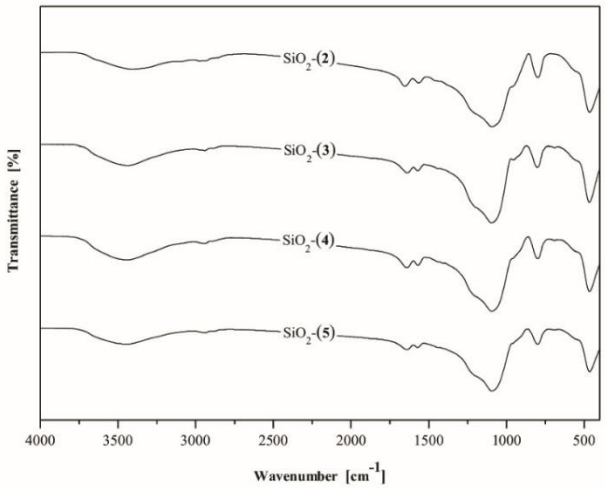


**Fig. 4.** FT-IR spectra of hybrid materials $SiO_2$-dendrimer.

assumed adsorbent surface heterogeneity [36]. The well-known linear form of Freundlich isotherm was used for $Cu^{2+}$ adsorption on synthesized materials (Fig. A. 5b.; SI), and it is expressed as:

$$\log q_{eq} = \log K_F + \frac{1}{n} \log c_{eq}$$

where: $c_{eq}$ – is the equilibrium $Cu^{2+}$ ions concentration in the solution [mg $L^{-1}$]; $q_{eq}$ – the equilibrium amount of metal adsorbed on material, $K_F$ – the Freundlich constant connected with adsorption capacity [mg $g^{-1}$ (L $mg^{-1})^{1/n}$]; $1/n$ – the empirical coefficient characterizing heterogeneity of material and adsorption intensity. The linear plot of logarithmized series is characterized with the slope and intercept, which are the basis for determination of $K_F$ and $1/n$ parameters, describing adsorptive properties of the examined materials, which are listed in Table 2.

Linear regressions of Langmuir and Freundlich isotherms are described with two coefficients ($R^2$ and $\chi^2$), both are the fitting parameters of the plots linearity. As shown in Table 2, the silica material grafted with dendrimer **2** ($SiO_2$-(**2**)) strictly follows the Langmuir isotherm ($R^2 = 0.9888$), rather than Freundlich isotherm ($R^2 = 0.9754$). The opposite conclusion was drawn for the material decorated with PAMAM dendrimer **5** ($SiO_2$-(**5**)), on which the adsorption process follows Freundlich isotherm much more favorably than Langmuir, reaching $R^2$

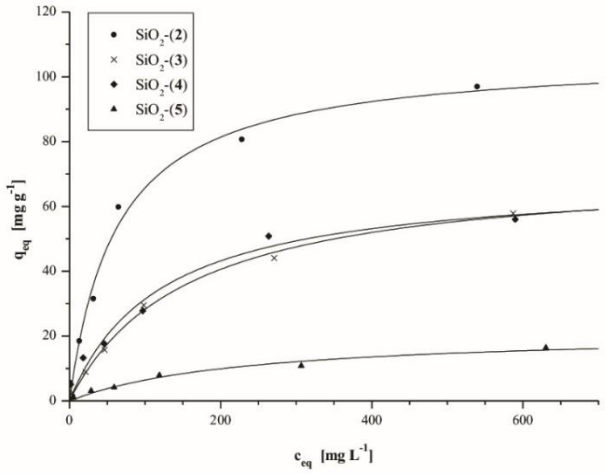


**Fig. 5.** Isotherms for adsorption of $Cu^{2+}$ ions on $SiO_2$-dendrimer hybrid materials.

**Table 2**
Adsorption isothermal parameters for binding $Cu^{2+}$ ions on hybrid materials $SiO_2$-dendrimer.

| Hybrid material | Langmuir isotherm | | | | | Freundlich isotherm | | | |
|---|---|---|---|---|---|---|---|---|---|
| | $K_L$ [L $mg^{-1}$] | $q_m$ [mg $g^{-1}$] | $R^2$ | $\chi^2$ | $R_L$ | $K_F$ [mg $g^{-1}$ (L $mg^{-1})^{1/n}$] | 1/n | $R^2$ | $\chi^2$ |
| $SiO_2$-(**2**) | 0.020 ± 0.006 | 104.6 ± 5.6 | 0.9888 | 0.3681 | 0.0717 | 6.81 ± 1.02 | 0.45 ± 0.04 | 0.9754 | 0.0164 |
| $SiO_2$-(**3**) | 0.007 ± 0.001 | 70.6 ± 3.4 | 0.9908 | 0.1795 | 0.1808 | 1.24 ± 0.26 | 0.64 ± 0.05 | 0.9847 | 0.0085 |
| $SiO_2$-(**4**) | 0.013 ± 0.005 | 62.9 ± 5.5 | 0.9707 | 1.1810 | 0.1062 | 4.12 ± 0.47 | 0.42 ± 0.03 | 0.9788 | 0.0242 |
| $SiO_2$-(**5**) | 0.006 ± 0.002 | 19.8 ± 2.2 | 0.9504 | 2.6240 | 0.2048 | 0.59 ± 0.03 | 0.59 ± 0.03 | 0.9882 | 0.0894 |

values at the level of 0.9882 and 0.9504, respectively. Experimental data obtained for $SiO_2$-(**3**) point to the Langmuir isotherm model ($R^2 > 0.99$), while the adsorption process on the material functionalized with dendrimer **4** follows partially the Freundlich and Langmuir isotherm models, according to not determinedly high $R^2$-values and also relatively small difference between $R^2$ coefficients obtained for both models - 0.9788 and 0.9707, respectively. Concluding, there is no uniform manner for isothermal modeling of copper (II) ions adsorption on the obtained hybrid materials. Such a differentiation might be caused mostly by structural differences in the grafting agents, i.e. the length of used amine chain and the presence of additional secondary or tertiary amine groups. Dendrimer **2** contains the most compact amino-termini (ethylenediamine), thus it readily forms only monolayer of adsorbate, after saturation of binding sites. On the other hand, dendrimers **3** and **4** contain additional secondary and tertiary amino groups, respectively, which might cause further interactions with $Cu^{2+}$ ions. However, dendrimer **4** has terminal tris(2-aminoethyl)amine, which restrict diffusion of adsorbate molecules inside the dendritic structure, triggered by steric hindrance, in contrast to the straight chain of triethylenetetramine (dendrimer **3**). PAMAM dendrimer **5** containing 4,7,10-trioxa-1,13-tridecanediamine contributes to formation of multilayer adsorbate coverage, primarily by the presence of three oxygen atoms inside the terminal amine-chain, which might interact with $Cu^{2+}$ ions, causing entering the interior of dendritic structure. The same sequence is observed for maximum adsorption capacities. The material modified with PAMAM dendrimer having the most compact terminal amino-component ($SiO_2$-(**2**)) exhibited the highest adsorption capacity of 104.6 mg $g^{-1}$, which could be related either to the easiest diffusion into its dendritic structure or the highest grafting value of dendritic structures on silica surface, affording the highest number of chelating groups. The materials which are grafted with dendrimers containing amine-rich terminal amino-components (triethylenetetramine – $SiO_2$-(**3**); tris(2-aminoethyl)amine – $SiO_2$(**4**)) show almost the same maximum adsorption capacities 70.6 and 62.9 mg $g^{-1}$, respectively. These values are lower than those for $SiO_2$-(**2**) material, because of the steric hindrance in the dendrimers used, however the dendrimers possess additional internal secondary or tertiary amine groups, able to interact with $Cu^{2+}$ ions, increasing adsorption capacities. For the material $SiO_2$-(**5**) the $q_m$ value is the lowest, leveling out at 19.8 mg $g^{-1}$, which is related to high steric hindrance in this compound and the lack of internal amine groups.

Moreover, Table 3 presents a comparison of the maximal adsorption capacities $q_m$ of the synthesized materials and the analogous values for other materials described in literature. Each synthesized material exhibited binding capability towards Cu(II), however the highest adsorptive properties were determined for $SiO_2$-(**2**), $SiO_2$-(**3**) and $SiO_2$-(**4**), which had considerably higher affinity to metal ions, compared with the other materials reported in literature.

**Table 3**
Comparison of maximal adsorption capacities of adsorbents dedicated to copper (II) ions adsorption.

| Adsorbent | Adsorption capacity [mg $g^{-1}$] | Reference |
|---|---|---|
| SBA-15–3.0 PAMAM | 13.4 | [22] |
| $SiO_2$–1.0 PAMAM | 78.7 | [24] |
| $SiO_2$–2.0 PAMAM | 65.3 | [24] |
| $SiO_2$–3.0 PAMAM | 18.0 | [24] |
| Graphene oxide – 2.0 PAMAM | 8.7 | [37] |
| Graphene oxide – 2.0 PAMAM | 68.7 | [38] |
| Cu(II) imprinted carbon-TEPA adsorbent | 33.3 | [39] |
| Loofah fibers | 14.2 | [40] |
| $SiO_2$–5.0 PPI | 460 | [41] |
| $SiO_2$-(**2**) | 104.6 | This study |
| $SiO_2$-(**3**) | 70.6 | This study |
| $SiO_2$-(**4**) | 62.9 | This study |
| $SiO_2$-(**5**) | 19.8 | This study |

*3.2.2. Adsorption kinetics*

To evaluate the effect of contact time between $Cu^{2+}$ ions and the synthesized adsorbents, kinetics experiments were conducted, using a 5 mM copper (II) solution, affording high excess of metal ions towards binding domain of dendrimers. There are several kinetic models describing interactions between adsorbent and metal ions, however the most frequently used are pseudo-first-order kinetics, introduced by Lagergren, and pseudo-second-order, proposed by Ho and McKay [42].

The pseudo-first-order model assumes that the rate-limiting step of adsorption process is connected with the adsorption capacity of the used material and it follows the equation whose plot $\log(q_e\text{-}q_t)$ versus $t$ (Fig. 6) is linear:

$$\log(q_e - q_t) = \log q_e - \frac{k_1}{2.303} t$$

where: $q_e$ and $q_t$ – are the amounts of metal adsorbed at the equilibrium and time $t$, respectively [mg $g^{-1}$]; $k_1$ – the rate constant of pseudo-first-order adsorption process [$h^{-1}$]. Nonlinear plot of the pseudo-first order kinetics is based on the following equation, which can also be used for prediction of the amount of metal adsorbed at the equilibrium state ($q_e$) (Fig. A. 6a.; SI):

$$q_t = q_e\left(1 - e^{-k_1 t}\right)$$

The obtained pseudo-first-kinetic data (Table 4) can be also used as a benchmark for defining the initial adsorption rate $k_i$ [mg $g^{-1}$ $h^{-1}$] and half-adsorption time $t_{1/2}$ [h] (which is the time needed for binding half of $Cu^{2+}$ ions bound at the equilibrium state) calculated from the following equations, respectively:

$$k_i = k_1 q_e$$

$$t_{1/2} = \frac{\ln 2}{k_1}$$

The pseudo-second-order kinetic model is based on the assumption that the rate limiting step of adsorption is the chemical adsorption, employing the process of sharing the exchange electrons between metal ion and adsorptive material [42]. Thus, the kinetics of adsorption depends on the saturation level of adsorbent at the time $t$, as well as the

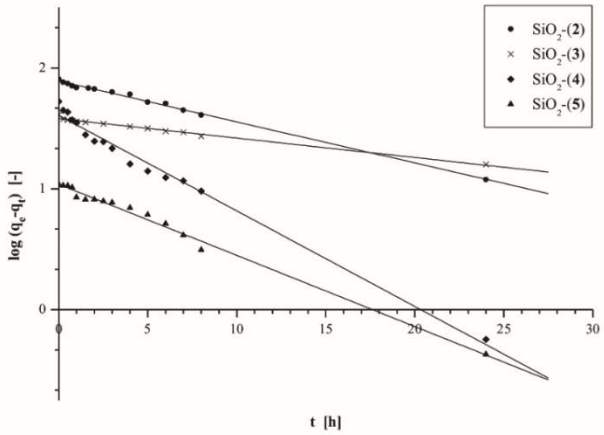


**Fig. 6.** Linear plot of pseudo-first-order kinetics for adsorption process of $Cu^{2+}$ ions on $SiO_2$-dendrimer hybrid materials.

amount of metal ion diffused on the surface of the adsorbent, and it can be expressed by the equation (Fig. A. 6b.; SI):

$$\frac{t}{q_t} = \frac{1}{k_2 {q_e}^2} + \frac{1}{q_e} t$$

where $k_2$ – is the rate constant for pseudo-second-order kinetics [g $mg^{-1}$ $h^{-1}$]. Similarly as for the pseudo-first-order kinetics, the half-adsorption time $t_{1/2}$ and initial adsorption rate $k_i$ were also investigated assuming the following equations:

$$t_{1/2} = \frac{1}{k_2 q_e}$$

$$k_i = k_2 {q_e}^2$$

In order to investigate the kinetic model of $Cu^{2+}$ adsorption process on

$SiO_2$-dendrimer materials, the correlation coefficients $R^2$ and $\chi^2$ were determined for both pseudo-first-order and pseudo-second-order kinetic linear plots, and collected in Tables 4 and 5, respectively. It is clearly visible that metal ions adsorption on the synthesized materials strictly follows the pseudo-first-order model, reaching all $R^2$-values higher than 0.98, fluctuating between 0.9859 and 0.9964, while for the pseudo-second-order kinetics only for one material (grafted with dendrimer **4**) the correlation coefficient $R^2$ value of 0.9874, indicating linearity of the plot. Therefore, the rate liming step of $Cu^{2+}$ adsorption on $SiO_2$-dendrimer materials is related to saturation of available binding sites on the materials surface. The only partly pseudo-first- and pseudo-second-order kinetic model was proposed for the material functionalized with dendrimer **4** (with triethylenetetramine as amino-terminus), which could be a result of the presence of dendrimer containing secondary amine groups in the amino-terminal component, which are capable of interaction with the adsorbate.

*3.2.3. Adsorption thermodynamics*

Temperature is one of the factors, which might have a significant influence on the proceeding of adsorption process. Determination of standard enthalpy (ΔH°), standard entropy (ΔS°) and Gibbs free energy (ΔG°) changes are necessary for characterization of thermodynamic aspects of copper (II) ions adsorption on silica-based hybrid materials. In order to determine ΔH° and ΔS° parameters, the following equation was used:

$$\ln K_d = \frac{\Delta S^\circ}{R} - \frac{\Delta H^\circ}{RT}$$

where: $T$ – is the temperature [K]; $R$ – the universal/ideal gas constant (8.314 J $mol^{-1}$ $K^{-1}$); $K_d$ – the distribution coefficient, defined as the ratio between ion metals bound to adsorbent and remaining in solution:

$$K_d = \frac{c_{Ae}}{c_e}$$

where $c_{Ae}$ and $c_e$ – are the equilibrium concentrations of the adsorbed metal [mg $g^{-1}$] and the metal in solution [mg $L^{-1}$], respectively. The

**Table 4**
Pseudo-first-order kinetics parameters for adsorption of $Cu^{2+}$ ions on $SiO_2$-dendrimer hybrid materials.

| Hybrid material | Pseudo-first-order | | | | |
|---|---|---|---|---|---|
| | $k_1$ [$h^{-1}$] | $R^2$ | $\chi^2$ | $k_i$ [mg $g^{-1}$ $h^{-1}$] | $t_{1/2}$ [h] |
| $SiO_2$-(**2**) | 0.078 ± 0.001 | 0.9964 | 0.0026 | 9.62 ± 0.32 | 8.89 ± 0.01 |
| $SiO_2$-(**3**) | 0.037 ± 0.001 | 0.9886 | 0.0682 | 1.63 ± 0.05 | 18.78 ± 0.26 |
| $SiO_2$-(**4**) | 0.182 ± 0.006 | 0.9859 | 0.0235 | 6.29 ± 0.10 | 3.81 ± 0.02 |
| $SiO_2$-(**5**) | 0.136 ± 0.003 | 0.9918 | 0.0200 | 1.47 ± 0.04 | 5.10 ± 0.32 |

**Table 5**
Pseudo-second-order kinetics parameters for adsorption of $Cu^{2+}$ ions on hybrid materials $SiO_2$-dendrimer.

| Hybrid material | Pseudo-second-order | | | | |
|---|---|---|---|---|---|
| | $k_2$ [g $mg^{-1}$ $h^{-1}$] | $R^2$ | $\chi^2$ | $k_i$ [mg $g^{-1}$ $h^{-1}$] | $t_{1/2}$ [h] |
| $SiO_2$-(**2**) | 0.0017 ± 0.0003 | 0.7841 | 0.0935 | 11.06 ± 1.95 | 7.29 ± 1.29 |
| $SiO_2$-(**3**) | 0.0024 ± 0.0006 | 0.7894 | 1.4492 | 4.67 ± 1.17 | 9.45 ± 2.36 |
| $SiO_2$-(**4**) | 0.0096 ± 0.0010 | 0.9874 | 0.0075 | 24.81 ± 2.58 | 2.05 ± 0.21 |
| $SiO_2$-(**5**) | 0.0112 ± 0.0020 | 0.4212 | 2.2174 | 1.32 ± 0.24 | 8.24 ± 1.47 |

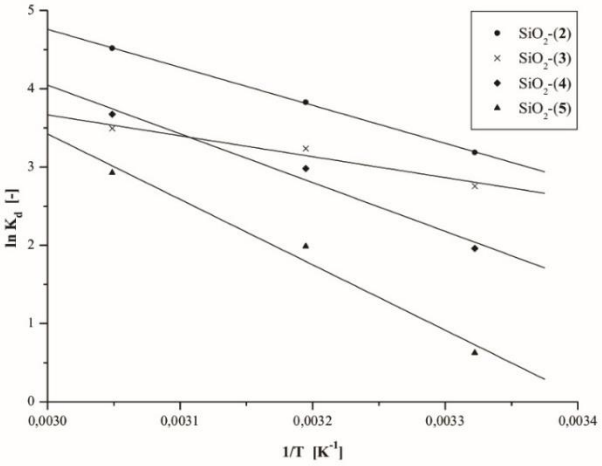


**Fig. 7.** Plot characterizing the thermodynamics of $Cu^{2+}$ adsorption process on $SiO_2$-dendrimer materials.

values of ΔS° and ΔH° were determined from the intercept and slope of the linear plot ln $K_d$ versus 1/$T$, respectively (Fig. 7). The obtained $K_d$ values were further used for the calculation of particular Gibbs free energies from the relation:

$$\Delta G^{\circ} = -RT \ln K_d$$

All calculated values, describing the thermodynamics of $Cu^{2+}$ adsorption process on materials $SiO_2$-dendrimers are listed in Table 6, provided with $R^2$ and $\chi^2$ linear correlation coefficients.

According to the experimental results, the adsorption of $Cu^{2+}$ ions on each material is an endothermic process, as indicated by positive values of standard enthalpy. Positive, and relatively high, values of ΔS° are a consequence of increase in randomness on the solid-solution interface, induced by progressive adsorption process.

The Gibbs free energies calculated for each adsorptive material, reached negative values, indicating the spontaneity of $Cu^{2+}$ adsorption in the whole range of temperatures. The lowest values were calculated for $SiO_2$-(**2**) grafted with ethylenediamine-containing PAMAM dendrimer, however the highest values indicating the least intensive and least spontaneous adsorption were obtained for silica-based $SiO_2$-(**5**), while the other materials grafted with dendrimers **3** and **4** gave the values in-between. The differences between the obtained data are related to the amino-termini component of obtained dendrimers, used as functionalizing agent for silica. The size and structural features (the presence of secondary and tertiary amine groups and oxygen atoms) affect the degree of surface grafting and the possibility of adsorbate diffusion inside the dendritic structure. Therefore, they influence the spontaneity of copper (II) ions binding to hybrid materials. Moreover, for each sample, ΔG° values increase with increasing temperature, which points to the endothermic character of adsorption process, as has been already indicated by the standard enthalpy results.

## 4. Conclusions

New hybrid materials consisting of silica platform and various poly (amidoamine) dendrimers as grafting agents were synthesized and tested for adsorption of $Cu^{2+}$ ions from water solutions. Four dendrimers were synthesized using tris(2-aminoethyl)amine as the core amino-component, methyl acrylate as the elongating agent and four structurally diverse amines: ethylenediamine (**2**), triethylenetetramine (**3**), tris(2-aminoethyl) amine (**4**) and 4,7,10-trioxa-1,13-triedecanediamine (**5**) as the terminal amino-components. Grafting of the synthesized dendrimers was achieved by the reaction of isocyanate-groups on silica surface with terminal amine group of dendritic structures. The obtained materials were characterized and then used as adsorbents of $Cu^{2+}$ ions under slightly acidic conditions. Adsorption isotherms of metal ions on the prepared materials provided the information on their maximal

**Table 6**
Thermodynamic parameters for adsorption of $Cu^{2+}$ ions on hybrid materials $SiO_2$-dendrimer.

| Hybrid material | ΔH° [kJ mol$^{-1}$] | ΔS° [kJ mol$^{-1}$ K$^{-1}$] | $R^2$ | $\chi^2$ | T [K] | ΔG° [kJ mol$^{-1}$] |
|---|---|---|---|---|---|---|
| $SiO_2$-(**2**) | 40.37 ± 0.75 | 0.161 ± 0.002 | 0.9997 | 0.0001 | 301 | −7.98 ± 0.03 |
| | | | | | 313 | −9.96 ± 0.03 |
| | | | | | 328 | −12.31 ± 0.04 |
| $SiO_2$-(**3**) | 22.20 ± 4.79 | 0.097 ± 0.015 | 0.9555 | 0.1151 | 301 | −4.91 ± 0.02 |
| | | | | | 313 | −7.76 ± 0.02 |
| | | | | | 328 | −10.02 ± 0.03 |
| $SiO_2$-(**4**) | 51.78 ± 7.82 | 0.189 ± 0.025 | 0.9777 | 0.1821 | 301 | −6.90 ± 0.02 |
| | | | | | 313 | −8.42 ± 0.03 |
| | | | | | 328 | −9.53 ± 0.03 |
| $SiO_2$-(**5**) | 69.48 ± 10.07 | 0.236 ± 0.032 | 0.9794 | 0.2343 | 301 | −1.57 ± 0.01 |
| | | | | | 313 | −5.17 ± 0.02 |
| | | | | | 328 | −7.98 ± 0.02 |

adsorption capacities, reaching values between 19.8 and 104.6 mg $g^{-1}$. Also kinetic and thermodynamic studies of adsorption process were conducted. Metal ions adsorption on all materials was found to be an endothermic and spontaneous process, following mainly the pseudo-first-order kinetic model. However, the differences between the calculated values describing particular materials were easily visible, which are related to the structural variety of used terminal amino-component, influencing the character of the adsorption process.

Nevertheless, three materials: $SiO_2$-(**2**), $SiO_2$-(**3**) and $SiO_2$-(**4**) were proved to be effective adsorbents of $Cu^{2+}$ ions, thus they could be highly effective adsorbents for not only other heavy metal ions, such as $Ni^{2+}$ or $Co^{2+}$, but also various toxic compounds, which may be bound to materials through either electrostatic or hydrogen bonds. These three materials ($SiO_2$-(**2**) – $SiO_2$-(**4**)) may lead to the novel tool for removal or preconcentration of particular analytes in radically diluted solutions, with further analytical techniques such as elemental analysis or X-ray fluorescence spectroscopy. Moreover, low toxicity of synthesized materials may be a key feature allowing the studies of adsorption/desorption of bioactive compounds, aiming at designing novel platforms for direct transport of drugs.

To sum up, the materials are of potential wide use, which is related to much further investigation our team intends to undertake.

## Conflict of interest

The authors declare no known financial or personal conflicts of interest associated with this publication.

## Acknowledgements

The work was supported by grant no. POWR.03.02.00-00-I026/16 co-financed by the European Union through the European Social Fund under the Operational Program Knowledge Education Development.

## Appendix A. Supplementary data

Supplementary Information associated with following article contain: Chemical structures of the used amino-terminal components; The $^{1}H$ NMR and $^{13}C$ NMR spectra of the synthesized dendrimer; The ESI-MS spectra of the obtained dendrimers; The additional plots related to investigated adsorption processes. Supplementary data associated with this article can be found in the online version, at doi: https://doi.org/10.1016/j.molliq.2019.02.043.

## References

[1] Y. Wang, Q. Zhao, N. Han, L. Bai, J. Li, J. Liu, E. Che, L. Hu, Q. Zhang, T. Jiang, S. Wang, Mesoporous silica nanoparticles in drug delivery and biomedical applications, Nanomedicine: NBM 11 (2015) 313–327.
[2] C. Deraedt, R. Ye, W.T. Ralston, F.D. Toste, G.A. Samorjai, Dendrimer-stabilized metal nanoparticles as efficient catalysts for reversible dehydrogenation/hydrogenation of N-heterocycles, J. Am. Chem. Soc. 139 (2017) 18084–18092.
[3] W.T. Tsai, K.J. Hsien, M.J. Yang, Silica adsorbent prepared from spent diatomaceous earth and its application to removal of dye from aqueous solution, J. Colloid Interface Sci. 275 (2004) 428–433.
[4] F. Chen, Q. Wu, Q. Lu, Y. Xu, Y. Yu, Synthesis and characterization of bifunctional mesoporous silica adsorbent for simultaneous removal of lead and nitrate ions, Sep. Purif. Technol. 151 (2015) 225–231.
[5] E. Da'na, Adsorption of heavy metals on functionalized-mesoporous silica: a review, Microporous Mesoporous Mater. 247 (2017) 145–157.
[6] C. Chu, N. Ueno, T. Imae, Solid-phase synthesis of amphiphilic dendron-surface-modified silica particles and their application toward water purification, Chem. Mater. 20 (2008) 2669–2676.
[7] C. Sanchez, K.J. Shea, S. Kitagawa, Recent progress in hybrid materials science, Chem. Soc. Rev. 40 (2011) 471–472.
[8] P. Kesherwani, K. Jain, N.K. Jain, Dendrimer as nanocarrier for drug delivery, Prog. Polym. Sci. 39 (2014) 268–307.
[9] M. Pawlaczyk, J. Kurczewska, G. Schroeder, Nanomaterials modification by dendrimers - a review, World J. Res. Rev. 6 (2018) 14–30.
[10] N.A. Ebelegi, T.A. Ekubo, N. Ayawei, D. Wankasi, A review of synthesis, characterization and applications of functionalized dendrimers, Am. J. Polym. Sci. 7 (2017) 8–14.
[11] R. Esfand, D.A. Tomalia, Poly (amidoamine)(PAMAM) dendrimers: from biomimicry to drug delivery and biomedical applications, Drug Deliv. Today 6 (2001) 427–436.
[12] E. Abbasi, S.F. Aval, A. Akbarzadeh, M. Milani, H.T. Nasrabadi, S.W. Joo, Y. Hanifehpour, K. Nejati-Koshki, R. Pashaei-Asl, Dendrimers: synthesis, applications, and properties, Nanoscale Res. Lett. 9 (2014) 247–256.
[13] J.T. Sun, C.Y. Hong, C.Y. Pan, Surface modification of carbon nanotubes with dendrimers or hyperbranched polymers, Polym. Chem. 2 (2011) 998–1007.
[14] K. Gerrans, A. Luhrs, C. Feider, L.D. Margerum, Silica nanoparticles functionalized with polyamidoamine (PAMAM) dendrimers as platforms for photoluminescence (PL) sensing of copper and cyanide ions, J. Colloid Interface Sci. 470 (2016) 276–283.
[15] J. Kurczewska, M. Ceglowski, B. Messyasz, G. Schroeder, Dendrimer-functionalized halloysite nanotubes for effective drug delivery, Appl. Clay Sci. 153 (2018) 134–143.
[16] J. Kurczewska, M. Ceglowski, G. Schroeder, Preparation of multifunctional cascade iron oxide nanoparticles for drug delivery, Mater. Chem. Phys. 211 (2018) 34–41.
[17] I. Saeedi, P. Hashemi, Z. Ramezani, A. Badiei, Dendrimer grafted nanoporous silica as a new coating for headspace solid-phase microextraction fibers, Anal. Methods 7 (2015) 10185–10191.
[18] X. Wu, L. Luo, Z. Chen, K. Liang, Xiongzhi Wu, et al., Syntheses, characterization and adsorption properties for Pb2+ of silica-gel functionalized by dendrimer-like polyamidoamine and 5-sulfosalicylic acid, Appl. Surf. Sci. 364 (2016) 86–95.
[19] R. Qu, Y. Niu, C. Sun, C. Ji, C. Wang, G. Cheng, Syntheses, characterization, and adsorption properties for metal ions of silica-gel functionalized by ester-and amino-terminated dendrimer-like polyamidoamine polimer, Microporous Mesoporous Mater. 97 (2006) 58–65.
[20] R. Qu, Y. Niu, J. Liu, C. Sun, Y. Zhang, H. Chen, C. Ji, Adsorption and desorption behaviors of Pd (II) on silica-gel functionalized with ester-and amino-terminated dendrimer-like polyamidoamine polymers, React. Funct. Polym. 68 (2008) 1272–1280.
[21] C.H. Yen, H.L. Lien, J.S. Chung, H.D. Yeh, Adsorption of precious metals in water by dendrimer modified magnetic nanoparticles, J. Hazard. Mater. 322 (2017) 215–222.
[22] Y. Jiang, Q. Gao, H. Yu, Y. Chen, F. Deng, Intensively competitive adsorption for heavy metal ions by PAMAM-SBA-15 and EDTA-PAMAM-SBA-15 inorganic–organic hybrid materials, Microporous Mesoporous Mater. 103 (2007) 316–324.
[23] R. Qu, X. Ma, M. Wang, C. Sun, X. Sun, S. Sun, Y. Zhang, P. Yin, Homogeneous preparation of polyamidoamine grafted silica gels and their adsorption properties as Au3 + adsorbents, J. Ind. Eng. Chem. 20 (2014) 4382–4392.
[24] R. Qu, C. Sun, F. Ma, Z. Cui, Y. Zhang, X. Sun, C. Ji, C. Wang, P. Yin, Adsorption kinetics and equilibrium of copper from ethanol fuel on silica-gel functionalized with amino-terminated dendrimer-like polyamidoamine polymers, Fuel 92 (2012) 204–210.
[25] X. Song, Y. Niu, Z. Qiu, Z. Zhang, Y. Zhou, J. Zhao, H. Chen, Adsorption of Hg (II) and Ag (I) from fuel ethanol by silica gel supported sulfur-containing PAMAM dendrimers: kinetics, equilibrium and thermodynamics, Fuel 206 (2017) 80–88.
[26] J. Bu, R. Li, C.W. Quah, K.J. Carpenter, Propagation of PAMAM dendrons on silica gel: a study on the reaction kinetics, Macromolecules 37 (2004) 6687–6694.
[27] C. Zhang, P. Su, M.U. Farooq, Y. Yang, X. Gao, E. Hongjun, Synthesis of polyamidoamine dendrimer-grafted silica with microwave assisted protocol, React. Funct. Polym. 70 (2010) 129–133.
[28] D.A. Tomalia, H. Baker, J. Dewald, M. Hall, G. Kallos, S. Martin, J. Roeck, J. Ryder, P. Smith, A new class of polymers: starburst-dendritic macromolecules, Polym. J. 17 (1985) 117–132.
[29] N. Oddone, A.I. Zambrana, M. Tassano, W. Porcal, P. Cabral, J.C. Benech, Cell uptake mechanisms of PAMAM G4-FITC dendrimer in human myometrial cells, J. Nanopart. Res. 15 (2013) 1776–1789.
[30] N. Tsubokawa, H. Ichioka, T. Satoh, S. Hayashi, K. Fujiki, Grafting of 'dendrimer-like' highly branched polymer onto ultrafine silica surface, React. Funct. Polym. 37 (1998) 75–82.
[31] P.K. Maiti, T. Cagin, G. Wang, W.A. Goddard, Structure of PAMAM dendrimers: generations 1 through 11, Macromolecules 37 (2004) 6236–6254.
[32] Y. Niu, R. Qu, H. Chen, L. Mu, X. Liu, T. Wang, Y. Zheng, C. Sun, Synthesis of silica gel supported salicylaldehyde modified PAMAM dendrimers for the effective removal of Hg (II) from aqueous solution, J. Hazard. Mater. 278 (2014) 267–278.
[33] N. Ayawei, A.N. Ebelegi, D. Wankasi, Modelling and interpretation of adsorption isotherms, J. Chem. 2017 (2017).
[34] K.Y. Foo, B.H. Hameed, Insights into the modeling of adsorption isotherm systems, Chem. Eng. J. 156 (2010) 2–10.
[35] M. Kumar, R. Tamilarasan, Kinetics, equilibrium data and modeling studies for the sorption of chromium by Prosopis juliflora bark carbon, Arab. J. Chem. 10 (2017) 1567–1577.
[36] Y. Niu, R. Qu, C. Sun, C. Wang, H. Chen, C. Ji, Y. Zhang, X. Shao, F. Bu, Adsorption of Pb (II) from aqueous solution by silica-gel supported hyperbranched polyamidoamine dendrimers, J. Hazard. Mater. 244-245 (2013) 276–286.
[37] Y. Yuan, G. Zhang, Y. Li, G. Zhang, F. Zhang, X. Fan, Poly(amidoamine) modified grapheme oxide as an efficient adsorbent for heavy metal ions, Polym. Chem. 4 (2013) 2164–2167.
[38] F. Zhang, B. Wang, S. He, R. Man, Preparation of graphene-oxide/polyamidoamine dendrimers and their adsorption properties toward some heavy metal ions, J. Chem. Eng. Data 59 (2014) 1719–1726.
[39] W. Peng, Z. Xie, G. Cheng, L. Shi, Y. Zhang, Amino-functionalized adsorbent prepared by means of cu(II) imprinted method and its selective removal of copper from aqueous solutions, J. Hazard. Mater. 294 (2015) 9–16.
[40] X. Tang, Q. Zhang, Z. Liu, K. Pan, Y. Dong, Y. Li, Removal of Cu(II) by loofah fibers as a natural and low-cost adsorbent from aqueous solutions, J. Mol. Liq. 199 (2014) 401–407.
[41] B. Hayati, A. Maleki, F. Najafi, H. Daraei, F. Gharibi, G. McKay, Adsorption of Pb2+, Ni2+, Cu2+, Co2+ metal ions from aqueous solution by PPI/SiO2 as new high performance adsorbent: preparation, characterization, isotherm, kinetic, thermodynamic studies, J. Mol. Liq. 237 (2017) 428–436.
[42] H. Qiu, L. Lv, B. Pan, Q. Zhang, W. Zhang, Q. Zhang, Critical review in adsorption kinetic models, J. Zhejiang Univ. Sci. A 10 (2009) 716–724.

**1. Structures of utilized amines**

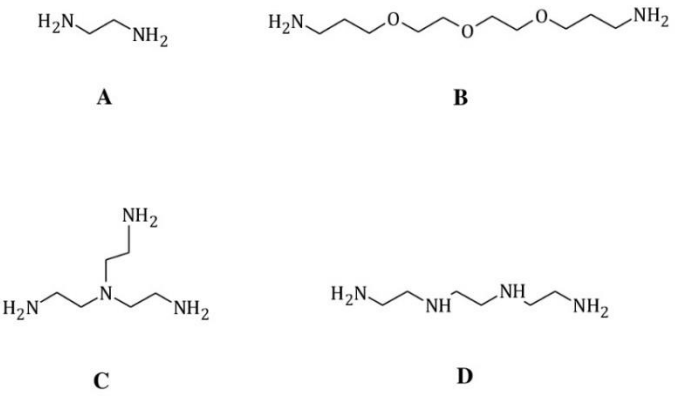


Figure A.1. Structures of: (**A**) ethylenediamine, (**B**) 4,7,10-trioxa-1,13-tridecanediamine, (**C**) tris(2-aminoethyl)amine and (**D**) triethylenetetramine.

**2. The $^{1}$H-NMR spectra of synthesized dendrimers**

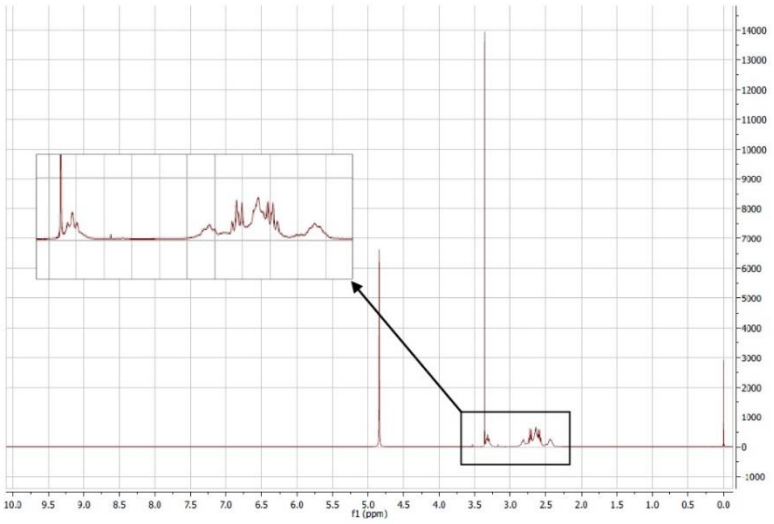

Figure A.2a. $^{1}$H-NMR spectrum of dendrimer containing tris(2-aminoethyl)amine as amino-terminal component

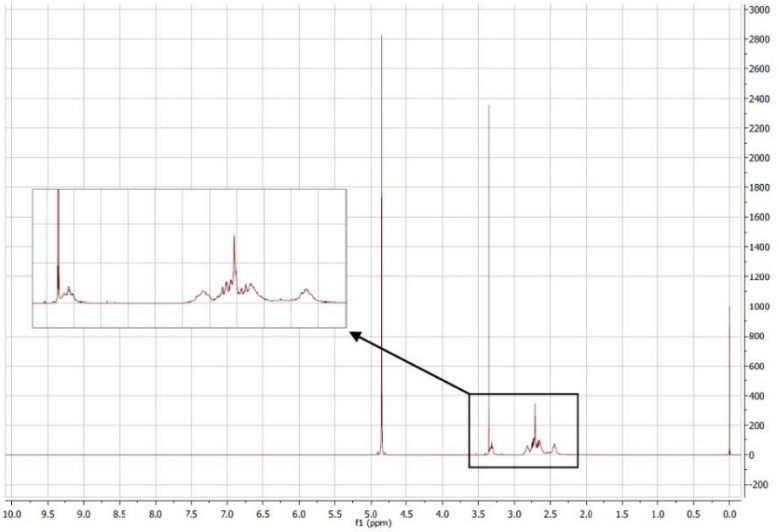


Figure A.2b. $^{1}$H-NMR spectrum of dendrimer containing triethylenetetramine as amino-terminal component

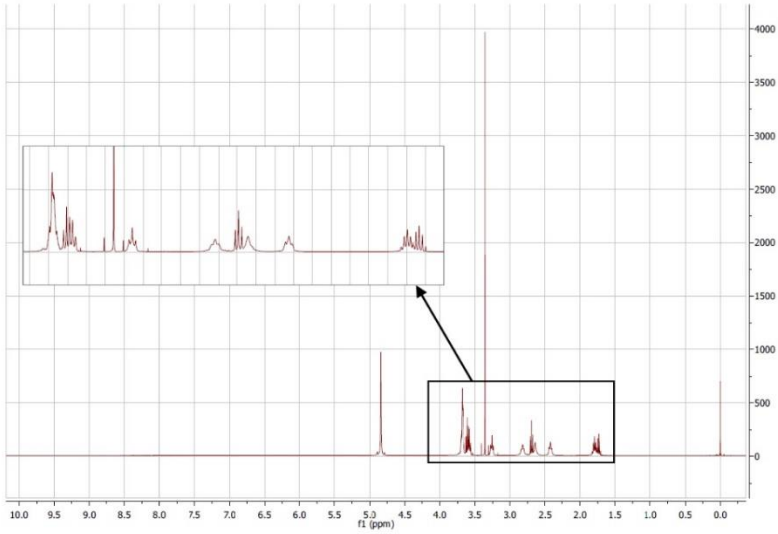


Figure A.2c. $^{1}$H-NMR spectrum of dendrimer containing 4,7,10-trioxa-1,13-tridecanediamine as amino-terminal component

**3. The $^{13}$C-NMR spectra of synthesized dendrimers**

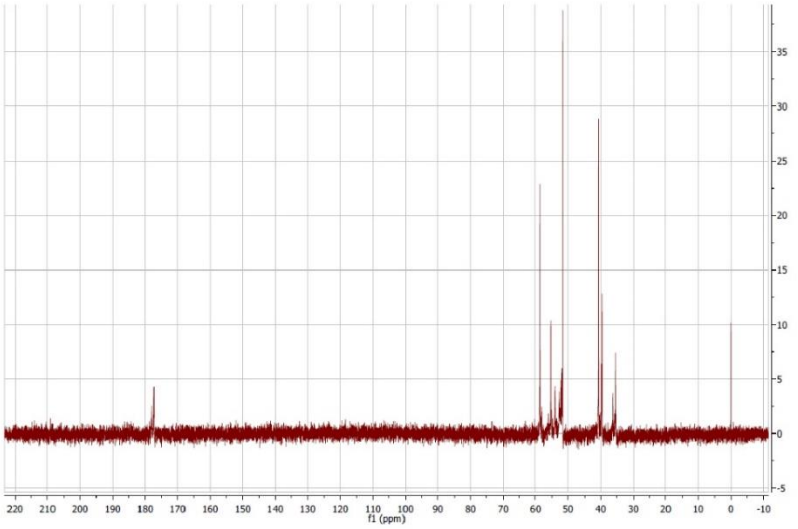


Figure A.3a. $^{13}$C-NMR spectrum of dendrimer containing tris(2-aminoethyl)amine as amino-terminal component

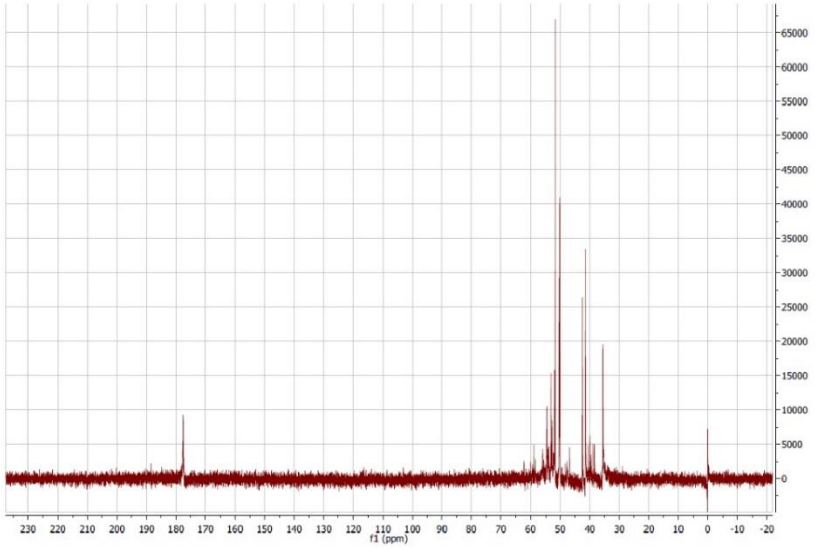


Figure A.3b. $^{13}$C-NMR spectrum of dendrimer containing triethylenetetramine as amino-terminal component

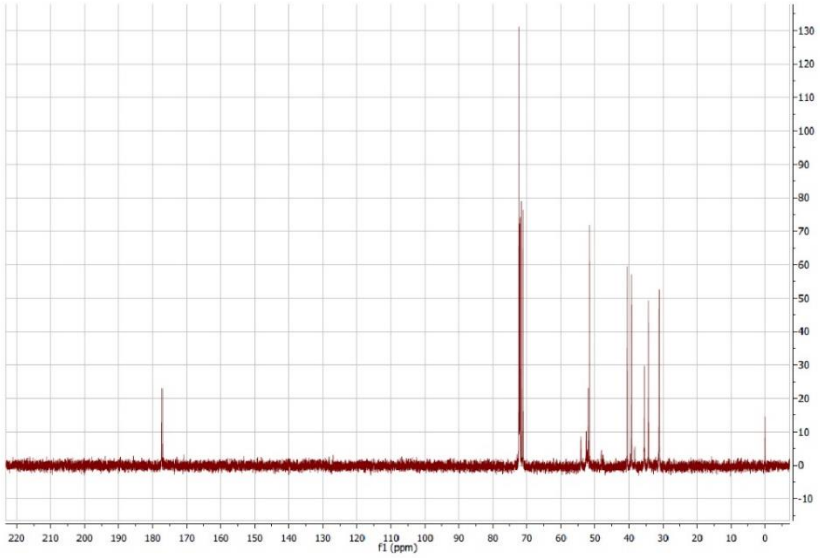


Figure A.3c. $^{13}$C-NMR spectrum of dendrimer containing 4,7,10-trioxa-1,13-tridecanediamine as amino-terminal component

**4. The ESI-MS spectra of synthesized dendrimers**

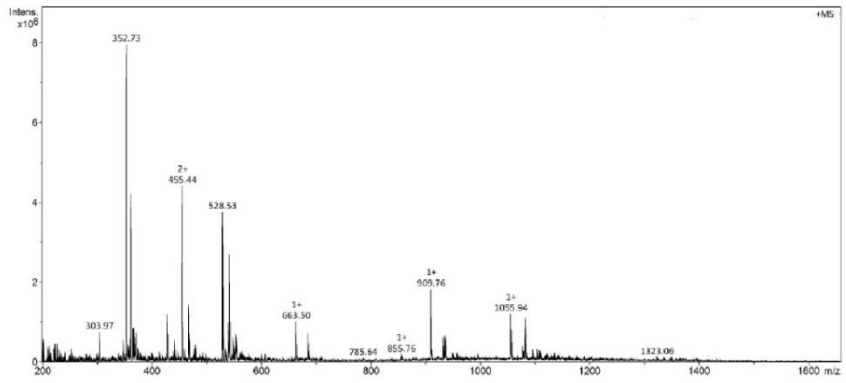


Figure A.4a. ESI-MS positive spectrum of dendrimer containing tris(2-aminoethyl)amine as amino-terminal component

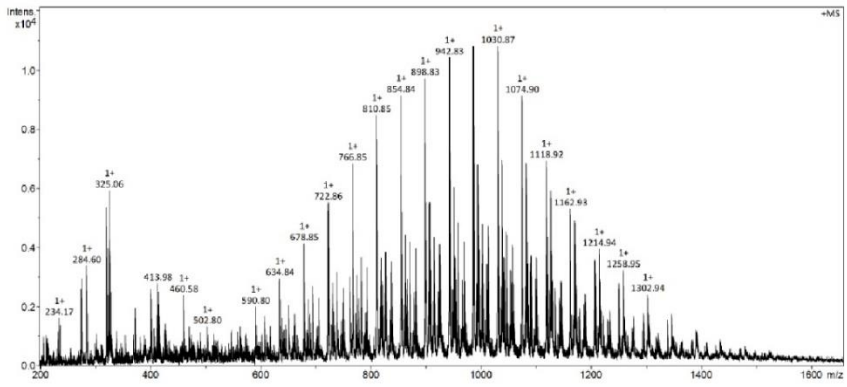


Figure A.4b. ESI-MS positive spectrum of dendrimer containing triethylenetetramine as amino-terminal component

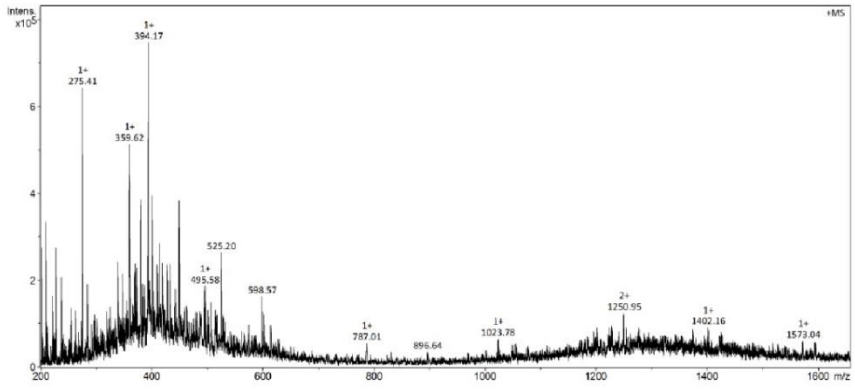


Figure A.4c. ESI-MS positive spectrum of dendrimer containing 4,7,10-trioxa-1,13-tridecanediamine as amino-terminal component

**5. The Langmuir and Freundlich isotherms for adsorption of $Cu^{2+}$ ions on $SiO_2$-dendrimer hybrid materials**

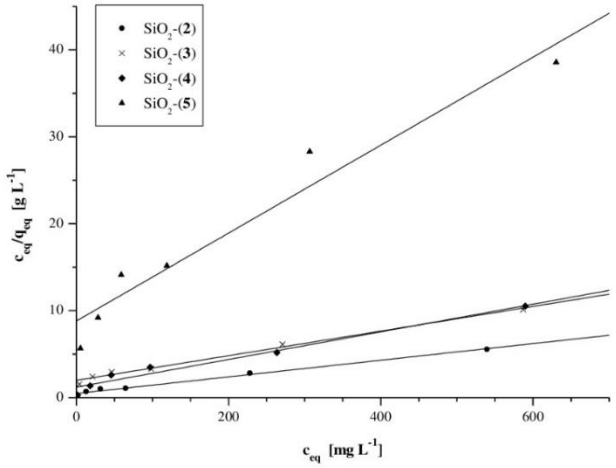


Figure A.5a. Langmuir isotherms for adsorption of $Cu^{2+}$ ions on $SiO_2$-dendrimer hybrid materials

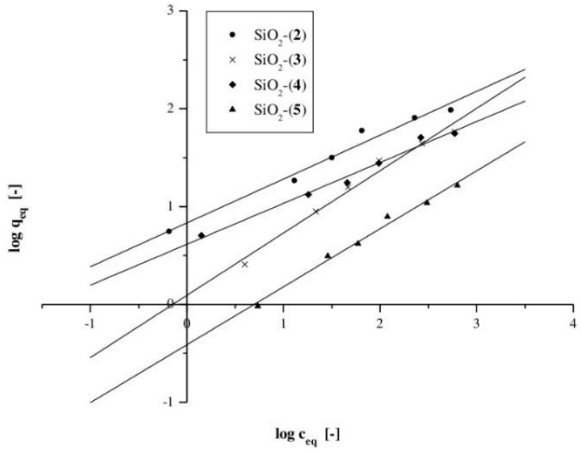


Figure A.5b. Freundlich isotherms for adsorption of $Cu^{2+}$ ions on $SiO_2$-dendrimer hybrid materials

**6. Kinetic plots depicting nonlinear pseudo-first-order model and pseudo-second-order models for adsorption of $Cu^{2+}$ ions on $SiO_2$-dendrimer hybrid materials**

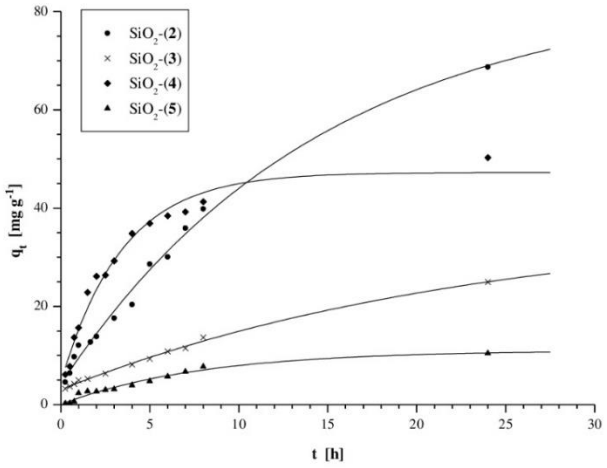


Figure A.6a. Nonlinear plot of pseudo-first-order kinetics for adsorption of $Cu^{2+}$ ions on $SiO_2$-dendrimer hybrid materials

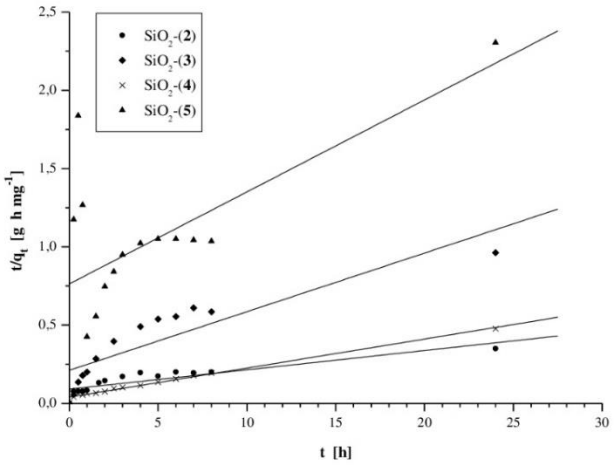


Figure A.6b. Pseudo-second-order kinetic plot for adsorption of $Cu^{2+}$ ions on $SiO_2$-dendrimer hybrid materials

SOLVENT EXTRACTION AND ION EXCHANGE
https://doi.org/10.1080/07366299.2020.1766742

Taylor & Francis
Taylor & Francis Group

Check for updates

# Efficient Removal of Ni(II) and Co(II) Ions from Aqueous Solutions Using Silica-based Hybrid Materials Functionalized with PAMAM Dendrimers

Mateusz Pawlaczyk and Grzegorz Schroeder

Faculty of Chemistry, Adam Mickiewicz University in Poznań, Poznań, Poland

**ABSTRACT**

Many techniques of metal ions removal have been already implemented; however, there is still need for novel, efficient, and non-toxic adsorbents dedicated to heavy metals. In a recent study, the adsorptive properties of four hybrid materials consisting of silica platform surface grafted with poly(amidoamine) dendrimers (PAMAM) with different amino-terminal components, toward two heavy metal ions: Ni(II) and Co(II), were examined. The materials showed maximal scavenging properties at pH 5.4. To determine the adsorptive nature of the hybrid materials, experimental isotherms were fitted by the Langmuir, the Freundlich, and the Dubinin–Radushkevich models. All materials exhibited adsorption capability best described by the Langmuir model. The calculated adsorption capacities $q_m$ ranged between 86.7 and 116.6 mg $g^{-1}$ for Ni(II) ions and 32.8 and 101.1 mg $g^{-1}$ for Co(II) ions, which strictly indicate the influence of grafting agent structure on adsorptive properties of hybrid materials. The values of mean free energy $E$ and adsorption enthalpy $\Delta H°$ jointly indicated the physical nature of adsorption processes. From the thermodynamic studies, the values of $\Delta H°$, $\Delta S°$, and $\Delta G°$ were obtained, indicating the spontaneous and endothermic character of investigated Ni(II)/Co(II) metal ions adsorption process on $SiO_2$–dendrimer hybrid materials. Moreover, the materials exhibited selectivity toward Ni(II) ions.

**KEYWORDS**

Hybrid materials; PAMAM dendrimers; heavy metal ions; adsorption; scavengers

## Introduction

Increasing industrialization and a positive rate of natural increase have the greatest impact on contamination of the natural environment with heavy metals, which come mostly from metallurgical industry, combustion of contaminated fuels, batteries manufacturers, and chemical or electroplating industries.[1] The main concern about the appearance of cadmium(II), mercury(II), copper(II), nickel(II), cobalt(II), and lead(II) ions in the environment is connected with their non-degradability and high toxicity. Once absorbed into the soil, they enter the food chain including plants, animals, and humans. Although, the acute metal ions poisoning is very rare, permanent accumulation of the metal ions present even at trace concentrations may lead to many diseases triggered by e.g. kidney, liver, nervous, and circulatory systems or even brain damages.[1,2] Hence, incorporation of novel, efficient, low-cost, time, and energy efficient methods for the removal of heavy metals has become a high priority for environmental protection research.

Up to now, many techniques for removal of heavy metal ions from water samples have been proposed. They employ precipitation of metal hydroxides or sulfides, electrocoagulation, membrane filtration, electrodialysis, and photocatalysis.[3–11] However, a significant attention is paid to

**CONTACT** Mateusz Pawlaczyk mateusz.pawlaczyk@amu.edu.pl Faculty of Chemistry, Adam Mickiewicz University in Poznań, Uniwersytetu Poznańskiego 8, Poznań 61-614, Poland

The supplemental data for this article can be accessed here.

the use of various novel and non-toxic adsorbents, including such systems as industrial wastes (fly ash, scoria, sludge, etc.),[12–14] modified metal oxides nanoparticles,[15–19] metal-organic frameworks,[20,21] and also natural materials or biomass.[22–26] Furthermore, the most numerous group of efficient adsorbents are hybrid materials, which can be classified as the materials combining a solid platform (silica-gel, titania, carbon nanotubes, metal surface, halloysite nanotubes, polymeric resins, biopolymers, etc.) with various organic structures such as chelating agents, Schiff's bases, surfactants, carboxylic acids, sugar, and protein domains or dendrimers, leading to highly efficient, easily separable, easily accessible and relatively cheap adsorbents, finding application in removal of heavy metals, organic dyes and organic toxins.[27–31]

A highly interesting group of adsorbents dedicated mostly for the removal of toxic metal ions is ion-exchange resins, which are cross-linked polymeric chains with covalently attached functional groups affording binding of particular ionic entities through electrostatic interactions or coordination.[32,33] The most extensively used monomer for ion-exchange resins synthesis is polystyrene (PS), undergoing cross-linking process using divinylbenzene (DVB), while attached surface groups are usually sulphonic residue and iminodiacetic acid (IDA) moiety. An ion exchange between $H^+/Na^+$ ions on virgin resin and metal ions in a solution is provided by electrostatic interaction between sulphonic group and metal cations, while IDA moieties may interact with metal cations through electrostatic interaction afforded with two carboxylate groups and coordination by nitrogen lone pair electrons. There is a plethora of commercially available resins including various types of Dowex®, Amberlite®, Purolite®, Ceralite® or Lewatit® resins, varying in matrix type, functional groups type (weak/strong acidic or basic groups), exchange capacity, size, range of operating pH and temperature, and particle size.[34] Nevertheless, many attempts of toxic metals adsorption studies using ion exchangers have been conducted. Several virgin resins have been tested for their adsorptive properties toward metal ion pollutants, achieving satisfactory results at 111, 66, and 42 mg $g^{-1}$ for Zn(II), Cu(II), and Ni(II), respectively, or >95% removal of Co(II), Ni(II), and Cr(III) after 100 minutes of contact time.[35–38] Also, Lewitat® TP 207 resin containing IDA pendant groups has been studied for its capability of Fe(II) ion recovery from the Fenton's treatment of winery effluent at the level of 63 mg $g^{-1}$.[39]

To improve the rate of ion exchange, several modification of bare resins were introduced, such as dispersing of iron(III) oxide nanoparticles or polyethyleneimine clusters within resin matrix, and surface modification with Crystal Violet dye, di(2-ethylhexyl)phosphoric acid (D2EHPA), aminomethylphosphoric acid, L-methionine or *N*-methylglucamine.[40–46] The dispersion of metal ion binding enhancing agents elevated Mn(II), Cr(VI), and Cu(II) adsorption capacity to 831, 29, and 99 mg $g^{-1}$, respectively, while surface functionalization enhanced Co(II), Ni(II), and Cu(II) binding with final adsorption efficiencies of 167, 83, and 71 mg $g^{-1}$, respectively. Moreover, in order to assess the ion exchange resins' utility as purifying materials of industrial wastewaters, there is a need for adsorption experiments implementing the fixed-bed method. For instance, a resin containing sulphonic pendant groups was utilized as column fillings for purification of Pb(II), Ni(II), and Zn(II) aqueous solution.[47] The study revealed the adsorption capacity values of 100, 12, and 15 mg $g^{-1}$ for given ions, respectively. Also, two resins with the same $-SO_3^-$ surface groups were demonstrated to achieve 97% removal of Ni(II) from real wastewater samples, as well as for high adsorption capacity of ciprofloxacin (a basic antibacterial therapeutic containing piperazine ring in its structure) ranging between 410 and 497 mg $g^{-1}$, highly depending on a concentration of HCl as regenerating agent used.[48,49] Such efficiently adsorbing polymeric systems also found application in removal of toxic metal complexes with 1-hydroxyethylene-1,1-diphosphonic acid (HEDP; a detergents' component) or tetrasodium salt of *N,N*-bis(carboxymethyl)glutamic acid, as materials for $Cl^-$, $NO_3^-$, $SO_4^{2-}$, $[Fe(CN)_6]^{3-}$, $[Fe(CN)_6]^{4-}$ anions or ammonia removal, as well as tasteless carriers of Fe(II) ions dedicated for children with ferrous ion deficiency.[50–55]

Another interesting group of materials finding application especially in toxic metal ions removal are ion-imprinted polymers (IIP) and cross-linked biopolymers with possible ion imprinting. A technique of ion imprinting allows for creating of selective recognition cavities

using a particular ion as a template molecule which is accessible for both synthetic and biological polymers. The selectivity is strictly connected with size, charge, and coordination chemistry of the target ion.[56] For example, a polymer obtained using 2-hydroxyethylmethacrylate, complex of Ni-vinylbenzoate and ethylene glycol dimethacrylate (EGDMA) exhibited high adsorption capacity toward Ni(II) ions of 89 mg $g^{-1}$ and high selectivity toward Zn(II), Cu(II), and Co(II) ions.[57] The ion-imprinting technique also was introduced during chitosan cross-polymerization with glutaraldehyde, epichlorohydrin, aminobenzaldehyde or anthranilic acid-glutaraldehyde Schiff's base. Obtained chitosan-based IIP exhibited efficient adsorption capacities toward particular ions, good selectivity coefficients, and high reusability.[58–61] On the other hand, non-imprinted cross-linked biopolymers may be highly adsorbing materials toward metal ions; however, their selectivity coefficients decrease, as a consequence of the absence of a templating ion. Nevertheless, chitosan cross-linked by 2-aminopyridine-glyoxal Schiff's base was confirmed for adsorption of Cu(II), Ni(II), and Cd(II) ions with maximal rates of 124, 67, and 87 mg $g^{-1}$, respectively, while magnetite nanoparticles encapsulated in cross-linked chitosan by diacetylmonoxie was proved for 95, 65, and 47 mg $g^{-1}$ adsorption capacities toward Cu(II), Co(II), and Ni(II) ions, respectively.[62,63] Moreover, lignosulfonate condensed with 5-hydroxymethylfurfural gave an efficient biopolymer-based adsorbent dedicated toward Cu(II), Pb(II), Ni(II), Cd(II), and Cr(III) ions.[64]

Classical inorganic–organic hybrid materials based on inorganic supporter surface functionalized with organic residues may be represented by silica particles grafted with poly(amidoamine) (PAMAM) dendrimers. This kind of highly-branched, symmetric macromolecules built of amine core surrounded by amido-amine branches (dendrons), usually with repetitive building blocks, is one of the most extensively explored dendritic families. A synthetic protocol involves repetitive Michael addition of methyl acrylate to terminal amine groups and its subsequent amidation using an appropriate amino-functional group, leading to multiple branching levels, called generation G*n*, which equals the number of Michael addition-amidation cycles. For amino-terminated dendrimers *n* takes the value 1, 2, 3, etc., while for ester-terminated 0.5, 1.5, 2.5, etc. The structural features of PAMAM dendrimers, which are the numerous amide and primary amine groups, afford the capability of various molecules binding. Immobilization of poly(amidoamine) dendrimers on a solid support does not alter the binding effectiveness of bare dendrimers, which leads to a versatility of the PAMAM-functionalized materials analytical applications.

There are two synthetic approaches for functionalization of supporter surface with dendrimers: (1) 'grafting from' approach, which is based on the repetitive Michael addition and an amidation step performed on the surface amine-functionalized supporter particles; and (2) 'grafting to' approach, which is based on the anchoring of a ready-made dendrimer to the supporter surface via isocyanate-, glycidoxy- or chloro-terminated linker. Although the 'grafting from' approach is a less demanding solid-phase synthesis, it leads to a formation of the materials functionalized with dendrimer-like structures (PAMAM dendrons); using 'grafting to' approach the fully dendritic character of grafting agent is maintained. No matter which synthetic approach used, host–guest complexes between this kind of dendrimers on the material surface and particular analytes may be formed via three different interaction models: (a) electrostatic interactions between protonated terminal primary amine groups and acidic analytes, such as simple and complex anions, acidic biocompounds, acidic dyes, or nucleic acids; (b) chelation of metal cations via coordination through amide -NH-C(O)- and amine NH-$R_2$ (R = C, H) groups by polydentate coordination; (c) cation exchange between weak acid iminol resonance form of amide bond (O=C-N(H)-R ↔ $^-$O-C=N$^+$(H)-R) and cationic species. Accordingly, PAMAM-functionalized hybrid materials may be applied as generally described sorbents, including solid-phase extraction systems dedicated to various analytes such as organic solvents residues in edible oils, phenol and its chloro-derivatives or immunoextraction of male human hormones present in urine samples, metal cations and organic dyes pre-concentration tools, drug and gene delivery platforms, catalysts of various chemical reactions, or column chromatography fillings.[65–72]

Interestingly, biomedical application of non- or slightly *in vivo* toxic silica particles with immobilized PAMAM dendrimers with varying generation, i.e. branching level, is based on the adsorption of bioactive agents through electrostatic interactions with their further release under paraphysiological conditions. For example, silica nanoparticles grafted with APTES as a linker and PAMAM dendrimers with generation varying between G0 and G3 were tested for their adsorptive properties toward model drug – curcumin.[73] The materials showed curcumin loading efficiency at 31.3%, while its release in slightly acidic solution with pH 5.0 reached 40% in 24 hours. Also, a similar material was tested for its binding efficiency toward diclofenac, ibuprofen and ketoprofen as representatives of barely water-soluble nonsteroidal anti-inflammatory drugs (NSAIDs), which adsorption capacity reached 116, 137, and 127 mg $g^{-1}$, respectively.[74] Moreover, $Fe_3O_4/SiO_2$ components grafted with PAMAM dendrimers varying in branching level and aminocomponents used were applied as platforms for immobilization of *Candida rugosa* lipase.[75] The immobilized enzyme showed 68% of its starting catalytic activity after seven use/regeneration cycles. Also, the highly basic character of PAMAM dendrimers, owing to the numerous primary amine surface groups, affords their easy tunability. Therefore, incorporation of different residues, e.g. RGD-peptide as targeting peptide domain, folic acid as targeting molecule toward its over-expressed receptors on a surface of cancer cells, *N*-diazeniumdiolate residue as NO-release precursor, FITC (fluorescein isothiocyanate) as labeling agent and other various adsorption enhancing molecules, is easily accessible and economical.[76–79]

Thanks to many beneficial properties, which include high thermal and mechanical stability, simplicity in separation and storage, and non-dissociative character, the silica-poly(amidoamine) dendrimer hybrid materials have found broad application as adsorbents dedicated especially to heavy metal ions. A pioneer of metal ions adsorption on poly(amidoamine) dendrons-grafted silica materials, synthesized via 'grafting from' approach, is Qu, who conducted one of the first studies aiming to investigate adsorptive properties of either amino- or ester-terminated materials toward noble and base metals ions.[80] The comprehensive study permitted determination of the materials' saturated adsorption capacities toward noble metals ions: Au(III), Pd(II), Pt(IV), and Ag(I), and basic metals ions: Cu(II), Zn(II), Hg(II), and Cd(II) in their aqueous solutions. The main conclusion indicated that the binding affinities depended on differences between complexation constants of ester-metal ion and amine-metal ion, and the size of solvation layer of particular ions (some of them might exist as polyatomic ions). It is evident that a metal ion's ability to disperse within the dendritic matrix diminishes with increasing size, thus lowering the adsorption capacity. These results have prompted the exploration of binding capability of silica-dendrimer hybrid materials toward various metal ions. A series of ethylenediamine-containing G0.0-G4.0 PAMAM-grafted silica materials has been described as efficient adsorbents toward Mn(II), Cd(II), Pb(II), Pd(II), and Cr(III) ions from their aqueous solutions, which were evaluated for 0.78, 1.18, 0.80, 1.01, and 0.78 mmol $g^{-1}$ maximal adsorption capacities, respectively, highlighting differences between sorption capability of amine- and ester-terminated materials.[81–85] Another study concerned the dependence of materials' adsorptive properties on the amine used. Au(III) ions were tested for their adsorption on the materials containing diethylenetriamine (DETA) or triethylenetetramine (TETA) as terminal amine, reaching high adsorption capacities at the level of 1.97 and 2.18 mmol $g^{-1}$, respectively.[86,87] The observed very high adsorption rate has been proved established as resulting from the electrostatic interaction between highly basic PAMAM dendrimers and $AuCl_4^-$ ions – complex anions of Au(III) in aqueous solutions. The same conclusion was observed for the adsorption experiments of these ions on the materials grafted with G1–G3 dendrimers containing classic ethylenediamine component, which gave maximal adsorption capacity at 2.45 mmol $g^{-1}$.[88]

Furthermore, heavy metal ions removal is also a necessity for purification of ethanol fuel in order to prevent their emission into environment, but also to prevent their harmful influence on the engine and to avoid undesirable reactions with fuel components. For instance, adsorption of Ni(II), Hg(II), Cu(II), Co(II), and Fe(III) has been performed on $SiO_2$–PAMAM materials with grafted dendrimers of different generations, concluding that the highest adsorption capacity of

0.92, 1.39, 0.97, 1.00, and 0.66 mmol $g^{-1}$, respectively, is reached for less branched G1 and G2 generations.[89–93] Nevertheless, not only aqueous or ethanol solutions are considered to be contaminated with metal ions. In 2018, two reports have been published, whose authors aimed to investigate removal of Fe(III) and Ag(I) ions from *N,N*-dimethylformamide solution and also Cd(II) and Fe(III) ions from dimethyl sulfoxide solutions using silica–PAMAM dendrimer materials. The materials showed the adsorption capacity at 0.62 mmol $g^{-1}$ for both ions in DMF solution, while lower values 0.28 and 0.16 mmol $g^{-1}$ for cadmium and ferric ions, respectively, were achieved in DMSO solution, indicating the influence of solvent on adsorptive properties of synthesized materials.[94,95]

There were also several attempts for enhancing the metal ions adsorption on hybrid materials by a further functionalization of surface-grafted dendrimers. For instance, methyl isothiocyanate (MITC) was incorporated to terminal amine groups of G0-G2 PAMAM-grafted increasing Ag(I) and Hg(II) rate of removal from aqueous and ethanol solutions.[96–99] Moreover, various $SiO_2$–PAMAM functionalized with 5-sulfosalicylic acid, salicylaldehyde, or thiomalic acid were considered to be the effective materials for adsorption of Hg(II), Ag(I), or Pb(II).[100–102] It is interesting to note that there is a very few reports aiming 'grafting to' approach for the obtaining of dendrimer-grafted adsorbents dedicated to Pb(II) and Cu(II) ions.[103,104]

In a recent study, we proposed the synthesis of silica-based hybrid materials modified with PAMAM dendrimers on their surface, using 'grafting-to' synthetic approach, which allowed the maintenance of fully dendritic character of the modifier. Dendrimers containing tris(2-aminoethyl) amine as the amine core and different terminal amino-components were used as grafting agents. The obtained $SiO_2$–PAMAM hybrids were examined as adsorbents toward Ni(II) and Co(II) ions from their aqueous solutions. The choice of these two cations was based on their widespread contamination in metallurgic industries wastewaters, especially during electrogalvanization. Moreover, the structure of PAMAM dendrimers determines their usability as the effective Cu(II) ions scavenger (stability constant of $[Cu(PAMAM)H_4]^{6+}$ system reaches $10^{42}$).[105] Therefore, characterization of dendrimer-functionalized silica-based materials might be essential for designing of novel materials dedicated to various polluting metal ions. To describe the influence of functionalizing the agent's grafting on the adsorptive properties of particular materials, the isothermal, kinetic, and thermodynamic studies were performed. Also, the selectivity of each material toward Ni(II) and Co(II) ions was established.

## Materials and methods

### *Materials*

The silica-gel surface-modified with isocyanate groups ($SiO_2$-NCO) was purchased from SiliCycle Inc. (Quebec, QC, Canada). According to Certificate of Analysis, size of particles ranged between 40 and 63 μm, molecular loading – 1.33 mmol/g, surface coverage – 3.12 μmol/$m^2$ specific, surface area – 482 $m^2$/g, pore diameter – 59 Å, and pore volume – 0.71 ml/g. All purchased reagents and solvents were used without any further purification. Nickel(II) perchlorate hexahydrate $Ni(ClO_4)_2 \times 6H_2O$, cobalt(II) perchlorate hexahydrate $Co(ClO_4)_2 \times 6H_2O$, methyl acrylate, tris(2-aminoethyl)amine, 4,7,10-trioxa-1,13-tridecanediamine, triethylenetetramine, and ethylenediamine were purchased from Sigma-Aldrich (St. Louis, MO, USA). All the commercially available pH buffers (pH 1 and 2: HCl/KCl buffers; pH 3: sodium citrate/$K_2HPO_4$ buffer; pH 4 and 5: AcOH/AcONa buffer; pH 6: $KH_2PO_4/K_2HPO_4$ buffer) were purchased from Eurochem (Tarnow, Poland). Acetic acid was obtained from Chempur (Piekary Slaskie, Poland), sodium acetate trihydrate and dichloromethane (purity grade p.a.) were purchased from Eurochem BGD (Tarnow, Poland). Methanol, diethyl ether, and isopropanol of the purity grade p.a. were obtained from POCH (Gliwice, Poland). Deionized water was used for preparation of all aqueous solutions.

### Instruments

The FT-IR spectra of the silica–PAMAM materials were recorded on a Bruker IFS 66/s spectrometer (Billerica, MA, USA) at the wavelength in the range of 400–4,000 $cm^{-1}$ with resolution set at 2 $cm^{-1}$. The samples were prepared by dilution of 1–1.5 mg of material in KBr. The equilibrium concentrations of metal ions in samples were determined by spectrophotometric measurements, using Agilent 8453 UV-Vis spectrophotometer. The XRF spectra were produced on a PANalytical MiniPal2 X-Ray Fluorescence (XRF) spectrometer equipped with a rhodium X-ray vacuum tube under given conditions: Al-filter used, time of the analysis: 600 s; X-ray tube voltage: 18 kV, and current generated in the electron beam was varying between 318 and 500 μA.

### Synthesis of hybrid materials $SiO_2$–PAMAM

Hybrid materials $SiO_2$-(**1**) – $SiO_2$-(**4**) were obtained by the 'grafting-to' approach reported in our previous study.[104] PAMAM dendrimers containing tris(2-aminoethyl)amine as the amine core were obtained by the two-step synthesis, including the branching step performed by Michael reaction between the amine core and methyl acrylate, and subsequent amidation using four structurally different amines: ethylenediamine, tris(2-aminoethyl)amine, triethylenetetramine, and 4,7,10-trioxa -1,13-tridecaneamine. They were labeled as dendrimers **1, 2, 3**, and **4**, respectively (Figure 1). The

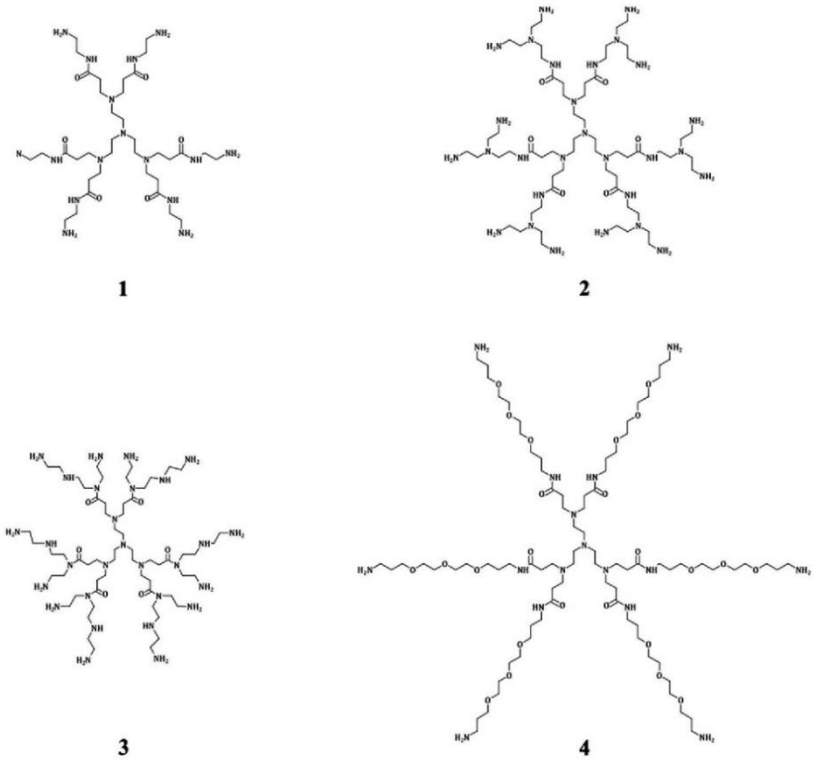


Figure 1. Structures of dendrimers **1–4** used as the grafting agents for the hybrid materials $SiO_2$–dendrimer.

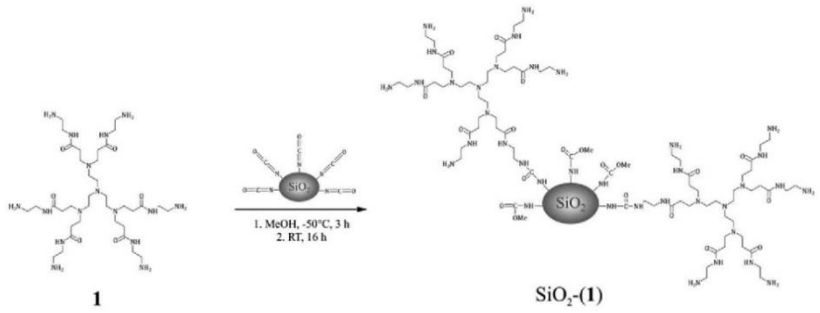


Figure 2. The synthetic route for obtaining of $SiO_2$–dendrimer materials on the example of $SiO_2$-(**1**) material.

obtained dendrimers were introduced onto silica surface by the reaction between terminal free amine groups of the dendrimers and isocyanate groups anchored to the silica-gel (Figure 2).

## Adsorption experiments

### Influence of pH on adsorptive properties

To investigate an influence of pH on the Ni(II) and Co(II) adsorption processes on the hybrid materials, the general following procedure was adopted: 10 mg of material was immersed into 10 mL of Ni(II)/Co(II) 15 mM solution in commercially available buffer solutions with pH at 1, 2, 3, 4, 5 and 6, and also prepared acetic acid/sodium acetate buffer solution at pH 5.4. The mixtures were shaken for 24 h at room temperature. Afterwards, the adsorptive materials were filtered off and the equilibrium concentrations of Ni(II) or Co(II) ions in solutions $c_{eq}$ [mg $L^{-1}$] were determined using spectrophotometric measurements, at 393 nm or 513 nm, respectively. The amounts of the metals adsorbed $q_{eq}$ [mg $g^{-1}$] were calculated using the following equation:

$$q_{eq} = \frac{(c_0 - c_{eq}) \cdot V}{m}$$

where: $c_0$ – the initial metal ions concentration [mg $L^{-1}$]; $m$ – the mass of the hybrid material sample [mg]; $V$ – the volume of ions solution [mL].

### Adsorption isotherms

To prepare stock solutions of both metal ions, 2.194 g of $Ni(ClO_4)_2 \times 6\ H_2O$ or 2.223 g of $Co(ClO_4)_2 \times 6\ H_2O$ were dissolved in 200 mL of acetic acid/sodium acetate buffer solution at pH 5.4. To prepare each isotherm, 10 mg of $SiO_2$–PAMAM material was immersed into 1, 2, 5, 10, 15, 20, and 30 mM solutions of Ni(II) or Co(II) ions. The mixtures were shaken for 24 h at room temperature. The equilibrium concentration $c_{eq}$ of the metal ions in solutions and the amount of the metal adsorbed $q_{eq}$ were determined in the same manner as described in the previous section.

The experimental data of isothermal studies were fitted to Langmuir and Freundlich isotherm models. The Langmuir model is described by the equation below:

$$\frac{c_{eq}}{q_{eq}} = \frac{c_{eq}}{q_m} + \frac{1}{q_m K_L}$$

where: $q_m$ [mg $g^{-1}$] – the maximal adsorption capacity of a material toward adsorbate; $K_L$ – the Langmuir constant connected with adsorption energy [L $mg^{-1}$]. Langmuir adsorption isotherm model also allows the calculation of a dimensionless separation coefficient $R_L$ [-]:

$$R_L = \frac{1}{1 + K_L c_{max}}$$

where: $c_{max}$ – the maximal starting concentration of the metal ions in the solution investigated for isothermal studies [mg $L^{-1}$]. Experimental data were also fitted to Freundlich adsorption isotherm, which is expressed with the following equation:

$$\log q_{eq} = \log K_F + \frac{1}{n} \log c_{eq}$$

where: $K_F$ – the Freundlich adsorption constant associated with the adsorption capacity [mg $g^{-1}$ (L $mg^{-1})^{1/n}$]; $1/n$ – the empirical constant, which corresponds to the intensity of adsorption process and heterogeneity of adsorbent's surface. Also, in order to determine the physical or chemical character of investigated adsorption processes, the Dubinin–Radushkevich isotherm model was employed, whose linear form is:

$$\ln q_{eq} = \ln q_m - \beta \varepsilon^2$$

where: $\beta$ – the activity coefficient strongly depended on adsorption capacity [$mol^2$ $J^{-2}$], $\varepsilon$ – the Polanyi potential [-], obtainable as $\varepsilon = RT \cdot \ln(1 + 1/c_{eq})$. The calculated $\beta$ values were further used for the calculation of mean free energies, $E$ [kJ $mol^{-1}$] as follows:

$$E = \frac{1}{\sqrt{-2\beta}}$$

### *Adsorption kinetics*

To perform kinetic studies, the general procedure was: 20 mg of $SiO_2$–PAMAM adsorbents was immersed in 20 mL of 15 mM metal ions solutions and shaken at room temperature. At pre-set time intervals, the amount of the metals adsorbed on the materials was determined using the equation given below:

$$q_t = \frac{(c_0 - c_t) \cdot V}{m}$$

where: $q_t$ – the amount of the metal adsorbed at time $t$ [mg $g^{-1}$]; $c_0$ – the initial concentration of metal ions in solution [mg $L^{-1}$]; $c_t$ – the concentration of metal ions in solution after time $t$ [mg $L^{-1}$], $V$ – the volume of added metal ions solutions [mL]; $m$ – the mass of samples [mg].

The pseudo-first-order and pseudo-second-order kinetic models were used for fitting of obtained experimental data. The pseudo-first-order model is described by the following equation:

$$\log(q_e - q_t) = \log q_e - \frac{k_1}{2.303} t$$

where: $q_e$ and $q_t$ – the amount of the metal adsorbed at the equilibrium state and after time $t$, respectively [mg $g^{-1}$]; $k_1$ – the pseudo-first-order kinetics rate constant [$h^{-1}$]. Calculated pseudo-first -order kinetic rate constants $k_1$ [$h^{-1}$] were further used to determine the initial adsorption rate $k_i$ [mg $g^{-1}$ $h^{-1}$] from the equation:

$$k_i = k_1 q_e$$

The linear form of the pseudo-second-order kinetic model is expressed with the following equation:

$$\frac{t}{q_t} = \frac{1}{k_2 q_e^2} + \frac{1}{q_e} t$$

where: $k_2$ – the pseudo-second-order rate constant [g $mg^{-1}$ $h^{-1}$]. The obtained $k_2$ values were also used to determine the pseudo-second-order half-adsorption time $t_{1/2}$ [h] and the initial adsorption rate $k_i$ [mg $g^{-1}$ $h^{-1}$], using the following expressions, respectively:

$$t_{1/2} = \frac{1}{k_2 q_e}$$

$$k_i = k_2 q_e^2$$

### Adsorption thermodynamics

Thermodynamic studies were performed according to the following general procedure, which involved introducing of 5 mg of $SiO_2$–PAMAM adsorbents into 10 mL of 15 mM metal ions solutions. The samples were stirred in aqueous solutions for 24 h at given temperatures: 301 ± 1 K, 313 ± 1 K, and 328 ± 1 K, to reach equilibrium state. The equilibrium amount of the metal ions adsorbed $q_{eq}$ were found in the same way as in the influence of pH studies.

The experimental data were fitted to the equation given below, in order to determine the thermodynamic coefficients:

$$\ln K_d = \frac{\Delta S^\circ}{R} - \frac{\Delta H^\circ}{RT}$$

where: $\Delta S°$ – the standard entropy [J mol$^{-1}$ K$^{-1}$]; $\Delta H°$ – the standard enthalpy [kJ mol$^{-1}$]; $T$ – the solution temperature [K]; $R$ – the universal gas constant (8.314 J mol$^{-1}$ K$^{-1}$); $K_d$ – the distribution coefficient which corresponded to the ratio of the amount of the metal adsorbed $c_{Ae}$ [mg g$^{-1}$] and the metal concentration that remained in the solution after reaching the equilibrium state $c_e$ [mg L$^{-1}$]:

$$K_d = \frac{c_{Ae}}{c_e}$$

The calculated distribution coefficients $K_d$ were also used to find out the standard Gibbs free energies $\Delta G°$ [kJ mol$^{-1}$], according to the equation given below:

$$\Delta G^\circ = -RT \ln K_d$$

### Adsorption selectivity

The determination of adsorption selectivity was based on the adsorption experiment in binary system, i.e. solution containing Ni(II) and Co(II) ions. The general procedure involved immersing of 10 mg of the hybrid materials into 10 mL of solution containing both metal ions at concentration 15 mM. The samples were shaken for 24 h at room temperature. Afterwards, the equilibrium amounts of the metals adsorbed $q_{eq}$ were determined in the same manner as described in the 'Influence of pH on adsorptive properties' section.

## Results and discussion

In 2014, Camarada et al. have postulated that the mechanism of bivalent metal cations binding to poly(amidoamine) dendrimers is based on the tri- or tetradentate coordination through nitrogen atoms of either amine or amide domains, and/or through oxygen atoms of amide domains, to metal ions.[106] Incorporation of additional atoms capable of coordination to metal cations, such as sulfur, may enhance binding abilities of materials functionalized with PAMAM-derivative, which was proved by DFT calculations revealing G1-PAMAM-MITC as a pentadentate ligand coordinating with Hg(II) ions.[98] Therefore, the mechanism of metal adsorption/extraction from their aqueous solution by $SiO_2$ materials grafted with poly(amidoamine) dendrimers may be classified as neutral extraction via coordination of PAMAM-residues to metal cations. Such a phenomenon is known to be counter ion-dependent, thus the choice of metals anions is an important issue having an impact on the adsorption experiments.

Among all the most widely used counter ions of metal cations undergoing adsorption, perchlorate $ClO_4^-$ is the one of the biggest ionic radius of 2.4 Å (while $Cl^-$, $NO_3^-$ and $SO_4^{2-}$ of 1.7, 1.9, and 2.1 Å,

respectively),[107] which low surface charge density in aqueous solutions affects its loosely packed hydration sphere, hindering its diffusion to adsorbing domain, enhancing metal cation adsorption efficiency. Such a phenomenon has been established for a study aiming to establish metal ions extraction of e.g. crown ethers.[108] Therefore, adsorption of Ni(II)/Co(II) ions from their perchlorate salts are not disturbed by PAMAM–anion interactions, which shows minimal tendency to adsorb to materials surface, indicating the affinity of surface dendrimers to the cations. Moreover, perchlorate as metal counter ion in non-volatile and kinetically inert to reduction.[109]

The following study aimed to demonstrate the binding ability of silica-based hybrid materials grafted with different PAMAM dendrimers toward Ni(II) and Co(II) ions, which are highly toxic contaminants of industrial wastewaters. However, there are several factors which may affect the quality of metal ions binding to the hybrid materials, especially the structure of used dendritic grafting agent, but also the contact time and the temperature of adsorbent-adsorbate samples. Thus, comprehensive studies, including isothermal, kinetic, and thermodynamic experiments, were undertaken.

The successful grafting of dendrimers **1**–**4** on silica surface via isocyanate linker was proved by the recorded FT-IR spectra (Figure A.1; SI). Presence of the new signals at around 1,560 and 1,650 $cm^{-1}$ corresponding to the stretching vibration of N–H and C=O motifs of amide groups, respectively, indicating proper functionalization of the silica platform. The amount of the dendrimers anchored to the silica surface were also established, employing a method based on a titration of the excess of hydrochloric acid remaining in the solution after its absorption by the terminal amine groups of the dendrimers, ranging between 0.078 and 0.310 mmol $g^{-1}$ (Table A.1; SI).

### *Influence of solution pH on adsorption process*

Determination of the pH solution influence on adsorptive properties of the hybrid materials is one of the most important parameters, as pH determines the choice of exact environment for further studies, affording the best quality of ions binding to the materials. Figure 3 presents the dependence of the metal ions uptake from samples on the pH of solution used for experiments.

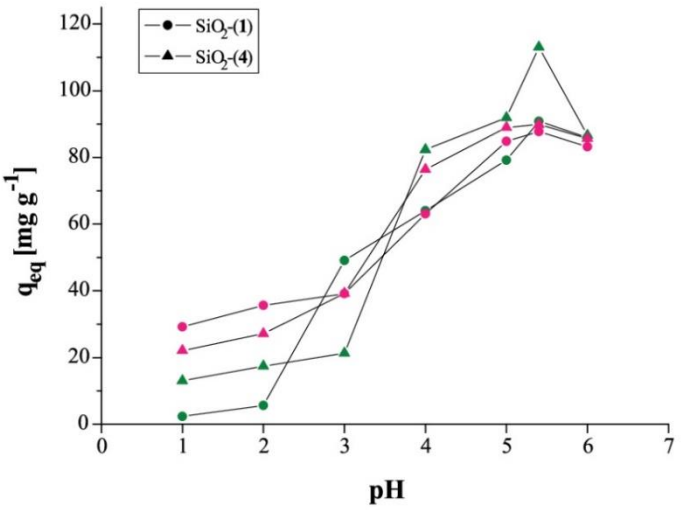


Figure 3. Representation of the influence of solution pH on adsorptive properties of materials $SiO_2$-(**1**) and $SiO_2$-(**4**) toward Ni(II) (green) and Co(II) (pink) ions ($c_0$ = 15 mM).

Common HCl/KCl, AcOH/AcONa, sodium citrate/$K_2HPO_4$, and $KH_2PO_4/K_2HPO_4$ buffers were used. For all the buffers, solutions did not change their pH under presence of Ni(II) and Co(II) salts. The representatives chosen for study were materials $SiO_2$-(**1**) and $SiO_2$-(**4**), functionalized with ethylenediamine- and 4,7,10-trioxa-1,13-tridecanediamine-containing dendrimers, respectively, as they might exhibit the greatest difference of binding abilities in various pH values caused by the structural diversity.

Nevertheless, both materials were found to demonstrate the highest adsorption capacity toward both Ni(II) and Co(II) ions in the solutions buffered to pH 5.4. The main reason of such a phenomenon is the fact that in a strongly acidic environment peripheral amine and internal amide groups exist in their protonated forms ($-NH_3^+$ and $-NH_2^+-$), hindering diffusion of positively charged metal ions into matrices by the repulsive interaction. Furthermore, the competitive binding of protons to surface dendritic domains may appear. On the other hand, in a slightly acidic environment (pH 6.0) metal ions might be inactivated by the formation of unhydrolyzed hydroxides due to the low values of their solubility equilibrium. Therefore, all the following adsorption experiments were conducted in slightly acidic environment at pH 5.4. Under such conditions only internal tertiary amine groups are protonated, while amide and primary amine groups remain in their unaltered form.[105] Thus, the metal ions binding in the materials structure is based on the neutral coordination of outer amine groups to the metal cations, but also on the ionic exchange between $H^+$ ions of protonated tertiary amines and $M^{2+}$ ions driven by ions diffusion, leading to coordination of tertiary amine and oxygen domains to metal cations/proton systems (Figure 4).

### Adsorption isotherms

Analysis of adsorption isotherms allows quantitative investigation of the interactions between a particular adsorbent and solute at the equilibrium state, but also is vital for evaluating the optimal use of the adsorbents. The adsorption capacities of each material toward metal ions are strongly related to the shapes of the isotherms (Figure 5).

To evaluate adsorptive properties of the $SiO_2$–dendrimer hybrid materials, experimental data were analyzed with two most extensively used equilibrium models, the Langmuir and Freundlich. The Langmuir model assumes the homogeneity of adsorbent surface, which is related to equal affinity of each binding site to adsorbate molecules, excluding any interactions or steric hindrance between adsorbed molecules. Therefore, the Langmuir model also assumes the ability for binding only a monolayer of adsorbate.[110] The obtained experimental data were fit to its linear plot of $c_{eq}/q_{eq}$ vs. $c_{eq}$ (Figure 6), which was employed for calculating the Langmuir isotherm parameters collected in Table 1.

The experimental data were also checked to fit the Freundlich isotherm model, which is based on the theory that adsorbent's surface is heterogeneous, thus differs in the values of binding sites

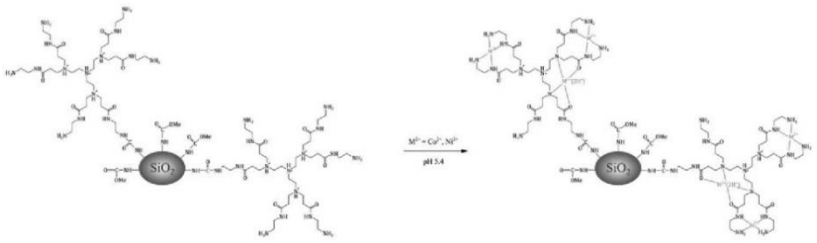


**Figure 4.** Adsorption process of heavy metal ions Ni(II) and Co(II) on $SiO_2$–dendrimer hybrid materials under slightly acidic conditions (pH 5.4).

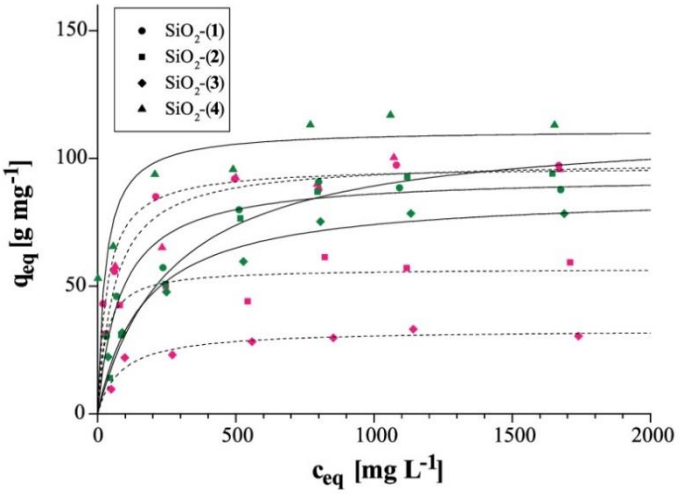


Figure 5. Adsorption isotherms of Ni(II) (green; solid lines) and Co(II) (pink; dashed lines) adsorption on $SiO_2$–dendrimer hybrid materials.

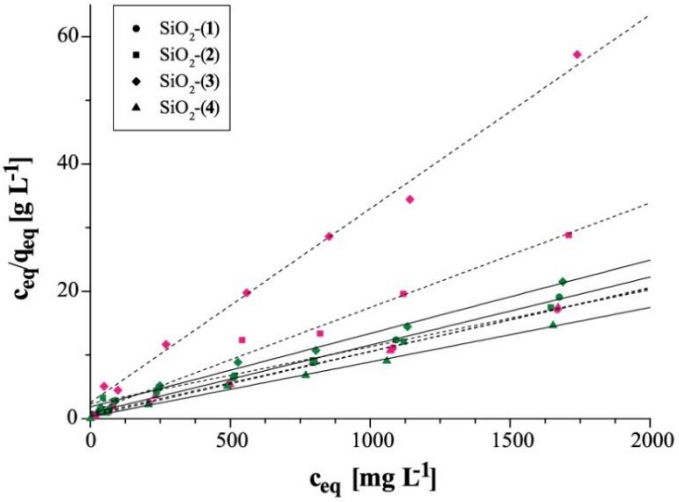


Figure 6. Langmuir isotherms for adsorption of Ni(II) (green; solid lines) and Co(II) (pink; dashed lines) on $SiO_2$–dendrimer hybrid materials.

energies. Therefore, it permits formation of a reversible adsorbate multilayer.[110] All parameters of Freundlich adsorption model for adsorption of metal ions on hybrid materials (Table 1) were calculated from the slope and intercept of the linear plot of *log* $q_{eq}$ vs. *log* $c_{eq}$ (Figure A.2; SI).

The adsorption of Ni(II) and Co(II) ions on each hybrid materials followed strictly the Langmuir isotherm model, reaching $R^2$-values higher than 0.99 (Table 1). It indicates the formation of an adsorbate monolayer on the adsorbents surface. According to the linear plot of

**Table 1.** Isothermal parameters for adsorption of Ni(II) and Co(II) ions on $SiO_2$–dendrimer hybrid materials.

| | | Langmuir isotherm | | | | Freundlich isotherm | | |
|---|---|---|---|---|---|---|---|---|
| Ion | Adsorbent | $K_L$ [L mg$^{-1}$] | $q_m$ [mg g$^{-1}$] | $R_L$ | $R^2$ | $K_F$ [mg g$^{-1}$ (L mg$^{-1}$)$^{1/n}$] | $1/n$ | $R^2$ |
| Ni(II) | $SiO_2$-(**1**) | 0.012 ± 0.004 | 93.6 ± 2.8 | 0.0452 | 0.9956 | 12.95 ± 2.33 | 0.28 ± 0.03 | 0.9436 |
| | $SiO_2$-(**2**) | 0.004 ± 0.001 | 111.7 ± 3.6 | 0.1243 | 0.9949 | 2.58 ± 0.98 | 0.52 ± 0.16 | 0.9298 |
| | $SiO_2$-(**3**) | 0.006 ± 0.001 | 86.7 ± 3.1 | 0.0865 | 0.9936 | 6.55 ± 0.90 | 0.35 ± 0.02 | 0.9792 |
| | $SiO_2$-(**4**) | 0.025 ± 0.015 | 116.6 ± 3.2 | 0.0222 | 0.9962 | 46.49 ± 4.13 | 0.12 ± 0.02 | 0.9275 |
| Co(II) | $SiO_2$-(**1**) | 0.023 ± 0.010 | 99.1 ± 2.0 | 0.0238 | 0.9979 | 26.33 ± 3.92 | 0.19 ± 0.02 | 0.9169 |
| | $SiO_2$-(**2**) | 0.016 ± 0.012 | 60.8 ± 3.1 | 0.0341 | 0.9875 | 20.48 ± 3.68 | 0.15 ± 0.03 | 0.8272 |
| | $SiO_2$-(**3**) | 0.012 ± 0.005 | 32.8 ± 1.2 | 0.0450 | 0.9934 | 4.40 ± 1.82 | 0.28 ± 0.07 | 0.7748 |
| | $SiO_2$-(**4**) | 0.014 ± 0.006 | 101.1 ± 3.0 | 0.0380 | 0.9955 | 15.84 ± 3.88 | 0.26 ± 0.04 | 0.8885 |

Langmuir isotherms, the adsorption capacities $q_m$ of the adsorbents for both ions were calculated. The highest $q_m$ values were obtained for $SiO_2$-(**4**) material grafted with dendrimer containing 4,7,10-trioxa-1,13-tridecanediamine, reaching 116.6 and 101.1 mg g$^{-1}$ for Ni(II) and Co(II), respectively. On the other hand, the lowest $q_m$ values were assigned to $SiO_2$-(**3**) material grafted with dendrimer containing triethylenetetramine, achieving 86.7 mg g$^{-1}$ for Ni(II) and 32.8 mg g$^{-1}$ for Co(II) ions. These results are strongly related to structural differences of terminal amino-components of dendrimers bound to the silica platform. Both triethylenetetramine and 4,7,10-trioxa-1,13-tridecanediamine are long-chained polyamines, however only the latter contains oxygen atoms, which might support interactions between the adsorbent and metal ions. Surprisingly, the material grafted with dendrimer containing the mostly branched tris(2-aminoethyl)amine $SiO_2$-(**2**) exhibited higher affinity toward metal ions (111.7 and 60.8 mg g$^{-1}$ for Ni(II) and Co(II), respectively) than $SiO_2$-(**3**) material, which is related to higher steric hindrance of dendritic component, hindering the elution of adsorbate from adsorbent's matrix.

Moreover, for each material, dimensionless Langmuir separation factors $R_L$ were calculated to define the favorability of adsorption processes. In principle, the adsorption process is either irreversible ($R_L = 0$), favorable ($0 < R_L < 1$), linear ($R_L = 1$) or unfavorable ($R_L > 1$).[111] All calculated data are listed in Table 1. They varied between 0.02 and 0.12, which indicated strong adsorption of metal ions on hybrid materials. Furthermore, on the basis of the obtained data, the distribution coefficients $K_d$ for each material at different metal ions initial concentrations were calculated (Figure 7). In general, the higher the distribution coefficient, the stronger the ability of adsorbent to bind solute in its matrix.[112] For both metal ions, the highest $K_d$ values were calculated for the lowest solutions concentrations. The increase in metals concentrations was accompanied by significant decrease in $K_d$ values. Hence, it may be concluded that the hybrid materials are preferably applicable as Ni(II) and Co(II) scavenging materials in their diluted solutions.

The linear regression analyses of the experimental data for Freundlich isotherm model were defined with considerably lower values of $R^2$ correlation coefficient than those for Langmuir model ($R^2 > 0.92$ for Ni(II) adsorption; $R^2 > 0.82$ for Co(II) adsorption). Nevertheless, on their basis, $1/n$ coefficients (equal to the Freundlich exponents) were calculated, which are strictly dependent on the adsorbent heterogeneity and adsorption efficiency. The lower the $1/n$ value, the more intensive the adsorption process. Table 1 contains the values obtained for all materials, which varied in the range of 0.12–0.52, indicating the efficient binding properties of hybrid materials toward Ni(II) and Co(II) metal ions.

To determine whether the adsorption of metal ions on $SiO_2$–dendrimer materials is a physical or chemical process, the Dubinin–Radushkevich model was employed. On the basis of linear regression $ln\ q_e$ vs. $\varepsilon^2$ (Figure A.3; SI), the values of $\beta$ parameter were calculated and further used for determination of energy values (Table A.2; SI). It is postulated that if value of $E$ energy

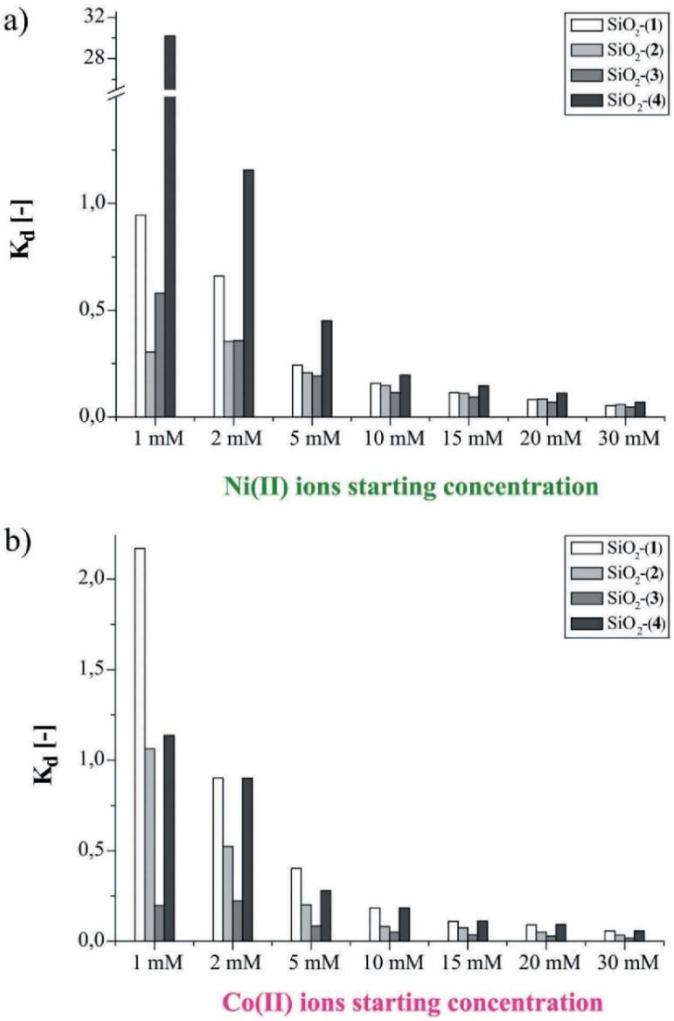


**Figure 7.** The distribution coefficients $K_d$ for each material at different toxic ions starting concentrations: (a) Ni(II), (b) Co(II).

is lower than 8 kJ $mol^{-1}$, the adsorption is a physical process, while if $E$ values range between 8 and 16 kJ $mol^{-1}$, it is a chemical process.[98] Although, the calculated energy values for all materials and metal ions varied between 0.028 and 1.008 kJ $mol^{-1}$, $R^2$ linear regression coefficients are relatively low, with average value of approximately 0.78, making these data only a supposition of physical nature of the investigated adsorption processes.

Moreover, Table 2 presents a comparison of adsorption capacity values reported in literature with these from our study. Among the reported materials there are various weak or strong acidic cation-exchange resins, IIP systems or functionalized biopolymers. It is clearly visible that $SiO_2$–dendrimer materials are very efficient adsorbents toward Ni(II)

**Table 2.** Comparison of the adsorption capacities for other materials reported in literature.

| Adsorbent | Adsorption capacity [mg $g^{-1}$] | | Reference |
|---|---|---|---|
| | Ni(II) | Co(II) | |
| Triethylenetetramine-crosslinked chitosan | | 59.5 | [113] |
| Dowex HCR-S/S cation exchange resin | | 69.0 | [114] |
| IRN 77 cation exchange resin | | 86.2 | [115] |
| SKN 1 cation exchange resin | | 69.4 | [115] |
| Lewitat MonoPlus SP 112 cation exchange resin | | 21.9 | [116] |
| Sodium titanate ($Na_2Ti_3O_5$) nanotubes | | 85.2 | [117] |
| G0.5-G3.0 PAMAM dendrons modified with methyl isothiocyanate grafted to silica | | 60.1 | [92] |
| G0.5-G3.0 PAMAM dendrons grafted to silica | 54.0 | | [89] |
| Spent Coffee Grounds/Calcium Alginate composite beads | 21.0 | | [118] |
| Dowex HCR-S/H cation exchange resin | 87.8 | | [119] |
| Ceralite IR 120 cation exchange resin | 28.6 | | [120] |
| Suqing D401 cation exchange resin | 41.1 | | [33] |
| Ni(II) ion imprinted polymer based on Ni-diphenylcarbazide complex | 86.3 | | [121] |
| $Fe_3O_4$ covered with cross-linked chitosan-isatin resin | 40.2 | 53.5 | [122] |
| Polyimide resins based on 2,5-bis-(amino-pyridine-2-yl)-1,3,4-oxadiazole | 59.7 | 65.6 | [123] |
| Copolymer of methylenebisacrylamide and *N*-methacryloxyphthalimide | 58.7 | 56.0 | [124] |
| Barley straw ash | 8.2 | 6.6 | [125] |
| $SiO_2$-5 G.PPI | 438.0 | 503.0 | [126] |
| Phthalate-functionalized sugarcane bagasse | 54.7 | 33.1 | [127] |
| $SiO_2$-(**1**) | 93.6 | 99.1 | This study |
| $SiO_2$-(**2**) | 111.7 | 60.8 | This study |
| $SiO_2$-(**3**) | 86.7 | 32.8 | This study |
| $SiO_2$-(**4**) | 116.6 | 101.1 | This study |

and Co(II), compared to other materials. The only exception is the several times higher adsorption capacity of $SiO_2$-5 G.PPI, which is related to very high branching level of dendrimer used as functionalizing agent for this material, affording high density of binding sites toward chosen adsorbates.

### *Adsorption kinetics*

Investigation of the contact time effect on the efficiency of adsorption process permits identification of the rate-limiting step. There are two widely used kinetic models: the pseudo-first-order model, which assumes that the rate-limiting step is strictly related to the saturation of the adsorbent binding sites and the pseudo-second-order model, which assumes that chemical adsorption related to electron exchange between adsorbent and metal ions is the rate-limiting step. The obtained experimental data were fitted to both pseudo-first-order kinetic model (Figure 8) and pseudo-second-order kinetic models (Figure 9), and the results are listed in Table 3.

Table 3 presents the values obtained for fitting of experimental data to the pseudo-first- and pseudo-second-order kinetic models. The adsorption process of Ni(II) ions as well as Co(II) on hybrid materials follows strictly the pseudo-second-order model as proved by $R^2$ correlation coefficient higher than 0.99, which means that each adsorption process was limited by the chemical interactions between adsorbent and metal ions. Moreover, the fit of the experimental data to such a kinetic model indicates the material applicability for diluted solutes,[46] which is clearly consistent with the results presented in Adsorption isotherms, based on comparison of $K_d$ parameters. Assuming the pseudo-second-order kinetic model, the half-adsorption times $t_{1/2}$, which is the time needed for binding half of adsorbate Ni(II)/Co(II) at the equilibrium state, were estimated. The highest half-adsorption time for both metal ions was obtained for $SiO_2$-(**4**) material, which is related to the highest adsorption capacity of this material and also the oxygen

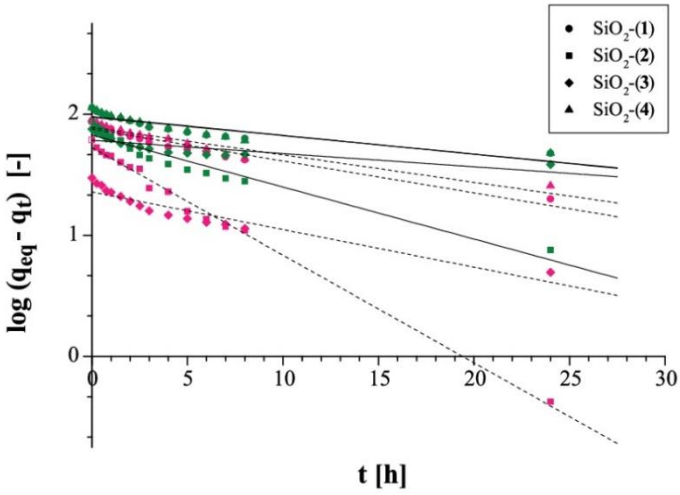


**Figure 8.** The pseudo-first-order kinetic model of Ni(II) (green; solid lines) and Co(II) (pink; dashed lines) adsorption on $SiO_2$–dendrimer hybrid materials ($c_0$ = 15 mM).

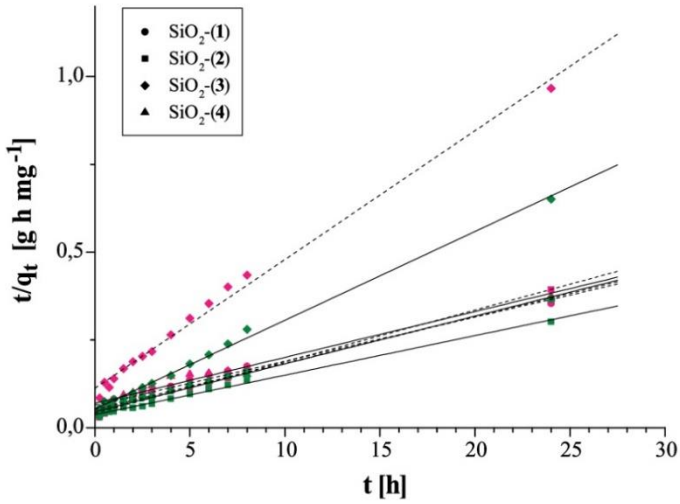


**Figure 9.** The pseudo-second-order kinetic model of Ni(II) (green; solid lines) and Co(II) (pink; dashed lines) adsorption on $SiO_2$–dendrimer hybrid materials ($c_0$ = 15 mM).

atoms in the grafting agent structure, whose presence has a significant impact on the interaction between the material and the solute.

In contrast, the lowest half-adsorption time values were calculated for materials $SiO_2$-(**2**) and $SiO_2$-(**3**), which contain tris(2-aminoethyl)amine and triethylenetetramine as an ultimate amino-components of dendrimers grafted on their surface, respectively. This phenomenon is related either to the lowest adsorption capacities ($SiO_2$-(**3**)) or to the presence of highly branched amino terminus

**Table 3.** Kinetic parameters for adsorption of Ni(II) and Co(II) ions on $SiO_2$–dendrimer hybrid materials.

| | | Pseudo-first-order | | | Pseudo-second-order | | | |
|---|---|---|---|---|---|---|---|---|
| Ion | Adsorbent | $k_1$ [$h^{-1}$] | $k_i$ [mg $g^{-1}$ $h^{-1}$] | $R^2$ | $k_2$ [g $mg^{-1}$ $h^{-1}$] | $k_i$ [mg $g^{-1}$ $h^{-1}$] | $t_{1/2}$ [h] | $R^2$ |
| Ni(II) | $SiO_2$-(**1**) | 0.035 ± 0.005 | 2.6 ± 0.4 | 0.7930 | 0.0040 ± 0.0003 | 21.6 ± 2.7 | 3.40 | 0.9922 |
| | $SiO_2$-(**2**) | 0.099 ± 0.007 | 8.8 ± 0.8 | 0.9384 | 0.0034 ± 0.0002 | 26.9 ± 2.6 | 3.31 | 0.9958 |
| | $SiO_2$-(**3**) | 0.025 ± 0.005 | 1.0 ± 0.2 | 0.6261 | 0.0119 ± 0.0008 | 18.7 ± 1.9 | 2.12 | 0.9966 |
| | $SiO_2$-(**4**) | 0.036 ± 0.005 | 2.7 ± 0.4 | 0.7881 | 0.0034 ± 0.0002 | 19.4 ± 1.7 | 3.89 | 0.9948 |
| Co(II) | $SiO_2$-(**1**) | 0.061 ± 0.004 | 5.3 ± 0.4 | 0.9417 | 0.0024 ± 0.0002 | 15.6 ± 2.2 | 5.12 | 0.9922 |
| | $SiO_2$-(**2**) | 0.205 ± 0.004 | 12.6 ± 0.3 | 0.9937 | 0.0052 ± 0.0004 | 24.2 ± 3.2 | 2.81 | 0.9958 |
| | $SiO_2$-(**3**) | 0.072 ± 0.007 | 2.1 ± 0.2 | 0.8950 | 0.0119 ± 0.0009 | 8.9 ± 1.1 | 3.08 | 0.9966 |
| | $SiO_2$-(**4**) | 0.052 ± 0.004 | 4.7 ± 0.4 | 0.9158 | 0.0024 ± 0.0002 | 14.3 ± 2.6 | 5.35 | 0.9948 |

in the dendritic structure, which contributes to the numerous binding sites and low elutability of adsorbate ($SiO_2$-(**2**)). Nevertheless, as presented in Table 3, $t_{1/2}$ values are relatively high with average of 3.5 h. Therefore, several structural changes in the hybrid materials may lead to an intensification of adsorption process. For instance, a utilization of another linker on the silica precursor, contributing to higher grafting percentage of dendritic structures, as well as an incorporation of particular domains to dendrimer's terminal amine groups enhancing binding effectiveness, e.g. a residue of thioamide.

### *Adsorption thermodynamics*

Temperature is one of the most important factors that affect the adsorptive capability of adsorbing systems and determination of its effect permits characterization of thermodynamic nature of adsorption process. The thermodynamic behavior of Ni(II) and Co(II) adsorption on hybrid materials is illustrated by the linear plot of $1/T$ vs. $ln\ K_d$, which is depicted in Figure 10. On the

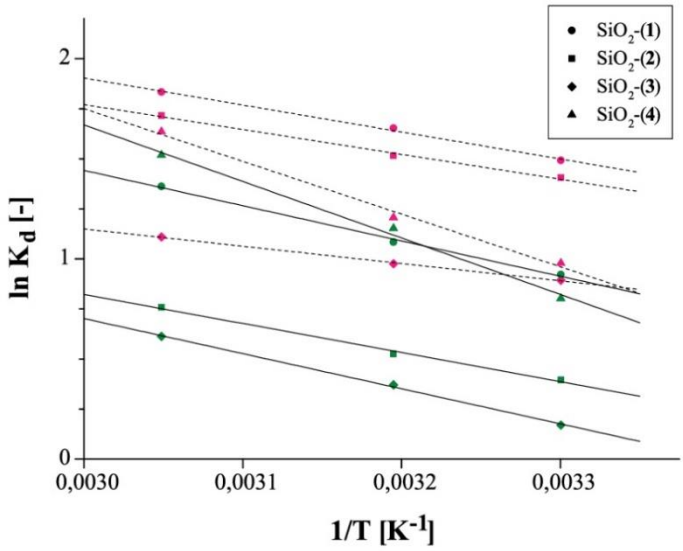


**Figure 10.** Thermodynamics of adsorption of Ni(II) (solid line) and Co(II) (dashed line) on $SiO_2$–dendrimer hybrid materials ($c_0$ = 15 mM).

**Table 4.** Thermodynamic parameters of adsorption of Ni(II) and Co(II) ions on $SiO_2$–dendrimer hybrid materials.

| Ion | Adsorbent | $\Delta H°$ [kJ mol$^{-1}$] | $\Delta S°$ [J mol$^{-1}$ K$^{-1}$] | $R^2$ | $T$ [K] | $\Delta G°$ [kJ mol$^{-1}$] |
|---|---|---|---|---|---|---|
| Ni(II) | $SiO_2$-(**1**) | 14.65 ± 0.84 | 55.93 ± 2.66 | 0.9967 | 301 | −2.31 ± 0.01 |
| | | | | | 313 | −2.82 ± 0.01 |
| | | | | | 328 | −3.72 ± 0.01 |
| | $SiO_2$-(**2**) | 12.08 ± 0.86 | 43.07 ± 2.74 | 0.9949 | 301 | −0.99 ± 0.01 |
| | | | | | 313 | −1.36 ± 0.01 |
| | | | | | 328 | −2.07 ± 0.01 |
| | $SiO_2$-(**3**) | 14.58 ± 0.61 | 49.57 ± 1.93 | 0.9983 | 301 | −0.42 ± 0.01 |
| | | | | | 313 | −0.97 ± 0.01 |
| | | | | | 328 | −1.67 ± 0.01 |
| | $SiO_2$-(**4**) | 23.47 ± 1.91 | 84.29 ± 6.08 | 0.9934 | 301 | −2.00 ± 0.01 |
| | | | | | 313 | −3.00 ± 0.01 |
| | | | | | 328 | −4.14 ± 0.01 |
| Co(II) | $SiO_2$-(**1**) | 11.21 ± 0.70 | 49.46 ± 2.22 | 0.9961 | 301 | −3.73 ± 0.01 |
| | | | | | 313 | −4.30 ± 0.01 |
| | | | | | 328 | −5.00 ± 0.02 |
| | $SiO_2$-(**2**) | 10.34 ± 0.79 | 45.74 ± 2.50 | 0.9942 | 301 | −3.52 ± 0.01 |
| | | | | | 313 | −3.94 ± 0.01 |
| | | | | | 328 | −4.68 ± 0.01 |
| | $SiO_2$-(**3**) | 7.18 ± 0.33 | 31.09 ± 1.06 | 0.9978 | 301 | −2.24 ± 0.01 |
| | | | | | 313 | −2.54 ± 0.01 |
| | | | | | 328 | −3.03 ± 0.01 |
| | $SiO_2$-(**4**) | 21.89 ± 1.78 | 80.23 ± 5.68 | 0.9934 | 301 | −2.45 ± 0.01 |
| | | | | | 313 | −3.14 ± 0.01 |
| | | | | | 328 | −4.46 ± 0.01 |

basis of the slope and intercept of linear regressions, all thermodynamic parameters were calculated (Table 4).

Table 4 presents a comparison of standard enthalpy changes ($\Delta H°$), standard entropy ($\Delta S°$), and standard free Gibbs energy changes ($\Delta G°$) calculated for Ni(II) and Co(II) ions adsorption process on $SiO_2$–dendrimer hybrid materials. For all materials, the adsorption process is described as endothermic, as follows from the positive values of standard enthalpy. The enthalpies values range between 7.18 and 23.47 kJ mol$^{-1}$, classifying the investigated binding processes as physisorption, basing on a general theory that ΔH° values of physisorption are between -20 and 40 kJ mol$^{-1}$,[128] which is in a good agreement with values of mean free energies E Adsorption isotherms. Moreover, all $\Delta G°$ values are negative, which indicates the spontaneity of investigated adsorption processes. The most pronounced influence of temperature is observed for adsorption of metal ions on $SiO_2$-(**4**) material, which is described with $\Delta H°$ of approximately 20 kJ mol$^{-1}$. The positive values of $\Delta S°$ indicate increasing randomness at the adsorbent–solution interface, which might be attributed as the driving force of the adsorption progress.

### *Selectivity of adsorption process*

The adsorption experiments conducted in binary system may deliver an information about the selectivity of the adsorption processes toward the particular metal ions used. Table 5 presents the amount of the competitive metals adsorbed $q_{Ni}/q_{Co}$ by the hybrid materials, calculated using spectrophotometric assays and also the percentage uptake of the metals determined by XRF analysis (Figure 11). Moreover, the separation factors ($\alpha_{Co}^{Ni}$) were calculated, which values may indicate the adsorption preferability:

$$\alpha_{Co}^{Ni} = \frac{q_{Ni} \cdot c_{Co}}{q_{Co} \cdot c_{Ni}}$$

Table 5. Selectivity of the metal ions adsorption processes on the hybrid materials.

| | UV–vis analysis | | | XRF analysis | |
|---|---|---|---|---|---|
| Adsorbent | $q_{Ni}$ [mg g$^{-1}$] | $q_{Co}$ [mg g$^{-1}$] | $\alpha_{Co}^{Ni}$ | % Ni | % Co |
| $SiO_2$-(**1**) | 101.3 | 97.4 | 1.05 | 59.8 | 40.2 |
| $SiO_2$-(**2**) | 70.3 | 33.6 | 2.45 | 85.2 | 14.8 |
| $SiO_2$-(**3**) | 69.9 | 25.6 | 3.19 | 97.4 | 2.6 |
| $SiO_2$-(**4**) | 89.6 | 81.1 | 1.23 | 65.8 | 34.2 |

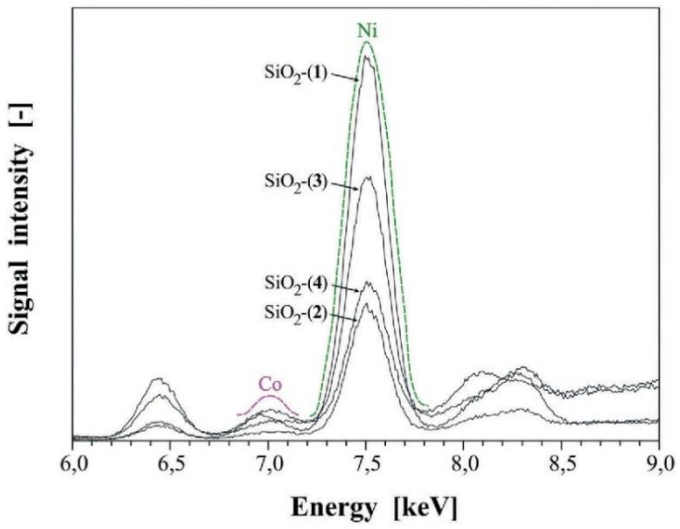


Figure 11. XRF analysis of hybrid materials $SiO_2$-(**1**) – $SiO_2$-(**4**) after metals adsorption from their binary system Ni(II)/Co(II).

where: $q_{Ni}/q_{Co}$ – the amount of the metals absorbed on the hybrid materials, $c_{Ni}/c_{Co}$ – the equilibrium concentration of the metals in the solution. For the investigated binary system, the value of separation factor $\alpha_{Co}^{Ni}$ lower than 1 would indicate the selectivity of Co(II) ions adsorption on the hybrid materials, and higher than 1 – the selectivity of Ni(II) ions adsorption.

The selectivity of the metal ions adsorption on the PAMAM-grafted hybrid materials is strictly connected with either electronegativity of the metals or the hydrated radii of the metal ions.[129] The most efficient adsorption takes place for those metals which have the highest electronegativity values, but also for those metal ions which have the smallest hydrated radii, enabling their easier diffusion into the matrix of a material. According to the fact that Ni(II) ions have higher electronegativity values and smaller hydrated radius than Co(II) ions, the selectivity of adsorption process in Ni(II)/Co(II) binary system should be directed toward Ni(II) ions. Such principle is proved for all of the hybrid materials using both, classic UV-Vis and XRF, analysis. Materials $SiO_2$-(**2**) and $SiO_2$-(**3**) exhibit good selectivity toward Ni(II) which might be related to the highest branching level of the dendrimers on their surface causing a steric hindrance for Co(II) ions with bigger hydrated radii. For materials $SiO_2$-(**1**) and $SiO_2$-(**4**) the selectivity for Ni(II) ions is seen, where adsorption differentiation is based only on the minor difference in the electronegativity values of both metal ions.

## Conclusions

The main objective of our study was to identify the ability of the $SiO_2$–dendrimer hybrid materials for coordination of two heavy metal ions, nickel(II) and cobalt(II), in surface dendrimer structures, leading to the metal ions extraction. Comprehensive research involved isothermal, kinetic and thermodynamic experiments, as well as investigation of the adsorption selectivity conducted in the metal ions solutions buffered at pH 5.4. Adsorption process of metal ions on the examined materials was found to be dependent especially on the structure of dendrimer grafted on the adsorbents surface. Nevertheless, the adsorption capacities calculated from linear plot of Langmuir isotherms ranged between 86.7–116.6 mg $g^{-1}$ for Ni(II) ions and 32.8–101.1 mg $g^{-1}$ for Co(II). The highest values were obtained for $SiO_2$-(**4**) material, which contained on its surface the dendrimer built of 4,7,10-trioxa-1,13-tridecanediamine as amino-terminus, while the lowest for the material containing triethylenetetramine as terminal amino-component of grafted dendrimer. Thus, it may be concluded that general structure of the grafting agent (branching level, presence of oxygen atoms, or tertiary amine groups) leads to the binding affinity increase. Moreover, the highest distribution coefficients were achieved for the lowest initial metal ions concentrations, which is consistent with determined pseudo-second-order kinetic models of each adsorption process, indicating the scavenging properties of hybrid materials. The calculated mean free energies and the calculated values of adsorption enthalpy strictly indicate the physical nature of adsorption processes. Furthermore, thermodynamic experiments proved the endothermic, spontaneous, and feasible character of investigated processes of Ni(II) and Co(II) metal ions adsorption on the four $SiO_2$–dendrimer materials studied. Moreover, the selectivity of the hybrid materials was found to be directed toward Ni(II) ions, which is consistent with the principle of the influence of ion features, for example, electronegativity and hydrated radius, on its affinity to the adsorptive material.

In summary, the obtained materials were characterized for their efficiency in toxic metal ions binding. Nevertheless, their further investigation as binding materials is useful, in order to establish the materials' pre-concentrating abilities (scavenging of contaminants from highly diluted solutions), reusability using EDTA re-chelating agent or HCl, and applicability of the materials for purification of real-life or simulated wastewater and ground water samples containing complex matrices. Such experiments would also allow for determination of common matrix metal ions ($Na^+$, $K^+$, $NH_4^+$, $Ca^{2+}$, etc.) influence on the adsorptive properties. Moreover, highly satisfactory results of adsorptive properties of studied materials may lead to designing other hybrids grafted with structurally diverse dendrimers and their further application as either scavenging materials or drug delivery systems.

## Declaration of Interest Statement

The authors declare no known financial or personal conflicts of interest associated with this publication.

## Funding

The work was supported by Grant no. [POWR.03.02.00-00-I026/16] co-financed by the European Union through the European Social Fund under the Operational Program Knowledge Education Development.

## ORCID

Mateusz Pawlaczyk http://orcid.org/0000-0002-2340-1363
Grzegorz Schroeder http://orcid.org/0000-0002-6626-9542

## References


[1] Barakat, M. A.;. New Trends in Removing Heavy Metals from Industrial Wastewater. *Arab. J. Chem.* 2011, *4*, 361–377.

[2] Ge, F.; Li, M. M.; Ye, H.; Zhao, B. X. Effective Removal of Heavy Metal Ions Cd2+, Zn2+, Pb2+, Cu2+ from Aqueous Solution by Polymer-Modified Magnetic Nanoparticles. *J. Haz. Mater.* 2012, *211–212*, 366–372.

[3] Peligro, F. R.; Pavlovic, I.; Rojas, R.; Barriga, C. Removal of Heavy Metals from Simulated Wastewater by in Situ Formation of Layered Double Hydroxides. *Chem. Eng. J.* 2016, *306*, 1035–1040.

[4] Ye, M.; Li, G.; Yan, P.; Ren, J.; Zheng, L.; Han, D.; Sun, S.; Huang, S.; Zhong, Y. Removal of Metals from Lead-Zinc Mine Tailings Using Bioleaching and Followed by Sulfide Precipitation. *Chemosphere.* 2017, *185*, 1189–1196.

[5] Al-Shannag, M.; Al-Qodah, Z.; Bani-Melhem, K.; Qtaishat, M. R.; Alkasrawi, M. Heavy Metal Ions Removal from Metal Plating Wastewater Using Electrocoagulation: Kinetic Study and Process Performance. *Chem. Eng. J.* 2015, *260*, 749–756.

[6] Lu, J.; Li, Y.; Yin, M.; Ma, X.; Lin, S. Removing Heavy Metal Ions with Continuous Aluminum Electrocoagulation: A Study on Back Mixing and Utilization Rate of Electro-Generated Al Ions. *Chem. Eng. J.* 2015, *267*, 86–92.

[7] Al-Rashdi, B. A. M.; Johnson, D. J.; Hilal, N. Removal of Heavy Metal Ions by Nanofiltration. *Desalination.* 2013, *315*, 2–17.

[8] Huang, J.; Yuan, F.; Zeng, G.; Li, X.; Gu, Y.; Shi, L.; Liu, W.; Shi, Y. Influence of pH on Heavy Metal Speciation and Removal from Wastewater Using Micellar Enhanced Ultrafiltration. *Chemosphere.* 2017, *173*, 199–206.

[9] Kirkelund, G. M.; Jensen, P. E.; Ottosen, L. M.; Pedersen, K. B. Comparison of Two- and Three-Compartment Cells for Electrodialytic Removal of Heavy Metals from Contaminated Material Suspensions. *J. Haz. Mater.* 2019, *367*, 68–76.

[10] Nemati, M.; Hosseini, S. M.; Shabanian, M. Novel Electrodialysis Cation Exchange Membrane Prepared by 2-Acrylamido-2-Methylpropane Sulfonic Acid; Heavy Metal Ions Removal. *J. Haz. Mater.* 2017, *337*, 90–104.

[11] Harraz, F. A.; Abdel-Salam, O. E.; Mostafa, A. A.; Mohamed, R. M.; Hanafy, M. Rapid Synthesis of Titania–Silica Nanoparticles Photocatalyst by a Modified Sol–Gel Method for Cyanide Degradation and Heavy Metals Removal. *J. Alloys Comp.* 2013, *551*, 1–7.

[12] Ahmed, M. J. K.; Ahmaruzzaman, M. A Review on Potential Usage of Industrial Waste Materials for Binding Heavy Metal Ions from Aqueous Solutions. *J. Water Process. Eng.* 2016, *10*, 39–47.

[13] Kwon, J. S.; Yun, S. T.; Lee, J. H.; Kim, S. O.; Jo, H. Y. Removal of Divalent Heavy Metals (Cd, Cu, Pb, and Zn) and Arsenic(III) from Aqueous Solutions Using Scoria: Kinetics and Equilibria of Sorption. *J. Haz. Mater.* 2010, *174*, 307–313.

[14] Al-Harahsheh, M. S.; Al Zboon, K.; Al-Makhadmeh, L.; Hararah, M.; Mahasneh, M. Fly Ash Based Geopolymer for Heavy Metal Removal: A Case Study on Copper Removal. *J. Env. Chem. Eng.* 2015, *3*, 1669–1677.

[15] Sheela, T.; Arthoba Nayaka, Y.; Viswanatha, R.; Basavanna, S.; Venkatesha, T. G. Kinetics and Thermodynamics Studies on the Adsorption of Zn(II), Cd(II) and Hg(II) from Aqueous Solution Using Zinc Oxide Nanoparticles. *Powder Technol.* 2012, *217*, 163–170.

[16] Ghasemi, Z.; Seif, A.; Ahmadi, T. S.; Zargar, B.; Rashidi, F.; Rouzbahani, G. M. Thermodynamic and Kinetic Studies for the Adsorption of Hg(II) by Nano-Tio2 from Aqueous Solution. *Adv. Powder Technol.* 2012, *23*, 148–156.

[17] Badsha, M. A. H., .; Lo, I. M. C. An Innovative pH-Independent Magnetically Separable Hydrogel for the Removal of Cu(II) and Ni(II) Ions from Electroplating Wastewater. *J. Haz. Mater.* 2020, *381*, 121000.

[18] Agarwal, S.; Tyagi, I.; Gupta, V. K.; Dehghani, M. H.; Jaafari, J.; Balarak, D.; Asif, M. Rapid Removal of Noxious Nickel (II) Using Novel Γ-alumina Nanoparticles and Multiwalled Carbon Nanotubes: Kinetic and Isotherm Studies. *J. Mol. Liq.* 2016, *224*, 618–623.

[19] Zhu, Q.; Zhang, B.; Wang, T.; Feng, X. Synthesis and Properties of Porous δ-Mno2/Polymer Millimeter-Sized Beads for Ni(II) Removal. *Micropor. Mesopor. Mater.* 2019, *273*, 90–98.

[20] Efome, J. E.; Rana, D.; Matsuura, T.; Lan, C. Q. Metal–Organic Frameworks Supported on Nanofibers to Remove Heavy Metals. *J. Mater. Chem. A.* 2018, *6*, 4550–4555.

[21] Kobielska, P. A.; Howarth, A. J.; Farha, O. K.; Nayak, S. Metal–Organic Frameworks for Heavy Metal Removal from Water. *Coordination Chem. Rev.* 2018, *358*, 92–107.

[22] Wang, H.; Tang, H.; Liu, Z.; Zhang, X.; Hao, Z.; Liu, Z. Removal of Cobalt(II) Ion from Aqueous Solution by Chitosan–Montmorillonite. *J. Environ. Sci.* 2014, *26*, 1879–1884.

[23] Sheha, R. R.; Moussa, S. I.; Attia, M. A.; Sadeek, S. A.; Someda, H. H. Novel Substituted Hydroxyapatite Nanoparticles as a Solid Phase for Removal of Co(II) and Eu(III) Ions from Aqueous Solutions. *J. Environ. Chem. Eng.* 2016, *4*, 4808–4816.

[24] Tounsadi, H.; Khalidi, A.; Abdennouri, M.; Barka, N. Biosorption Potential of Diplotaxis Harra and Glebionis Coronaria L. Biomasses for the Removal of Cd(II) and Co(II) from Aqueous Solutions. *J. Environ. Chem. Eng.* 2015, *3*, 822–830.

[25] Foroutan, R.; Esmaeili, H.; Rishehri, S. D.; Sadeghzadeh, F.; Mirahmadi, S.; Kosarifard, M.; Ramavandi, B. Zinc, Nickel, and Cobalt Ions Removal from Aqueous Solution and Plating Plant Wastewater by Modified Aspergillus Flavus Biomass: A Dataset. *Data Brief.* 2017, *12*, 485–492.
[26] Gopi Kiran, M.; Pakshirajan, K.; Das, G. Heavy Metal Removal from Multicomponent System by Sulfate Reducing Bacteria: Mechanism and Cell Surface Characterization. *J. Haz. Mater.* 2017, *324*, 62–70.
[27] Samiey, B.; Cheng, C. H.; Wu, J. Organic-Inorganic Hybrid Polymers as Adsorbents for Removal of Heavy Metal Ions from Solutions: A Review. *Materials.* 2014, *7*, 673–726.
[28] Das, S. K.; Khan, M. M. R.; Parandhaman, T.; Laffir, F.; Guha, A. K.; Sekaran, G.; Mandal, A. B. Nano-Silica Fabricated with Silver Nanoparticles: Antifouling Adsorbent for Efficient Dye Removal, Effective Water Disinfection and Biofouling Control. *Nanoscale.* 2013, *5*, 5549–5560.
[29] Zhao, C.; Ma, L.; You, J.; Qu, F.; Priestley, R. D. EDTA-and Amine-Functionalized Graphene Oxide as Sorbents for Ni (II) Removal. *Desalin. Water Treat.* 2016, *57*, 8942–8951.
[30] Shahat, A.; Awual, M. R.; Naushad, M. Functional Ligand Anchored Nanomaterial Based Facial Adsorbent for Cobalt (II) Detection and Removal from Water Samples. *Chem. Eng. J.* 2015, *271*, 155–163.
[31] Thakur, A. K.; Nisola, G. M.; Limjuco, L. A.; Parohinog, K. J.; Torrejos, R. E. C.; Shahi, V. K.; Chung, W. J. Polyethylenimine-Modified Mesoporous Silica Adsorbent for Simultaneous Removal of Cd (II) and Ni (II) from Aqueous Solution. *J. Ind. Eng. Chem.* 2017, *49*, 133–144.
[32] Eser, E.; Tirtom, V. N.; Aydemir, T.; Becerik, S.; Dinçer, A. Removal of Nickel (II) Ions by Histidine Modified Chitosan Beads. *Chem. Eng. J.* 2012, *210*, 590–596.
[33] Ma, A.; Abushaikha, A.; Allen, S. J.; McKay, G. Ion Exchange Homogeneous Surface Diffusion Modelling by Binary Site Resin for the Removal of Nickel Ions from Wastewater in Fixed Beds. *Chem. Eng. J.* 2019, *358*, 1–10.
[34] Wołowicz, A.; Hubicki, Z. Comparison of Ion-Exchange Resins for Efficient Cobalt(II) Removal from Acidic Streams, *Chem.. Eng. Comm.* 2018, *205*, 1207–1225.
[35] Misra, R. K.; Jain, S. K.; Khatri, P. K. Iminodiacetic Acid Functionalized Cation Exchange Resin for Adsorptive Removal of Cr(VI), Cd(II), Ni(II) and Pb(II) from Their Aqueous Solutions. *J. Haz. Mater.* 2011, *185*, 1508–1512.
[36] Bohdana, C. M.; Pincovschi, E.; Oancea, A. M. S. Proton/Cu(II) and Proton/Ni(II) Ion Exchange Equilibria on Sulfonated Hypercrosslinked Resin Sorption and Surface Complexation Models. *Rev. Chim.* 2012, *63*, 159–165.
[37] Rengaraj, S.; Yeon, K. H.; Kang, S. Y.; Lee, J. U.; Kim, K. W.; Moon, S. H. Studies on Adsorptive Removal of Co(II), Cr(III) and Ni(II) by IRN77 Cation-Exchange Resin. *J. Haz. Mater.* 2002, *B92*, 185–198.
[38] Fil, B. A.; Boncukcuoglu, R.; Yilmaz, A. E.; Bayar, S. Adsorption Kinetics and Isotherms for the Removal of Zinc Ions from Aqueous Solutions by an Ion-Exchange Resin. *J. Chem. Soc. Pak.* 2012, *34*, 841.
[39] Martins, P. J. M.; Reis, P. M.; Martins, R. C.; Gando-Ferreira, L. M.; Quinta-Ferreira, R. M. Iron Recovery from the Fenton's Treatment of Winery Effluent Using an Ion-Exchange Resin. *J. Mol. Liq.* 2017, *242*, 505–511.
[40] Puttamat, S.; Pavarajarn, V. Adsorption Study for Removal of Mn(II) Ion in Aqueous Solution by Hydrated Ferric (III) Oxides. *Int. J. Chem. Eng. Appl.* 2016, *7*, 239–243.
[41] Rafati, L.; Mahvi, A. H.; Asgari, A. R.; Hosseini, S. S. Removal of Chromium (VI) from Aqueous Solutions Using Lewatit FO36 Nano Ion Exchange Resin. *Int. J. Environ. Sci. Tech.* 2010, *7*, 147–156.
[42] Chen, Y.; Pan, B.; Li, H.; Zhang, W.; Lv, L.; Wu, J. Selective Removal of Cu(II) Ions by Using Cation-exchange Resin-Supported Polyethyleneimine (PEI) Nanoclusters. *Environ. Sci. Technol.* 2010, *44*, 3508–3513.
[43] Otrembska, P.; Gega, J. Separation of Nickel(II) and Cadmium(II) Ions with Ion-Exchange and Membrane Processes. *Sep. Sci. Technol.* 2016, *51*, 2675–2680.
[44] Naushad, M.; ALOthman, Z. A.; Sharma, G. Inamuddin, Kinetics, Isotherm and Thermodynamic Investigations for the Adsorption of Co(II) Ion onto Crystal Violet Modified Amberlite IR-120 Resin. *Ionics.* 2015, *21*, 1453–1459.
[45] Kumar, R.; Kumar, M.; Ahmad, R.; Barakat, M. A. L-Methionine Modified Dowex-50 Ion-Exchanger of Reduced Size for the Separation and Removal of Cu(II) and Ni(II) from Aqueous Solution. *Chem. Eng. J.* 2013, *218*, 32–38.
[46] Nekouei, R. K.; Pahlevani, F.; Assefi, M.; Maroufi, S.; Sahajwalla, V. Selective Isolation of Heavy Metals from Spent Electronic Waste Solution by Macroporous Ion-Exchange Resins. *J. Haz. Mater.* 2019, *371*, 389–396.
[47] Hamdzah, M.; Ujang, Z.; Nasef, M. M.; Abdullah, N.; Dahalan, F. A. Removal of Ni(II), Zn(II) and Pb(II) from Aqueous Solutions Using Cation-Exchange Resin in Fixed-Bed Column. *Desalin. Water Treat.* 2016, *57*, 18770–18781.
[48] Shaidan, N. H.; Eldemerdash, U.; Awad, S. Removal of Ni(II) Ions from Aqueous Solutions Using Fixed-Bed Ion Exchange Column Technique. *J. Taiwan Inst. Chem. Eng.* 2012, *43*, 40–45.
[49] Staudt, J.; Scheufele, F. B.; Ribeiro, C.; Sato, T. Y.; Canevesi, R.; Borba, C. E. Ciprofloxacin Desorption from Gel Type Ion Exchange Resin: Desorption Modeling in Batch System and Fixed Bed Column. *Sep. Purif. Technol.* 2020, *230*, 115857.
[50] Kolodynska, D.;. Cu(II), Zn(II), Ni(II), and Cd(II) Complexes with HEDP Removal from Industrial Effluents on Different Ion Exchangers. *Ind. Eng. Chem. Res.* 2010, *49*, 2388–2400.

[51] Kolodynska, D.;. Cu(II), Zn(II), Co(II) and Pb(II) Removal in the Presence of the Complexing Agent of a New Generation. *Desalination*. 2011, *267*, 175–183.
[52] Dron, J.; Dodi, A. Comparison of Adsorption Equilibrium Models for the Study of Cl–, NO3– and SO42– Removal from Aqueous Solutions by an Anion Exchange Resin. *J. Haz. Mater*. 2011, *190*, 300–307.
[53] Parajuli, D.; Noguchi, H.; Tanaka, H.; Kawasaki, T.; Kawatsu, Y.; Kobayashi, T.; Kawamoto, T. Effective Removal of Hexacyanoferrate Anions Using Quaternary Amine Type Ion Exchange Resin. *J. Environ. Chem. Eng*. 2015, *3*, 2448–2452.
[54] Sica, M.; Duta, A.; Teodosiu, C.; Draghici, C. Thermodynamic and Kinetic Study on Ammonium Removal from a Synthetic Water Solution Using Ion Exchange Resin. *Clean Techn. Environ. Policy*. 2014, *16*, 351–359.
[55] Kouchak, M.; Ramezani, Z.; Bagheri, F. Preparation and Evaluation of Taste Masking Iron Suspension: Taking Advantage of Weak Cationic Exchange Resin. *AAPS Pharm. Sci. Tech*. 2018, *19*, 719–729.
[56] Tamahkar, E.; Bakhshpour, M.; Andac, M.; Denizli, A. Ion Imprinted Cryogels for Selective Removal of Ni(II) Ions from Aqueous Solutions. *Sep. Purif. Technol*. 2017, *179*, 36–44.
[57] Singh, D. K.; Mishra, S. Synthesis, Characterization and Analytical Applications of Ni(II)-Ion Imprinted Polimer. *App. Surf. Sci*. 2010, *256*, 7632–7637.
[58] Liu, B.; Wang, D.; Xu, J.; Huang, G. Adsorption Properties of Cd(II)-Imprinted Chitosan Resin, *J.. Mater. Sci*. 2011, *46*, 1535–1541.
[59] Chen, C. Y.; Yang, C. Y.; Chen, A. H. Biosorption of Cu(II), Zn(II), Ni(II) and Pb(II) Ions by Cross-Linked Metal-Imprinted Chitosans with Epichlorohydrin. *J. Environ. Manag*. 2011, *92*, 796–802.
[60] Monier, M.; Abdel-Latif, D. A.; Abou El-Reash, Y. G. Ion-Imprinted Modified Chitosan Resin for Selective Removal of Pd(II) Ions. *J. Colloid Interfaces Sci*. 2016, *469*, 344–354.
[61] Abou El-Reash, Y. G.; Otto, M.; Kenawy, I. M.; Ouf, A. M. Adsorption of Cr(VI) and As(V) Ions by Modified Magnetic Chitosan Chelating Resin. *Int. J. Biol. Macromol*. 2011, *49*, 513–522.
[62] Monier, M.; Ayad, D. M.; Abdel-Latif, D. A. Adsorption of Cu(II), Cd(II) and Ni(II) Ions by Cross-Linked Magnetic Chitosan-2-Aminopyridine Glyoxal Schiff's Base. *Colloids Surf. B Biointerf*. 2012, *94*, 250–258.
[63] Monier, M.; Ayad, D. M.; Wei, Y.; Sarhan, A. A. Preparation and Characterization of Magnetic Chelating Resin Based on Chitosan for Adsorption of Cu(II), Co(II), and Ni(II) Ions. *React. Funct. Polym*. 2010, *70*, 257–266.
[64] Liang, F. B.; Song, Y. L.; Huang, C. P.; Li, Y. X.; Chen, B. H. Synthesis of Novel Lignin-Based Ion-Exchange Resin and Its Utilization in Heavy Metals Removal. *Ind. Eng. Chem. Res*. 2013, *52*, 1267–1274.
[65] Pawlaczyk, M.; Kurczewska, J.; Schroeder, G. Nanomaterials Modification by Dendrimers – A Review. *World J. Res. Rev*. 2018, *6*, 14–30.
[66] Wu, X. Z.; Liu, P.; Pu, Q. S.; Sun, Q. Y.; Su, Z. X. Preparation of Dendrimer-Like Polyamidoamine Immobilized Silica Gel and Its Application to Online Preconcentration and Separation Palladium Prior to FAAS Determination. *Talanta*. 2004, *62*, 918–923.
[67] Yuan, Y.; Wu, Y.; Wang, H.; Tong, Y.; Sheng, X.; Sun, Y.; Zhou, X.; Zhou, Q. Simultaneous Enrichment and Determination of Cadmium and Mercury Ions Using Magnetic PAMAM Dendrimers as the Adsorbents for Magnetic Solid Phase Extraction Coupled with High Performance Liquid Chromatography. *J. Haz. Mater*. 2020, *386*, 121658.
[68] Zhang, C.; Su, P.; Wang, S.; Ding, F.; Yang, Y.; Yang, Y. Immunoextraction of Testosterone and Epitestosterone from Human Urine Sample Based on Polyamidoamine Modified Silica. *J. Immunoassay Immunochem*. 2013, *34*, 246–254.
[69] Yesil-Celiktas, O.; Pala, C.; Cetin-Uyanikgil, E. O.; Sevimli-Gur, C. Synthesis of Silica-PAMAM Dendrimer Nanoparticles as Promising Carriers in Neuro Blastoma Cells. *Anal. Biochem*. 2017, *519*, 1–7.
[70] Esmaeilpour, M.; Sardarian, A.; Javidi, J. Dendrimer-Encapsulated Pd(0) Nanoparticles Immobilized on Nanosilica as a Highly Active and Recyclable Catalyst for the Copper- and Phosphine-Free Sonogashira–Hagihara Coupling Reactions in Water. *Catal. Sci. Technol*. 2016, *6*, 4005–4019.
[71] Saeedi, I.; Hashemi, P.; Ramezani, Z.; Badiei, A. Dendrimer Grafted Nanoporous Silica as a New Coating for Headspace Solid-Phase Microextraction Fibers. *Anal. Methods*. 2015, *7*, 10185–10191.
[72] Ramezani, Z.; Saeedi, I.; Hashemi, P. Dendrimer Grafted Nanoporous Silica Fiber for Headspace Solid Phase Microextraction Coupled to Gas Chromatography Determination of Solvents Residues in Edible Oil. *Anal. Methods*. 2018, *11*, 1379–1384.
[73] Xu, X.; Lu, S.; Gao, C.; Wang, X.; Bai, X.; Gao, N.; Liu, M. Facile Preparation of pH-Sensitive and Self-fluorescent Mesoporous Silica Nanoparticles Modified with PAMAM Dendrimers for Label-free Imaging and Drug Delivery. *Chem. Eng. J*. 2015, *266*, 171–178.
[74] Lotfi, R.; Hayati, B.; Rahimi, S.; Shekarchi, A. A.; Mahmoodi, N. M.; Bagheri, A. Synthesis and Characterization of PAMAM/SiO2 Nanohybrid as a New Promising Adsorbent for Pharmaceuticals. *Microchem. J*. 2019, *146*, 1150–1159.
[75] Zhao, P.; Tian, L.; Li, X.; Ali, Z.; Zhang, B.; Zhang, H.; Zhang, Q. Effect of the Structure and Length of Flexible Chains on Dendrimers Grafted Fe3O4@SiO2/PAMAM Magnetic Nanocarriers for Lipase Immobilization. *ACS Sustainable Chem. Eng*. 2016, *4*, 6382–6390.

[76] Li, T.; Chen, Q.; Zheng, Y.; Zhang, P.; Chen, X.; Lu, J.; Lv, Y.; Sun, S.; Zeng, W. PAMAM-Crgd Mediating Efficient Sirna Delivery to Spermatogonial Stem Cells. *Stem Cell Res. Therapy.* 2019, *10*, 1–15.
[77] Hu, Y.; Chen, J.; Li, X.; Sun, Y.; Huang, S.; Li, Y.; Liu, H.; Xu, J.; Zhong, S. Multifunctional Halloysite Nanotubes Ffor Targeted Delivery and Controlled Release of Doxorubicin In-Vitro and In-Vivo Studies. *Nanotechnology.* 2017, *28*, 375101.
[78] Yu, S.; Li, G.; Liu, R.; Ma, D.; Xue, W. Dendritic Fe3O4@Poly(dopamine)@PAMAM Nanocomposite as Controllable NO-Releasing Material: A Synergistic Photothermal and NO Antibacterial Study. *Adv. Funct. Mater.* 2018, *28*, 1707440.
[79] Wen, S.; Liu, H.; Cai, H.; Shen, M.; Shi, X. Targeted and pH-Responsive Delivery of Doxorubicin to Cancer Cells Using Multifunctional Dendrimer-Modified Multi-Walled Carbon Nanotubes. *Adv. Healthcare Mater.* 2013, *2*, 1267–1276.
[80] Qu, R.; Niu, Y.; Sun, C.; Ji, C.; Wang, C.; Cheng, G. Syntheses, Characterization, and Adsorption Properties for Metal Ions of Silica-Gel Functionalized by Ester- and Amino-Terminated Dendrimer-like Polyamidoamine Polymer. *Micropor. Mesopor. Mater.* 2006, *97*, 58–65.
[81] Fu, T.; Niu, Y.; Zhou, Y.; Wang, K.; Mu, Q.; Qu, R.; Chen, H.; Yuan, B.; Yang, H. Adsorption of Mn(II) from Aqueous Solution by Silica-Gel Supported Polyamidoamine Dendrimers: Experimental and DFT Study. *J. Taiwan Inst. Chem. Eng.* 2019, *97*, 189–199.
[82] Ren, B.; Wang, K.; Zhang, B.; Li, H.; Niu, Y.; Chen, H.; Yang, Z.; Li, X.; Zhang, H. Adsorption Behavior of PAMAM Dendrimers Functionalized Silica for Cd(II) from Aqueous Solution: Experimental and Theoretical Calculation. *J. Taiwan Inst. Chem. Eng.* 2019, *101*, 80–91.
[83] Niu, Y.; Qu, R.; Sun, C.; Wang, C.; Chen, H.; Ji, C.; Zhang, Y.; Shao, X.; Bu, F. Adsorption of Pb(II) from Aqueous Solution by Silica-Gel Supported Hyperbranched Polyamidoamine Dendrimers. *J. Haz. Mater.* 2013, *244– 245*, 276–286.
[84] Qu, R.; Niu, Y.; Liu, J.; Sun, C.; Zhang, Y.; Chen, H.; Ji, C. Adsorption and Desorption Behaviors of Pd(II) on Silica-Gel Functionalized with Ester- and Amino-Terminated Dendrimer-Like Polyamidoamine Polymers. *React. Funct. Polym.* 2008, *68*, 1272–1280.
[85] Yin, R.; Niu, Y.; Zhang, B.; Chen, H.; Yang, Z.; Yang, L.; Cu, Y. Removal of Cr(III) from Aqueous Solution by Silica-Gel/PAMAM Dendrimer Hybrid Materials. *Environ. Sci. Pollution Res.* 2019, *26*, 18098–18112.
[86] Zhang, Y.; Qu, R.; Sun, C.; Ji, C.; Chen, H.; Yin, P. Improved Synthesis of Silica-Gel-Based Dendrimer-Like Highly Branched Polymer as the Au(III) Adsorbents. *Chem. Eng. J.* 2015, *270*, 110–121.
[87] Zhang, Y.; Qu, R.; Xu, T.; Zhang, Y.; Sun, C.; Ji, C.; Wang, Y. Fabrication of Triethylenetetramine Terminal Hyperbranched Dendrimer-Like Polymer Modified Silica Gel and Its Prominent Recovery toward Au (III). *Front. Chem.* 2019, *7*, 577–589.
[88] Qu, R.; Ma, X.; Wang, M.; Sun, C.; Sun, X.; Sun, S.; Zhang, Y.; Yin, P. Homogeneous Preparation of Polyamidoamine Grafted Silica Gels and Their Adsorption Properties as Au3+ Adsorbents. *J. Industr. Eng. Chem.* 2014, *20*, 4382–4392.
[89] Qiu, Z.; Niu, Y.; Fu, T.; Wang, K.; Mu, Q. Removal of Ni(II) from Fuel Ethanol by PAMAM Dendrimers/Silica Hybrid Materials: Combined Experimental and Theoretical Study. *Chem. Eng. Res. Des.* 2019, *144*, 174–184.
[90] Sun, C.; Ma, F.; Zhang, G.; Qu, R.; Zhang, Y. Removal of Mercury Ions from Ethanol Solution Using Silica Gel Functionalized with Amino-Terminated Dendrimer-Like Polyamidoamine Polymers: Kinetics and Equilibrium Studies. *J. Chem. Eng. Data.* 2011, *56*, 4407–4415.
[91] Qu, R.; Sun, C.; Ma, F.; Zhang, C.; Zhang, Y.; Sun, X.; Ji, C.; Wang, C.; Yin, P. Adsorption Kinetics and Equilibrium of Copper from Ethanol Fuel on Silica-Gel Functionalized with Amino-Terminated Dendrimer-like Polyamidoamine Polymers. *Fuel.* 2012, *92*, 204–210.
[92] Song, X.; Niu, Y.; Zhang, P.; Zhang, C.; Zhang, Z.; Zhu, Y.; Qu, R. Removal of Co(II) from Fuel Ethanol by Silica-Gel Supported PAMAM Dendrimers: Combined Experimental and Theoretical Study. *Fuel.* 2017, *199*, 91–101.
[93] Qu, R.; Sun, C.; Ma, F.; Zhang, Y.; Ji, C.; Yin, P. Removal of Fe(III) from Ethanol Solution by Silica-Gel Supported Dendrimer-like Polyamidoamine Polymers. *Fuel.* 2018, *219*, 205–213.
[94] Li, H.; Niu, Y.; Xue, Z.; Mu, Q.; Wang, K.; Qu, R.; Chen, H.; Bai, L.; Yang, H.; Wei, D. Adsorption Property and Mechanism of PAMAM Dendrimer/Silica Gel Hybrids for Fe(III) and Ag(I) from N,N-Dimethylformamide. *J. Mol. Liq.* 2019, *273*, 305–313.
[95] Zhu, Y.; Niu, Y.; Li, H.; Ren, B.; Qu, R.; Chen, H.; Zhang, Y. Removal of Cd(II) and Fe(III) from DMSO by Silica Gel Supported PAMAM Dendrimers: Equilibrium, Thermodynamics, Kinetics and Mechanism. *Ecotoxic. Environm. Safety.* 2018, *162*, 253–260.
[96] Song, X.; Niu, Y.; Qiu, Z.; Zhang, Z.; Zhou, Y.; Zhao, J.; Chen, H. Adsorption of Hg(II) and Ag(I) from Fuel Ethanol by Silica Gel Supported Sulfur-Containing PAMAM Dendrimers: Kinetics, Equilibrium and Thermodynamics. *Fuel.* 2017, *206*, 80–88.
[97] Zhang, P.; Niu, Y.; Qiao, W.; Xue, Z.; Bai, L.; Chen, H. Experimental and DFT Investigation on the Adsorption Mechanism of Silica Gel Supported Sulfur-Capped PAMAM Dendrimers for Ag(I). *J. Mol. Liq.* 2018, *263*, 390–398.

[98] Niu, Y.; Yang, J.; Qu, R.; Gao, Y.; Du, N.; Chen, H.; Sun, C.; Wang, W. Synthesis of Silica-Gel-Supported Sulfur-Capped PAMAM Dendrimers for Efficient Hg(II) Adsorption: Experimental and DFT Study. *Ind. Eng. Chem. Res.* 2016, *55*, 3679–3688.
[99] Song, X.; Niu, Y.; Qiu, Z.; Zhang, Z.; Zhou, Y.; Zhao, J.; Chen, H. Adsorption of Hg(II) and Ag(I) from Fuel Ethanol by Silica Gel Supported Sulfur-Containing PAMAM Dendrimers: Kinetics, Equilibrium and Thermodynamics. *Fuel.* 2017, *206*, 80–88.
[100] Wu, X.; Luo, L.; Chen, Z.; Liang, K. Syntheses, Characterization and Adsorption Properties for Pb2+ of Silica-Gel Functionalized by Dendrimer-like Polyamidoamine and 5-Sulfosalicylic Acid. *Appl. Surf. Sci.* 2016, *364*, 86–95.
[101] Niu, Y.; Qu, R.; Chen, H.; Mu, L.; Liu, X.; Wang, T.; Zhang, Y.; Sun, C. Synthesis of Silica Gel Supported Salicylaldehyde Modified PAMAM Dendrimers for the Effective Removal of Hg(II) from Aqueous Solution. *J. Haz. Mater.* 2014, *278*, 267–278.
[102] Wu, X.; Cheh, Z.; Luo, L.; Li, L.; Liu, Y. Adsorption of Lead with Silica Gel Modified with Polyamidoamine Dendrimer and Thiomalic Acid. *MATEC Web Conf.* 2016, *67*, 06099.
[103] Ebelegi, A. N.; Ayawei, N.; Wankasi, D.; Dikio, E. D.; Diagboya, P. N.; Mtunzi, F. M. Covalently Bonded Polyamidoamine Functionalized Silica Used as a Pb(II) Scavenger from Aqueous Solution. *J. Env. Chem. Eng.* 2019, *7*, 103214.
[104] Pawlaczyk, M.; Schroeder, G. Adsorption Studies of Cu(II) Ions on Dendrimer-Grafted Silica-Based Materials. *J. Mol. Liq.* 2019, *281*, 176–185.
[105] Krot, K. A.; de Namor, D.; Aguilar-Cornejo, A. F.; Nolan, A.; Speciation, K. B. Stability Constants and Structures of Complexes of Copper(II), Nickel(II), Silver(I) and Mercury(II) with PAMAM Dendrimer and Related Tetraamide Ligands. *Inorg. Chim. Acta.* 2005, *358*, 3497–3505.
[106] Camarada, M. B.; Zuniga, M.; Alzate-Morales, J.; Santos, L. S. Computational Study of the Complexation of Metal Ions with Poly(amidoamine) PAMAM G0 Dendrimers. *Chem. Phys. Lett.* 2014, *616–617*, 171–177.
[107] Tansel, B.;. Significance of Thermodynamic and Physical Characteristics on Permeation of Ions during Membrane Separation: Hydrated Radius, Hydration Free Energy and Viscous Effects. *Sep. Purif. Technol.* 2012, *86*, 119–126.
[108] Olsher, U.; Hankins, M. G.; Kim, Y. D.; Bartsch, R. A. Anion Effect on Selectivity in Crown Ether Extraction of Alkali Metal Cations. *J. Am. Chem. Soc.* 1993, *115*, 3370–3371.
[109] Zhu, Y.; Gao, N.; Wang, Q.; Wei, X. Adsorption of Perchlorate from Aqueous Solutions by Anion Exchange Resins: Effects of Resin Properties and Solution Chemistry. *Colloids Surf. A. Physicochem. Eng. Aspects.* 2015, *468*, 114–121.
[110] Foo, K. Y.; Hameed, B. H. Insights into the Modeling of Adsorption Isotherm Systems. *Chem. Eng. J.* 2010, *156*, 2–10.
[111] Ayawei, N.; Ebelegi, A. N.; Wankasi, D. Modelling and Interpretation of Adsorption *Isotherms. J. Chem.* 2017, *2017*, 1–11.
[112] Engates, K. E.; Shipley, H. J. Adsorption of Pb, Cd, Cu, Zn, and Ni to Titanium Dioxide Nanoparticles: Effect of Particle Size, Solid Concentration, and Exhaustion. *Environ. Sci. Pollut. Res.* 2011, *18*, 386–395.
[113] Liao, B.; Sun, W.; Guo, N.; Ding, S.; Su, S. Comparison of Co2+ Adsorption by Chitosan and Its Triethylene-Tetramine Derivative: Performance and Mechanism. *Carbohydr. Polym.* 2016, *151*, 20–28.
[114] Hamed, M. M.;. Adsorption Kinetics and Modeling of Gadolinium and Cobalt Ions Sorption by an Ion-exchange Resin. *Part. Sci. Technol.* 2016, *34*, 716–724.
[115] Rengaraj, S.; Moon, S. H. Kinetics of Adsorption of Co(II) Removal from Water and Wastewater by Ion Exchange Resins. *Water Res.* 2002, *36*, 1783–1793.
[116] Asci, Y.; Kaya, S. Removal of Cobalt Ions from Water by Ion-Exchange Method. *Desalin. Water Treat.* 2014, *52*, 267–273.
[117] Li, D. M.; Li, F. Z.; Liao, J. L.; Yang, J. J.; Li, B.; Chen, Y. M.; Yang, Y. Y.; Zhang, J. S.; Tang, J.; Liu, N. Efficient Removal of Co (II) from Aqueous Solution by Titanate Sodium Nanotubes. *Nuclear Sci. Tech.* 2016, *27*, 143–154.
[118] Torres-Caban, R.; Vega-Olivencia, C. A.; Mina-Camilde, N. Adsorption of Ni2+ and Cd2+ from Water by Calcium Alginate/Spent Coffee Grounds Composite Beads. *Appl. Sci.* 2019, *9*, 4531–4551.
[119] Fil, B. A.; Boncukcuolu, R.; Yilmaz, A. E.; Bayar, S. Adsorption of Ni(II) on Ion Exchange Resin: Kinetics, Equilibrium and Thermodynamic Studies. *Korean J. Chem. Eng.* 2012, *29*, 1232–1238.
[120] Kumar, P. S.; Ramakrishnan, K.; Gayathri, R. Removal of Nickel(II) from Aqueous Solutions by Ceralite IR 120 Cationic Exchange Resins. *J. Eng. Sci. Tech.* 2010, *5*, 232–243.
[121] Zhou, Z.; Kong, D.; Zhu, H.; Wang, N.; Wang, Z.; Wang, Q.; Liu, W.; Li, Q.; Zhang, W.; Ren, Z. Preparation and Adsorption Characteristics of an Ion-Imprinted Polymer for Fast Removal of Ni(II) Ions from Aqueous Solution. *J. Haz. Mater.* 2018, *341*, 355–364.
[122] Monier, M.; Ayad, D. M.; Wei, Y.; Sarhan, A. A. Adsorption of Cu(II), Co(II), and Ni(II) Ions by Modified Magnetic Chitosan Chelating Resin. *J. Haz. Mater.* 2010, *177*, 962–970.

[123] Mansoori, Y.; Ghanbari, M. Novel Polyimides Obtained from a New Aromatic Diamine (BAPO) Containing Pyridine and 1,3,4-Oxadiazole Moieties for Removal of Co(II) and Ni(II) Ions. *Polym. Adv. Technol.* 2015, *26*, 658–664.
[124] Shaaban, A. F.; Khalill, A. A.; Radwan, M.; El Hefnawy, M.; El Khawaga, H. A. Synthesis, Characterization and Application of A Novel Nanometer-Sized Chelating Resin for Removal of Cu(II), Co(II) and Ni(II) Ions from Aqueous Solutions. *J. Polym. Res.* 2017, *24*, 165–179.
[125] Arshadi, M.; Amiri, M. J.; Mousavi, S. Kinetic, Equilibrium and Thermodynamic Investigations of Ni(II), Cd(II), Cu(II) and Co(II) Adsorption on Barley Straw Ash. *Water Res. Industry*. 2014, *6*, 1–7.
[126] Hayati, B.; Maleki, A.; Najafi, F.; Daraei, H.; Gharibi, F.; McKay, G. Adsorption of Pb2+, Ni2+, Cu2+, Co2+ Metal Ions from Aqueous Solution by PPI/SiO2 as New High Performance Adsorbent: Preparation, Characterization, Isotherm, Kinetic, Thermodynamic Studies. *J. Mol. Liq.* 2017, *237*, 428–436.
[127] Carmo Ramos, S. N.; Xavier, A. L. P.; Teodoro, F. S.; Gil, L. F.; Gurgel, L. V. A. Removal of Cobalt(II), Copper(II), and Nickel(II) Ions from Aqueous Solutions Using Phthalate-Functionalized Sugarcane Bagasse: Mono and Multicomponent Adsorption in Batch Mode. *Ind. Crop Prod.* 2016, *79*, 116–130.
[128] Khan, M.; Kim, S. W.; Rao, R. A. K.; Abou-Shanab, R. A. I.; Bhatnagar, A.; Song, H.; Jeon, B. H. Adsorption Studies of Dichloromethane on Some Commercially Available GACS: Effect of Kinetics, Thermodynamics and Competitive Ions. *J. Haz. Mater.* 2010, *178*, 963–972.
[129] Ray, J.; Jana, S.; Bhanja, S. K.; Tripathy, T. Efficient Removal of Co(II), Ni(II), and Zn(II) Metal Ions from Binary and Ternary Solutions Using a pH Responsive Bifunctional Graft Copolymer. *Colloid Polym. Sci.* 2018, *296*, 1275–1291.

## Supplementary Information

**Efficient removal of Ni(II) and Co(II) ions from aqueous solutions using silica-based hybrid materials functionalized with PAMAM dendrimers**

Mateusz Pawlaczyk*, Grzegorz Schroeder

Faculty of Chemistry, Adam Mickiewicz University in Poznań, Uniwersytetu Poznańskiego 8, 61-614 Poznań, Poland

*corresponding author: Mateusz Pawlaczyk
e-mail address: mateusz.pawlaczyk@amu.edu.pl
tel: +48 61 829 17 97

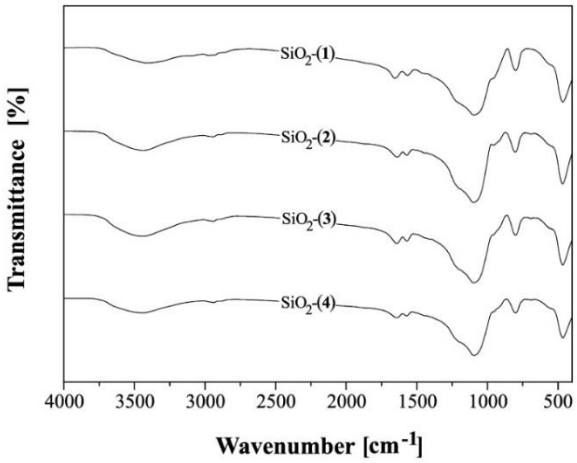


Figure A.1. The FT-IR spectra of the hybrid materials $SiO_2$-(**1**) – $SiO_2$-(**4**)

Table A.1. The values of the dendrimers loading on the hybrid materials

| Hybrid material | Loading [mmol $g^{-1}$] |
|---|---|
| $SiO_2$-(**2**) | 0.310 |
| $SiO_2$-(**3**) | 0.152 |
| $SiO_2$-(**4**) | 0.155 |
| $SiO_2$-(**5**) | 0.078 |

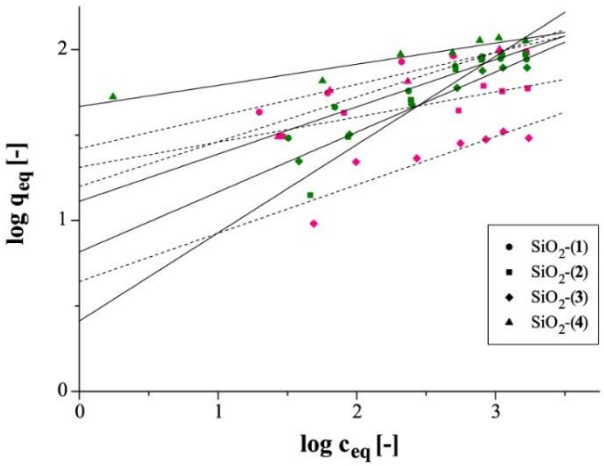


Figure A.2. Freundlich isotherms for adsorption of Ni(II) (green; solid lines) and Co(II) (pink; dashed lines) on $SiO_2$-dendrimer hybrid materials

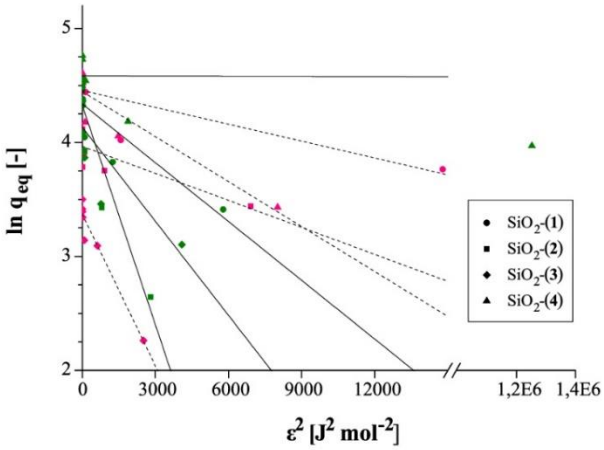


Figure A.3. Dubinin-Radushkevich isotherms for adsorption of Ni(II) (green; solid lines) and Co(II) (pink; dashed lines) on $SiO_2$-dendrimer hybrid materials

Table A.2. Dubinin-Radushkevich isothermal parameters for adsorption of Ni(II) and Co(II) ions on $SiO_2$-dendrimer hybrid materials

| Ion | Adsorbent | Langmuir isotherm | | | |
|---|---|---|---|---|---|
| | | $10^4 \cdot \beta$ [$mol^2\ J^{-2}$] | E [$kJ\ mol^{-1}$] | $q_{m,cal.}$ [$mg\ g^{-1}$] | $R^2$ |
| Ni(II) | $SiO_2$-(**1**) | -1.720 ± 0.414 | 0.054 ± 0.006 | 76.6 ± 7.1 | 0.8754 |
| | $SiO_2$-(**2**) | -6.417 ± 1.082 | 0.028 ± 0.002 | 75.7 ± 9.1 | 0.7116 |
| | $SiO_2$-(**3**) | -2.752 ± 0.784 | 0.043 ± 0.006 | 62.4 ± 7.7 | 0.7751 |
| | $SiO_2$-(**4**) | -0.005 ± 0.002 | 1.008 ± 0.192 | 97.9 ± 8.7 | 0.5946 |
| Co(II) | $SiO_2$-(**1**) | -0.495 ± 0.134 | 0.100 ± 0.014 | 86.2 ± 6.5 | 0.7308 |
| | $SiO_2$-(**2**) | -0.790 ± 0.220 | 0.080 ± 0.011 | 52.8 ± 3.1 | 0.7167 |
| | $SiO_2$-(**3**) | -4.433 ± 0.469 | 0.034 ± 0.002 | 29.1 ± 1.3 | 0.9470 |
| | $SiO_2$-(**4**) | -1.316 ± 0.242 | 0.062 ± 0.006 | 85.3 ± 6.4 | 0.8552 |

*molecules*

MDPI

*Article*

# Dendrimer-Functionalized Hybrid Materials Based on Silica as Novel Carriers of Bioactive Acids

**Mateusz Pawlaczyk * and Grzegorz Schroeder**

Faculty of Chemistry, Adam Mickiewicz University in Poznań, Uniwersytetu Poznańskiego 8, 61-614 Poznań, Poland; schroede@amu.edu.pl

* Correspondence: mateusz.pawlaczyk@amu.edu.pl; Tel.: +48-61-829-17-97

Received: 9 May 2020; Accepted: 3 June 2020; Published: 8 June 2020

check for updates

**Abstract:** One of the major goals in the materials science is the design and development of non-toxic, versatile, and efficient drug delivery systems. The study reported in this paper concerns the syntheses of poly(amidoamine) (PAMAM) dendrimers with tris(2-aminoethyl)amine as an amine core and different terminal amines, and their attachment to silica matrix. The obtained ethylenediamine (EDA), triethylenetetramine (TETA), tris(2-aminoethyl)amine (TREN) and 4,7,10-trioxa-1,13-tridecanediamine (TRI-OXA) dendrimers were introduced to the support surface via an epoxy linker, leading to a loading efficiency in the range of 0.054–0.113 mmol $g^{-1}$, determined using elemental and thermogravimetric analyses. The materials exhibited high adsorption capacities towards the chosen model drugs: folic, salicylic and nicotinic acid. The investigated adsorption processes were found to follow the Freundlich isotherm model, with indication of the drugs' structure influence on the binding efficiency. Drug-loaded hybrid materials were also described for in vitro drug release in three pH-different paraphysiological media. The highest percentage release was obtained in the tests performed at pH 2.0, ranging between 35.42 and 99.83%. Satisfactory results and the versatility of PAMAM dendrimers may lead to the application of such materials not only as drug carriers dedicated to a wide range of pharmaceutics, but also as analytical tools for pre-concentration and/or the determination of biocompound contamination in samples.

**Keywords:** drug delivery; hybrid materials; PAMAM dendrimers; bioactive acids; in vitro drug release

## 1. Introduction

In recent decades, much attention has been paid to design synthesis and the final utilization of organic grafting agents dedicated to various solid supports, aiming at obtaining hybrid materials exhibiting versatile chemical and analytical applications. The common characteristic feature of such organic agents is their polyfunctionality, which affords interactions with particular analytes through non-covalent binding, such as electrostatic and hydrogen bonding, chelation, hydrophobic effect or π-π stacking of aromatic rings. Non-covalent bonds are desirable because of their high effectiveness, in particular if different types of bonds impose each other. Moreover, the low energy of non-covalent bonds permits the easy desorption of the adsorbed analytes so the materials with such bonds can be used as recyclable adsorbents and delivery systems.

One family of molecules exhibiting applicability towards diverse compounds, are dendrimers, especially poly(amidoamine) (PAMAM) dendrimers invented and introduced in 1980s by Tomalia [1]. The idea of introducing a dendritic structure as a polyfunctional domain could have originated from dendritic topology found in the natural environment, including snow crystals, neuron branches or tree roots [2]. The common features of dendrimers are: repetitiveness of structural units afforded by the repeated binding of monomers to a chosen core (branching center), multifunctionality gained with

the introduction of peripheral functional groups and the presence of internal cavities as a series of gaps between the synthesized branches. More precisely, PAMAM dendrimers consist of an amine core (ammonia or polyamine, e.g., ethylenediamine, diethylenetriamine, etc.), which makes the starting point for building amidoamine branches and undergoes sequential expansion. Each step of introducing the next peripheral amino component leads to the layered expansion of the molecule called dendrimer generation (G*x*, where x is the generation number). As the dendrimer generation increases, the value of the stability constant of the dendrimer-analyte complex increases. What is more, multiple free terminal amino groups on the dendrimers' ultimate layer allow their further functionalization with several organic domains, which may tune or introduce new interacting sources, such as: polyethylene glycol (PEG), acetyl, long-chain fatty acids, amino acids or targeting domains [3]. Therefore, PAMAM dendrimers and their derivatives may find attractive biological applications either in the native form or immobilized on a support surface. These two types of species of dendrimers and their derivatives can be subjected to in vitro and in vivo studies, in order to assess their desirable biological effectiveness and also cytotoxicity, permeability or degradability.

The drug delivery potential of bare PAMAM dendrimers is strictly related to their multifunctional structure. Namely, multiple amine and amide groups on the surface or in the dendrimer's interior allow the non-covalent electrostatic or hydrogen bonding between the dendrimers and drug molecules [4]. Moreover, the 'internal architecture' of PAMAM dendrimers allows the effective physical entrapment of drugs in dendritic internal cavities, whose size is dependent on the size of the core molecule and branching units, determining the distance between the subsequent branches. The aforementioned structural features of dendrimers permit the adsorption of drug molecules to the dendrimer's surface or permit their diffusion into the dendrimer's interior, leading to host-guest supramolecular complexes. Although PAMAM-drug conjugates may be used as therapeutics targeted delivery systems with an enhanced transmembrane permeability which may dissolute already in blood plasma, the increase in the dendrimer generation leads to its higher cytotoxic effect towards cells. It is strongly connected with the interaction between the polycationic macromolecule and the negatively charged glycocalices, which are one of the major cell membrane constituents, triggering apoptotic cell death [5–9]. Densely charged PAMAM dendrimers of generation 7.0 have been also proved to enhance the aggregation of several proteins in the bloodstream, causing their deactivation [8]. The prevention of negative interactions of the dendrimers with proteins, membrane constituents, etc. is therefore connected with a decrease in the surface amine groups reactivity by their conjugation with e.g., PEG, lipophilic carboxylic acid with short hydrocarbon chains, surfactants, acetyl groups, amino acids (arginine and ornithine), biotin or dimethyl itaconate [10–17], as well as with folic acid or octeroide (somatostatin analogue) as targeting domains [18,19].

Another possibility of shielding the polycationic character of PAMAM dendrimers is their immobilization on support, leading to the group of novel dendrimer-functionalized hybrid materials. Such hybrids exhibit physicochemical features common for native dendrimers and platforms, but also gain the character of a functionalized material-finding application as sorbents: molecular scavengers, materials for analytes extraction, pre-concentration systems and delivery systems of biomolecules or nucleic acids [20]. Among the well known supports, superparamagnetic iron oxide nanoparticles ($Fe_3O_4$; SPIONs) are of great interest, due to the easiness of obtaining them, their size and shape control, but mostly because of their magnetic properties, affording easy separation, targeting within samples and organisms and their visualization with either microscopic or resonance imagining [21,22]. Hitherto literature presents several papers devoted to the synthesis, characterization and final biomedical applications of $Fe_3O_4$ nanoparticles functionalized with PAMAM dendrimers of various structures and generations [23–26]. For instance, G3.5 PAMAM grafted on the iron oxide nanoparticles' surface was proved to be negligibly more cytotoxic towards HeLa cells than bare particles, indicating the cytocompatibility of such systems with a simultaneous ability of penetration into bacteria cells [27]. A similar PEGylated material decorated with folic acid as a targeting residue was tested for the delivery properties of paclitaxel towards MCF-7 human breast cancer cell line, which resulted in the cancer cell

viability decreasing by 34% [28]. Moreover, the efficiency of $Fe_3O_4$ particles modified with PAMAM dendrimers through various linkers has been studied in delivery of doxorubicin (versatile anticancer drug) and epigallocatechin gallate (therapeutic agent against various cancers, stroke or Parkinson's and Alzheimer's diseases) and has been explored towards HeLa cells [29–31]. The high efficiency of the drug loading of the materials and their proper cytocompatibility have been reported, which make them potential materials for therapeutics delivery with minimized side effects. Furthermore, iron oxide nanoparticles modified with citric acid and G5.0 PAMAM dendrimer have been considered to play the role of curcumin delivery platforms [32]. The material incubated with human breast adenocarcinoma (MCF-7 cell line) showed 45% cell viability at a micromolar concentration of the $Fe_3O_4$/PAMAM/curcumin system. In addition, a PAMAM dendrimer made of unusual branching units, which were 1,3-propanodiamine and glutaraldehyde, was branched around $Fe_3O_4$ nanoparticles and proved to show efficient antimicrobial activity towards two cell lines: *Escherichia coli* and *Staphylococcus Aureus* [33]. However, such hybrid materials find application not only as supports for the targeted delivery of biomolecules, but also as supporting materials for the delivery of nitrogen oxide (NO), which might be classified as an endogenous agent taking part in many physiological and pathophysiological pathways, e.g., wound healing and immune response. Yu et al. [34] have presented a method for the synthesis of *N*-diazeniumdiolate-functionalized hybrid material as a new NO-release precursor. The material was obtained in a reaction between $Fe_3O_4$/polydopamine/G3.0 PAMAM and nitrogen oxide under elevated pressure. The same material was investigated for antimicrobial activity against *E. coli* and *S. Aureus* under infrared irradiation to ensure NO-releasing conditions. The studies resulted in obtaining highly effective material with the controllable release of nitrogen oxide performed in IR switch-on/off mode.

Biological applications of the PAMAM-grafted hybrid materials based on other platforms such as single- or multi-walled carbon nanotubes [35–37], halloysite nanotubes [38–40], mesoporous silica [41,42], titania [43], gold nanorods [44], polymeric chains [45] and quantum dots made of CdSe/ZnS or CdSe/CdTe binary systems [46,47] have also been studied. Nevertheless, the pressing need for novel transporting systems has prompted us to focus on silica-based hybrid materials functionalized with PAMAM dendrimers. Our recent study was aimed at the synthesis of a series of structurally different dendritic structures with tris(2-aminoethyl)amine as a core molecule and ethylenediamine, tris(2-aminoethyl)amine, triethylenetetramine and 4,7,10-trioxa-1,13-tridecanediamine as surface amine residues. The dendrimers were introduced onto a silica surface via a linker with epoxy groups using a 'grafting to' approach, which allowed the retention of the fully dendritic feature of modifying agents. The obtained group of PAMAM-modified materials was investigated to establish their adsorptive properties towards folic acid, salicylic acid and nicotinic acid as the model bioactive molecules, with their further in vitro release studies under various paraphysiological conditions.

## 2. Results and Discussion

### *2.1. Synthesis of PAMAM Dendrimers*

The PAMAM dendrimers consisting of tris(2-aminoethyl)amine as the amine core molecule were obtained using the two-step synthetic protocol. The first step involved the branching of the amine core molecule using the Michael addition between tris(2-aminoethyl)amine and methyl acrylate, leading to an ester intermediate, which was the precursor of desired dendritic structures. The second step was based on the amidation of the ester intermediate with proper amine, which led to obtaining each of the designed PAMAM dendrimers (Figure 1a). The choice of structurally different terminal amino-components was made on the basis of the expected influence of the terminal amine structure on the adsorptive properties of the final hybrid materials. The semi-product and the products were characterized by the electrospray ionization mass spectrometry (ESI-MS) technique. The spectrum of the ester intermediate (Figure S1) shows a highly intensive molecular peak $m/z$ = 663.62 and its sodium derivative $m/z$ = 685.55. On the other hand, the spectra of PAMAM dendrimers (Figure S2) show

several signals corresponding to fragmentation peaks, which are strongly connected to the capability of dendrimers to fragmentation, which is a result of their chemical structure (several polyamine and carbonyl domains) and the choice of ionization mode [48]. The spectra also show several signals corresponding to sodium adducts, as well as mono-, di- or even triprotonated signals, regarding the polyamine character of the studied dendrimers.

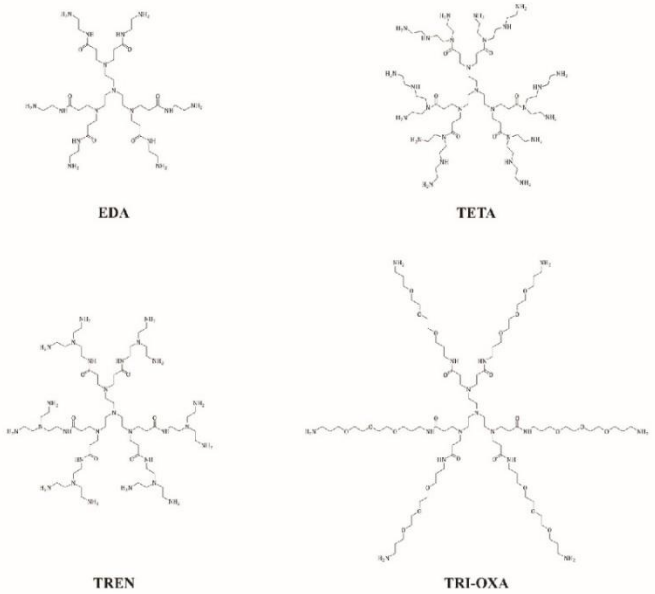


**Figure 1.** (**a**) The structures of the synthesized poly(amidoamine) (PAMAM) dendrimers containing tris(2-aminoethyl)amine as an amine core and different terminal amino-components: EDA (ethylenediamine), TETA (triethylenetetramine), TREN (tris(2-aminoethyl)amine) and TRI-OXA (4,7,10-trioxa-1,13-tridecanediamine); (**b**) the synthetic approach to obtaining hybrid materials grafted with poly(amidoamine) (PAMAM) dendrimers (on the example of tris(2-aminoethyl)amine (TREN) dendrimer grafting).

*2.2. Synthesis and Characterization of the Hybrid Materials*

The hybrid materials functionalized with the synthesized PAMAM dendrimers were obtained in the reaction between the free terminal amine group of the dendrimer and the easy opening epoxy ring on the silica surface (Figure 1b). The choice of *N*,*N*-dimethylformamide (DMF) instead of the usual PAMAM dendrimers' solvent, which is methanol, was driven by the non-nucleophilic character of DMF, decreasing the possibility of a side reaction between epoxy silica-surface groups and solvent molecules. The successful grafting of dendrimers on the silica surface was proven by Fourier-transformed photoacoustic infrared (FT-IR/PAS) spectra results (Figure 2a). All the spectra are similar, which is a consequence of the utilization of epoxy-modified silica gel as the support for PAMAM-functionalized hybrid materials. Each spectrum shows two signals assigned to the asymmetric stretching of silica matrix, which have their maxima approximately at 797 and 952 $cm^{-1}$. Morevoer, broad bands between 1000 and 1250 $cm^{-1}$ are related to the symmetric stretching of Si-O-Si domains. Nevertheless, the proper functionalization of silica support with particular PAMAM dendrimers is proved by the presence of signals at 1560 and 1640 $cm^{-1}$, which correspond to the bending of N-H and the stretching of C=O, respectively, both present in amide-rich dendrimers anchored to the silica surface. These signals are not present in the spectrum of the silica precursor ($SiO_2$-epoxy), which undoubtedly proves the PAMAM-functionalization of the hybrid materials. Moreover, several signals at 2889, 2936 and 2974 $cm^{-1}$ are related to the symmetric and asymmetric stretching of methylene groups -$CH_2$- present in the studied dendritic structures. These signals are noticeable on each spectrum, which might be attributed to the presence of multiple methylene groups in PAMAM dendrimers (the spectra of the hybrid materials) or to the methylene groups originating from the propylosilane epoxy-linker ($SiO_2$-epoxy). In addition, the broad bands between 3050 and 3450 $cm^{-1}$ in the hybrid materials spectra can be attributed to the overlapped stretching modes of N-H and O-H vibrations, originating in multiple terminal primary amine groups and free hydroxyl groups remaining after the functionalization of silica by the epoxy-ring opening [49]. The broad signal in $SiO_2$-epoxy, however, may originate in free hydroxyl groups as a result of trace humidity in the material leading to the ring opening. The successful functionalization of silica particles with PAMAM dendrimers was also indicated by the thermogravimetric analysis (Figure 2b), which showed the samples' mass loss up to 20%. Each spectrum shows two distinct decomposition steps. The first one is visible upon heating to around 200 °C and is strictly connected to the trace humidity removal from the samples studied. This step is manifested as approximately 2.5% mass loss of the samples and it is followed by the slow oxidation of the organic residue anchored to the inorganic platforms. This thermal decomposition takes place in the temperature range between 250 and 700 °C, leading to 10–16% mass loss of the samples.

Moreover, the hybrid materials obtained were subjected to the CHN elemental analysis to assess the percentage contents of carbon, hydrogen and nitrogen. The most informative results of the elemental analysis were those of the nitrogen percentage contents, as carbon and hydrogen appear also in the glycidoxypropyl linker between the silica matrix and the grafted PAMAM dendrimers. The nitrogen percentage content was 2.521%, 2.122%, 3.196% and 2.010% for $SiO_2$-EDA, $SiO_2$-TETA, $SiO_2$-TREN and $SiO_2$-TRI-OXA, respectively. The loadings of dendritic structures on the silica support were calculated on the basis of these values to be 0.113, 0.054, 0.082 and 0.094 mmol $g^{-1}$, respectively, so in good agreement with approximations following from the thermogravimetric analysis. The highest loading efficiency was calculated for the material containing surface EDA dendrimer molecules, which consist of the most compact and the least branched terminal amine used—ethylenediamine. On the other hand, the lowest loading values were calculated for the materials functionalized with TETA and TREN dendrimers with amine terminal domains whose branched character was defined before the synthesis (tris(2-aminoethyl)amine) or was a consequence of the polyamine structure that determined the differentiation in the reactivity of primary and secondary amine groups (triethylenetetramine). Furthermore, Figure 3 presents the SEM images of the synthesized hybrid materials. All the silica gel particles can be classified as microparticles with the mean size of approximately 40 μm. The functionalization of the support with more branched dendrimers TETA and TRI-OXA led to a formation

of the particles with a higher mean size, as a result of the bulky dendritic structures (Figure 3C,D). The silica precursor used was described as a porous, micro-sized material, therefore the attachment of the dendrimers did not greatly enhance the size of the final hybrid materials.

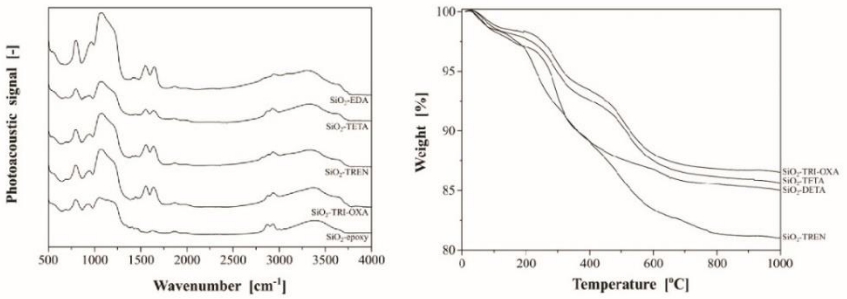


**Figure 2.** (**a**) The Fourier-transformed photoacoustic infrared (FT-IR/PAS) spectra of the PAMAM-modified hybrid materials; (**b**) the thermogravimetric analysis of the synthesized hybrid materials.

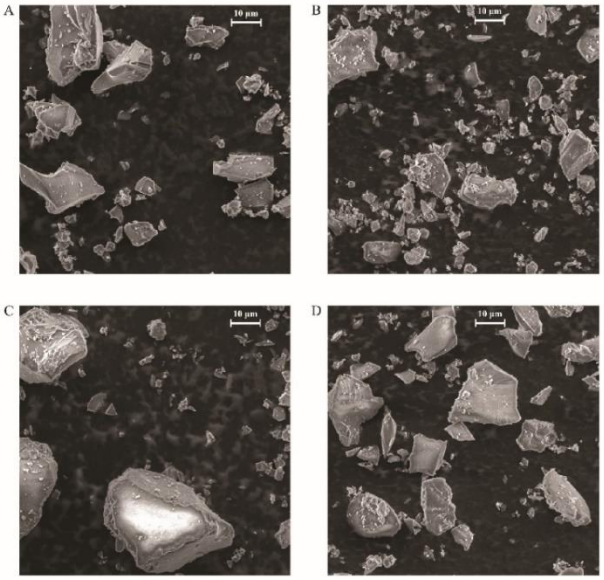


**Figure 3.** The SEM images of the obtained PAMAM-modified hybrid materials: (**A**) $SiO_2$-EDA, (**B**) $SiO_2$-TETA, (**C**) $SiO_2$-TREN and (**D**) $SiO_2$-TRI-OXA. The scale bar is 10 µm.

### 2.3. Adsorption of Bioactive Compounds on the Hybrid Materials

The adsorptive properties of the obtained materials were tested for three bioactive compounds: folic, salicylic and nicotinic acids. The choice was driven by their highly broad application as drugs and vitamin supplements, while folic acid is also a preferable candidate for drug-delivery investigation, as it is chemically similar to the broadly used anticancer agent, methotrexate. Moreover, the chosen bioactive compounds are structurally different, which may bring preliminary information of the relationship between the adsorption ability and structure of the analyte. The investigation of the $SiO_2$-PAMAM adsorption properties was based on the possibility of proton exchange between the highly basic PAMAM dendrimers on the silica surface and the acidic adsorbate molecules. Such an exchange, leading to the formation of a cationic form of the dendrimers (-$NH_3^+$) and an anionic form of biomolecules (-$COO^-$), enables effective electrostatic interactions between the hybrid materials and the adsorbates. The ESI-MS spectra of the complexes of exemplary PAMAM dendrimers containing tris(2-aminoethyl)amine as the terminal amine and each of the bioactive compounds used (Figure S3) proved the proton exchange between the tested components. The ESI-MS spectra of TREN-salicylic acid (Figure S3a) and TREN-nicotinic acid (Figure S3b) in positive mode showed signals originating mostly from the monoprotonated forms (z 1+) of the dendrimers' fragmentation products (the signal at *m*/*z* 1201.98, 1055.84, 983.20, 909.70), which strictly indicated the single proton exchange between the dendrimer and the drug. The corresponding spectra in negative mode presented the most intensive signals related to the deprotonated forms of the salicylic and nicotinic acids at *m*/*z* 137.36 and *m*/*z* 122.45, respectively. Moreover, several mono-negative signals (z 1−), corresponding to the adducts of the fragmented -COOH domain of biomolecules and the fragmented dendritic structures appear, e.g., at *m*/*z* 570.47, 643.55, 907.61, 951.59, 1097.77 or 1243.93, which are similar in both the TREN-salicylic acid and TREN-nicotinic acid complex spectra. In the case of the TREN-folic acid (Figure S3c), an exchange of the two protons derived from dicarboxylic drug takes place, determining the appearance of mostly di-, but also tri- or even tetra-positive signals in the positive ESI-MS spectrum corresponding to the dendrimers' fragmentation ions or their sodium adducts (*m*/*z* (z 2+) 612.65, 601.68, 539.60, 528.65, 466.53, 455.55; *m*/*z* (z 3+) 401.61, 352.87; *m*/*z* (z 4+) 301.64). The least intensive signals at *m*/*z* 909.64 and 1055.81 related to the monoprotonated (z 1+) fragmentation ions of the dendrimer might be a consequence of the single proton exchange between the folic acid and TREN dendrimer. In the negative spectrum, the most intensive signals are related to the di-negative ion (z 2−) of folic acid *m*/*z* 219.69, however the spectrum also exhibits several mono-, di- and tri-negative signals at *m*/*z* 1243.98, 1097.74, 951.55, 644.08, 570.48, 544.82, 462.80 or 380.89, corresponding to the adducts of the fragmented dendrimer and the fragmented carboxylic group of biomolecules. There is also a mono-negative signal at *m*/*z* 440.23, which is connected with the exchange of a single proton, which when interpreted together with the previous results proves the formation of the dendrimer-drug complex, indicating the PAMAM-grafted materials' capability of binding the acidic drugs, which is shown in Figure 4. Therefore, the ESI-MS analysis showed that the chosen drugs can be bound to surface dendritic structures only via electrostatic interactions with terminal amine groups. Although, the amine groups are also utilized in the dendrimers' immobilization process, the dendrimers may easily interact with analytes through the other multiple free -$NH_2$ domains.

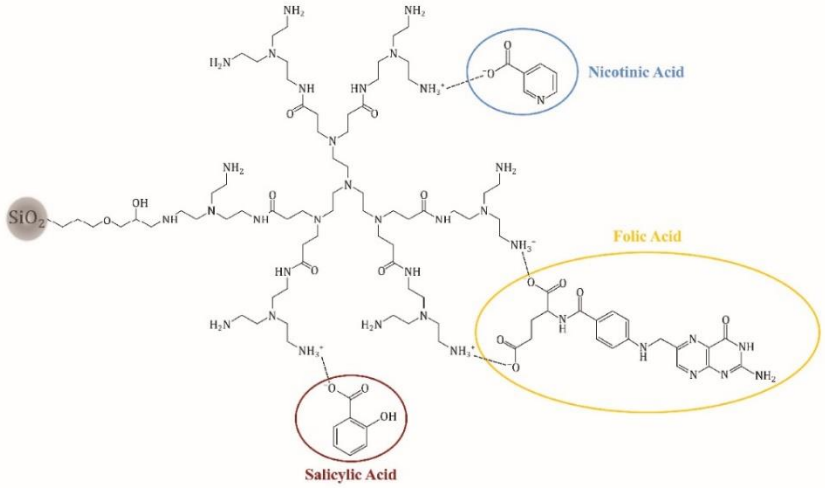


**Figure 4.** The possible electrostatic interactions (dotted line) between the PAMAM-grafted silica particles and bioactive compounds, the example of $SiO_2$-TREN material.

The adsorptive properties of the obtained PAMAM-grafted materials were tested in isothermal studies (Figure 5), which delivered information about the behavior of adsorbent-adsorbate interactions and their efficiency at equilibrium state. Therefore, the experimental data were fitted to several adsorption isotherm models for the assessment of particular physicochemical quantities. The most broadly used models are the Langmuir and Freundlich ones, which take into account the distribution of the binding places on the adsorbents' surface and the interactions between the adsorbate molecules [50]. The Langmuir model (Figure S4) assumes the formation of the adsorbate monolayer on the homogenous adsorbent surface, neglecting the adsorbate molecules' interaction, and can be expressed by Equation (1), where $c_{eq}$ is the concentration of the drug remaining in the solution at equilibrium (mg $L^{-1}$), $q_{eq}$ and $q_{max}$ are the equilibrium and the maximal amount of the drug adsorbed, respectively (mg $g^{-1}$), while $K_L$ is the Langmuir constant (L $mg^{-1}$):

$$\frac{c_{eq}}{q_{eq}} = \frac{c_{eq}}{q_{max}} + \frac{1}{q_{max} K_L} \quad (1)$$

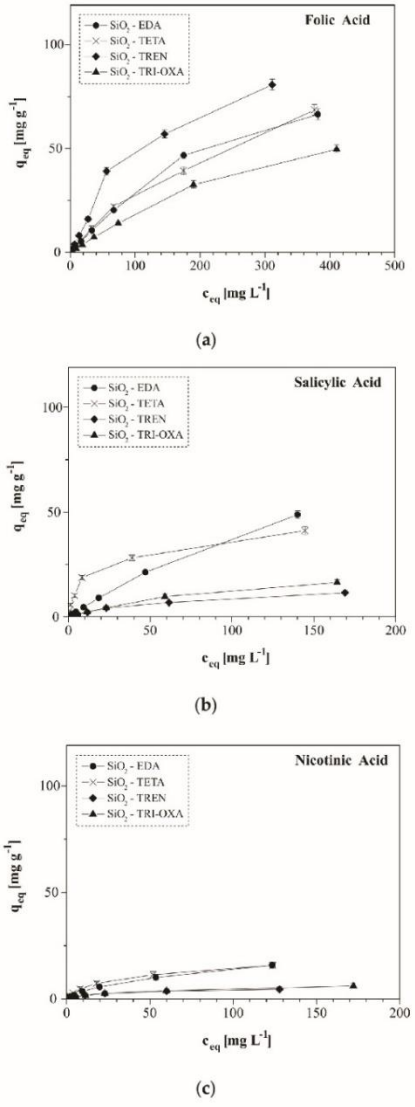


**Figure 5.** The isotherms of the acidic drugs' adsorption on the obtained hybrid materials: (**a**) folic acid; (**b**) salicylic acid; and (**c**) nicotinic acid. For some points, the SDs are smaller than the plotted symbols.

In contrast, the Freundlich isotherm model (Figure S5) indicates the possibility of adsorbate multilayer formation, which is a consequence of the interactions of adsorbate molecules. Moreover, it

assumes the heterogeneity of the adsorbent surface, influencing the adsorptive properties of materials, and is expressed as Equation (2):

$$\log q_{eq} = \frac{1}{n} \log c_{eq} + \log K_F \quad (2)$$

where 1/n is the coefficient related to the heterogeneity of the adsorptive material (−) and $K_F$ is the Freundlich constant (mg $g^{-1}$ (L $mg^{-1})^{1/n}$). On the basis of both aforementioned linear plots of the isothermal models, all the parameters and their standard deviations can be easily calculated from slopes and intercepts; the relevant values are collected in Table 1.

**Table 1.** Isothermal parameters of the drugs' adsorption on the PAMAM-modified materials.

| Biomolecule | Adsorbent | Langmuir Isotherm | | | | Freundlich Isotherm | | |
|---|---|---|---|---|---|---|---|---|
| | | $q_m$ (mg $g^{-1}$) | $R_L$ (-) | $R^2$ | $\chi^2$ | 1/n (−) | $R^2$ | $\chi^2$ |
| Folic Acid | $SiO_2$-epoxy | 12.46 ± 0.96 | 0.9966 | 0.9654 | 1.000 | 0.80 ± 0.03 | 0.9907 | 0.054 |
| | $SiO_2$-EDA | 274.72 ± 6.87 | 0.9987 | 0.9963 | 0.003 | 0.93 ± 0.02 | 0.9979 | 0.017 |
| | $SiO_2$-TETA | 230.95 ± 18.18 | 0.9882 | 0.9977 | 0.025 | 0.96 ± 0.01 | 0.9994 | 0.029 |
| | $SiO_2$-TREN | 236.97 ± 11.79 | 0.9984 | 0.9853 | 0.008 | 0.91 ± 0.02 | 0.9978 | 0.012 |
| | $SiO_2$-TRI-OXA | 202.43 ± 4.34 | 0.9972 | 0.9972 | 0.727 | 0.93 ± 0.02 | 0.9982 | 0.010 |
| Salicylic Acid | $SiO_2$-epoxy | 1.50 ± 0.09 | 0.9549 | 0.9827 | 8.739 | 0.50 ± 0.02 | 0.9887 | 0.072 |
| | $SiO_2$-EDA | 157.48 ± 9.67 | 0.9956 | 0.9777 | 0.006 | 0.93 ± 0.02 | 0.9973 | 0.013 |
| | $SiO_2$-TETA | 15.44 ± 1.17 | 0.9803 | 0.9667 | 0.056 | 0.70 ± 0.03 | 0.9858 | 0.046 |
| | $SiO_2$-TREN | 42.92 ± 2.10 | 0.8741 | 0.9848 | 0.222 | 0.46 ± 0.03 | 0.9855 | 0.037 |
| | $SiO_2$-TRI-OXA | 29.53 ± 1.69 | 0.9902 | 0.9807 | 0.104 | 0.84 ± 0.03 | 0.9914 | 0.028 |
| Nicotinic Acid | $SiO_2$-epoxy | 1.33 ± 0.10 | 0.9610 | 0.9641 | 8.190 | 0.54 ± 0.02 | 0.9871 | 0.030 |
| | $SiO_2$-EDA | 20.11 ± 2.25 | 0.8758 | 0.9408 | 0.673 | 0.64 ± 0.03 | 0.9907 | 0.073 |
| | $SiO_2$-TETA | 4.86 ± 0.25 | 0.8499 | 0.9870 | 1.245 | 0.54 ± 0.03 | 0.9866 | 0.052 |
| | $SiO_2$-TREN | 17.74 ± 1.08 | 0.7724 | 0.9816 | 0.353 | 0.42 ± 0.08 | 0.9888 | 0.032 |
| | $SiO_2$-TRI-OXA | 7.18 ± 0.46 | 0.9508 | 0.9803 | 1.002 | 0.60 ± 0.03 | 0.9857 | 0.072 |

All the materials, including the $SiO_2$-epoxy material, which is a bare precursor of the synthesized hybrid materials, exhibit an adsorption capacity towards all the biocompounds studied, which is in agreement with the Freundlich isothermal model, as confirmed by the $R^2$ correlation coefficients higher than 0.985 for all the experiments. It is also indicated in Table 1, where the $R^2$ values for the Freundlich model are higher or equal to the $R^2$ values calculated for the Langmuir model, that the $\chi^2$ values calculated for the Freundlich model are mostly lower than those calculated for the Langmuir fitting. Therefore, the adsorption of the biocompounds studied on the materials obtained is possible thanks to the materials' surface heterogeneity, proved by the Freundlich 1/n factors values ranging between 0 and 1 and also the intermolecular interactions between the adsorbate molecules, which are easily proved by the structural features of the bioactive compounds used. Namely, folic acid contains three aromatic rings, which may easily interact with each other by the π-π stacking effect, as well as electrostatic interactions between two carboxylic groups and several amine groups (terminal, internal or even the one contained in pteridyl domain), while nicotinic and salicylic acids may be engaged in intermolecular interactions thanks to the presence of aromatic rings in both structures. Therefore, folic acid is the most intensively adsorbed, independently of the material used. Moreover, the amount of hydrogen-bonding acceptors and donors in the biocompounds' structure, and also their $pK_a$ values, influence the intensity of the interaction with basic PAMAM dendrimers. The ratio of the hydrogen-bonding acceptors to donors is 10/6 for folic acid, 3/2 for salicylic acid and 3/1 for nicotinic acid, which firmly indicates the formation of the strongest interactions between the basic PAMAM dendrimers and folic acid, while the weakest is with nicotinic acid. In addition, the acid-base interaction of the surface dendrimers with biocompounds is dependent on their $pK_a$ values, namely the lower the $pK_a$ value, the stronger the interaction. The $pK_a$ values are 3.49 for folic acid, 2.97 for salicylic acid and 4.75 for nicotinic acid. On the basis of the mentioned chemical features of the studied bioactive acids, the biocompounds can be ordered according to their binding efficiency as: folic acid > salicylic acid > nicotinic acid. Nevertheless, the reliable fitting of the experimental data to the Langmuir isothermal model led to the determination of maximal adsorption capacities ($q_m$) for all the hybrid and

bare materials. As expected, $SiO_2$-epoxy material (bare silica support) showed the lowest adsorption capacity towards the bioactive acids among all the adsorbents, reaching approximately 12.5 mg $g^{-1}$ for folic acid, and 1.5 and 1.3 mg $g^{-1}$ for salicylic and nicotinic acid, respectively. The binding of therapeutic substances in the material that does not contain dendrimer as the domain biding through electrostatic interactions of the physical entrapment is thus based on the physical diffusion of drugs into the material pores. $SiO_2$-EDA which contains the dendrimer having the shortest and the least branched terminal aminocomponent used, ethylenediamine, turned out to be the most effective adsorbent of all the acidic bioactive compounds studied. The use of ethylenediamine ensured the highest dendrimer-grafting efficiency at the level of 0.113 mmol $g^{-1}$, which contributed to the significantly increased adsorption capacity of the material containing it, towards the bioactive acidic compounds, reaching the maximal adsorption capacities of 274.72, 157.48 and 20.11 mg $g^{-1}$ for folic, salicylic and nicotinic acids, respectively. A high-adsorption efficiency was also noted for the $SiO_2$-TREN material, containing a surface dendritic structure built of symmetric tris(2-aminoethyl)amine. The doubled number of the ultimate interacting amine groups and the increased number of cavities in the interior of the dendrimer should have significantly enhanced the $q_m$ values, however, the steric hindrance of the TREN dendrimer contributed to its lower loading onto the silica surface (0.082 mmol $g^{-1}$), which jointly led to high, but not the highest, adsorption effectiveness. The least adsorptive materials were the ones decorated with the TETA and TRI-OXA dendrimers, which might be a consequence of steric hindrance and the low functionalization percentage of the dendritic structures. In addition, the long-chained dendrimer containing additional oxygen atoms (TRI-OXA dendrimer) may not be capable of the effective binding of compounds because of the presence of a long methylene-rich chain which does not improve the interaction with acidic adsorbates. Thus, the adsorptive efficiency of the materials may be ordered as: $SiO_2$-EDA > $SiO_2$-TREN > $SiO_2$-TETA ~ $SiO_2$-TRI-OXA. Moreover, for all the adsorption experiments, the dimensionless separation Langmuir factors $R_L$ were calculated using Equation (3), where $c_{max}$ is the maximal concentration of the drug solutions used for the isothermal experiments (mg $L^{-1}$):

$$R_L = \frac{1}{1 + K_L c_{max}} \quad (3)$$

For all the experiments, the $R_L$ factors ranged between 0 and 1, which indicates the favorability of the adsorption processes [51]. Furthermore, the experimental data were fitted to the Temkin and Dubinin-Radushkevich isothermal models, which are strictly connected with specific values of the energy of adsorption, therefore making useful tools for the investigation of physical or chemical characters of adsorptive processes studied [50]. The Temkin isotherm linear plot (Figure S6) is given by Equation (4), where $K_T$ is the Temkin isotherm constant, while B is the Temkin constant strictly related to the heat of adsorption:

$$q_{eq} = B \ln c_{eq} + B \ln K_T \quad (4)$$

Specific values, which determine whether chemi- or physisorption takes place, may be calculated using the linear plot of the Dubinin-Radushkevich isotherms model (Figure S7) presented below (Equation (5)), which is described by ln $q_{eq}$ vs. $\varepsilon^2$, where $\varepsilon$ is the Polanyi potential (J $mol^{-1}$), calculable as $\varepsilon = RT \cdot \ln(1+1/c_{eq})$; R is the ideal gas constant (8.314 J $mol^{-1}K^{-1}$), and T is the temperature of the process:

$$\ln q_{eq} = -\beta \ln \varepsilon^2 + \ln q_m \quad (5)$$

According to the above plot, the slope of the linear plot, which equals to the activity coefficient $\beta$ ($mol^2$ $J^{-2}$), is necessary for the determination of the mean energy of adsorption $E$ (J $mol^{-1}$) using Equation (6):

$$E = \sqrt{\frac{1}{-2\beta}} \quad (6)$$

The calculated values of the Temkin constants $B$ (Table S1) show that the adsorption energy is significantly smaller for the precursor material ($SiO_2$-epoxy) than for the hybrid materials functionalized

with PAMAM dendrimers. These parameters also indicate the physical character of sorption processes as *B* values are lower than 20 J $mol^{-1}$ for each experiment. Physisorption is also proved by the calculated mean energy of the adsorption value *E* (Table S1), which varies between 0.02 and 2.45 kJ $mol^{-1}$ for all the conducted experiments, remaining lower than 8 kJ $mol^{-1}$, which is a limit for physical sorption [52].

### *2.4. Thermodynamic Studies of the Drug Adsorption Processes on the Hybrid Materials*

The processes of complex formation between the chosen bioactive acids and the hybrid materials were also described with thermodynamic parameters. Therefore, thermochemical parameters such as the adsorption enthalpy $\Delta H°$ and the adsorption entropy $\Delta S°$ may be determined using an appropriate principle. The van't Hoff equation, given below as Equation (7), shows a relation between these parameters and the temperature:

$$\ln K_d = -\frac{\Delta H}{RT} + \frac{\Delta S}{R} \quad (7)$$

where: $K_d$ is the equilibrium constant defined as the ratio of the amount of the drug adsorbed at equilibrium to the concentration of the drug remaining in the solution ($K_d = q_{eq}/c_{eq}$) (L $g^{-1}$), T is the temperature (K) and R is the ideal gas constant (8.314 J $mol^{-1}$ $K^{-1}$). From the slope and intercept of the linear plot of $\ln K_d$ vs. 1/T (Figure S8), all the parameters are obtainable. In addition, Gibbs free energy values of the biomolecules' adsorption process at different temperatures were calculated using Equation (8):

$$\Delta G = -RT \cdot \ln K_d \quad (8)$$

The calculated thermodynamic parameters are collected in Table 2. High-correlation coefficients $R^2$ and extremely low $\chi^2$ values highlight the reliability of the obtained energy values. Very low and positive adsorption enthalpies, which for most of the adsorption processes are lower than 15 kJ $mol^{-1}$, clearly indicate the endothermic physisorption, which is stabilized only by non-covalent binding, such as electrostatic interactions and hydrogen bonds [53]. In addition, the adsorption processes are driven by the entropy, whose positive values indicate the increased randomness in the adsorbent-solution interface with the temperature rise. Moreover, the endothermic character of bioactive acids' adsorption is proved by the decrease in negative $\Delta G°$ values with increasing temperature, reaching the lowest values at 328 K indicating the highest intensity of adsorption ($\Delta G°_{328K} < \Delta G°_{313K} < \Delta G°_{301K}$). Their negative values also indicate the spontaneity of the processes.

**Table 2.** Thermodynamic parameters of the biomolecules' adsorption processes on the dendrimer-grafted silica-supported materials.

| Biomolecule | Adsorbent | $\Delta H°$ (kJ $mol^{-1}$) | $\Delta S°$ (J $mol^{-1}$ $K^{-1}$) | $R^2$ | $\chi^2 \cdot 10^3$ | $\Delta G°$ (kJ $mol^{-1}$) | | |
|---|---|---|---|---|---|---|---|---|
| | | | | | | 301 K | 313 K | 328 K |
| Folic Acid | $SiO_2$-EDA | 1.41 ± 0.12 | 43.8 ± 0.4 | 0.9855 | 0.002 | −11.78 | −12.32 | −12.96 |
| | $SiO_2$-TETA | 2.29 ± 0.02 | 51.8 ± 0.1 | 0.9998 | 0.001 | −13.31 | −13.93 | −14.71 |
| | $SiO_2$-TREN | 1.43 ± 0.09 | 44.2 ± 0.3 | 0.9924 | 0.001 | −11.86 | −12.39 | −13.06 |
| | $SiO_2$-TRI-OXA | 4.64 ± 0.28 | 53.3 ± 0.9 | 0.9929 | 0.007 | −11.41 | −12.03 | −12.85 |
| Salicylic Acid | $SiO_2$-EDA | 4.40 ± 0.13 | 47.3 ± 0.4 | 0.9982 | 0.641 | −9.84 | −10.42 | −11.12 |
| | $SiO_2$-TETA | 42.94 ± 3.02 | 147.6 ± 9.6 | 0.9901 | 4.545 | −1.58 | −3.12 | −5.56 |
| | $SiO_2$-TREN | 6.35 ± 0.21 | 53.7 ± 0.7 | 0.9979 | 0.649 | −9.81 | −10.43 | −11.25 |
| | $SiO_2$-TRI-OXA | 13.59 ± 0.76 | 60.0 ± 2.4 | 0.9938 | 0.157 | −4.44 | −5.22 | −6.07 |
| Nicotinic Acid | $SiO_2$-EDA | 4.38 ± 0.25 | 38.1 ± 0.8 | 0.9936 | 0.011 | −7.10 | −7.57 | −8.13 |
| | $SiO_2$-TETA | 9.42 ± 0.36 | 49.8 ± 1.1 | 0.9972 | 0.029 | −5.59 | −6.16 | −6.94 |
| | $SiO_2$-TREN | 6.26 ± 0.49 | 43.2 ± 1.6 | 0.9879 | 0.046 | −6.72 | −7.28 | −7.89 |
| | $SiO_2$-TRI-OXA | 10.45 ± 0.74 | 44.7 ± 2.4 | 0.9899 | 0.221 | −3.04 | −3.52 | −4.25 |

### *2.5. pH-Dependent Drug Release from the Drug-Loaded Hybrid Materials*

The release of drugs anchored to the surface of the hybrid materials studied was performed in three different media: phosphate buffered saline (PBS) (pH 7.4), acetic acid/sodium acetate buffer (pH 5.4) and hydrochloric acid/potassium chloride buffer (pH 2.0). The choice of such environments was driven by the different pH values of blood, plasma and saliva (pH 7.4); skin (pH 5.5); and gastric

juice (pH 1.5–3.0). Moreover, the main interactions taking part in the material-drug complexes are electrostatic ones, which are labile towards pH changes and ionic strength. In vitro release experiments were held at 37 °C, imitating paraphysiological conditions.

Figure 6 presents the release profiles of folic acid (A, D, G, J), salicylic acid (B, E, H, K) and nicotinic acid (C, F, I, L) from the PAMAM-grafted hybrid materials as a function of the cumulative percentage of drug released $Q_t$ in 20 h of incubation. From among all the experiments, the ones performed in the most acidic environment, which was HCl/KCl buffer at pH 2.0, gave the highest release levels ranging between 37.22% and 99.83%. The main reason for such a phenomenon is connected with introducing the excess of $H^+$, which readily binds with negatively charged acidic residue, leading to repulsive interactions with the protonated amine groups of PAMAM dendrimers grafted on the silica supports. On the other hand, the lowest percentage of drug released were established for the desorption processes held in the PBS buffer. A composition of such a buffer was based on the sodium and potassium cations, and the hydrogen phosphate and chloride anions, whose proportion matches the ionic strength and osmolarity of human plasma. These ions are easily exchanging between protonated amine groups of surface PAMAM dendrimers and deprotonated biocompounds' molecules, which does not afford the highest effectiveness of electrostatic interaction disruption, hindering the drugs' desorption. Nevertheless, the percentage amount of drugs released from the drug-loaded hybrid materials at pH 7.4 ranges between 5.45% and 49.28% for all the experiments performed. The analysis of the relation between the chemical structure of the drugs and their release profiles has shown that the lowest efficiency of desorption was obtained for folic acid. The strongest binding affinity of folic acid to the support and the acid's steric hindrance may both hinder its elution to an aqueous medium, irrespectively of the solution pH, thus the desorbed folic acid molecules are usually contained in external layers of the adsorbate multilayer. Therefore, the maximal folic acid releases at pH 2.0 are 35.42%, 54.90%, 42.40% and 41.59% from $SiO_2$-EDA (Figure 6A), $SiO_2$-TREN (Figure 6D), $SiO_2$-TETA (Figure 6G) and $SiO_2$-TRI-OXA (Figure 6J), respectively. Salicylic and nicotinic acid, however, have significantly smaller molecules than folic acid and exhibit a weaker binding affinity to the PAMAM-grafted hybrid materials, which allows their greater release to aqueous solutions. The highest percentage of released salicylic and nicotinic acid was calculated for $SiO_2$-EDA (Figure 6B,C) and $SiO_2$-TREN (Figure 6H,I), which is strictly connected with the high dendrimer grafting values of these materials and the presence of tight internal cavities within the dendrimers' interior, jointly improving the sorption parameters. The experiments conducted in the acidic environment in pH 2.0 gave very high release percentage values ranging between 86.88% and 99.83%. On the other hand, $SiO_2$-TETA, containing a TETA dendrimer grafted on the surface (branched and with larger cavities) may tightly bind salicylic and nicotinic acid by both electrostatic/hydrogen bonding and physical entrapment, hindering their elution, leading to maximal release percentage values at 40.75% for salicylic acid (Figure 6E) and 37.22% for nicotinic acid (Figure 6F). A similar observation was made when studying the release of salicylic acid and nicotinic acid from $SiO_2$-TRI-OXA. The profiles of their release are shown in Figure 6K,L. The exception was the release of nicotinic acid from the same material at pH 2.0, which was much stronger than at pH 5.4 and 7.4, which can be explained by a considerable excess of protons in the HCl/KCl buffer. This excess of protons permits the effective desorption of nicotinic acid from the complex.

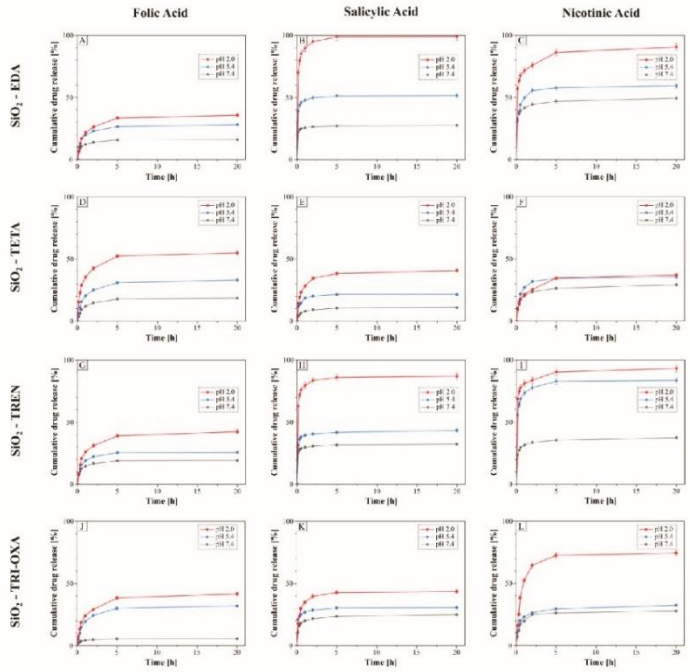


**Figure 6.** Release profiles of the biocompounds (folic acid: **A, D, G, J**; salicylic acid: **B, E, H, K**; nicotinic acid: **C, F, I, L**) from the drug-loaded hybrid materials: $SiO_2$-EDA (**A–C**); $SiO_2$-TETA (**D–F**), $SiO_2$-TREN (**G–I**), $SiO_2$-TRI-OXA (**J–L**) in three different environments. For some points, the SDs are smaller than the plotted symbols.

In order to propose a mechanism which triggers the drug release from the PAMAM-grafted hybrid materials, the experimental in vitro release at pH 2.0 (the highest release efficiency) was fitted to several kinetic models [54,55]: the zero-order model, the first-order model, the Higuchi model, the Korsmeyer-Peppas model and the Hixson-Crowell model, whose linear representations are given below in the same order:

$$F_t = F_0 + k_0 t \quad (9)$$

$$\log(100 - Q_t) = -k_1 t \quad (10)$$

$$Q_t = k_H \sqrt{t} \quad (11)$$

$$\log Q_t = n \log t + \log k_{K-P} \quad (12)$$

$$\sqrt[3]{F_0} - \sqrt[3]{F_t} = k_{H-C} t \quad (13)$$

where: $F_t$ is the cumulative amount of the drug released at time t (mg), $F_0$ is the initial amount of the drug loaded in the hybrid material (mg), $k_0$ is the zero-order release constant (mg $h^{-1}$), $Q_t$ is the cumulative percentage of the drug release at time t (%), $k_1$ is the first-order release constant (% $h^{-1}$), $k_H$ is the Higuchi release constant (% $h^{-1/2}$), n is the Korsmeyer-Peppas exponent of release (-), $k_{K-P}$ is the Korsmeyer-Peppas release constant (% $h^{-1}$), and $k_{H-C}$ is the Hixson-Crowell release constant ($mg^{1/3}$ $h^{-1}$).

Table 3 presents a comparison of the experimental data fit to the first-order, the Higuchi and the Korsemeyer-Peppas release models, which are most extensively used for the description of drug release from various delivery platforms. The highest correlation coefficients $R^2$ of the bioactive acids release from the PAMAM-functionalized silica materials were calculated for the Korsmeyer-Peppas release model and were equal to or higher than 0.8. Moreover, the experimental data fitted to this kinetic model were described with statistical $\chi^2$ coefficients, the values of which were determined to be the lowest among the values calculated for fitting to the Higuchi and the first-order kinetic models. In addition, in this model, the n value is strictly dependent on the mechanism of drug release and if n is lower than 0.45, the release follows a Fickian or quasi-Fickian diffusion model [56]. Such a conclusion can be drawn for the experiments of bioactive acids released from the materials studied, which gave n values lower than 0.34, indicating the quasi-Fickian diffusion as a mechanism of folic, salicylic and nicotinic acid release from the dendrimer-grafted materials. In addition, the experimental data were fitted to the zero-order and the Hixson-Crowell models (Table S2), however the obtained $R^2$ values reached maximally 0.62, which clearly shows that the release profiles do not follow these models.

**Table 3.** The drug release parameters calculated for the first-order, the Higuchi and the Korsmeyer-Peppas release models, based on the drug desorption experiments at pH 2.0.

| Biomolecule | Adsorbent | First-Order Model | | Higuchi Model | | Korsemeyer-Peppas Model | | |
|---|---|---|---|---|---|---|---|---|
| | | $k_1$ (% $h^{-1}$) | $R^2$ ($\chi^2$) | $k_H$ (% $h^{-1/2}$) | $R^2$ ($\chi^2$) | n | $k_{K\text{-}P}$ (% $h^{-1}$) | $R^2$ ($\chi^2$) |
| Folic Acid | $SiO_2$-EDA | 0.006 ± 0.002 | 0.5519 (0.039) | 6.5 ± 1.8 | 0.7205 (10.340) | 0.34 | 17.1 ± 1.8 | 0.8311 (0.064) |
| | $SiO_2$-TETA | 0.011 ± 0.004 | 0.5748 (0.116) | 8.8 ± 2.4 | 0.7224 (10.763) | 0.26 | 31.1 ± 2.1 | 0.8743 (0.020) |
| | $SiO_2$-TREN | 0.008 ± 0.003 | 0.5883 (0.058) | 7.3 ± 1.9 | 0.7399 (9.740) | 0.31 | 21.8 ± 2.0 | 0.8476 (0.041) |
| | $SiO_2$-TRI-OXA | 0.008 ± 0.003 | 0.6061 (0.061) | 7.7 ± 1.9 | 0.7602 (10.207) | 0.34 | 19.6 ± 1.9 | 0.8594 (0.048) |
| Salicylic Acid | $SiO_2$-EDA | 0.103 ± 0.030 | 0.7071 (7.928) | 5.6 ± 2.3 | 0.5520 (3.596) | 0.07 | 86.9 ± 2.0 | 0.8118 (0.002) |
| | $SiO_2$-TETA | 0.006 ± 0.003 | 0.5238 (0.038) | 5.8 ± 1.7 | 0.6941 (6.777) | 0.22 | 25.4 ± 1.5 | 0.8735 (0.015) |
| | $SiO_2$-TREN | 0.016 ± 0.008 | 0.4629 (0.319) | 4.5 ± 1.8 | 0.5522 (2.629) | 0.06 | 76.4 ± 1.6 | 0.8024 (0.002) |
| | $SiO_2$-TRI-OXA | 0.006 ± 0.003 | 0.4110 (0.036) | 5.3 ± 2.0 | 0.5822 (7.903) | 0.18 | 30.2 ± 1.9 | 0.7974 (0.018) |
| Nicotinic Acid | $SiO_2$-EDA | 0.029 ± 0.007 | 0.7707 (0.781) | 7.6 ± 1.7 | 0.8062 (2.315) | 0.10 | 70.5 ± 1.0 | 0.9613 (0.001) |
| | $SiO_2$-TETA | 0.007 ± 0.002 | 0.6211 (0.041) | 6.5 ± 1.5 | 0.7847 (6.462) | 0.29 | 19.1 ± 1.2 | 0.9061 (0.021) |
| | $SiO_2$-TREN | 0.028 ± 0.008 | 0.7378 (0.820) | 5.2 ± 1.3 | 0.7596 (1.318) | 0.06 | 79.8 ± 0.8 | 0.9443 (0.001) |
| | $SiO_2$-TRI-OXA | 0.020 ± 0.009 | 0.5047 (0.418) | 12.7 ± 4.5 | 0.6164 (27.616) | 0.31 | 40.1 ± 4.4 | 0.7941 (0.049) |

## 3. Materials and Methods

### *3.1. Materials*

The support 3-(glycidoxy)propyl-functionalized silica-gel ($SiO_2$-epoxy) was obtained from SiliCycle Inc. (Quebec, QC, Canada). According to the specification card, the particle sizes ranged between 40 and 63 μm, the molecular loading (grafting level) was 1.21 mmol $g^{-1}$, the specific surface area equaled 494 $m^2$ $g^{-1}$, the pore diameter was 60 Å and pore volume was 0.74 mL $g^{-1}$. All the reagents were commercially available products used with no further purification. Ethylenediamine, triethylenetetramine, tris(2-aminoethyl)amine, 4,7,10-trioxa-1,13-tridecanediamine, methyl acrylate, folic acid, salicylic acid, nicotinic acid were purchased from Sigma-Aldrich (St. Louis, MO, USA). All the solvents and salts used for the buffers preparation were of the purity grade p.a. Methanol and hydrochloric acid (HCl) were purchased from STANLAB (Lublin, Poland). *N*,*N*-dimethylformamide (DMF), dichloromethane (DCM), acetic acid (AcOH), sodium acetate (AcONa) and potassium chloride (KCl) were obtained from Eurochem (Tarnow, Poland). Di- and monosodium phosphates ($Na_2HPO_4$ and $NaH_2PO_4$) were purchased from POCH (Gliwice, Poland).

### 3.2. Instruments

The ESI-MS spectra of the dendrimers and the dendrimer-biocompound complexes were recorded on amaZon SL ion trap Bruker mass spectrometer (Bremen, Germany), using electrospray ion source (ESI) in infusion mode. Sample solutions were introduced to the spectrometer using a syringe pump, at a flow rate of 10 μL $min^{-1}$ into the ionization source. Analyses were performed in the so-called "enhanced resolution mode" with mass ranges between 100 and 2200 *m*/*z*. Capillary voltage was determined at −4.5 kV and −500 V for the endplate offset. The source temperature was set at 80 °C and the desolvation temperature at 250 °C. Helium and nitrogen were used as the cone and the desolvating gases, respectively. The flow rate of helium was set at 50 L $h^{-1}$ and 800 L $h^{-1}$ for nitrogen. The Fourier-transformed photoacoustic infrared (FT-IR/PAS) spectra of the synthesized hybrid materials were obtained by means of Bio-Rad Excalibur FTIR 3000 MX spectrometer (Hercules, CA, USA), using the MTEC Model 300 photoacoustic cell and carbon black standard as a reference sample. Before the data collection within the wavenumber range between 4000 and 400 $cm^{-1}$, the cell was purged with dry helium. The thermogravimetric measurements were performed using Setaram Setsys 1200 analyser (Caluire, France). The hybrid materials were investigated for thermal stability in air stream within the temperature range of 20–1000 °C (a heating rate: 5 °C $min^{-1}$). The elemental analyses of the materials were carried out in Elementar Vario EL III analyzer (Langenselbold, Germany) in CHN mode. The SEM images of the hybrid materials were performed using the Quanta FEG 250 scanning electron microscope. The images were recorded in high vacuum conditions (1.21–5.33·$10^{-3}$ Pa) and high voltage, set at 5 kV. The working distance during the image production ranged between 9.7 and 10.1 mm. Concentration of the drugs in the samples of adsorption and in vitro release studies was determined by spectrophotometric method, using the Agilent 8453 UV-Vis spectrophotometer (Santa Clara, CA, USA). All the measurements were performed at least in triplicate, in order to overcome disturbances.

### 3.3. Synthesis of PAMAM Dendrimers

To a solution of methyl acrylate (12.23 mL, 0.135 mol) in 50 mL of anhydrous methanol, cooled to temperature 0 °C, a solution of tris(2-aminoethyl)amine (4.49 mL, 0.03 mol) of in 30 mL of anhydrous methanol was added dropwise within 2 h, under nitrogen atmosphere, not to allow temperature rise above 5 °C. Then, the reaction mixture was allowed to warm to room temperature and stirred for 5 days. Afterwards, the solvent and the excess of methyl acrylate were evaporated, and the product was dried under vacuum at 40 °C. The orange liquid ester intermediate was obtained with 98% yield. ESI-MS: *m*/*z* (z 1+) 663.62, 685.55.

The synthesis of final PAMAM dendrimers was performed according to the following procedure: to the solutions of particular amines cooled to the temperature of 0 °C: ethylenediamine (3.00 mL, 45 mmol), triethylenetetramine (6.71 mL, 45 mmol), tris(2-aminoethyl)amine (6.73 mL, 45 mmol) or 4,7,10-trioxa-1,13-tridecanediamine (9.95 mL, 45 mmol) in 50 mL of anhydrous methanol, the solution of ester intermediate (3.31 g, 5 mmol) in 20 mL of anhydrous methanol was added dropwise within 2 h not to let the temperature rise above 5 °C. Afterwards, the mixtures were warmed to room temperature and stirred for 5 days in the atmosphere of inert gas ($N_2$). The crude products were obtained by extraction with cold diethyl ether (3 × 30 mL). The products were then evaporated and dried under vacuum at 40 °C, obtaining pure EDA, TETA, TREN and TRI-OXA dendrimers, respectively.

**EDA:** yield = 95%; ESI-MS: *m*/*z* (z 1+) 831.78, 771.71, 717.73, 657.68, 603.69

**TETA:** yield = 71%; ESI-MS: *m*/*z* (z 1+) 1255.94, 1227.94, 1201.99, 1174.02, 1147.99, 1081.84, 1055.83, 1027.86, 1001.84, 973.86, 909.69, 855.73; *m*/*z* (z 2+) 628.63, 614.67, 601.68, 587.68, 574.67, 528.58, 501.57

**TREN:** yield = 83%; ESI-MS: *m*/*z* (z 1+) 1348.11, 1223.96, 1201.99, 1077.83, 1055.84, 931.68, 909.72; *m*/*z* (z 2+) 612.69, 601.71, 539.60, 528.62

**TRI-OXA:** yield = 91%; ESI-MS: *m*/*z* (z 1+) 1792.11, 1682.47, 1572.96, 1518.06, 1297.95; *m*/*z* (z 2+) 897.17; *m*/*z* (z 3+) 598.36

### 3.4. Synthesis of Hybrid Materials

Briefly, 2 mmol of each dendrimer (1.6 g EDA; 2.7 g TREN; 2.7 g TETA or 3.6 g TRI-OXA) was dissolved in 50 mL of anhydrous DMF, and then 5 g of silica modified with glycidoxypropyl linker (1.21 mmol $g^{-1}$; 6.05 mmol of epoxy groups) were added in a few portions under a nitrogen atmosphere. The stirring was continued for 24 h at room temperature. Afterwards, the solids were filtered off and washed with DMF (2 × 10 mL) and DCM (1 × 15 mL). The pale yellow solids were dried in a vacuum at 40 °C, obtaining $SiO_2$-EDA, $SiO_2$-TETA, $SiO_2$-TREN and $SiO_2$-TRI-OXA materials, respectively.

### 3.5. Biomolecules Adsorption Isotherms

Isothermal studies were performed individually for each hybrid material towards each of the three bioactive compounds, i.e., folic, salicylic and nicotinic acid. The general procedure was as follows: 10 mg samples of the hybrid material were poured into a series of 10 mL of bioactive compound aqueous solutions with various concentrations: 0.01, 0.05, 0.1, 0.2, 0.5 and 1 mM. Salicylic and nicotinic acids were dissolved in distilled water, while folic acid in phosphate buffer at pH 8.0. The materials were stirred in the drug solutions for 24 h at room temperature. Afterwards, the solids were filtered off and the amount of the drug adsorbed was calculated using Equation (14):

$$q_{eq} = \left(c_0 - c_{eq}\right) \cdot \frac{V}{m} \cdot M \quad (14)$$

where: $c_0$ is the starting concentration of the biomolecule (mM), $c_{eq}$ is the equilibrium concentration of the biomolecule that remained in the solution (mM), V is the volume of the biomolecule solution (mL), M is the molar mass of the biomolecule (g $mol^{-1}$), and m is the mass of the hybrid material sample (mg). The concentrations of the drug remaining in the solution were calculated using UV-Vis spectrophotometric assays with absorption maxima at 365, 297 and 263 nm for folic, salicylic and nicotinic acid, respectively.

### 3.6. Thermodynamic Studies of Biomolecules Adsorption on the Hybrid Materials

Thermodynamic studies were also conducted for each of the hybrid samples towards each drug, individually. The general procedure was based on the stirring of 10 mg samples of the hybrid material in 10 mL of 1 mM solution of particular biocompound (salicylic or nicotinic acid dissolved in distilled water, while folic acid was dissolved in phosphate buffer at pH 8.0) at 298, 313 and 328 K for 24 h. Then, the materials were filtered off and the amount of the acid adsorbed was calculated as described in Section 3.5.

### 3.7. In-Vitro Release of Bioactive Compounds

The hybrid materials loaded with either folic, salicylic or nicotinic acid were tested for the release of the drug in three different environments: pH 2.4 (hydrochloric acid/potassium chloride buffer), pH 5.4 (acetic acid/sodium acetate buffer) and pH 7.4 (phosphate buffered saline: PBS). The general procedure involved the incubation of 15 mg of the drug-loaded materials in 5 mL of the desorbing aqueous solutions at a temperature of 37 °C. The buffers aliquots were collected at the pre-set time intervals, with the subsequent addition of 5 mL of fresh buffers. The cumulative percentages of the drug released $Q_t$ at time t were calculated using Equation (15), where $c_t$ is the concentration of the drug released at time t (mM), V is the volume of the desorbing solution (mL), M is the molar mass of the drug (g $mol^{-1}$), and m is the amount of the drug in the material-drug complex used (mg):

$$Q_t = \frac{\sum_{i=0}^{t}(c_t \cdot V \cdot M)}{m} \cdot 100\% \quad (15)$$

The drug concentrations were calculated using UV-Vis spectrophotometric measurements of folic, salicylic and nicotinic acids at a wavelength of 365, 297 and 263 nm, respectively.

## 4. Conclusions

The study reported was aimed at determination of the adsorption properties of silica-PAMAM dendrimer hybrid materials towards chosen model biocompounds. The materials obtained by the anchoring of ready-made poly(amidoamine) dendrimer on the silica surface via epoxy linker ('grafting to' approach) were successfully characterized using several analytical techniques, indicating the dendrimers' loading values variation between 0.054 and 0.113 mmol $g^{-1}$. Although the dendrimers' loading values were relatively low, the final hybrid materials exhibited binding efficiency towards chosen biocompounds, which is related to the branched and amine-rich character of the grafting agents. The highest adsorption capacity of the biocompounds studied was found for $SiO_2$-EDA (274.72, 157.48 and 20.11 mg $g^{-1}$ for folic, salicylic and nicotinic acid, respectively) and $SiO_2$-TREN (236.97, 42.92 and 17.74 mg $g^{-1}$ for folic, salicylic and nicotinic acid, respectively) materials. The adsorption performance was dependent on the structural features of the studied bioactive acids. Moreover, each drug-loaded material was investigated for the drugs' in vitro release in three different aqueous media. The release percentage was found to be pH-dependent, which can be presented in a series pH 2.0 > pH 5.4 > pH 7.4. In addition, the amount of the drug released was affected by its chemical structure either hindering or improving its desorption from the material matrices, reaching maximal release between 35.42% and 54.90% for folic acid release, 40.75% and 99.83% for salicylic acid release, and 37.22% and 93.24% for nicotinic acid release.

The synthesized hybrid materials were found to be characterized with effective adsorption and in vitro release of the model drugs, which was possible thanks to the versatility of PAMAM dendrimer applications. The universality of $SiO_2$-PAMAM complexes makes them attractive candidates for their future use as the systems for the adsorption/desorption of selected anticancer drugs as well as pre-concentration tools for bioactive water pollutants. In addition, the enhancement of the adsorptive properties as well as the biomedical applicability of the hybrid materials obtained are planned to be studied using different supports, such as iron oxide ($Fe_3O_4$) nanoparticles or biocompatible polymeric chains.

**Supplementary Materials:** The following are available online, Figure S1. The ESI-MS positive spectrum of ester intermediate, Figure S2. The ESI-MS positive spectra of the synthesized PAMAM dendrimers: (a) EDA, (b) TETA, (c) TREN and (d) TRI-OXA, Figure S3. The ESI-MS spectra (positive—top; negative—bottom) of exemplary TREN poly(amidoamine) dendrimer complexes with the studied biomolecules: (a) salicylic acid, (b) nicotinic acid, (c) folic acid, Figure S4. The Langmuir isotherm model fitted to the experimental data of the adsorption processes, Figure S5. The Freundlich isotherm model fitted to the experimental data of the adsorption processes, Figure S6. The Temkin isotherm model fitted to the experimental data of the adsorption processes, Figure S7. The Dubinin-Radushkevich isotherm model fitted to the experimental data of the adsorption processes, Figure S8. The thermodynamic plots of the biomolecules adsorption processes corresponding the van't Hoff equation, Table S1. Fitting of the experimental data to the Tekmin and the Dubinin-Radushkevich isothermal models, Table S2. The drug release parameters calculated for the fitting of experimental data to the zero-order and the Hixson-Crowell release models.

**Author Contributions:** Conceptualization, M.P. and G.S.; methodology, M.P.; software, M.P.; validation, M.P. and G.S.; formal analysis, M.P.; investigation, M.P.; resources, G.S.; data curation, M.P.; writing—original draft preparation, M.P.; writing—review and editing, G.S.; visualization, M.P.; supervision, G.S.; project administration, M.P. and G.S.; funding acquisition, M.P. and G.S. All authors have read and agreed to the published version of the manuscript.

**Funding:** This research was funded by the European Union through the European Social Fund under the Operational Program Knowledge Education Development, grant number POWR.03.02.00-00-I026/16.

**Conflicts of Interest:** The authors declare no conflict of interest. The funders had no role in the design of the study; in the collection, analyses, or interpretation of data; in the writing of the manuscript, or in the decision to publish the results.

## References

1. Tomalia, D.A.; Baker, H.; Dewald, J.; Hall, M.; Kallos, G.; Martin, S.; Roeck, J.; Ryder, J.; Smith, P. Dendritic macromolecules: Synthesis of starburst dendrimers. *Macromolecules* **1986**, *19*, 2466–2468. [CrossRef]

2. Silva, N.P., Jr.; Menacho, F.P.; Chorilli, M. Dendrimers as potential platform in nanotechnology-based drug delivery systems. *IOSE J. Pharm.* **2012**, *2*, 23–30.
3. Sadekar, S.; Ghandehari, H. Transepithelial transport and toxicity of PAMAM dendrimers: Implications for oral drug delivery. *Adv. Drug. Deliv. Rev.* **2012**, *64*, 571–588. [CrossRef]
4. Chanphai, P.; Tajmir–Riahi, H.A. Characterization of folic acid-PAMAM conjugates: Drug loading efficacy and dendrimer morphology. *J. Biomol. Struct. Dynamics* **2018**, *36*, 1918–1924. [CrossRef] [PubMed]
5. Li, J.; Liang, H.; Liu, J.; Wang, Z. Poly (amidoamine) (PAMAM) dendrimer mediated delivery of drug and pDNA/siRNA for cancer therapy. *Int. J. Pharm.* **2018**, *546*, 215–225. [CrossRef]
6. Fox, L.J.; Richardson, R.M.; Briscoe, W.H. PAMAM dendrimer-cell membrane interactions. *Adv. Colloid Interf. Sci.* **2018**, *257*, 1–18. [CrossRef]
7. Ehsan, M.; Kharat, A.N.; Adeli, M. Polyamidoamine and polyglycerol; their linear, dendritic and linear-dendritic architectures as anticancer drug delivery systems. *J. Mater. Chem. B* **2015**, *3*, 3896–3921.
8. Jones, C.F.; Campbell, R.A.; Brooks, A.E.; Assemi, S.; Tadjiki, S.; Thiagarajan, G.; Mulcock, C.; Weyrich, A.S.; Brooks, B.D.; Ghandehari, H.; et al. Cationic PAMAM Dendrimers Aggressively Initiate Blood Clot Formation. *ACS Nano* **2012**, *6*, 9900–9910. [CrossRef] [PubMed]
9. Patel, M.; De Paoli, S.H.; Elhelu, O.K.; Farooq, S.; Simak, J. Cell membrane disintegration and extracellular vesicle release in a model of different size and charge PAMAM dendrimers effects on cultured endothelial cells. *Nanotoxicology* **2019**, *13*, 664–681. [CrossRef]
10. Sweet, D.M.; Kolhatkar, R.B.; Ray, A.; Swaan, P.; Ghandehari, H. Transepithelial transport of PEGylated anionic poly (amidoamine) dendrimers: Implications for oral drug delivery. *J. Control. Release* **2009**, *138*, 78–85. [CrossRef]
11. Kumar, P.D.; Kumar, P.V.; Selvam, T.P.; Sambasiva Rao, K.R.S. Prolonged Drug Delivery System of PEGylated PAMAM Dendrimers with a Anti-HIV Drug. *Res. Pharm.* **2013**, *3*, 8–17.
12. Yan, C.; Gu, J.; Lv, Y.; Shi, W.; Wang, Y.; Liao, Y.; Deng, Y. Caproyl-Modified G2 PAMAM Dendrimer (G2-AC) Nanocomplexes Increases the Pulmonary Absorption of Insulin. *AAPS Pharm. Sci. Tech.* **2019**, *20*, 298–304. [CrossRef]
13. Nguyen, T.T.C.; Nguyen, C.K.; Nguyen, T.H.; Tran, N.Q. Highly lipophilic pluronics-conjugated polyamidoamine dendrimer nanocarriers as potential delivery system for hydrophobic drugs. *Mater. Sci. Eng. C* **2017**, *70*, 992–999. [CrossRef] [PubMed]
14. Kolhatkar, R.B.; Kitchens, K.M.; Swaan, P.W.; Ghandehari, H. Surface acetylation of polyamidoamine (PAMAM) dendrimers decreases cytotoxicity while maintaining membrane permeability. *Bioconjug. Chem.* **2007**, *18*, 2054–2060. [CrossRef]
15. Pisal, D.S.; Yellepeddi, V.K.; Kumar, A.; Kaushik, R.S.; Hildreth, M.B.; Guan, X.; Palakurthi, S. Permeability of surface-modified polyamidoamine (PAMAM) dendrimers across Caco-2 cell monolayers. *Int. J. Pharm.* **2008**, *350*, 113–121. [CrossRef] [PubMed]
16. Pourianazar, N.T.; Mutlu, P.; Gunduz, U. Bioapplications of poly(amidoamine) (PAMAM) dendrimers in nanomedicine. *J. Nanopart. Res.* **2014**, *16*, 2342–2379. [CrossRef]
17. Ciolkowski, M.; Petersen, J.F.; Ficker, M.; Janaszewska, A.; Christensen, J.B.; Klajnert, B.; Bryszewska, M. Surface modification of PAMAM dendrimer improves its biocompability. *Nanomed. Nanotechnol. Biol. Med.* **2012**, *8*, 815–817. [CrossRef] [PubMed]
18. Kesharwani, P.; Xie, L.; Mao, G.; Padhye, S.; Iyer, A.K. Hyaluronic acid-conjugated polyamidoamine dendrimers for targeted delivery of 3,4-difluorobenzylidene curcumin to CD44 overexpressing pancreatic cancer cells. *Colloids Surf. B Biointerf.* **2015**, *136*, 413–423. [CrossRef] [PubMed]
19. Peng, J.; Qi, X.; Chen, Y.; Ma, N.; Zhang, Z.; Xing, J.; Zhu, X.; Li, Z.; Wu, Z. Octreotide-conjugated PAMAM for targeted delivery to somatostatin receptors over–expressed tumor cells. *J. Drug Target.* **2014**, *22*, 428–438. [CrossRef] [PubMed]
20. Pawlaczyk, M.; Kurczewska, J.; Schroeder, G. Nanomaterials Modification by Dendrimers—A review. *World J. Res. Rev.* **2018**, *6*, 14–30.
21. Zhou, L.; Yuan, J.; Wei, Y. Core-shell structural iron oxide hybrid nanoparticles: From controlled synthesis to biomedical applications. *J. Mater. Chm.* **2010**, *21*, 2823–2840. [CrossRef]
22. Arachchige, M.P.; Laha, S.S.; Naik, A.R.; Lewis, K.T.; Naik, R.; Jena, B.P. Functionalized nanoparticles enable tracking the rapid entry and release of doxorubicin in human pancreatic cancer cells. *Micron* **2017**, *92*, 25–31. [CrossRef] [PubMed]

23. Zhang, Y.; Liu, J.Y.; Yang, F.; Zhang, Y.J.; Yao, Q.; Cui, T.Y.; Zhao, X.; Zhang, Z.D. A new strategy for assembling multifunctional nanocomposites with iron oxide and amino-terminated PAMAM dendrimers. *J. Mater. Sci. Mater. Med.* **2009**, *20*, 2433–2440. [CrossRef] [PubMed]
24. Tajabadi, M.; Khosroshahi, M.E.; Bonakdar, S. An efficient method of SPION synthesis coated with third generation PAMAM dendrimer. *Colloids Surf. A Physicochem. Eng. Aspects* **2013**, *431*, 18–26. [CrossRef]
25. Zhao, H.; Gu, W.; Ye, L.; Yang, H. Biodistribution of PAMAM dendrimer conjugated magnetic nanoparticles in mice. *J. Mater. Sci. Mater. Med.* **2014**, *25*, 769–776. [CrossRef] [PubMed]
26. Khodadust, R.; Unsoy, G.; Yalcin, S.; Gunduz, G.; Gunduz, U. PAMAM dendrimer-coated iron oxide nanoparticles: Synthesis and characterization of different generations. *J. Nanopart. Res.* **2013**, *15*, 1488–1500. [CrossRef]
27. Banei, M.; Salami-Kalajahi, M. A "Grafting to" Approach to Synthesize Low Cytotoxic Poly(aminoamide)-Dendrimer-grafted Fe3O4 Magnetic Nanoparticles. *Adv. Polym. Technol.* **2018**, *37*, 943–948. [CrossRef]
28. Chang, Y.; Li, Y.; Meng, X.; Liu, N.; Sun, D.; Liu, H.; Wang, J. Dendrimer functionalized water soluble magnetic iron oxide conjugates as dual imaging probe for tumor targeting and drug delivery. *Polym. Chem.* **2013**, *4*, 789–794. [CrossRef]
29. Xu, S.; Wu, J.; Jiang, W.; Tian, R. Synthesis and Characterization of a Poly(amido amine) Modified Magnetic Nanocarrier for Controlled Delivery of Doxorubicin. *J. Nanosci. Nanotechnol.* **2016**, *16*, 1363–1369. [CrossRef]
30. Nigam, S.; Chandra, S.; Newgreen, D.F.; Bahadur, D.; Chen, Q. Poly(ethylene glycol)-Modified PAMAM–Fe3O4-Doxorubicin Triads with the Potential for Improved Therapeutic Efficacy: Generation-Dependent Increased Drug Loading and Retention at Neutral pH and Increased Release at Acidic pH. *Langmuir* **2014**, *30*, 1004–1011. [CrossRef]
31. Nigam, S.; Bahadur, D. Dendrimerized Magnetic Nanoparticles as Carriers for the Anticancer Compound, Epigallocatechin Gallate. *IEEE Trans. Magnet.* **2016**, *52*, 1–5. [CrossRef]
32. Nosrati, H.; Adibtabar, M.; Sharafi, A.; Danafar, H.; Kheiri, M.H. PAMAM-modified citric acid-coated magnetic nanoparticles as pH sensitive biocompatible carrier against human breast cancer cells. *Drug Dev. Ind. Pharm.* **2018**, *44*, 1377–1384. [CrossRef]
33. El-Sigeny, S.M.; Abou Taleb, M.F. Synthesis, Characterization, and Application of Dendrimer Modified Magnetite Nanoparticles as Antimicrobial Agent. *Life Sci. J.* **2015**, *12*, 161–170.
34. Yu, S.; Li, G.; Liu, R.; Ma, D.; Xue, W. Dendritic Fe3O4@Poly(dopamine)@PAMAM Nanocomposite as Controllable NO-Releasing Material: A Synergistic Photothermal and NO Antibacterial Study. *Adv. Funct. Mater.* **2018**, *28*, 1707440. [CrossRef]
35. Cancino, J.; Paino, I.M.M.; Micocci, K.C.; Selistre de Araujo, H.S.; Zucolotto, V. In vitro nanotoxicity of single-walled carbon nanotube–dendrimer nanocomplexes against murine myoblast cells. *Toxic. Letters* **2013**, *219*, 18–25. [CrossRef]
36. Zheng, X.; Wang, T.; Jiang, H.; Li, Y.; Jiang, T.; Zhang, J.; Wang, S. Incorporation of Carvedilol into PAMAM-functionalized MWNTs as a sustained drug delivery system for enhanced dissolution and drug-loading capacity. *Asian J. Pharm. Sci.* **2013**, *8*, 278–286. [CrossRef]
37. Wen, S.; Liu, H.; Cai, H.; Shen, M.; Shi, X. Targeted and pH-Responsive Delivery of Doxorubicin to Cancer Cells Using Multifunctional Dendrimer-Modified Multi-Walled Carbon Nanotubes. *Adv. Healthcare Mater.* **2013**, *2*, 1267–1276. [CrossRef]
38. Kurczewska, J.; Cegłowski, M.; Messyasz, B.; Schroeder, G. Dendrimer-functionalized halloysite nanotubes for effective drug delivery. *Appl. Clay Sci.* **2018**, *153*, 134–143. [CrossRef]
39. Eskandarloo, H.; Arshadi, M.; Abbaspourrad, A. Magnetic Dendritic Halloysite Nanotube for Highly Selective Recovery of Heparin Digested from Porcine Intestinal Mucosa. *ACS Sustain. Chem. Eng.* **2018**, *6*, 14561–14573. [CrossRef]
40. Hu, Y.; Chen, J.; Li, X.; Sun, Y.; Huang, S.; Li, Y.; Liu, H.; Xu, J.; Zhong, S. Multifunctional halloysite nanotubes for targeted delivery and controlled release of doxorubicin in-vitro and in-vivo studies. *Nanotechnology* **2017**, *28*, 375101. [CrossRef]
41. Xu, X.; Lu, S.; Gao, C.; Wang, X.; Bai, X.; Gao, N.; Liu, M. Facile preparation of pH-sensitive and self-fluorescent mesoporous silica nanoparticles modified with PAMAM dendrimers for label-free imaging and drug delivery. *Chem. Eng. J.* **2015**, *266*, 171–178. [CrossRef]

42. Lotfi, R.; Hayati, B.; Rahimi, S.; Shekarchi, A.A.; Mahmoodi, N.M.; Bagheri, A. Synthesis and characterization of PAMAM/SiO2 nanohybrid as a new promising adsorbent for pharmaceutical. *Microchem. J.* **2019**, *146*, 1150–1159. [CrossRef]
43. Torres, C.C.; Campos, C.H.; Díáz, C.; Jiménez, V.A.; Vidal, F.; Guzmán, L.; Alderete, J.B. PAMAM-grafted TiO2 nanotubes as novel versatile materials for drug delivery applications. *Mater. Sci. Eng. C* **2016**, *65*, 164–171. [CrossRef]
44. Zhang, Q.; Wang, L.; Jiang, Y.; Gao, W.; Wang, Y.; Yang, X.; Yang, X.; Liu, Z. Gold Nanorods with Silica Shell and PAMAM Dendrimers for Efficient Photothermal Therapy and Low Toxic Codelivery of Anticancer Drug and siRNA. *Adv. Mater. Interfaces* **2017**, *4*, 1701166. [CrossRef]
45. Xiao, H.; Yan, L.; Dempsey, E.M.; Song, W.; Qi, R.; Li, W.; Huang, Y.; Jing, X.; Zhou, D.; Ding, J.; et al. Recent progress in polymer-based platinum drug delivery systems. *Progress Polym. Sci.* **2018**, *87*, 70–106. [CrossRef]
46. Akin, M.; Bongartz, R.; Walter, J.G.; Demirkol, D.O.; Stahl, F.; Timur, S.; Scheper, T. PAMAM–functionalized water soluble quantum dots for cancer cell targeting. *J. Mater. Chem.* **2012**, *22*, 11529–11536. [CrossRef]
47. Geraldo, D.A.; Duran–Lara, E.F.; Aguayo, D.; Cachau, R.E.; Tapia, J.; Esparza, R.; Yacaman, M.J.; Gonzalez-Nilo, F.D.; Santos, L.S. Supramolecular complexes of quantum dots and a polyamidoamine (PAMAM)–folate derivative for molecular imaging of cancer cells. *Anal. Bioanal. Chem.* **2011**, *400*, 483–492. [CrossRef]
48. Kaczorowska, M.A.; Cooper, H.J. Electron Capture Dissociation, Electron Detachment Dissociation, and Collision-Induced Dissociation of Polyamidoamine (PAMAM) Dendrimer Ions with Amino, Amidoethanol, and Sodium Carboxylate Surface Groups. *J. Am. Soc. Mass Spectrom.* **2008**, *19*, 1312–1319. [CrossRef]
49. Socrates, G. *Infrared and Raman Characteristic Group Frequencies. Tables and Charts*, 3rd ed.; John Wiley and Sons Ltd.: Chichester, UK, 2001; pp. 50–53, 94–108, 139–148.
50. Foo, K.Y.; Hameed, B.H. Insights into the modeling of adsorption isotherm systems. *Chem. Eng. J.* **2010**, *156*, 2–10. [CrossRef]
51. Ayawei, N.; Ebelegi, A.N.; Wankasi, D. Modelling and Interpretation of Adsorption Isotherms. *J. Chem.* **2017**, *2017*, 1–11. [CrossRef]
52. Vahidhabanu, S.; Idowu, A.A.; Babu, R.B. Magnetic core layered double hydroxide over halloysite as a robust adsorbent for the treatment of dye-contaminated wastewater: A clean approach for industrial applications. *Desalin. Water Treat.* **2019**, *138*, 379–388. [CrossRef]
53. Sanchez Zambrano, K.S.; Vilarassa–Garcia, E.; Maia, D.A.S.; Bastos-Neto, M.; Rodriguez-Castellon, E.; Azevedo, D.C.S. Adsorption microcalorimetry as a tool in the characterization of amine-grafted mesoporous silicas for $CO_2$ capture. *Adsorption* **2019**, *26*, 165–175. [CrossRef]
54. Bohrey, S.; Chourasiya, V.; Pandey, A. Polymeric nanoparticles containing diazepam: Preparation, optimization, characterization, in–vitro drug release and release kinetic study. *Nano Converg.* **2016**, *3*, 1–7. [CrossRef]
55. Somanathan, T.; Krishna, V.M.; Saravanan, V.; Kumar, R.; Kumar, R. MgO Nanoparticles for Effective Uptake and Release of Doxorubicin Drug: pH Sensitive Controlled Drug Release. *J. Nanosci. Nanotechnol.* **2016**, *16*, 9421–9431. [CrossRef]
56. Wua, I.Y.; Balaa, S.; Skalko–Basneta, N.; Pio di Cagno, M. Interpreting non-linear drug diffusion data: Utilizing Korsmeyer-Peppas model to study drug release from liposomes. *Eur. J. Pharm. Sci.* **2019**, *138*, 105026. [CrossRef] [PubMed]


**Sample Availability:** Samples of the compounds SiO2-EDA, SiO2-TETA, SiO2-TREN and SiO2-TRI-OXA are available from the authors.

# Dendrimer–functionalized hybrid materials based on silica as novel carriers of bioactive acids

**Mateusz Pawlaczyk [1,*], Grzegorz Schroeder [1]**

[1] Faculty of Chemistry, Adam Mickiewicz University in Poznań, Uniwersytetu Poznańskiego 8, 61–614, Poznań, Poland

* Corresponding Author: mateusz.pawlaczyk@amu.edu.pl

## Supplementary Information

**Section A: The ESI-MS spectra of the synthesized dendrimers and their complexes with bioactive compounds studied**

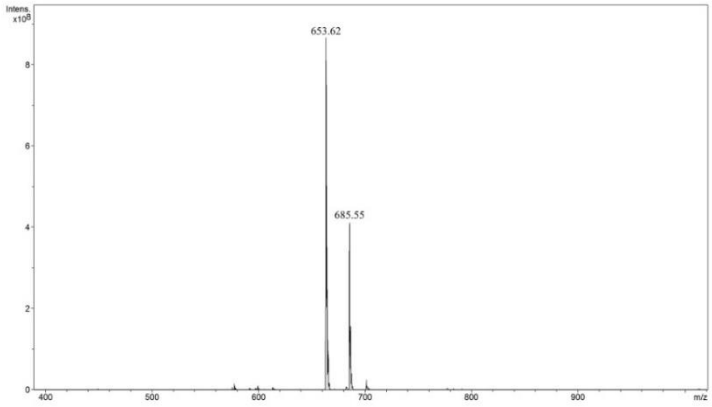


**Figure S1.** The ESI-MS positive spectrum of ester intermediate.

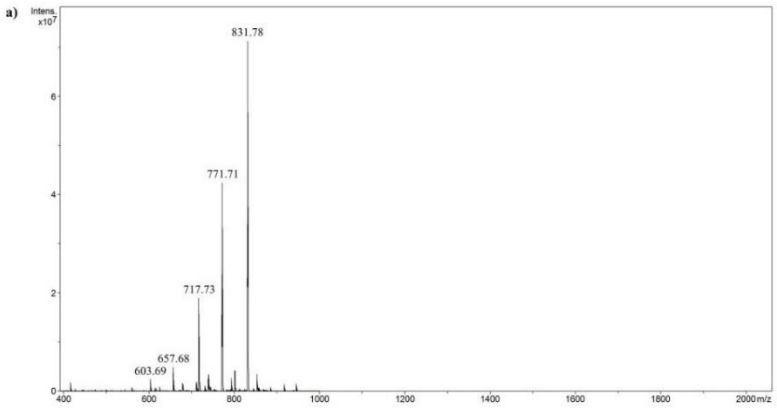

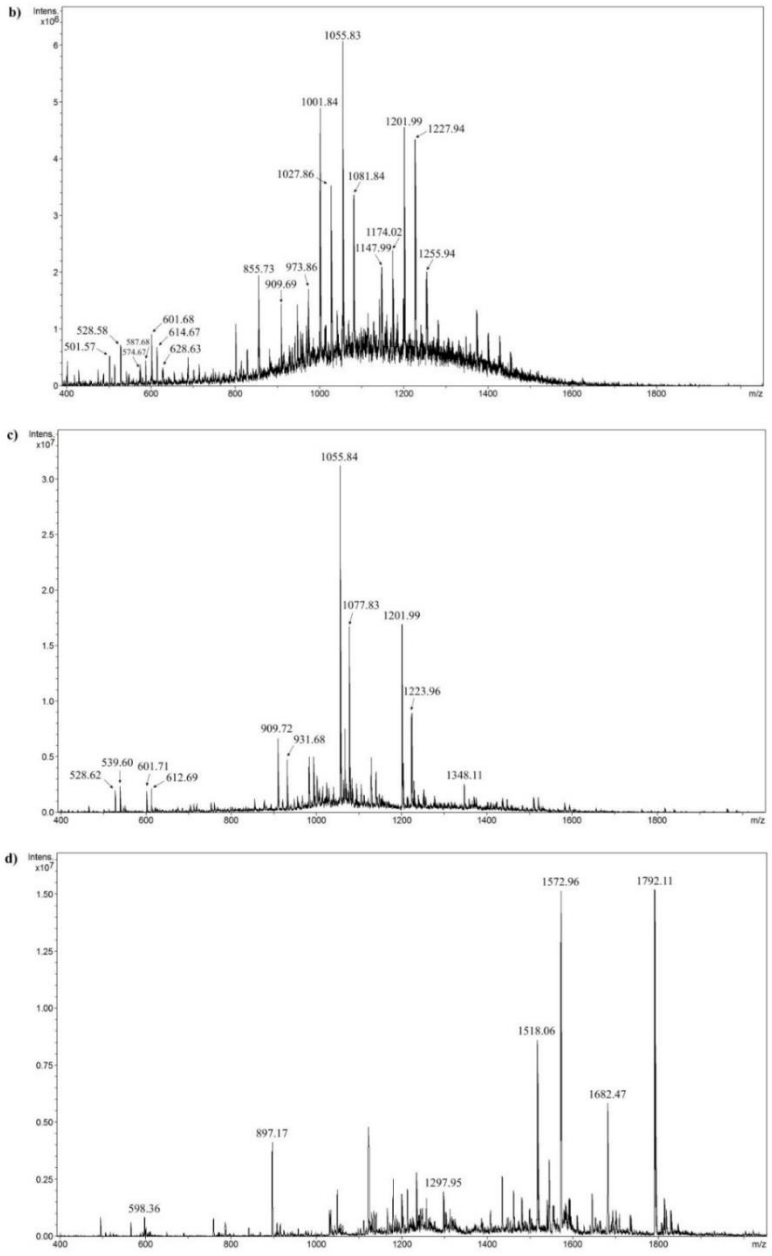


**Figure S2.** The ESI-MS positive spectra of the synthesized PAMAM dendrimers: (**a**) EDA, (**b**) TETA, (**c**) TREN and (**d**) TRI-OXA.

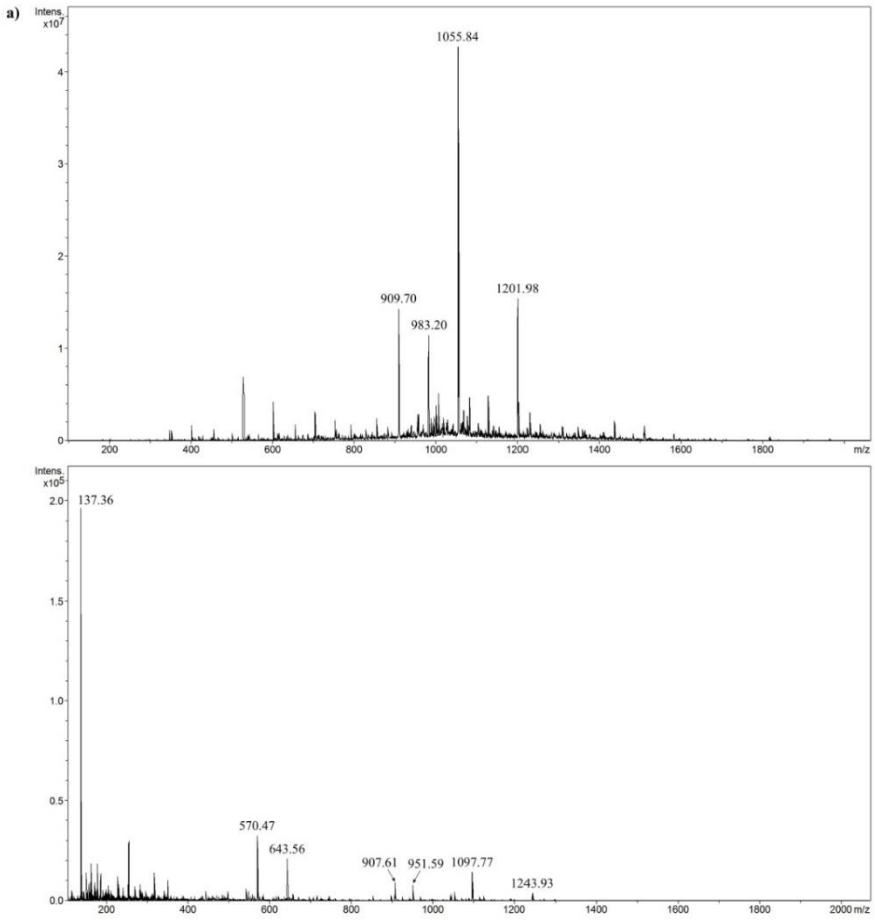
a)
Intens.
x10^7
1055.84
909.70
983.20
1201.98
m/z
Intens.
x10^5
137.36
570.47
643.56
907.61
951.59
1097.77
1243.93
2000 m/z

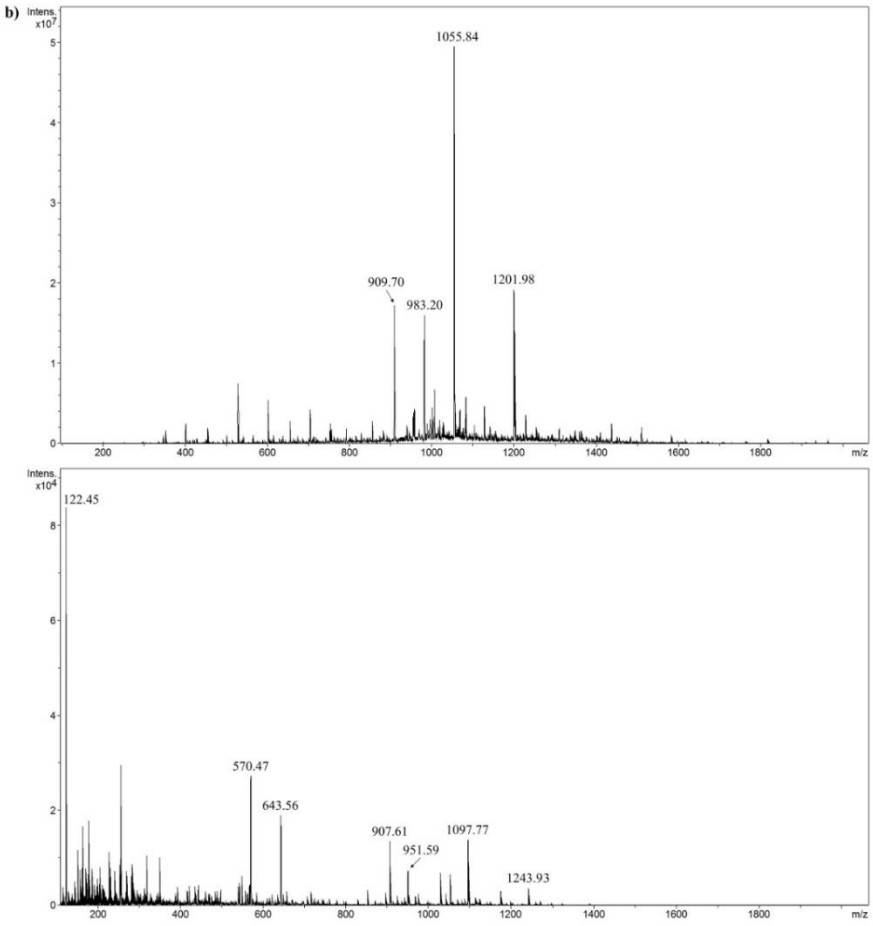
b)
Intens.
x10^7
1055.84
909.70
983.20
1201.98
m/z
Intens.
x10^4
122.45
570.47
643.56
907.61
951.59
1097.77
1243.93
m/z

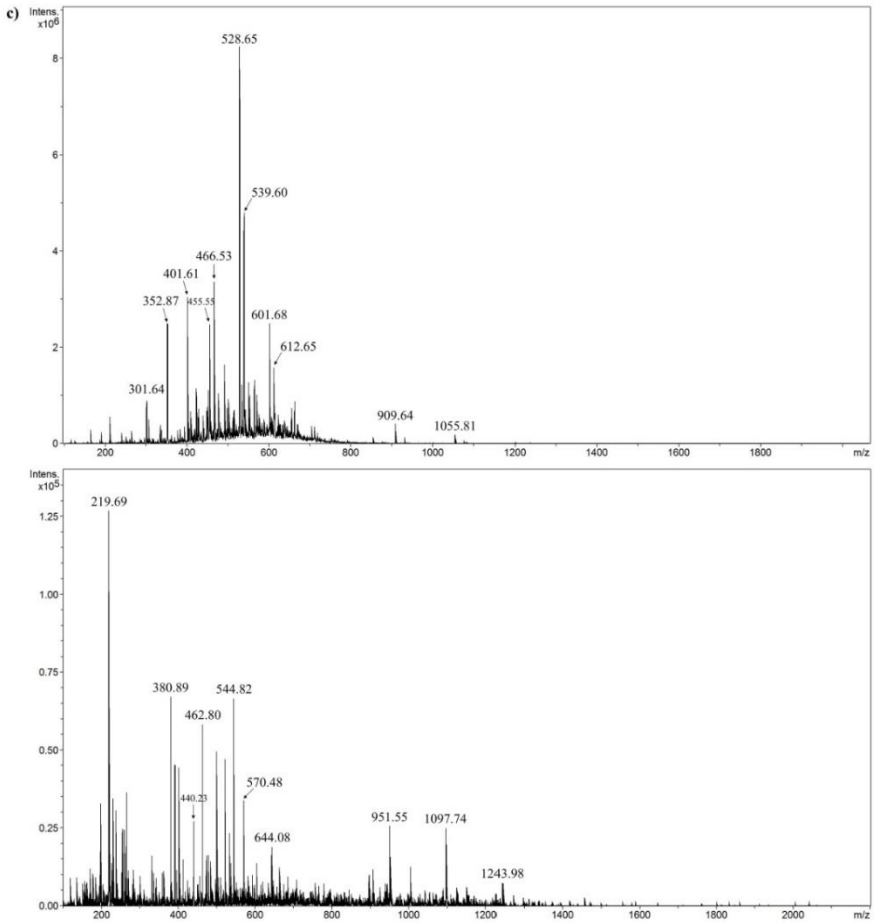


**Figure S3.** The ESI-MS spectra (positive – top; negative – bottom) of exemplary TREN poly(amidoamine) dendrimer complexes with the studied biomolecules: (**a**) salicylic acid, (**b**) nicotinic acid, (**c**) folic acid.

**Section B: The supplement of the conducted adsorption experiments**

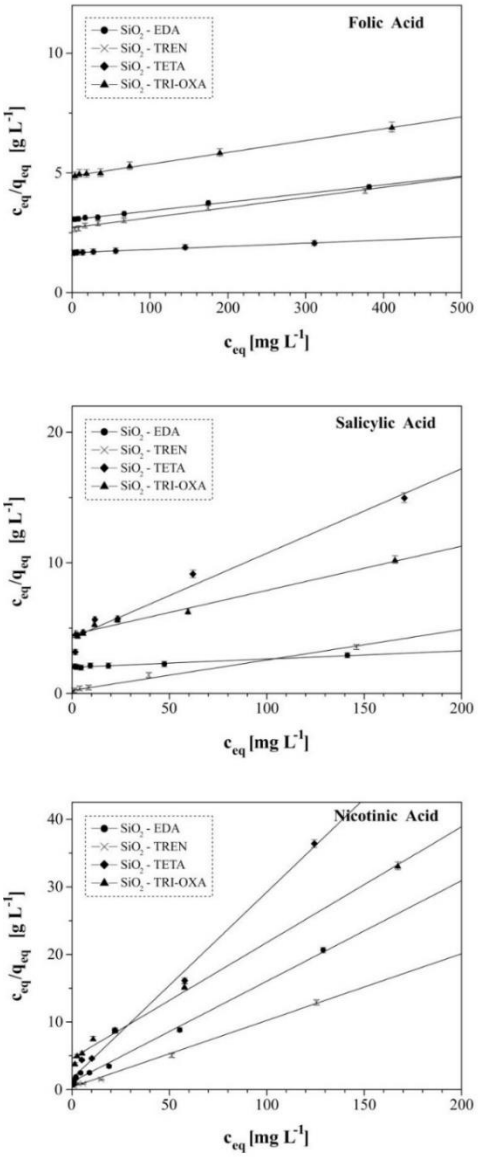


**Figure S4.** The Langmuir isotherm model fitted to the experimental data of the adsorption processes. For some points SDs are smaller than the plotted symbols.

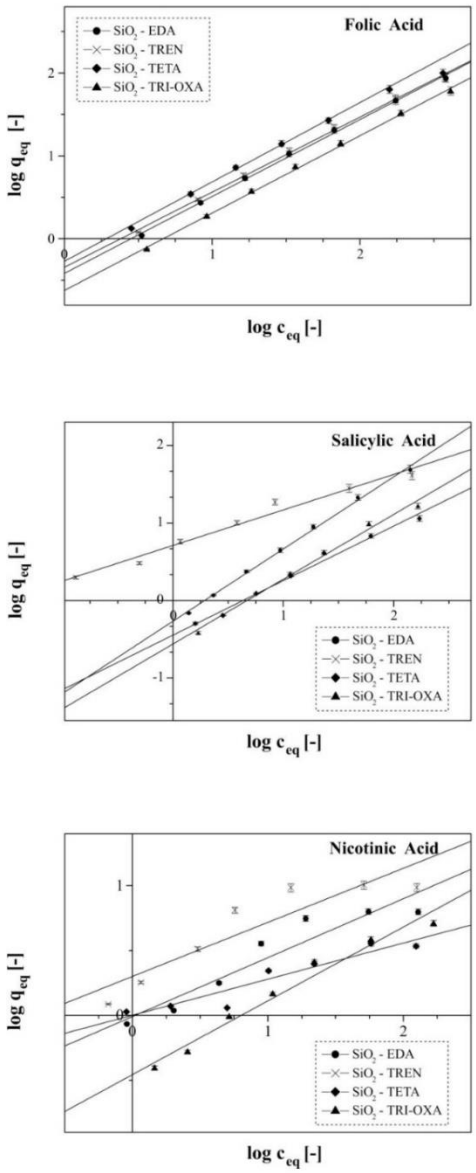


**Figure S5.** The Freundlich isotherm model fitted to the experimental data of the adsorption processes. For some points SDs are smaller than the plotted symbols.

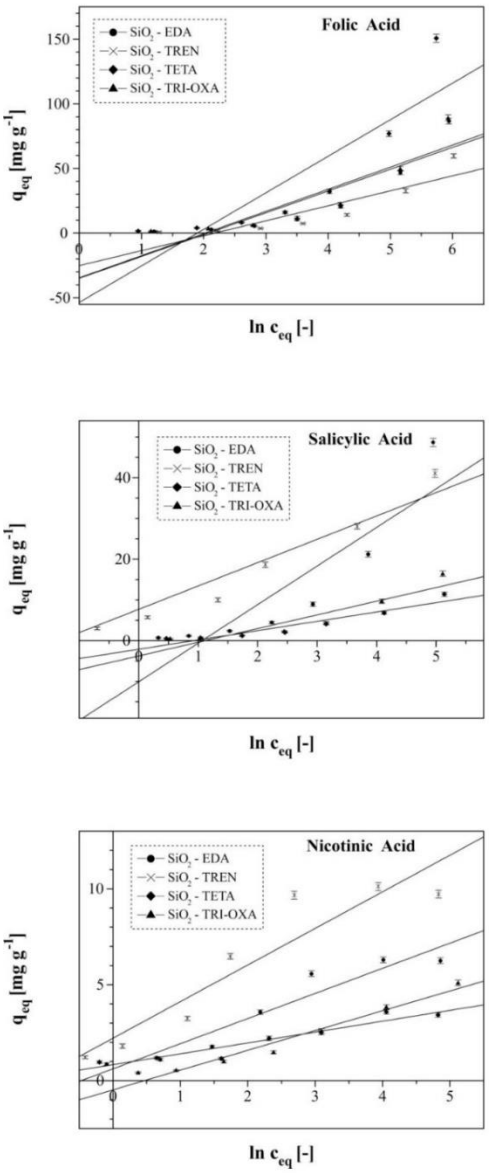


**Figure S6.** The Temkin isotherm model fitted to the experimental data of the adsorption processes. For some points SDs are smaller than the plotted symbols.

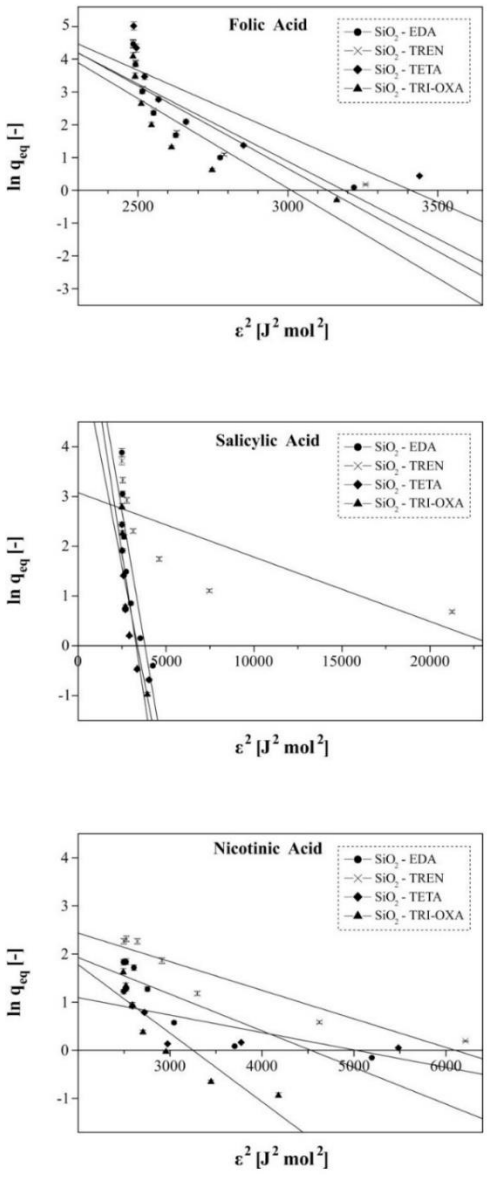


**Figure S7.** The Dubinin–Radushkevich isotherm model fitted to the experimental data of the adsorption processes. For some points SDs are smaller than the plotted symbols.

**Table S1.** Fitting of the experimental data to the Tekmin and the Dubinin–Radushkevich isothermal models.

| Biomolecule | Adsorbent | Temkin isotherm | | | Dubinin–Raduschkevich isotherm | | |
|---|---|---|---|---|---|---|---|
| | | B [J mol$^{-1}$] | $R^2$ | $\chi^2$ | E [kJ mol$^{-1}$] | $R^2$ | $\chi^2$ |
| Folic Acid | $SiO_2$–epoxy | 1.54 | 0.8608 | 0.010 | 0.209 ± 0.075 | 0.6052 | 43.592 |
| | $SiO_2$–EDA | 16.75 | 0.7564 | 16.250 | 0.260 ± 0.106 | 0.5474 | 9.514 |
| | $SiO_2$–TETA | 19.83 | 0.8038 | 7.689 | 0.296 ± 0.115 | 0.5717 | 9.091 |
| | $SiO_2$–TREN | 17.07 | 0.7635 | 12.862 | 0.273 ± 0.110 | 0.5508 | 9.160 |
| | $SiO_2$–TRI–OXA | 11.58 | 0.7532 | 9.980 | 0.242 ± 0.099 | 0.5440 | 10.392 |
| Salicylic Acid | $SiO_2$–epoxy | 0.25 | 0.9490 | 0.512 | 0.406 ± 0.108 | 0.7376 | 6.140 |
| | $SiO_2$–EDA | 9.47 | 0.7628 | 27.602 | 0.526 ± 0.185 | 0.6173 | 12.798 |
| | $SiO_2$–TETA | 3.31 | 0.8354 | 8.626 | 0.462 ± 0.156 | 0.6366 | 14.136 |
| | $SiO_2$–TREN | 5.73 | 0.9098 | 12.498 | 2.448 ± 0.927 | 0.5824 | 6.369 |
| | $SiO_2$–TRI–OXA | 2.82 | 0.8713 | 19.115 | 0.496 ± 0.166 | 0.6426 | 12.631 |
| Nicotinic Acid | $SiO_2$–epoxy | 0.22 | 0.9299 | 0.636 | 0.020 ± 0.005 | 0.7540 | 61.718 |
| | $SiO_2$–EDA | 2.99 | 0.8557 | 6.049 | 0.871 ± 0.373 | 0.5207 | 8.278 |
| | $SiO_2$–TETA | 0.84 | 0.9587 | 0.473 | 0.813 ± 0.257 | 0.6676 | 6.779 |
| | $SiO_2$–TREN | 2.90 | 0.9294 | 6.128 | 0.997 ± 0.314 | 0.6593 | 7.170 |
| | $SiO_2$–TRI–OXA | 1.18 | 0.9221 | 2.068 | 0.620 ± 0.219 | 0.6359 | 11.258 |

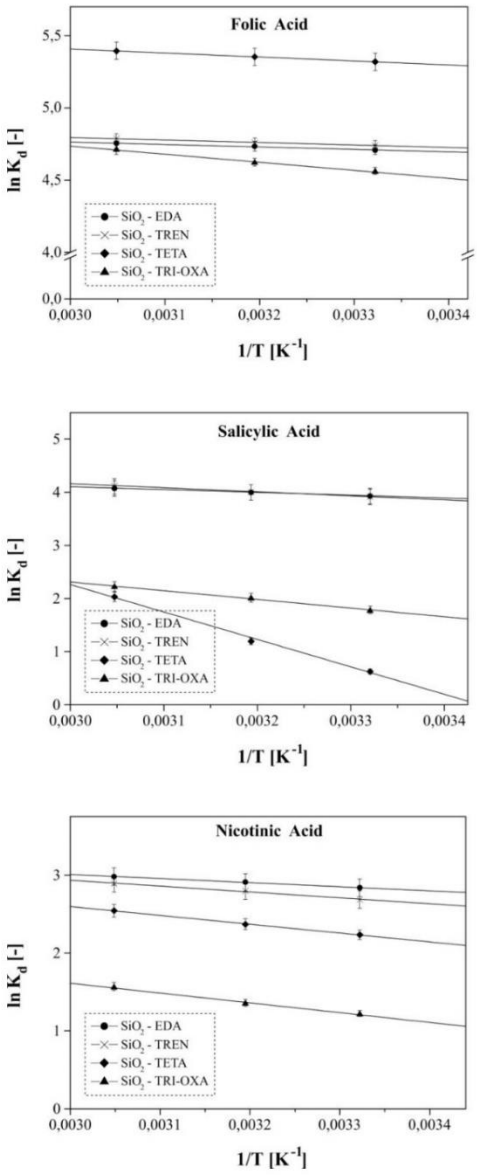


**Figure S8.** The thermodynamic plots of the biomolecules adsorption processes corresponding the van't Hoff equation. For some points SDs are smaller than the plotted symbols.

## Section C: The supplement of the conducted drug-release experiments

**Table S2.** The drug release parameters calculated for the fitting of experimental data to the zero–order and the Hixson–Crowell release models.

| Biomolecule | Adsorbent | Zero–order model | | Hixson–Crowell model | |
|---|---|---|---|---|---|
| | | $k_1$ [mg $h^{-1}$] | $R^2$ ($\chi^2$) | $k_{H-C}$ [$mg^{1/3}$ $h^{-1}$] | $R^2$ ($\chi^2$) |
| Folic Acid | $SiO_2$–EDA | 0.006 ± 0.002 | 0.5433 (0.085) | 0.008 ± 0.004 | 0.4265 (0.078) |
| | $SiO_2$–TETA | 0.005 ± 0.002 | 0.5477 (0.058) | 0.007 ± 0.003 | 0.4596 (0.073) |
| | $SiO_2$–TREN | 0.005 ± 0.002 | 0.5698 (0.061) | 0.007 ± 0.004 | 0.4599 (0.063) |
| | $SiO_2$–TRI–OXA | 0.004 ± 0.001 | 0.5860 (0.059) | 0.008 ± 0.004 | 0.4649 (0.072) |
| Salicylic Acid | $SiO_2$–EDA | 0.007 ± 0.004 | 0.3547 (0.042) | 0.003 ± 0.002 | 0.3371 (0.111) |
| | $SiO_2$–TETA | 0.006 ± 0.002 | 0.4885 (0.066) | 0.006 ± 0.003 | 0.4280 (0.039) |
| | $SiO_2$–TREN | 0.006 ± 0.004 | 0.3611 (0.032) | 0.003 ± 0.002 | 0.3416 (0.071) |
| | $SiO_2$–TRI–OXA | 0.005 ± 0.003 | 0.3809 (0.069) | 0.005 ± 0.003 | 0.3374 (0.056) |
| Nicotinic Acid | $SiO_2$–EDA | 0.004 ± 0.001 | 0.6156 (0.013) | 0.004 ± 0.001 | 0.5821 (0.043) |
| | $SiO_2$–TETA | 0.004 ± 0.001 | 0.5863 (0.045) | 0.006 ± 0.002 | 0.5729 (0.032) |
| | $SiO_2$–TREN | 0.004 ± 0.002 | 0.5655 (0.011) | 0.001 ± 0.002 | 0.0592 (0.156) |
| | $SiO_2$–TRI–OXA | 0.008 ± 0.004 | 0.4099 (0.159) | 0.008 ± 0.005 | 0.3438 (0.235) |

ACS APPLIED POLYMER MATERIALS

pubs.acs.org/acsapm Article

# Dual-Polymeric Resin Based on Poly(methyl vinyl ether-*alt*-maleic anhydride) and PAMAM Dendrimer as a Versatile Supramolecular Adsorbent

Mateusz Pawlaczyk* and Grzegorz Schroeder

Cite This: *ACS Appl. Polym. Mater.* 2021, 3, 956–967 Read Online

ACCESS | Metrics & More | Article Recommendations | Supporting Information

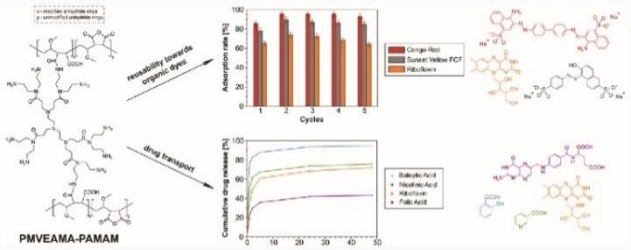


**ABSTRACT:** Adsorptive materials demand meeting several criteria, including the versatility of applications, synthetic easiness, reusability, eco-friendliness, and low-cost production. Therefore, the following study aimed at the synthesis of dual-polymeric material containing biocompatible poly(methyl vinyl ether–*alt*–maleic anhydride) (PMVEAMA) matrix functionalized with multifunctional and branched poly(amidoamine) (PAMAM) dendrimer. The obtained PMVEAMA–PAMAM material was characterized with several analytical techniques and investigated as an adsorbent of several analytes, which belong to a class of either water contaminants or bioactive molecules. Adsorption isothermal studies have been performed, using aqueous solutions of analytes (conditions: distilled water or phosphate buffer pH 8.0 solutions of concentration ranging between 0.1 and 1 mM; room temperature; 24 h incubation), which revealed highly satisfactory results of the maximal adsorption capacity $q_m$ values, e.g. 367.65 and 304.88 mg $g^{-1}$ for Congo Red and folic acid, respectively. The studies aiming to a description of the material–dye complexes included also adsorption kinetic studies and 5 cycles of adsorption/desorption steps, showing fast and intense dye adsorption and high reusability of the material toward dye scavenging. Moreover, PMVEAMA–PAMAM has been investigated for the drug delivery of four biocompounds. The release studies performed in three different media showed that material–drug complexes dissociate to the highest extent at pH 2.0, reaching maximally 94.90% for salicylic acid. The performed experiments indicate the versatility of PMVEAMA–PAMAM applications, including chemical analysis, environmental protection, and *in vitro* biomedical application.

**KEYWORDS:** *adsorption, polymeric adsorbent, PAMAM dendrimer, organic dyes, biocompounds, in vitro drug release*

## 1. INTRODUCTION

Over the past few decades, hybrid materials gained significant attention according to a versatility of their components allowing for a wide range of applications, especially as drug delivery systems, tools for targeted gene therapy, scavenging materials for aqueous or organic media purification, or tools finding application in analytical chemistry. A classic hybrid material is composed of a supporter undergoing surface functionalization with a particular organic domain. Silica either in amorphous or mesoporous form, magnetite nanoparticles, clay nanotubes, titania particles, quantum dots, and metal nanoparticles are the most commonly used inorganic supporters for the preparation of hybrid materials. Also, in recent years, synthetic and biosourced polymers exhibiting interesting physicochemical properties have become an attractive group of platforms for the creation of functional materials. Among such polymeric chains, the alternating copolymer of methyl vinyl ether and maleic anhydride (PMVEAMA) has been considered to find versatile chemical and biomedical applications related to its biocompatibility, biodegradability, easy functionalization, and mucoadhesive properties.[1,2] Since PMVEAMA is water-soluble, easiness in

Received: November 12, 2020
Accepted: December 28, 2020
Published: January 6, 2021





https://dx.doi.org/10.1021/acsapm.0c01254
ACS Appl. Polym. Mater. 2021, 3, 956–967

its functionalization is highly important, which allows for tuning solubility and dispersibility of polymer-based materials through various modifications, such as surface functionalization, cross-linking, or encapsulation.

The biomedical applications of PMVEAMA-based materials are mostly connected with the synthesis of drug-loaded nanovehicles, which therapeutic effects may be stimulated by several functionalizations leading to prolonged drug release, increase in biocompatibility, or improvement of mucoadhesive properties. Although the main domains responsible for enhanced hydrogen bonding between the polymeric chain and mucosa components are the two carboxylic groups available as anhydride ring hydrolysis products, functionalization of polymers may improve adhesive properties. Such a phenomenon was observed for PMVEAMA cross−linked with 1,3−diaminopropane or glycerine, as well as coated with vitamin B12.[3−5] The nanoparticles were studied for *in vivo* bioadhesion, as the rate of particles adhered to the animal gut (stomach, intestine, and cecum regions) in the administration time, revealing improved interacting time. Moreover, the polymer was also functionalized with PEGs with different molecular weights, showing the dependence between the functionalizing PEG length and the affinity to adsorb mucin.[6] Nevertheless, improved adhesive properties of the polymeric materials are only a beneficial feature of their therapeutic effect as drug−delivery or cell−penetrating systems. For instance, PMVEAMA was characterized as an efficient platform for prolonged delivery of propranolol hydrochloride, a nonselective $\beta$-adrenergic blocking agent, or L-$\alpha$-dimyristoylphosphatidylcholine (DMPC), as well as a candidate for intravaginal administration of glycyrrhizic acid, the triterpenic saponin exhibiting therapeutic effects for the treatment of HPV and cervical cancer lesions. 5, 7, and 8 The polymer chains cross−linked with diols of different lengths were designed as percutaneous drug−delivery platforms, studied for *in vitro* permeation of pyridoxine hydrochloride.[9] Studies showed higher permeation ability of cross−linked polymer materials, indicating an influence of cross−linking agent's length on the improvement rate. Moreover, Luzardo-Álvarez et al. proposed a synthesis of PMVEAMA−based sponges by cross−linking of the polymer chains with glutaraldehyde or genipin for delivery of amoxicillin, an antibiotic used for the treatment of dental root canals infected with *Enterococcus faecalis*.[10] What is interesting, cross−linking of PMVEAMA chains may be also performed with a use of metal cations, such as $Zn^{2+}$ or $Ca^{2+}$, resulting in microwave irradiation−sensitive matrices for the targeted delivery of bioactive compounds.[11] The nanoparticles of methyl vinyl ether and maleic anhydride copolymer were also investigated for transfection or direct binding to cancer cells.[12] The ones associated with aluminum−phthalocyanine chloride by electrostatic interactions between the negative carboxylate groups of opened anhydride rings of PMVEAMA and the positive metallic center of phthalocyanine were tested for their photodynamic activity towards chosen cancer cell lines.[13] The material was successfully described as a singlet oxygen−generating system causing cell death after its prior transfection. The polymer may also play a role of coating material, which was implemented for encapsulation of hydrophobic selol nanocapsules−a mixture of selenitetriacylglycerides, exhibiting proved anticancer activity.[14,15] The PMVEAMA/selol nanoparticles surface−functionalized with folic acid as a targeting marker exhibited high cytotoxicity towards 4T1, MCF−7, HeLa, and NIH−3T3 cancer cell lines, reaching cell viabilities approximately of 15%.

Physicochemical properties of PMVEAMA have also prompted its implementation as a network of biocompatible hydrogels. The polymer−based hydrogels exhibit increased water dispersibility, excellent swelling properties, high cytocompatibility, increased adhesiveness, and satisfactory mechanical properties. Mostly, hydrogels are formed by a cross−linking process using polyfunctional nonionic surfactants, such as PEG and Pluronic F127, and polysugar domains, e.g. pectin, cellulose, or cellulose derivatives.[16−21] The choice of a particular cross−linker affects the materials plasticity, hardness, and swelling abilities of final materials, as well as their ability to adhere, effectiveness in biocompounds permeation, and drug controlled release potential. Also, a few reports describe the gelation process performed by autoclaving of PMVEAMA with poly(vinyl alcohol), Diels−Alder coupling between furfurylamine− and (2−aminoethyl)−*N*−maleimide derivatives of the polymer, and supramolecular assembly of PMVEAMA−$\beta$−cyclodextrin and PMVEAMA−*p*−aminobenzene chains.[22−24] Nevertheless, it needs to be highlighted that despite the synthetic routes, all the hydrogels were found to be highly biocompatible and effective tools for biomedical applications. The described versatile and biocompatible polymer has also found its application as a platform for various analytical tools. For instance, core/shell particles based on magnetic beads encapsulated with poly(methyl vinyl ether−maleic anhydride) were successfully used for human influenza A and B viruses capture from nasal aspirates and allantoic fluid.[25] Also, bare PMVEAMA and its poly(vinyl alcohol)−blended nanofibers were proved for efficient amino acids and protein adsorption, while the polymer's particles functionalized with structurally different amines and 2,4−dichlorophenoxyacetic acid chloride were confirmed for excellent delivery of 2,4−D as a model herbicide, using hydrolytic release mechanism in basic and acidic media.[26−28] Moreover, the polymer functionalized with 3−aminophenylboronic acid found an application as a platform for diol sensing (such as ribonucleosides and carbohydrates), while a membrane based on PMVEAMA and poly(vinylidene fluoride) with doped $TiO_2$ particles offered satisfactory photodegradative properties toward organic Reactive Black 5 (RB5) dye.[29,30]

Our present research aims to investigate poly(methyl vinyl ether−*alt*−maleic anhydride) functionalization with highly branched, symmetric, and monodisperse poly(amidoamine) dendrimer. The choice of PAMAM dendrimer is strictly related to its proved biocompatibility and versatility in the formation of PAMAM−analyte complexes. The structural features of this kind of dendrimers (multiple terminal amine groups, internal amide domains, and cavities between dendrimer's branches) allow for binding of several compounds through various physicochemical processes, which are electrostatic interactions and coordination of metal cations, as well as physical entrapment within a dendritic matrix. Therefore, PMVEAMA−PAMAM dual−polymeric material should exhibit the versatility of applications, especially as an effective scavenger of various contaminants and a tool for drug delivery, concerning the biocompatibility of both reagents. Moreover, the polyamine character of PAMAM dendrimer may lead to cross−linking of the polymeric support, which makes the material insoluble in aqueous samples and more stable in either acidic or basic environments, affording broad usability perspectives. Although, a creation of such material may find a wide range of applications, as a consequence of highly utilizable physicochemical features of both polymeric components, to the best of our knowledge the



https://dx.doi.org/10.1021/acsapm.0c01254
ACS Appl. Polym. Mater. 2021, 3, 956−967

following study is a very first attempt to synthesis and analytical applications of the aforementioned polymeric material. The obtained material was characterized with several analytical techniques and subsequently investigated for binding efficiency toward chosen organic dyes as model water contaminants and bioactive acids as model biocompounds.

## 2. MATERIALS AND METHODS

**2.1. Materials.** All the reagents and solvents without any further purification, otherwise indicated. Poly(methyl vinyl ether−*alt*−maleic anhydride) (PMVEAMA) (average $M_w \sim 216\,000$, average $M_n \sim 80\,000$) of p.a. purity grade, diethylenetriamine ≥99%, tris(2-aminoethyl)-amine ≥96%, maleic anhydride ≥99%, and all the analytes used for adsorption experiments (folic acid ≥97%, salicylic acid ≥99%, nicotinic acid ≥99.5%, riboflavin ≥98%, Congo Red ≥85%, and Sunset Yellow FCF ≥ 90%) were purchased from Sigma-Aldrich (St. Louis, MO). The solvents and the ingredients of buffers were described as of p.a. purity grade. Diethyl ether, potassium chloride, disodium hydrophosphate dehydrate, and sodium dihydrophosphate hydrate were obtained from POCH (Gliwice, Poland). Methanol, toluene, and hydrochloric acid were supplied by Stanlab (Lublin, Poland), acetic acid was obtained from Chempur (Piekary Śląskie, Poland), and sodium acetate trihydrate was purchased from Eurochem BGD (Tarnów, Poland). The dimethyl sulfoxide used in experiments was purchased from Merck (Darmstadt, Germany) and dried over molecular sieves 4 Å for 24 h before use.

**2.2. Instruments.** The ESI−MS spectra of the ester-intermediate and the PAMAM dendrimer were recorded on an amaZon SL ion trap Bruker mass spectrometer (Bremen, Germany). Electrospray ion source (ESI) worked in infusion mode. The samples were introduced to spectrometer using a syringe pump, at a flow rate of 10 $\mu$L min$^{-1}$ into the ionization source. The analysis was performed in so−called "enhanced resolution mode" with a detection range between 50 and 2200 $m/z$ and scanning rate at 8100 $m/z$ per second. The instrument used two types of gases: the cone gas (helium) flowing at a flow rate of 50 L h$^{-1}$ and the desolvating gas (nitrogen) flowing at a rate of 800 L h$^{-1}$. The capillary voltage was set at −4.5 kV, while the voltage for the end plate offset was set at −0.5 kV. The $^{13}$C NMR spectrum of PAMAM dendrimer was recorded on Varian VNMR−S 400 MHz spectrometer (Palo Alto, CA). The FT−IR spectrum of the synthesized polymeric material was recorded in photoacoustic mode (PAS/FT−IR) using Bio-Rad Excalibur FTIR 3000 MX spectrometer (Hercules, CA) equipped with MTEC Model 300 photoacoustic cell. A reference sample used during spectroscopic assays was carbon black standard. The operating wavelength range was set between 4000 and 400 cm$^{-1}$. The thermal stability of the polymeric material was studied employing Setaram Setsys 1200 analyzer (Caluire, France). Thermogravimetric measurements were conducted in an airstream in the range of 20−1000 °C with a heating rate of 5 °C min$^{-1}$. The percentage of carbon, hydrogen, and nitrogen contents (CHN elemental analysis) in the material was established using Elementar Vario EL III analyzer (Langenselbold, Germany). PMVEAMA−PAMAM material was also described with microscopic images obtained using FEI Quanta FEG 250 (Hillsboro, OR, USA) scanning electron microscope. The microscopic imagining was performed using a high accelerating voltage of 10 kV with a working distance of 10.2 mm and was carried out under vacuum conditions (70 Pa). The analytes adsorption on the polymeric material was monitored by UV−Vis spectrophotometric assays using Agilent 8453 spectrophotometer (Santa Clara, CA). The spectra were recorded in the range of 200−1000 cm$^{-1}$ using PMMA cuvettes with an optical path length of 10 mm. Each measurement was done in triplicate, selecting a mean value of absorbance ascribed to the particular wavelength as a final value.

**2.3. Synthesis of PMVEAMA−PAMAM.** *2.3.1. Synthesis of the Ester Intermediate (1).* A three−necked flask was purged with $N_2$, charged with an anhydrous solution of methyl acrylate (8.16 mL; 90 mmol) in 50 mL of MeOH, and placed in a water−ice bath. When the solution temperature had lowered to 0 °C, a solution of diethylenetri-amine (DETA) (1.63 mL; 15 mmol) in 20 mL of anhydrous MeOH was added dropwise within 1.5 h under nitrogen atmosphere, not to let the temperature rise above 4 °C. Afterwards, the cooling bath was removed, and the reaction mixture was stirred at room temperature for 5 days ($N_2$). After reaction completion, monitored with ESI−MS analysis, solvent and excess of reagent were evaporated and the crude product was dried under reduced pressure at 40 °C, yielding pale yellow liquid ester intermediate (**1**). Yield: 97.7% (7.82 g; 14.66 mmol). ESI-MS: ($z$ +1) $m/z$ 534.77.

*2.3.2. Synthesis of PAMAM Dendrimer (2).* An anhydrous solution of 8.14 mL of diethylenetriamine (75 mmol) in 50 mL of MeOH was cooled to temperature 0 °C in a water−ice bath under nitrogen atmosphere. Then, an anhydrous solution of 5.34 g of ester intermediate (**1**) (10 mmol) in 30 mL of MeOH was added dropwise, maintaining a low temperature. Afterwards, the mixture was subsequently warmed to room temperature and stirring was held for 5 days under $N_2$ atmosphere. Reaction completion was confirmed with ESI−MS analysis. An excess of solvent was evaporated, and then the product was extracted with cooled $Et_2O$. The crude product was dried under reduced pressure at 45 °C, yielding in orange honey−like dendrimer (**2**). Yield: 89.7% (7.98 g; 8.97 mmol). ESI-MS: ($z$ +1) $m/z$ 889.78, 786.71, 732.77, 629.68, 575.68, 440.49, 418.50, 283.32, 261.35. $^{13}$C−NMR ($CD_3OD$, 400 MHz), $\delta$: 34.64, 36.56, 38.61, 40.00, 41.68, 41.87, 44.80, 46.51, 51.81, 52.51, 164.09, 175.06.

*2.3.3. Immobilization of PAMAM Dendrimer (2) on Poly(methyl vinyl−alt−maleic anhydride).* In a three−necked flask equipped with a reflux condenser, 4.55 g of dendrimer (**2**) (5.12 mmol) was dissolved in 40 mL of DMSO. The mixture was heated to 110 °C under nitrogen atmosphere, and then a suspension of PMVEAMA (1.6 g) in 30 mL of toluene was added in a few portions. The mixture was stirred under the atmosphere of neutral gas for 16 h. Afterward, solvents were evaporated and the crude product was crystallized in $Et_2O$. The material was filtered off, washed with cold $Et_2O$ (2 × 10 mL), and dried under vacuum at 50 °C, yielding green−blue solid PMVEAMA-PAMAM. Yield: 93.4% (5.74 g).

*2.3.4. Quantification of PAMAM Content in PMVEAMA−PAMAM.* To a series of three samples of PMVEAMA−PAMAM (20 mg), 20 mL of 0.01 M aqueous solution of HCl were added. The mixtures were stirred for 2 h at room temperature. Afterward, the solids were filtered off and the solutes were titrated with 0.005 M aqueous solution of NaOH, using phenolphthalein as an indicator, until the color changed to permanent pink.

*2.3.5. pH−Influenced Stability Measurements of the Material.* PMVEAMA samples (10 mg) were added to a series of prepared buffer solutions of pH ranging between 1 and 13. The buffer systems were: HCl/KCl (pH 1, 2), citric acid/$Na_2HPO_4$ (pH 3, 4, 5, 6) $NaH_2PO_4$/$Na_2HPO_4$ (pH 7, 8), $NaHCO_3$/$Na_2CO_3$ (pH 9) $NaHCO_3$/NaOH (pH 10, 11), and NaOH/KCl (pH 12, 13). The material was incubated in 10 mL of each of the given buffers for 3 h at room temperature. Afterward, the solid was filtered off and the solutes were analyzed using the ESI−MS technique in positive and negative mode.

**2.4. Adsorption of Drugs and Organic Dyes on PMVEAMA−-PAMAM.** For isothermal experiments, a general procedure was adopted, which was based on incubation of 10 mg of PMVEAMA−-PAMAM in 10 mL of analytes solutions of seven different concentrations: 0.01, 0.025, 0.05, 0.1, 0.2, 0.5, and 1 mM. Distilled water was a solvent for the preparation of salicylic and nicotinic acid, and Sunset Yellow FCF solutions, while folic acid Congo Red and Riboflavin solutions were prepared using phosphate buffer ($Na_2HPO_4$/$NaH_2PO_4$) of pH 8.0. The adsorption experiments were handled for 24 h at room temperature. Afterwards, the material−analyte complexes were filtered off and the amount of the analytes remaining in the filtrates was established using UV−Vis spectrophotometric assays. The absorbance values were determined at wavelength $\lambda$ = 365, 297, 265, 498, 484, and 430 nm for folic acid, salicylic acid, nicotinic acid, Congo Red, Sunset Yellow FCF, and riboflavin, respectively. Therefore, the amount of the analyte adsorbed to PMVEAMA−PAMAM material $q_{eq}$ was calculated using the below presented eq 1, where $c_0$ is the starting concentration of the analyte [mM], $c_{eq}$ is the equilibrium concentration of the analyte [mM], $m$ is the sample mass [mg], $V$ is the solution volume [mL], and $M$ is the molar mass of the analyte [g mol$^{-1}$]:



https://dx.doi.org/10.1021/acsapm.0c01254
ACS Appl. Polym. Mater. 2021, 3, 956−967

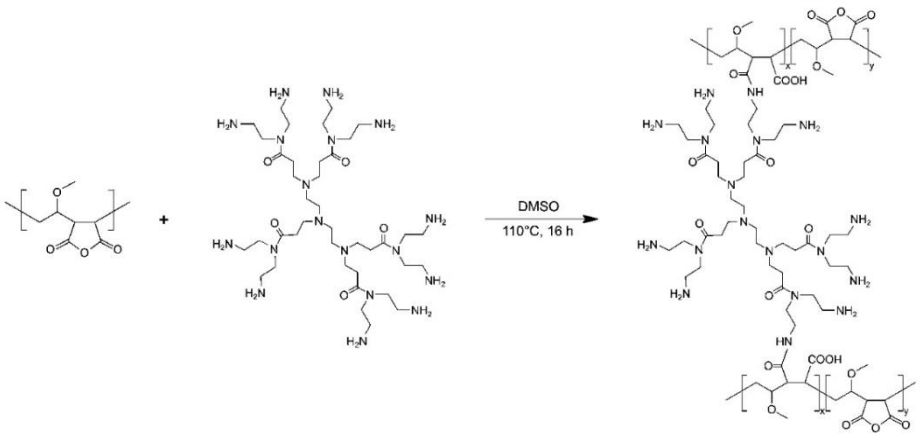


**Figure 1.** Synthetic route for obtaining PAMAM−functionalized poly(methyl vinyl ether−*alt*−maleic anhydride) chain; *x* and *y* indexes are related to a number of modified and unmodified anhydride rings, respectively.

$$q_{eq} = \frac{(c_0 - c_{eq}) \times V}{m} \times M \quad (1)$$

Thermodynamic and pH studies were based on the same experimental protocol, however, for thermodynamic studies the material samples were incubated in 0.1 mM solutions of the analytes at three different temperatures: 298 ± 1, 313 ± 1, and 328 ± 1 K for thermodynamic experiments, while for pH tests, the material was incubated in 1 mM Congo Red or folic acid solutions buffered to pH values 8 (phosphate buffer) 9, 10, and 11 (bicarbonate buffer). The material isolation, UV−Vis measurements, and calculation of the amount of the analytes adsorbed were performed as described for isothermal studies.

**2.5. Kinetic Studies of the Organic Dyes Adsorption on PMVEAMA−PAMAM.** The kinetic studies of the uptake of the organic dye by the polymeric material were performed using a procedure as follows: 20 mg of PMVEAMA−PAMAM material was added to 20 mL of 0.5 mM solution of the organic dye (Congo Red, Sunset Yellow FCF, or riboflavin) and stirred at room temperature. The experiments involved the use of aqueous solutions of the dyes: distilled water as a solvent for Sunset Yellow FCF and phosphate buffer (pH 8.0) for Congo Red and riboflavin. In preset time intervals, the filtrate was investigated for the amount of the dye remaining in the solution using UV−Vis spectroscopic assays. The amount of the dye adsorbed on the material $q_t$ at time $t$ was then established using eq 2, where $c_t$ is the concentration of the organic dye at time $t$ [mM]:

$$q_t = \frac{(c_0 - c_t) \times V}{m} \times M \quad (2)$$

**2.6. Reusability Studies of PMVEAMA−PAMAM toward Organic Dyes.** Investigation of the material reusability toward organic dyes scavenging was based on the repetitive adsorption/desorption cycles. Briefly, 20 mg of PMVEAMA−PAMAM material was added to 10 mL of 0.01 mM solution of Congo Red (phosphate buffer, pH 8.0), Sunset Yellow FCF ($H_2O$), or riboflavin (phosphate buffer, pH 8.0). The mixtures were stirred at room temperature for 24 h. Afterwards, the material was filtered off, and the amount of the dye adsorbed was investigated using UV−Vis assay. The material−dye complexes were then treated with 10 mL of 0.01 M HCl at room temperature for 24 h, as the desorption step. Subsequently, the dye-desorbed material was filtered off, dried, and used for another 4 cycles of adsorption/desorption processes handled under the described conditions.

**2.7. Drug Loading and *In Vitro* Release of the Drugs from PMVEAMA−PAMAM.** Drug loading on the material surface was performed using 100 mg of PMVEAMA−PAMAM stirred in 20 mL of 1 mM solution of the biocompounds (folic, salicylic, and nicotinic acid or riboflavin) at room temperature for 24 h. Then, 20 mg of the dried material−biocompound complexes were incubated in 5 mL of three different release media: HCl/KCl buffer of pH 2.4, AcOH/AcONa buffer of pH 5.4, and PBS buffer of pH 7.4. At preset time intervals, the buffers' aliquots were collected and replaced with 5 mL of fresh buffer. The amount of the drugs released in buffer aliquots at time $t$ was determined using UV−Vis measurements. The cumulative amount of the drug released $F_t$ [mg] and percentage of the drug released $Q_t$ [%] at time $t$ was established using eq 3 and eq 4, respectively:

$$F_t = V \times M \sum_{i=t_1}^{t} c_t \quad (3)$$

$$Q_t = \frac{F_t}{m_0} \times 100\% \quad (4)$$

where $c_t$ is the concentration of the drug released at time $t$ [mM], $V$ is the volume of buffer aliquot [L], $M$ is the molar mass of the drug [g mol$^{-1}$], and $m_0$ is the initial mass of the drug in the material-drug complex [mg].

## 3. RESULTS AND DISCUSSION

**3.1. Synthesis and Characterization of the Dual−-Polymeric Material.** The preparation of PMVEAMA−PAMAM was achieved by the nucleophilic addition of free terminal amine group of PAMAM dendrimer to the easy−opening maleic ring as a pendant group of PMVEAMA polymeric chain (Figure 1). The ring opening led to the formation of an amide bond between both polymeric constituents and the free carboxyl group. The anchorage of poly(amidoamine) dendrimer to the polymer chain was, therefore, also stabilized by electrostatic interactions between formed free −COOH group of anhydride domain and the neighboring free terminal $-NH_2$ residue of the dendrimer. Moreover, the polyamine character of the grafting agent might have also triggered the bare polymer cross−linking


https://dx.doi.org/10.1021/acsapm.0c01254
ACS Appl. Polym. Mater. 2021, 3, 956−967

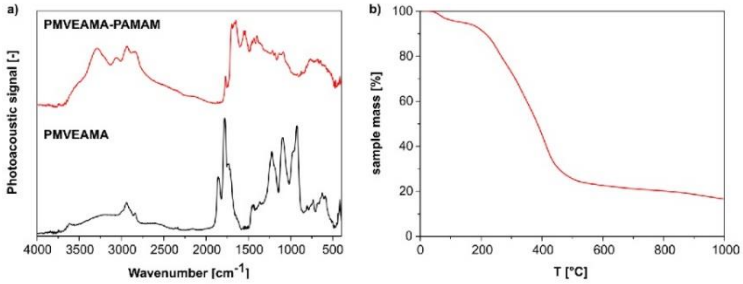


**Figure 2.** (a) FT−IR/PAS spectra and (b) the TG curve obtained for the prepared dual−polymeric material PMVEAMA−PAMAM

processes. Nevertheless, it may have decreased the utility of dendritic structure only by an inconsiderable extent.

PAMAM dendrimer was obtained in the classic two−step synthetic protocol which was based on (1) the branching of tris(2−aminoethyl)amine as an amine core using methyl acrylate, leading to a formation of the polyester product, and (2) the amidation of the obtained polyester with diethylenetriamine (DETA). The amidation process was directed toward the internal amine group, which is the most reactive one among all three accessible amine groups, as a consequence of the highest electrodonating effect. The final PAMAM dendrimer was characterized by ESI−MS and $^{13}$C−NMR analysis. The recorded ESI−MS spectra in positive mode shows several signals, which correspond to either molecular ion ($m/z$ 889.78), fragmentation ions ($m/z$ 786.71, 732.77, 629.68, 575.68, 418.50, 261.35) or sodium adducts of fragmentation ions ($m/z$ 440.49, 283.22) (Figure S1a). Easy fragmentation of the obtained poly(amidoamine) dendrimer during MS analysis is mostly caused by the vulnerability of multiple amide− and amino−-domains, which are prone to breakage under analysis conditions.[31] Also, the dendrimer was characterized using the $^{13}$C−NMR technique, which spectrum exhibits several signals of doubled intensity, related to symmetrically distributed carbon atoms at terminal branches ($\delta$ = 34.64, 40.00, 41.87, 52.51, 175.06 ppm) (Figure S1b). The signals corresponding to the middle dendritic branch are visible as slightly shifted than those of terminal branches ($\delta$ = 36.56, 38.61, 41.68, 51.81, 164.09 ppm). Also, carbon atoms in the amine core (DETA) are symmetrically equal and are attributed to signals at 44.80 and 46.51 ppm.

The immobilization of the obtained poly(amidoamine) dendrimer on PMVEAMA chain was performed at elevated temperature, which allowed for a complete ring opening of maleic anhydride, affording the highest possible dendrimer loading efficiency. The bare polymeric support and the obtained material were characterized with infrared spectroscopy in photoacoustic mode (FT−IR/PAS), which spectra are presented in Figure 2a. The success of PMVEAMA amidation with PAMAM dendrimer is strictly proved by the appearance of N−H$_{(amide)}$ (Amide II) stretching vibrations observed at 3288 cm$^{-1}$ with their overtones at 3058 cm$^{-1}$ and bending vibration observed as a doublet at 1541 and 1556 cm$^{-1}$, comparing with PMVEAMA spectrum. Moreover, the presence of the amide carbonyl group (Amide I) is proved by the appearance of a highly intensive signal at 1637 cm$^{-1}$, evidencing the successful functionalization of the polymer chain with PAMAM dendrimer. Also, a drastic decrease of signals at 927 and 1771 cm$^{-1}$ corresponding to the stretching of C−O−C domain of 5−membered anhydride ring and the stretching of the carbonyl group of anhydride, respectively, in the spectrum of the hybrid polymeric material indicates almost full ring−opening of PMVEAMA reactive maleic anhydride domain. The ring−-opening also leads to the free carboxyl group which absorbs at 1697 cm$^{-1}$ (C═O stretching) and 878 cm$^{-1}$ (O−H out-of-plane bending) visible on the spectrum of PMVEAMA-PAMAM. The spectra exhibit also several common signals related to PMVEAMA structural domains staying unaltered after the amidation process, e.g. signals at 419 and 1131 cm$^{-1}$, which might be both assigned to the stretching of ether domain (C−O−C). The presence of numerous methylene groups −CH$_2$−, as structural domains of both the polymeric support and the hybrid material is proved by their asymmetric and symmetric stretching at 2937 and 2862 cm$^{-1}$, respectively, and also by signals at 1436 cm$^{-1}$ corresponding to C−H scissoring vibrations or at 1456 cm$^{-1}$ related to C−H asymmetric bending vibrations. Furthermore, PMVEAMA−PAMAM spectrum shows a broad band between 500 and 850 cm$^{-1}$, which may correspond to overlapped various C−H bending vibrations of −CH$_2$− and −CH$_3$ groups and N−C−O in−plane bending mode of amide, while a signal at 1398 cm$^{-1}$ may be assigned for O−H deformation vibrations or −CH$_2$− wagging vibrations.[32]

The obtained dual−polymeric material was also characterized with thermogravimetric analysis (Figure 2b). The spectrum shows two distinct decomposition steps: the first one between 80 and 110 °C may be attributed to the removal of trace humidity or organic solvents remaining in the material's structure and the second one between 210 and 470 °C related to the slow decomposition/oxidation of both organic residues as material components. The broad single step corresponding to the oxidation of organic residues, which is not divided into two steps related to the decomposition of a particular organic domain, proves that the chemical nature of the dendrimer used led to a formation of a cross−linking product. Therefore, we expect the two−step character of PAMAM conjugation to the polymeric support, based on the amidation of a single polymer chain followed by the nucleophilic attack of the dendrimer's terminal amine remaining unmodified to another polymeric chain. The material was also characterized with elemental analysis in CHN mode, assessing the percentage of carbon, nitrogen, and hydrogen in the sample at the level of 52.06, 17.70, and 7.01%, respectively. Even though the cross−linking process took place, the fitting of the obtained values to a theoretical


https://dx.doi.org/10.1021/acsapm.0c01254
ACS Appl. Polym. Mater. 2021, 3, 956−967

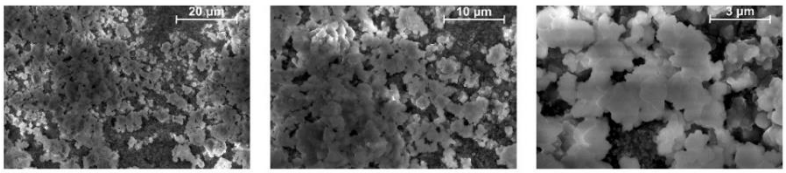


**Figure 3.** SEM images of PMVEAMA−PAMAM material of different magnitudes (left−magnitude 5000×, scale bar equals 20 $\mu$m; middle−magnitude 10 000×, scale bar equals 10 $\mu$m; right−magnitude 30 000×, scale bar equals 3 $\mu$m).

**Table 1. Isothermal Parameters of the Equilibrium State of the Analytes Adsorption on the Polymeric Material PMVEAMA−PAMAM**

| | | Langmuir isotherm | | | | Freundlich isotherm | | |
|---|---|---|---|---|---|---|---|---|
| | adsorbate | $q_m$ [mg g$^{-1}$] | $10^2 \cdot K_L$ [L mg$^{-1}$] | $R^2$ | $\chi^2$ | $1/n$ [−] | $R^2$ | $\chi^2$ |
| biomolecules | folic acid | 304.9 ± 20.7 | 0.49 ± 0.02 | 0.9728 | 0.271 | 0.83 ± 0.03 | 0.9932 | 0.192 |
| | salicylic acid | 134.2 ± 5.4 | 0.20 ± 0.01 | 0.9903 | 0.014 | 0.96 ± 0.01 | 0.9992 | 0.003 |
| | nicotinic acid | 91.6 ± 4.5 | 0.57 ± 0.01 | 0.9856 | 0.079 | 0.89 ± 0.03 | 0.9945 | 0.025 |
| | riboflavin | 26.5 ± 2.3 | 0.86 ± 0.11 | 0.9549 | 1.168 | 0.62 ± 0.02 | 0.9910 | 0.031 |
| dyes | Congo Red | 367.7 ± 10.8 | 2.01 ± 0.22 | 0.9923 | 0.988 | 0.58 ± 0.02 | 0.9930 | 0.006 |
| | Sunset Yellow FCF | 310.6 ± 11.2 | 0.21 ± 0.01 | 0.9922 | 0.098 | 0.89 ± 0.03 | 0.9936 | 0.012 |

percentage calculated for a particular ratio of modified anhydride rings to unmodified ones was performed. The closest calculation values were obtained for a 2:5 ratio (modified:unmodified anhydride rings), which is connected with the percentage of 52.86, 17.47, and 8.17% for nitrogen, carbon, and hydrogen, respectively, showing good comparability to the obtained analytical data. Also, the percentage of nitrogen content in the adsorbent is related to the grafting level of the dendrimer to the polymeric support. The calculated grafting level of 0.702 mmol g$^{-1}$ is consistent with the value obtained during materials characterization by acid−base titration, which equaled 0.687 mmol g$^{-1}$. Furthermore, the stability of the dual polymeric material under acidic and alkaline conditions was investigated. The material's samples were incubated in a series of prepared buffers ranging from pH 1 to 14. The ESI−MS spectra of the solutes showed no signals corresponding to PAMAM dendrimer, which indicates that materials are stable in given conditions and no dissociation of the dendrimer from the material takes place.

Moreover, the polymeric material was characterized using scanning electron microscopy (SEM) imagining. The obtained images of two different magnitudes are presented in Figure 3. According to the obtained images, the studied material might be classified as the microsized one, which is strictly connected to either application of polymeric chain as the material's support or functionalization involving multifunctional PAMAM dendrimer, which structure enhances the possibility of PMVEAMA chains cross−linking. As a result, the material tends to form aggregates of size ranging between approximately 2 and 3 $\mu$m. Since the material's adsorptive properties are predominantly dependent on the structural features of PAMAM dendrimer as a supramolecular receptor, the material's size is satisfactory, taking the synthetic approach into account.

**3.2. Investigation of PMVEAMA−PAMAM Adsorptive Properties.** The synthesized dual−polymeric material containing poly(amidoamine) dendrimer as terminal molecular receptor has been investigated for its binding ability toward various analytes. The chosen analytes were organic dyes (Congo Red, Sunset Yellow FCF, and riboflavin), as well as bioactive compounds (folic, salicylic, and nicotinic acids and riboflavin), which aimed to confirm an application versatility of the obtained material. Their structures are presented in Table S1. Moreover, riboflavin has been treated both as a biomolecule and as an organic dye; therefore, it was used for all of the experiments. Theoretically, the polymer's binding effectiveness is mostly afforded by the formation of strong electrostatic interactions between multiple basic amine groups of the dendrimer and acidic groups of analytes. Moreover, material−analyte interactions might be also enhanced by other factors, such as hydrogen bonding formation or physical entrapment of small molecules inside dendritic cavities, which should lead in overall to efficient binding of either acidic organic or bioorganic molecules on the external surface of the dendrimer−functionalized polymer chain.

*3.2.1. Adsorption Isotherms.* In order to define the material's effectiveness for attaching the bioactive acids and the organic dyes, isothermal studies have been performed, which give information about equilibrium state, in response. Although, there are several models, which mathematically describe adsorption isotherms, the Langmuir and the Freundlich isotherms are the most extensively used, since they deliver key parameters for assessment of the adsorbent binding potential (Table S2). These parameters, such as adsorption constants and maximal adsorption capacities can be calculated basing on the slope and the intercept of linear plots of $c_{eq}/q_{eq}$ vs $c_{eq}$ and log $q_{eq}$ vs log $c_{eq}$, corresponding to the Langmuir (eq S1) and the Freundlich models (eq S2), respectively. The main theoretical difference between the two presented models is based on the interactions between adsorbent's surface and adsorbate; i.e., the Langmuir model assumes the formation of adsorbate's monolayer on the adsorbent surface as a consequence of equal binding energy of each binding sites of the material. It also postulates that adsorbate−adsorbate interactions are negligible; therefore, it is usually found as the contaminants adsorption model. On the other hand, the Freundlich theory assumes the formation of adsorbate multilayer triggered by intermolecular interactions between adsorbed molecules, such as electrostatic interactions, hydrogen bonding, dipole−dipole interactions, or


https://dx.doi.org/10.1021/acsapm.0c01254
ACS Appl. Polym. Mater. 2021, 3, 956−967

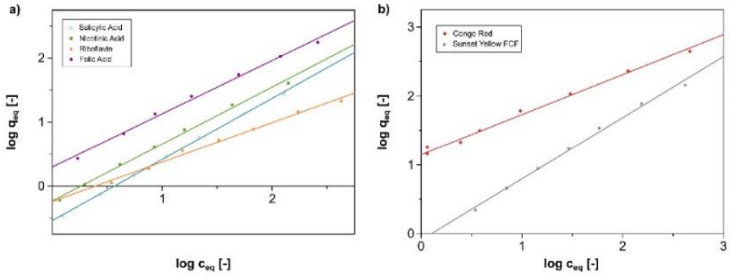


**Figure 4.** Linear fitting of the experimental data obtained during isothermal experiments of the biocompounds (a) and the synthetic organic dyes (b) adsorption on PMVEAMA−PAMAM to the Freundlich isotherm model.

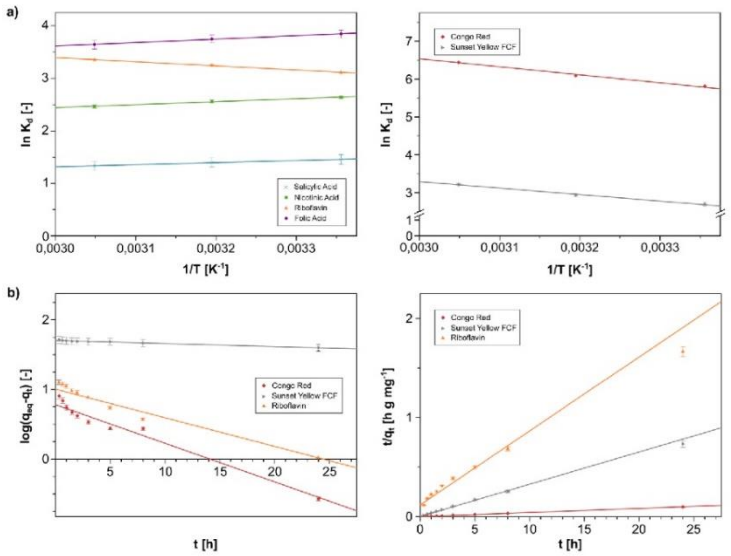


**Figure 5.** (a) Linear plots of van't Hoff equation presenting the adsorption of the biomolecules (left) and the synthetic organic dyes (right) at different temperatures. (b) Experimental data of the organic dyes adsorption kinetic studies fitted to the pseudo−first−order model (left) and the pseudo−second−order model (right).

$\pi-\pi$ stacking.[33] Table 1 presents collected adsorption parameters for the drugs and the anionic organic dyes adsorption on the obtained polymeric material. The best fitting of the isothermal models' linear plots to experimental data was achieved for the Freundlich model (Figure 4), which is confirmed by higher values of $R^2$ and lower values of $\chi^2$ parameters than the calculated for the Langmuir model. In the case of the studies including adsorption of bioactive molecules, the main reason is connected with their structural features, especially a presence of phenyl rings interacting with each other through their $\pi$−electrons, as well as particular domains, which might form hydrogen bonding between analyte molecules (carboxylic groups, amine groups, nitrogen atoms, hydroxyl groups, etc.). Nevertheless, correlation coefficients calculated for the Langmuir model (Figure S2) are also high enough, allowing for the investigation of a key parameter characterizing the adsorptive ability of the material toward a given analyte, which is maximal adsorption capacity $q_m$ (Table 1). The highest values of 305 and 134 mg $g^{-1}$ were obtained for folic and salicylic acid, respectively, as a result of analytes' structural complexity and the highest affinity to surface dendritic structure afforded by a presence of carboxylic and hydroxyl groups. Nicotinic acid and riboflavin were found to be adsorbed on the material's surface at a lower extent, reaching adsorption capacities of 92 and 26 mg $g^{-1}$, which is strictly related to the analytes structures: nicotinic acid, containing only one carboxylic group able to interact with the dendritic structure of the polymer, and riboflavin, consisting of isoalloxazine and ribitol domains unable to form strong


https://dx.doi.org/10.1021/acsapm.0c01254
ACS Appl. Polym. Mater. 2021, 3, 956−967

**Table 2. Thermodynamic Parameters of the Biomolecules and the Organic Dyes Adsorption on the Dual−Polymeric Material PMVEAMA−PAMAM**

| | Adsorbate | $\Delta H°$ [kJ mol$^{-1}$] | $\Delta S°$ [J mol$^{-1}$K$^{-1}$] | $R^2$ | $\Delta G°$ [kJ mol$^{-1}$] | | |
|---|---|---|---|---|---|---|---|
| | adsorbate | | | | 298 K | 313 K | 328 K |
| biomolecules | folic acid | −5.5 ± 0.4 | 13.6 ± 1.4 | 0.9881 | −9.53 | −9.76 | −9.93 |
| | salicylic acid | −3.3 ± 0.2 | 0.9 ± 0.2 | 0.9906 | −3.61 | −3.63 | −3.64 |
| | nicotinic acid | −4.7 ± 1.0 | 6.3 ± 1.4 | 0.9830 | −6.54 | −6.67 | −6.72 |
| | riboflavin | 19.6 ± 1.8 | 90.4 ± 5.8 | 0.9936 | −7.36 | −8.57 | −10.08 |
| Dyes | Congo Red | 17.6 ± 0.1 | 107.2 ± 3.3 | 0.9845 | −14.40 | −15.85 | −17.57 |
| | Sunset Yellow FCF | 14.3 ± 1.4 | 70.2 ± 4.4 | 0.9924 | −6.68 | −7.65 | −8.76 |

electrostatic interactions with basic PAMAM dendrimer. Nevertheless, the polymer exhibits adsorptive activity towards given analytes, which can be also related to the physical entrapment of the molecules inside internal cavities between dendrimers' amidoamine branches. The isothermal experiments performed using chosen organic dyes showed a very high adsorption capacity of 368 and 311 mg g$^{-1}$ for Congo Red and Sunset Yellow FCF, respectively. These azo dyes contain two sulfonate groups forming highly strong electrostatic interactions with terminal amine groups of PAMAM−domain of the polymeric adsorbent, but also contain multiple phenyl rings, which lead to intermolecular interaction between analytes' molecules through the stacking of $\pi$−electrons, increasing adsorption capacity values. Moreover, for two of the most extensively adsorbed analytes − folic acid and Congo Red − adsorption experiments in different environments were performed (Figure S3). An influence of the aqueous solution environment on their adsorption was investigated for folic acid and Congo Red incubated in buffer systems at pH 8, 9, 10, and 11. The choice of these conditions was driven by the very poor solubility of folic acid in acidic and neutral conditions, and the formation of a red or blue precipitate of Congo Red in a neutral or acidic environment, respectively. Nevertheless, the experiments revealed a decrease of the sorption capacity of the material toward analytes with solution's basicity increase, which is mainly due to an excess of $OH^-$ anions hindering attractive interactions between PAMAM residue and the analytes molecules.

The calculated values of adsorption capacity $q_m$ of the synthetic dyes used on PMVEAMA−PAMAM were also compared with some recent results obtained for different types of adsorbents. According to Table S3, Congo Red adsorption on the synthesized material was more intensive, comparing to functionalized or cross−linked biopolymer (chitosan), bio-sourced material, or $ZnO_2$ nanoparticles. Also, the rate of Sunset Yellow FCF adsorption is much greater than for the materials collected in Table S3, such as silica-based adsorbents, MOF hybrid material, and double hydroxide. The high adsorptive potential of the synthesized material toward the synthetic dyes might be explained by the appearance of multiple amine binding domains in PAMAM dendrimer structure.

*3.2.2. Thermodynamics of Adsorption Processes.* Adsorption experiments conducted in different temperatures bring several parameters, such as standard adsorption enthalpy ($\Delta H°$), entropy ($\Delta S°$), and Gibbs free energy ($\Delta G°$), which are useful for an assessment of the adsorbent−adsorbate interactions thermal behavior. The thermodynamic studies involved PMVEAMA-PAMAM contact with each of the analytes at three different temperatures −298, 313, and 328 K − to reach full saturation of the adsorbent. The values of $\Delta H°$ and $\Delta S°$ were directly calculated using slope and intercept of the linear plot $\ln K_d$ vs $1/T$ (eq S4), where $K_d$ is the distribution coefficient described as a ratio of the amount of the analyte adsorbed to its amount left in solution, presented as eq S3. The plots presenting the van't Hoff equation for all the adsorption−adsorbate systems are presented in Figure 5a. Moreover, the values of Gibbs free energies calculated for all the experiments at different temperatures were calculated using the expression of $\Delta G°$ definition (eq S5). The calculated parameters are collected in Table 2.

The calculated Gibbs free energy values clearly indicate that the adsorption of both the organic dyes and the biomolecules is a spontaneous process ($\Delta G° < 0$) determined by either enthalpy or entropy factor. For all three dyes chosen (riboflavin, Congo Red, and Sunset Yellow FCF) entropy values are high, varying between 70.19 and 107.22 J mol$^{-1}$ K$^{-1}$; therefore, the adsorption of the dyes on PMVEAMA−PAMAM is driven by the randomness increase at the solid−liquid interface, which is connected with the noncovalent nature of material−dye interactions (dipole−dipole interactions and/or hydrogen bonding). Also, positive values of enthalpy indicate the endothermic character, which is connected with an energy donation increasing attraction between analyte and adsorbent particles. The temperature increase led to the more intensive adsorption process, which is related to the significant decrease in Gibb's free energy values for the organic dyes.[34] On the other hand, the temperature changes had a very slight influence on the biomolecules' adsorption on PMVEAMA−PAMAM. The interactions between the material and bioactive acids (folic, salicylic, and nicotinic acid) are based on a proton exchange between the carboxylic group of the analytes and amine groups of the material. As the attachment of the biomolecules on the material is a spontaneous process, the enthalpy factor related to the formation of bonding between them by a proton exchange has a dominant impact on the spontaneity of these processes, leading to a slightly exothermic effect of the biomolecules adsorption on PMVEAMA−PAMAM. Nevertheless, the decrease in $\Delta G°$ values with temperature increase is relatively low.

*3.2.3. Kinetics of Dyes Adsorption.* Kinetics of pollutants adsorption from aqueous media, such as organic dyes, can be described by two most broadly used kinetic models, which are pseudo−first−order kinetics proposed by Lagergen and pseudo−second−order kinetics presented by Ho et al.[35] Equations of their linear plots are presented as eq S6 and eq S8, respectively. The experimental data were fitted to both pseudo−first−order and pseudo−second−order (Figure 5b) kinetic models, resulting in a better correlation with the pseudo−second−order model, for which calculated correlation coefficients $R^2$ were higher and $\chi^2$ coefficients were lower (Table S4). This may be attributed to the use of analytes at low concentration (0.5 mM), which has been proved to affect the better correlation with pseudo−second−order kinetics.[36] From



https://dx.doi.org/10.1021/acsapm.0c01254
ACS Appl. Polym. Mater. 2021, 3, 956−967

the slope and intercept of linear plots $t/q_t$ vs $t$ presented in Figure 5b, several parameters describing the rate of the adsorption of the dyes on PMVEAMA−PAMAM have been calculated, which are collected in Table S4. The adsorption of the synthetic dyes (Congo Red and Sunset Yellow FCF) has been described with the pseudo-second-order rate constants $k_2$ of 0.418 and 0.067 mg $g^{-1}$ $h^{-1}$, respectively, as well as with very low half a dsorption times $t_{1/2}$ (eq S9) of 0.02 h for Congo Red and 0.19 h for Sunset Yellow FCF, indicating fast and intensive dyes adsorption. Such a phenomenon is directly related to bicarboxylate domains contained in their structures, which afford strong electrostatic interactions with basic amine groups of PAMAM dendrimer. For riboflavin, half of the maximal adsorbate amount was calculated to bind after 1.83 h, which also proves the efficiency of the adsorbent analytical applications. Moreover, the pseudo−second−order kinetics initial adsorption rates $k_i$ ranging between 0.790 and 31.165 mg $g^{-1}$ $h^{-1}$ were established using eq S10, which shows an influence of analyte's structure on its binding affinity to the polymeric material.

**3.3. Reusability of the Polymeric Adsorbent towards Organic Dyes.** The obtained dual−polymeric material, which has been designed as an adsorbent dedicated to various analytes, should exhibit reusability in order to fulfill its applicability. Since the main interactions stabilizing the material−dye complexes are the electrostatic ones, a diluted water solution of HCl at a concentration of 0.01 M was used as a desorbing agent. Such desorption/adsorption cycles were performed 4 times in order to investigate the material's binding properties, which results are presented in Figure 6. The first adsorption experiments showed

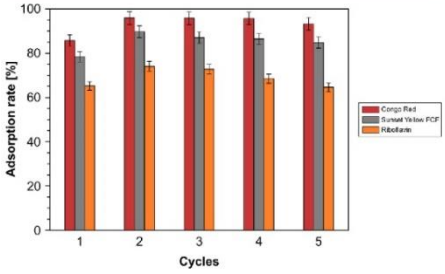


**Figure 6.** Percentage of the dyes adsorbed on PMVEAMA−PAMAM during adsorption/desorption cycles using 0.01 M HCl as the desorbing agent.

that Congo Red, Sunset Yellow FCF, and riboflavin were adsorbed at 85.72, 78.38, and 65.23%, respectively. However, after the first desorption step, the adsorption rate for each dye rose approximately by 10%, which is connected with (a) protonation of terminal amine groups of the pending PAMAM−domains of material, which leads to more intensive binding of anionic dyes, and (b) hydrolysis of unmodified anhydride rings under acidic conditions, leading to the appearance of new carboxylic domains as both hydrogen bonding donors and acceptors. During the further three desorption steps, the adsorption rate of Congo Red slightly decreased by 2.64%, Sunset Yellow FCF by 4.91%, and riboflavin by 9.49%, indicating effectiveness and reusability of the PMVEAMA−PAMAM as the adsorptive material.

**3.4. *In Vitro* Drugs Release Using PMVEAMA−PAMAM as Drug Transporting System.** The synthesized dual polymeric material was also tested for its application as a platform for effective drug transport. The drug−loaded material samples were incubated in three different media at pH 2.4 (HCl/KCl buffer), pH 5.4 (AcOH/AcONa buffer), and pH 7.4 (PBS) for 48 h at 37 °C, mimicking various physiological conditions of drug release. The release profiles of drugs used − folic acid, salicylic acid, nicotinic acid, and riboflavin − are presented in Figure 7. The main interactions stabilizing the material−drug complexes are electrostatic interactions, afforded by the proton transfer from the carboxylic domain of biomolecule to free amine groups of the material's dendritic domain. Therefore, the medium pH has a significant impact on the progress of the releases. The highest amounts of the drugs released were obtained in the most acidic environment (pH 2.4), which is attributed to the highest excess of $H^+$, causing the highest disruption of electrostatic interactions PAMAM−drug. After 48 h of incubation, the amounts of the drugs released reached 43.19% for folic acid, 94.90% for salicylic acid, 75.74% for nicotinic acid, and 72.02% for riboflavin. The greater the basic release environment, the less the drug desorbed. Desorbing abilities are also dependent on the structure of the biomolecules used. Folic acid as a bicarboxylic acid containing multiple phenyl rings binds to the materials surface the most strongly among the chosen drugs; thus, its desorption is mostly hindered. Nevertheless, almost half of the folic acid adsorbed to the material has been released. On the other hand, salicylic or nicotinic acid may desorb more easily and in a higher extent, taking their compactness and single binding domains into account.

Moreover, fitting of the release profiles at pH 2.4 (the most effective drug release) to chosen kinetic models has been performed. There are several known release models, however, the most broadly used are the zero−order model, the first−order model, the Higuchi model, the Hixson−Crowell model, and the Korsmeyer−Peppas model, which linear equations are presented in Table S6 (eqs S11−S15). The correlation coefficients $R^2$ of the experimental data to the first−order, the Higuchi and the Korsmeyer−Peppas release kinetic models are collected in Table 3, indicating the best correlation with the Korsmeyer−-Peppas model. According to its theoretical background, the release of the drugs (folic, salicylic and nicotinic acid, and riboflavin) is controlled by a mechanism of Fickian diffusion, which might be assigned to all $n$ values lower than 0.45.[37] Otherwise, the drugs' release would have been dependent on a non−Fickian (anomalous) diffusion mechanism strictly connected with the shape or the structural changes of the polymeric material. The lowest correlation of the data gained during release experiments was achieved for the zero−order and the Hixson−Crowell kinetic models (Table S7).

## 4. CONCLUSIONS

The dual−polymeric material comprising PMVEAMA as a support and PAMAM dendrimer as a supramolecular receptor was successfully synthesized and characterized with various analytical techniques. Despite the cross−linking phenomenon triggered by polyamine character of the functionalizing agent, the material exhibited satisfactory efficiency in binding the chosen biocompounds and the synthetic organic dyes. Although the adsorption processes follow the Freundlich isothermal model, maximal adsorption capacity values were calculated, which reached even 367.65 mg $g^{-1}$ for Congo Red or 304.88 mg $g^{-1}$ for folic acid. PMVEAMA−PAMAM was described as a


https://dx.doi.org/10.1021/acsapm.0c01254
ACS Appl. Polym. Mater. 2021, 3, 956−967

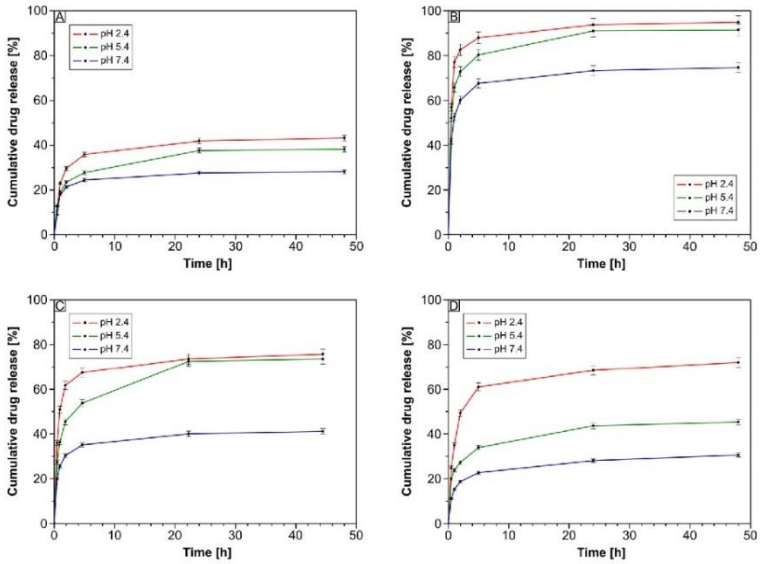


**Figure 7.** Drug release profiles of folic acid (A), salicylic acid (B), nicotinic acid (C), and riboflavin (D) performed in three different aqueous media: pH 2.4 (red), pH 5.4 (green), and pH 7.4 PBS (blue).

**Table 3. Kinetic release parameters calculated for the drugs desorption from PMVEAMA−PAMAM**

| | first-order model | | Higuchi model | | Korsemeyer−Peppas model | | |
|---|---|---|---|---|---|---|---|
| biomolecule | $k_1$ [% $h^{-1}$] | $R^2$ | $k_H$ [% $h^{-1/2}$] | $R^2$ | $n$ | $k_{K-P}$ [% $h^{-1}$] | $R^2$ |
| folic acid | 0.003 ± 0.001 | 0.6208 | 4.0 ± 1.2 | 0.7266 | 0.23 | 20.8 ± 2.5 | 0.8050 |
| salicylic acid | 0.015 ± 0.005 | 0.7186 | 4.3 ± 1.8 | 0.5861 | 0.09 | 71.1 ± 4.2 | 0.7334 |
| nicotinic acid | 0.007 ± 0.003 | 0.6226 | 4.9 ± 1.8 | 0.6538 | 0.14 | 48.3 ± 3.8 | 0.7866 |
| riboflavin | 0.006 ± 0.002 | 0.5962 | 6.0 ± 2.0 | 0.6903 | 0.23 | 31.9 ± 3.7 | 0.8222 |

reusable adsorbent towards organic dyes, which was proved by 2.64−9.49% decrease of sorption efficiency after 5 cycles of adsorption/desorption. Moreover, material−biocompound complexes were subjected to *in vitro* drug release, revealing satisfactory release profiles. The studies have shown material effectiveness, which may lead to its further implementation for wastewater contaminants removal and investigation of the biocompatibility and drug transporting delivery potential studied in *in vivo* mode.

## ■ ASSOCIATED CONTENT

### Supporting Information

The Supporting Information is available free of charge at https://pubs.acs.org/doi/10.1021/acsapm.0c01254.

Presentation of the structure of the analytes, the ESI−MS and $^{13}$C−NMR spectra of the synthesized PAMAM dendrimer, mathematical expressions of the models used during the analysis of the adsorption and *in vitro* release processes, the comparison of the obtained adsorption capacities toward synthetic organic dyes and other sorbent described in literature, and additional plots and parameters obtained for the performed adsorption and release experiments. (PDF)

## ■ AUTHOR INFORMATION


### Corresponding Author

**Mateusz Pawlaczyk** − *Faculty of Chemistry, Adam Mickiewicz University in Poznań, Poznań, Greater Poland Voivodeship 61-614, Poland;* orcid.org/0000-0002-2340-1363; Phone: +48 61 829 17 97; Email: mateusz.pawlaczyk@amu.edu.pl

### Author

**Grzegorz Schroeder** − *Faculty of Chemistry, Adam Mickiewicz University in Poznań, Poznań, Greater Poland Voivodeship 61-614, Poland;* orcid.org/0000-0002-6626-9542

Complete contact information is available at: https://pubs.acs.org/10.1021/acsapm.0c01254


### Notes

The authors declare no competing financial interest.

## ■ ACKNOWLEDGMENTS

The work was supported by Grant No. POWR.03.02.00−00−I026/16 cofinanced by the European Union through the European Social Fund under the Operational Program Knowledge Education Development.

## ■ REFERENCES

(1) Stewart, S. A.; Coulson, M. B.; Zhou, C.; Burke, N. A. D.; Stover, H. D. H. Synthetic hydrogels formed by thiol-ene crosslinking of vinyl sulfone-functional poly(methyl vinyl ether-alt-maleic acid) with α,ω-dithio-polyethyleneglycol. *Soft Matter* **2018**, *14*, 8317−8324.

(2) Larrañeta, E.; Dominguez-Robles, J.; Coogan, M.; Heaney, E.; Stewart, S. A.; Singh Thakur, R. R.; Donnelly, R. F. Poly(methyl vinyl ether-co-maleic acid) Hydrogels Containing Cyclodextrins and Tween 85 for Potential Application as Hydrophobic Drug Delivery Systems. *Macromol. Res.* **2019**, *27*, 396−403.

(3) Irache, J. M.; Huici, M.; Konecny, M.; Espuelas, S.; Campanero, M. A.; Arbos, P. Bioadhesive Properties of Gantrez Nanoparticles. *Molecules* **2005**, *10*, 126−145.

(4) Salman, H. H.; Gamazo, C.; de Smidt, P. C.; Russell-Jones, G.; Irache, J. M. Evaluation of Bioadhesive Capacity and Immunoadjuvant Properties of Vitamin B12-Gantrez Nanoparticles. *Pharm. Res.* **2008**, *25*, 2859−2868.

(5) Nunez, J. L.; Ballesteros, M. P.; Lastres, J. L.; Castro, R. M. Interaction of poly methyl vinyl ether/maleic anhydride-dimiristoyl phosphatidylcholine: a model bioadhesion study. *Biomaterials* **2000**, *21*, 2131−2135.

(6) Yoncheva, K.; Lizarraga, E.; Irache, J. M. Pegylated nanoparticles based on poly(methyl vinyl ether-co-maleic anhydride): preparation and evaluation of their bioadhesive properties. *Eur. J. Pharm. Sci.* **2005**, *24*, 411−419.

(7) Cerchiara, T.; Luppi, B.; Chidichimo, G.; Bigucci, F.; Zecchi, V. Chitosan and poly(methyl vinyl ether-co-maleic anhydride) microparticles as nasal sustained delivery systems. *Eur. J. Pharm. Biopharm.* **2005**, *61*, 195−200.

(8) Aguilar-Rosas, I.; Alcala-Alcala, S.; Llera-Rojas, V.; Ganem-Rondero, A. Preparation and characterization of mucoadhesive nanoparticles of poly (methyl vinyl ether-co-maleic anhydride) containing glycyrrhizic acid intended for vaginal administration. *Drug Dev. Ind. Pharm.* **2015**, *41*, 1632−1639.

(9) Luppi, B.; Cerchiara, T.; Bigucci, F.; Di Pietra, A. M.; Orienti, I.; Zecchi, V. Crosslinked Poly(Methyl Vinyl Ether-Co-Maleic Anhydride) as Topical Vehicles for Hydrophilic and Lipophilic Drugs. *Drug Delivery* **2003**, *10*, 239−244.

(10) Luzardo-Álvarez, A.; Blanco-Méndez, J.; Varela-Patiño, P.; Martín Biedma, B. Amoxicillin-Loaded Sponges Made of Collagen and Poly[(methyl vinyl ether)-*co*-(maleic anhydride)] for Root Canal Treatment: Preparation, Characterization and *In Vitro* Cell Compatibility. *J. Biomater. Sci., Polym. Ed.* **2011**, *22*, 329−342.

(11) Wong, T. W.; Wahab, S.; Anthony, Y. Drug release responses of zinc ion crosslinked poly(methyl vinyl ether-*co*-maleic acid) matrix towards microwave. *Int. J. Pharm.* **2008**, *357*, 154−163.

(12) Arbos, P.; Wirth, M.; Arangoa, M. A.; Gabor, F.; Irache, J. M. Gantrez®AN as a new polymer for the preparation of ligand-nanoparticle conjugates. *J. Controlled Release* **2002**, *83*, 321−330.

(13) Muehlmann, L. A.; Ma, B. C.; Figueiró Longo, J. P.; Almeida Santos, M.; Azevedo, R. B. Aluminum-phthalocyanine chloride associated to poly(methyl vinyl ether-co-maleic anhydride) nanoparticles as a new third-generation photosensitizer for anticancer photodynamic therapy. *Int. J. Nanomed.* **2014**, *9*, 1199−1213.

(14) Suchocki, P.; Jakoniuk, D.; Fitak, B. A. Specific spectrophotometric method with trifluoroacetic acid for the determination of selenium (IV) in selenitetriglycerides. *J. Pharm. Biomed. Anal.* **2003**, *32*, 1029−1036.

(15) Ganassin, R.; de Souza, L. R.; Py-Daniel, K. R.; Longo, J. P.; Coelho, J. M.; Rodrigues, M. C.; Jiang, C. S.; Gu, J.; de Morais, P. C.; Mosiniewicz-Szablewska, E.; Suchocki, P.; Báo, S. N.; Azevedo, R.; Muehlmann, L. A. Decoration of a Poly(methyl vinyl ether-co-maleic anhydride)-Shelled Selol Nanocapsule with Folic Acid Increases Its Activity Against Different Cancer Cell Lines In Vitro. *J. Nanosci. Nanotechnol.* **2018**, *18*, 522−528.

(16) Raj Singh, T. R.; McCarron, P. A.; Woolfson, A. D.; Donnelly, R. F. Investigation of swelling and network parameters of poly(ethylene glycol)-crosslinked poly(methyl vinyl ether-co-maleic acid) hydrogels. *Eur. Polym. J.* **2009**, *45*, 1239−1249.

(17) Raj Singh, T. R.; Woolfson, A. D.; Donnelly, R. F. Investigation of solute permeation across hydrogels composed of poly(methyl vinyl ether-*co*-maleic acid) and poly(ethylene glycol). *J. Pharm. Pharmacol.* **2010**, *62*, 829−837.

(18) Zhang, T.; Chen, J.; Zhang, Q.; Dou, J.; Gu, N. Poly(ethylene glycol)-cross linked poly(methyl vinyl ether-co-maleic acid) hydrogels for three-dimensional human ovarian cancer cell culture. *Colloids Surf., A* **2013**, *422*, 81−89.

(19) Demir, Y. K.; Metin, A.Ü.; Satiroglu, B.; Solmaz, M. E.; Kayser, V.; Mader, K. Poly (methyl vinyl ether-co-maleic acid) - Pectin based hydrogel forming systems: Gel, film, and microneedles. *Eur. J. Pharm. Biopharm.* **2017**, *117*, 182−194.

(20) Goetz, L.; Foston, M.; Mathew, A. P.; Oksman, K.; Ragauskas, A. J. Poly(methyl vinyl ether-*co*-maleic acid)-Polyethylene Glycol Nanocomposites Cross-Linked In Situ with Cellulose Nanowhiskers. *Biomacromolecules* **2010**, *11*, 2660−2666.

(21) Moreno, E.; Schwartz, J.; Larraneta, E.; Nguewa, P. A.; Sanmartin, C.; Agüeros, M.; Irache, J. M.; Espuelas, S. Thermosensitive hydrogels of poly(methyl vinyl ether-co-maleic anhydride) - Pluronic® F127 copolymers for controlled protein release. *Int. J. Pharm.* **2014**, *459*, 1−9.

(22) Caló, E.; de Barros, J. M. S.; Fernández-Gutiérrez, M.; San Román, J.; Ballamy, L.; Khutoryanskiy, V. V. Antimicrobial hydrogels based on autoclaved poly(vinyl alcohol) and poly(methyl vinyl ether-*alt*-maleic anhydride) mixtures for wound care applications. *RSC Adv.* **2016**, *6*, 55211−55219.

(23) Stewart, S. A.; Backholm, M.; Burke, N. A. D.; Stöver, H. D. H. Crosslinked Hydrogels formed through Diels-Alder coupling of Furan and Maleimide-modified Poly(methyl vinyl ether-alt-maleic acid). *Langmuir* **2016**, *32*, 1863−1870.

(24) Ma, X.; Zhou, N.; Zhang, T.; Guo, Z.; Hu, W.; Zhu, C.; Ma, D.; Gu, N. In situ formation of multiple stimuli-responsive poly[(methyl vinyl ether)-alt-(maleic acid)]-based supramolecular hydrogels by inclusion complexation between cyclodextrin and azobenzene. *RSC Adv.* **2016**, *6*, 13129−13136.

(25) Sakudo, A.; Baba, K.; Tsukamoto, M.; Sugimoto, A.; Okada, T.; Kobayashi, T.; Kawashita, N.; Takagi, T.; Ikuta, K. Anionic polymer, poly(methyl vinyl ether-maleic anhydride)-coated beads-based capture of human influenza A and B virus. *Bioorg. Med. Chem.* **2009**, *17*, 752−757.

(26) Najafi, M.; Chery, J.; Frey, M. M. Functionalized Electrospun Poly(Vinyl Alcohol) Nanofibrous Membranes with Poly(Methyl Vinyl Ether-Alt-Maleic Anhydride) for Protein Adsorption. *Materials* **2018**, *11*, 1002−1013.

(27) Ladaviere, C.; Lorenzo, C.; Elaissari, A.; Mandrand, B.; Delair, T. Electrostatically Driven Immobilization of Peptides onto (Maleic Anhydride-alt-methyl Vinyl Ether) Copolymers in Aqueous Media. *Bioconjugate Chem.* **2000**, *11*, 146−152.

(28) Kenawy, E. R.; Sakran, M. A. Controlled Release of Polymer Conjugated Agrochemicals. System Based on Poly(Methyl Vinyl Ether-alt-Maleic Anhydride). *J. Appl. Polym. Sci.* **2001**, *80*, 415−421.

(29) Cegłowski, M.; Gierczyk, B.; Schroeder, G. Poly(methyl vinyl ether-alt-maleic anhydride) Functionalized with 3-Aminophenylboronic Acid: A New Boronic Acid Polymer for Sensing Diols in Neutral Water. *J. Appl. Polym. Sci.* **2014**, *131*, 40778−40784.

(30) Semblante, G. U.; You, S. J.; Wu, G. H.; Chang, T. C.; Yen, F. C. Pore size and flux behavior of polyvinylidene fluoride and polymethyl vinyl ether-alt-maleic anhydride with TiO2. *Chem. Eng. J.* **2014**, *241*, 513−520.

(31) Kaczorowska, M. A.; Cooper, H. J. Electron Capture Dissociation, Electron Detachment Dissociation, and Collision-Induced Dissociation of Polyamidoamine (PAMAM) Dendrimer

Ions with Amino, Amidoethanol, and Sodium Carboxylate Surface Groups. *J. Am. Soc. Mass Spectrom.* **2008**, *19*, 1312−1319.
(32) Socrates, G. Infrared and Raman Characteristic Group Frequencies. *Tables and Charts 2001*, 3rd ed.; John Wiley and Sons, Ltd., England, 2001.
(33) Chen, S.; Qin, C.; Wang, T.; Chen, F.; Li, X.; Hou, H.; Zhou, M. Study on the adsorption of dyestuffs with different properties bysludge-rice husk biochar: Adsorption capacity, isotherm, kinetic, thermodynamics and mechanism. *J. Mol. Liq.* **2019**, *285*, 62−74.
(34) Siddiqui, S. I.; Rathi, G.; Chaudhry, S. A. Acid washed black cumin seed powder preparation for adsorption of methylene blue dye from aqueous solution: Thermodynamic, kinetic and isotherm studies. *J. Mol. Liq.* **2018**, *264*, 275−284.
(35) Dissanayake, D.M.R.E.A.; Wijesinghe, W.M.K.E.H.; Iqbal, S. S.; Priyantha, N.; Iqbal, M. C. M. Isotherm and kinetic study on Ni(II) and Pb(II) biosorption by the fern Asplenium nidus L. *Ecol. Eng.* **2016**, *88*, 237−241.
(36) Azizian, S. Kinetic models of sorption: a theoretical analysis. *J. Colloid Interface Sci.* **2004**, *276*, 47−52.
(37) Gouda, R.; Baishya, H.; Qing, Z. Application of Mathematical Models in Drug Release Kinetics of Carbidopa and Levodopa ER Tablets. *J. Dev. Drugs* **2017**, *06*, 171−178.



https://dx.doi.org/10.1021/acsapm.0c01254
*ACS Appl. Polym. Mater.* 2021, 3, 956−967

# Supporting Information

**Dual-polymeric resin based on poly(methyl vinyl ether-alt-maleic anhydride) and PAMAM dendrimer as a versatile supramolecular adsorbent**

Mateusz Pawlaczyk*, Grzegorz Schroeder

Faculty of Chemistry, Adam Mickiewicz University in Poznań, Poznań, Greater Poland Voivodeship, 61-614, Poland

* Corresponding author: Mateusz Pawlaczyk, mateusz.pawlaczyk@amu.edu.pl, tel: +48 61 829 17 97

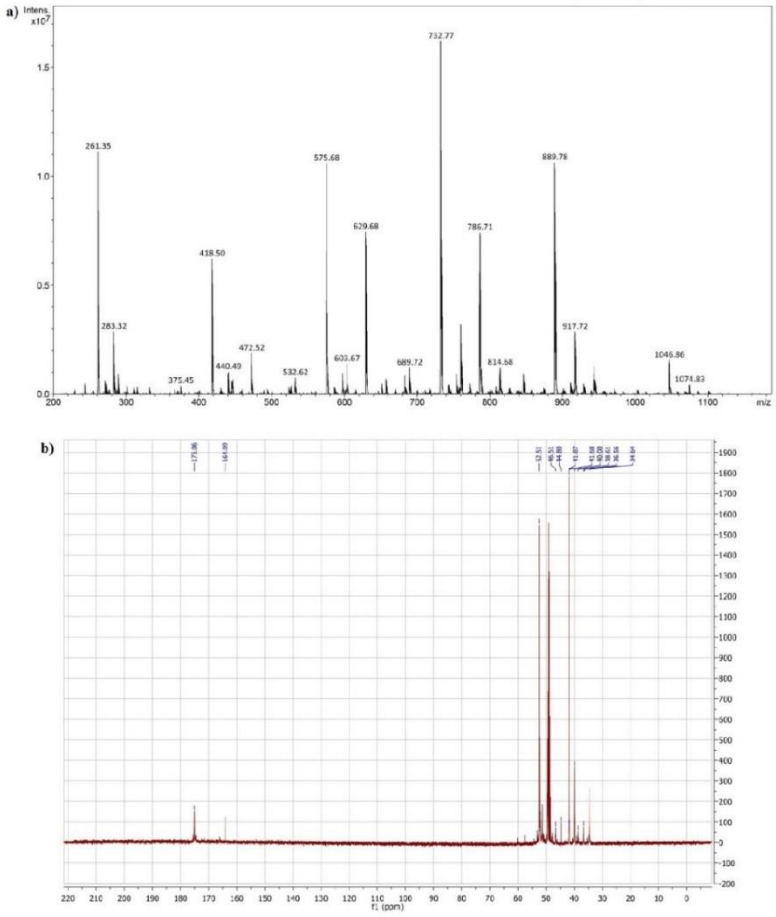


**Figure S1.** a) the ESI-MS spectrum of the synthesized PAMAM dendrimer, performed in positive mode; b) $^{13}$C-NMR analysis of the synthesized PAMAM dendrimer

**Table S1.** Structures of the analytes used in adsorption experiments

**Biomolecules**

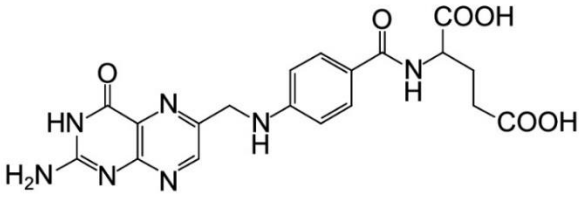

Folic Acid

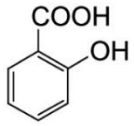

Salicylic Acid

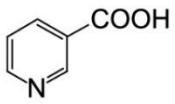

Nicotinic Acid

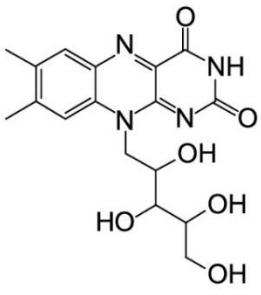

Riboflavin

**Organic dyes**

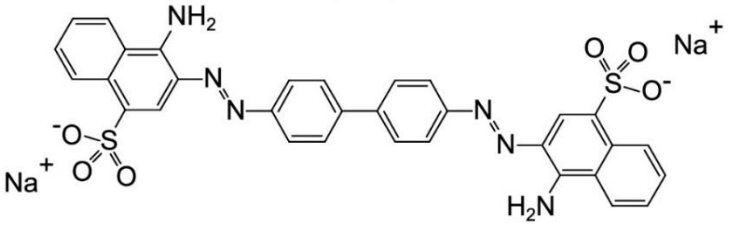

Congo Red

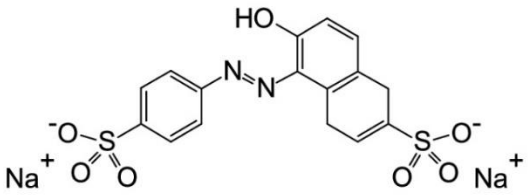

Sunset Yellow FCF

S-2

**Table S2**. Expressions representing the isothermal, kinetic and thermodynamic models used during analysis of the obtained experimental data of adsorption studies, with indication of the related parameters

| Theoretical model | | Representation of linear plot | Obtainable parameters |
|---|---|---|---|
| the Langmuir isotherm | (S1) | $\frac{c_{eq}}{q_{eq}} = \frac{c_{eq}}{q_m} + \frac{1}{K_L q_m}$ | $K_L$ – the Langmuir constant [L mg$^{-1}$]<br>$q_m$ – maximal adsorption capacity [mg g$^{-1}$] |
| the Freundlich isotherm | (S2) | $\log q_{eq} = \frac{1}{n}\log c_{eq} + \log K_F$ | $K_F$- the Freundlich constant [mg g$^{-1}$ (L mg$^{-1}$)$^{1/n}$]<br>$1/n$ – heterogeneity constant [–] |
| van't Hoff equation (thermodynamics) | (S3) | $K_d = \frac{c_A}{c_{eq}}$ | $K_d$ – distribution coefficient<br>$c_A$ – the amount of the analyte adsorbed on the solid |
| | (S4) | $\ln K_d = -\frac{\Delta H° 1}{R\ T} + \frac{\Delta S°}{R}$ | $\Delta H°$ - the standard enthalpy [J mol$^{-1}$]<br>$\Delta S°$ - the standard entropy [J mol$^{-1}$ K$^{-1}$] |
| | (S5) | $\Delta G° = -RT\ln K_d$ | $\Delta G°$ - the Gibbs free energy [J mol$^{-1}$] |
| Pseudo-1$^{st}$-order kinetics | (S6) | $\log(q_{eq} - q_t) = -\frac{k_1}{2.303}t + \log q_{eq}$ | $k_1$ – the first-order kinetics rate [h$^{-1}$] |
| | (S7) | $k_i = k_1 q_e$ | $k_i$ – the initial adsorption rate [mg g$^{-1}$ h$^{-1}$] |
| Pseudo-2$^{nd}$-order kinetics | (S8) | $\frac{t}{q_t} = \frac{1}{q_{eq}}t + \frac{1}{k_2 {q_{eq}}^2}$ | $k_2$ – the second-order kinetics [g mg$^{-1}$ h$^{-1}$] |
| | (S9) | $t_{\frac{1}{2}} = \frac{1}{k_2 q_e}$ | $t_{1/2}$ – the pseudo-second-order half-adsorption time [h] |
| | (S10) | $k_i = k_2 {q_e}^2$ | $k_i$ – the initial adsorption rate [mg g$^{-1}$ h$^{-1}$] |

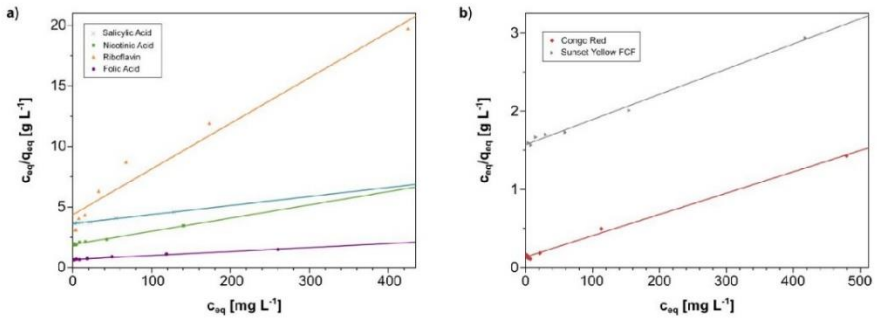


**Figure S2**. Representation of the experimental data fitting to the Langmuir isothermal model for biocompounds (**a**) and synthetic dyes (**b**)

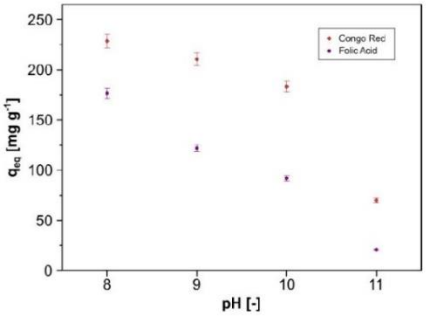


**Figure S3**. Dependence of the sorption capacity towards Congo Red and folic acid on the solution pH

**Table S3**. Comparison of maximal adsorption capacities towards Congo Red and Sunset Yellow FCF organic dyes with results found in literature

| Material | Maximal adsorption capacity $q_m$ [mg g$^{-1}$] | | Reference |
|---|---|---|---|
| | Congo Red | Sunset Yellow FCF | |
| PVA/melamine-formaldhyde composite | 221.4 | | 1 |
| sulphate-crosslinked chitosan | 91.8 | | 2 |
| $ZnO_2$ nanoparticles | 208.0 | | 3 |
| Banana Peel Powder | 164.6 | | 4 |
| glutaraldehyde-grafted chitosan modified with $NiFe_2O_4$ | 270.0 | | 5 |
| PMVEAMA-PAMAM | 367.6 | | This study |
| layered double hydroxide of $Mg(OH)_2$ and $Al(OH)_3$ | | 142.9 | 6 |
| hybrid of Cr(III) terephthalate MOF and grapheme oxide | | 81.3 | 7 |
| silica modified with cetylpyridinium cations | | 2.0 | 8 |
| Diasorb-130-C16 (silica sorbent modified with hexadecyl groups) | | 33.9 | 9 |
| PMVEAMA-PAMAM | | 310.6 | This study |

**Table S4**. The kinetic parameters of the organic dyes adsorption on PMVEAMA-PAMAM material

| Dye | Pseudo-first-order kinetics | | | Pseudo-second-order kinetics | | | |
|---|---|---|---|---|---|---|---|
| | $k_1$ [h$^{-1}$] | $R^2$ | $\chi^2$ | $k_2$ [mg g$^{-1}$ h$^{-1}$] | $t_{1/2}$ [h] | $R^2$ | $\chi^2$ |
| Congo Red | 0.127 ± 0.003 | 0.9597 | 0.092 | 0.41 ± 0.10 | 0.02 ± 0.01 | 0.9999 | 0.001 |
| Sunset Yellow FCF | 0.010 ± 0.005 | 0.9714 | 0.029 | 0.07 ± 0.02 | 0.19 ± 0.04 | 0.9969 | 0.001 |
| Riboflavin | 0.094 ± 0.001 | 0.9599 | 2.988 | 0.04 ± 0.01 | 1.83 ± 0.07 | 0.9774 | 0.038 |

**Table S5**. Additional parameters connected with the analytes adsorptive behavior

| Adsorbate | Freundlich isotherm | Pseudo-first-order kinetics | Pseudo-second-order kinetics |
|---|---|---|---|
| | $K_F$ [mg $g^{-1}$ (L $mg^{-1})^{1/n}$] | $k_i$ [mg $g^{-1}$ $h^{-1}$] | $k_i$ [mg $g^{-1}$ $h^{-1}$] |
| Congo Red | 1.98 ± 0.19 | 31.165 ± 0.812 | 24999.9 ± 7328.7 |
| Sunset Yellow FCF | 0.29 ± 0.01 | 0.790 ± 0.434 | 404.9 ± 118.7 |
| Riboflavin | 0.57 ± 0.03 | 1.459 ± 0.039 | 8.4 ± 0.5 |

**Table S6.** Representation of the release kinetic models used for fitting the experimental data

| **Theoretical model** | | **Representation of linear plot** | **Obtainable parameters** |
|---|---|---|---|
| the zero-order model | (S11) | $F_t = F_0 + k_0 t$ | $k_0$ – the zero-order release constant [mg $h^{-1}$]<br>$k_1$ – the first-order release constant [% $h^{-1}$]<br>$k_H$ – the Higchi release constant [% $h^{-1/2}$]<br>$k_{H\text{-}C}$ – the Hixson-Crowell release constant [$mg^{1/3}$ $h^{-1}$]<br>$n$ – the Korsmeyer-Peppas exponent of release [-]<br>$k_{K\text{-}P}$ – the Korsmeyer-Peppas release constant [% $h^{-1}$] |
| the first-order model | (S12) | $\log(100 - Q_t) = -k_1 t$ | |
| the Higuchi model | (S13) | $Q_t = k_H \sqrt{t}$ | |
| the Hixson-Crowell model | (S14) | $\sqrt[3]{F_0} - \sqrt[3]{F_t} = k_{H-C} t$ | |
| the Korsmeyer-Peppas model | (S15) | $\log Q_t = n \log t + \log k_{K-P}$ | |

**Table S7.** Kinetic release parameters of the zero-order and the Hixson-Crowell models calculated for the drugs desorption from PMVEAMA-PAMAM

| Biomolecule | Zero-order model | | Hixson-Crowell model | |
|---|---|---|---|---|
| | $k_1 \cdot 10^2$ [mg $h^{-1}$] | $R^2$ | $k_{H\text{-}C} \cdot 10^2$ [$mg^{1/3}$ $h^{-1}$] | $R^2$ |
| Folic Acid | 0.158 ± 0.068 | 0.5712 | 0.241 ± 0.125 | 0.4837 |
| Salicylic Acid | 0.032 ± 0.018 | 0.4437 | 0.076 ± 0.046 | 0.4039 |
| Nicotinic Acid | 0.061 ± 0.030 | 0.5038 | 0.127 ± 0.070 | 0.4494 |
| Riboflavin | 0.038 ± 0.018 | 0.5251 | 0.149 ± 0.080 | 0.4658 |

**References**

[1] Bhat, S.A.; Zafar, F.; Mondal, A.H.; Mirza, A.U.; Haq, Q.M.R.; Nishat, N. Efficient removal of Congo red dye from aqueous solution by adsorbent films of polyvinyl alcohol/melamine-formaldehyde composite and bactericidal effects, J. Cleaner Prod. 2020, 255, 120062.
[2] Jeyaseelan, C.; Chaudhary, N.; Jugade, E. Sulphate-Crosslinked Chitosan as an Adsorbent for the Removal of Congo Red Dye from Aqueous Solution, Air, Soil Water Res. 2018, 11, 1-8.
[3] Chawla, S.; Uppal, H.; Yadav, M.; Bahadur, N.; Singh, N. Zinc peroxide nanomaterial as an adsorbent for removal of Congo red dye from waste water, Ecotox. Environ. Safety 2017, 135, 68-74.
[4] Munagapati, V.S.; Yarramuthi, V.; Kim, Y.; Lee, K.M.; Kim, D.S. Removal of anionic dyes (Reactive Black 5 and Congo Red) from aqueous solutions using Banana Peel Powder as an adsorbent, Ecotox. Environ. Safety 2018, 148, 601-607.
[5] Moghaddam, A.Z.; Ghiamati, E.; Pourashuri, A.; Allahresani, A. Modified nickel ferrite nanocomposite/functionalized chitosan as a novel adsorbent for the removal of acidic dyes, Int. J. Biol. Macromol. 2018, 120, 1714-1725.
[6] Malek, A.H.A.; Yasin, Y. Use of Layered Double Hydroxides to Remove Sunset Yellow FCF Dye from Aqueous Solution, Chem. Sci. Trans. 2012, 1, 194-200.
[7] Li, L.; Shi, Z.; Zhu, H.; Hong, W.; Xie, F.; Sun, K. Adsorption of azo dyes from aqueous solution by the hybrid MOFs/GO, Water Sci. Technol. 2016, 73, 1728-1737.
[8] Bevziuk, K.; Chebotarev, A.; Koicheva, A.; Snigur, D. Adsorption of anionic food azo dyes from aqueous solution by silica modified with cetylpyridinium chloride, Monatsh. Chem. 2018, 149, 2153–2160.
[9] Tikhomirova, T.I.; Ramazanova, G.R.; Apyari, V.V. A hybrid sorption – Spectrometric method for determination of synthetic anionic dyes in foodstuffs, Food Chem. 2017, 221, 351-355.

ACS OMEGA

http://pubs.acs.org/journal/acsodf

Article

# Deferoxamine-Modified Hybrid Materials for Direct Chelation of Fe(III) Ions from Aqueous Solutions and Indication of the Competitiveness of *In Vitro* Complexing toward a Biological System

Mateusz Pawlaczyk* and Grzegorz Schroeder

Cite This: *ACS Omega* 2021, 6, 15168−15181

Read Online

ACCESS | Metrics & More | Article Recommendations | Supporting Information

**ABSTRACT:** Deferoxamine (DFO) is one of the most potent iron ion complexing agent belonging to a class of trihydroxamic acids. The extremely high stability constant of the DFO−Fe complex (log $\beta$ = 30.6) prompts the use of deferoxamine as a targeted receptor for scavenging Fe(III) ions. The following study aimed at deferoxamine immobilization on three different supports: poly(methyl vinyl ether-*alt*-maleic anhydride), silica particles, and magnetite nanoparticles, leading to a class of hybrid materials exhibiting effectiveness in ferric ion adsorption. The formed deferoxamine-loaded hybrid materials were characterized with several analytical techniques. Their adsorptive properties toward Fe(III) ions in aqueous samples, including pH-dependence, isothermal, kinetic, and thermodynamic experiments, were investigated. The materials were described with high values of maximal adsorption capacity $q_m$, which varied between 87.41 and 140.65 mg $g^{-1}$, indicating the high adsorptive potential of the DFO-functionalized materials. The adsorption processes were also described as intense, endothermic, and spontaneous. Moreover, an exemplary magnetically active deferoxamine-modified material has been proven for competitive *in vitro* binding of ferric ions from the biological complex protoporphyrin IX−Fe(III), which may lead to a further examination of the materials' biological or medical applicability.

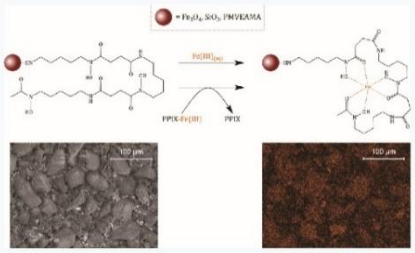

## 1. INTRODUCTION

Iron ions as microelements play a significant role in the stimulations of various functions in human organisms. Several health disorders may lead to an increased level of non-transferrin bound iron (NTBI), which might accumulate in healthy tissues, causing several dysfunctions, such as cardiac, hepatic, or pancreatic diseases. Burst release of iron also occurs during subarachnoid hemorrhage (a devastating subtype of stroke), which leads to hemoglobin breakdown, causing serious oxidative injuries and neuronal death. Moreover, iron excess promotes the formation of reactive oxygen species (ROS), which may oxidize various cell components such as lipid membranes, nucleic acids, or protein. Iron overload may also trigger a more rapid proliferation of iron-demanding cancer cells.[1−3]

Among many classes of domains responsible for effective chelation of metal ions, siderophores are the ones that bind iron selectively or exhibit extremely high binding constants. Deferoxamine (DFO) is a siderophore belonging to a class of trihydroxamic acids and is naturally secreted by bacterium species *Streptomyces pilosus*. Deferoxamine as a hexadentate molecule coordinates iron ions in a ratio of 1:1 with an extremely high stability constant $\beta$ at a level of $4.0 \times 10^{30}$. Its complexes with other metal ions are formed with much lower stability constants. This property has prompted deferoxamine-mediated ion overload treatment for many years of clinical therapy.[4−7] Moreover, free deferoxamine exhibits beneficial therapeutic effects, such as antifibrotic effects, protection against acetaminophen-induced liver injuries, or inhibition of neurodegenerative Alzheimer's and Huntington's diseases.[8−11]

Deferoxamine is being used in clinical treatment; however, its application is limited due to its poor *in vivo* absorption to the gut, rapid renal excretion causing short plasma half-time, and sunlight hypersensitivity, which leads to enhanced production of ROS.[1,12] Thus, several immobilization and functionalization approaches to incorporate different DFO formulations for analytical and biochemical applications have been investigated. Good pharmacokinetic parameters and improved bioapplicability were proven for deferoxamine conjugates with various adamantane derivatives,[13] reverse emulsion nanogels containing DFO and glycine,[14] a poly(D,L-

Received: March 16, 2021
Accepted: May 24, 2021
Published: June 3, 2021





https://doi.org/10.1021/acsomega.1c01411
*ACS Omega* 2021, 6, 15168−15181

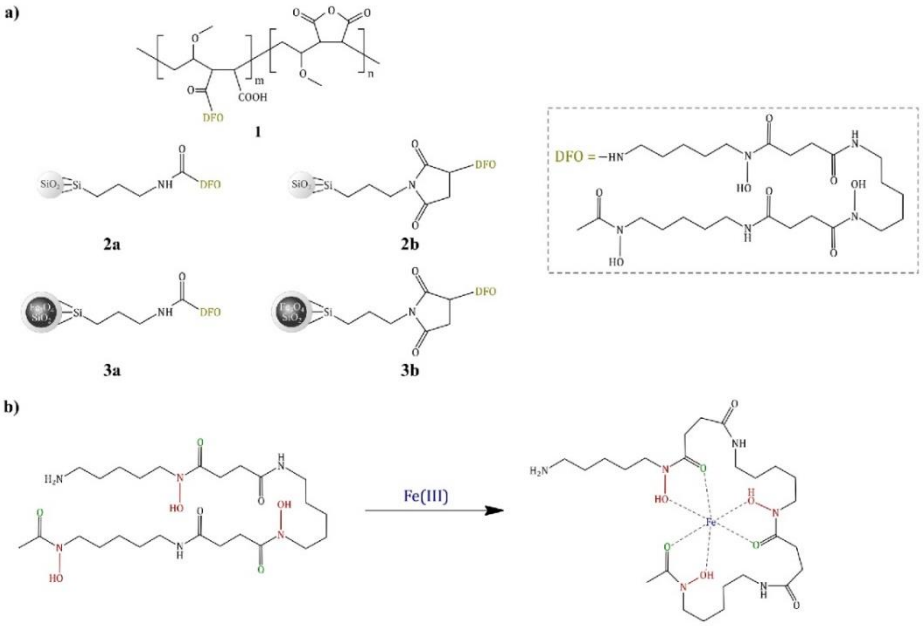


**Figure 1.** (a) Structures of the synthesized deferoxamine-functionalized hybrid materials; (b) formation of the Fe(III)−deferoxamine complex.

lactide) membrane modified with DFO,[15,16] or a synthesized c(RGDfK)−DFO−$^{89}$Zr system.[17,18]

DFO properties has also prompted a design of functional materials dedicated to adsorption or sensing of Fe(III) ions. The implemented DFO-functionalized materials were based on, e.g., mesoporous silica MCM-41,[19,20] Sepharose gel,[21] or filtration paper Whatman,[22] leading to biocompatible materials for direct Fe(III) sensing in aqueous or biological samples, using classic analytical techniques. Interestingly, a few reports aimed at application of a new approach for quantification of the amount of ferric ions chelated by DFO-functionalized materials, which involved a detection of Fe−O band signal intensities in FT-IR or surface-enhanced Raman scattering (SERS) spectra.[23−25]

The following research aimed to synthesize a series of deferoxamine-functionalized hybrid materials based on three different supports: poly(methyl vinyl ether-*alt*-maleic anhydride) (PMVEAMA), silica microparticles, and magnetite nanoparticles, which were implemented as ferric ion scavengers. The characterized materials were subjected to studies of their adsorptive properties toward Fe(III) ions, including a sequence of pH-dependence, isothermal, kinetic, and thermodynamic studies. The comprehensive studies led to several parameters describing the materials' applicability for the metal binding, such as the most effective adsorption environment, materials' adsorption capacities, rates of the adsorbate binding, or thermal coefficients. Moreover, the exemplary magnetite-based material was considered for competitive chelation of ferric ions from a biological complex of protoporphyrin IX (PPIX) and Fe(III) ions, which corresponds to a naturally occurring complex − hemin. The description of an adsorptive potential of the materials and characterization of their *in vitro* application toward competitive chelation of ferric ions may lead to a new class of eco-friendly and biocompatible adsorbents finding application in biomedical science.

## 2. RESULTS AND DISCUSSION

The designed deferoxamine-functionalized hybrid materials were synthesized, characterized with several analytical techniques, and subsequently subjected to adsorption of Fe(III) ions from aqueous solutions to establish an influence of the support used on the adsorptive properties of the materials. Predominantly, the matrices' size and functionalization potential would have had the most impact on the materials' adsorption efficiency, which has been investigated in the following article.

**2.1. Synthesis of Deferoxamine-Functionalized Hybrid Materials.** The designed adsorbents consisted of three different supports, which were biocompatible polymeric chains of poly(methyl vinyl ether-*alt*-maleic anhydride) (PMVEAMA), commercially available amorphous silica microparticles functionalized with surface isocyanate and maleimide groups, and synthesized $Fe_3O_4$ nanoparticles encapsulated within the silica matrix, which underwent functionalization with deferoxamine via isocyanate− and maleimide−silyl linkers. The functionalization strategy was based on a reaction between a terminal free amine group of deferoxamine with reactive


https://doi.org/10.1021/acsomega.1c01411
ACS Omega 2021, 6, 15168−15181

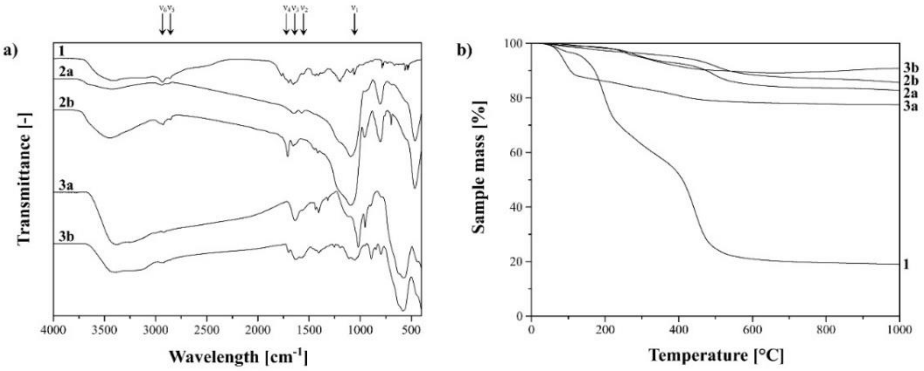


**Figure 2.** (a) FT-IR spectra of the adsorptive materials with indicated specific bands: $\nu_1$ = 1051 $cm^{-1}$; $\nu_2$ = 1570 $cm^{-1}$; $\nu_3$ = 1640 $cm^{-1}$; $\nu_4$ = 1705 $cm^{-1}$; $\nu_5$ = 2855 $cm^{-1}$; $\nu_6$ = 2930 $cm^{-1}$; (b) the thermogravimetric curves obtained during thermal analysis of the materials.

pendant groups on the supports' surface. Functionalization of PMVEAMA was afforded by maleic anhydride ring opening at elevated temperature under nucleophilic attack of the deferoxamine amine group. For both silica and $Fe_3O_4$, the attachment of deferoxamine was performed either by amine group addition to a highly electrophilic carbon atom of pendant isocyanate or by Michael addition of the amine group to carbon−carbon double bond of the maleimide ring. Accordingly, five hybrid materials were obtained, which structures are collected in Figure 1, and the synthetic routes are presented in Figure S1.

The $Fe_3O_4$ nanoparticles were obtained by coprecipitation from an aqueous solution containing Fe(III):Fe(II) salts in a ratio of 2:1 under alkaline conditions (pH ∼10).[26] The synthesized magnetite nanoparticles were subsequently covered with a $SiO_2$ layer, which was achieved by condensation of tetraethyl orthosilicate (TEOS) under alkaline conditions in a water/ethanol mixture. The obtained $Fe_3O_4/SiO_2$ particles were then treated as a starting material for obtaining the $Fe_3O_4$-based hybrid materials. An introduction of the deferoxamine domain onto $Fe_3O_4/SiO_2$ platform was achieved through two different linkers: isocyanate− and maleimide−silyl linkers. The isocyanate linker was reacted with a solution of deferoxamine in DMF under a $N_2$ atmosphere, and the resulting silyl derivative of deferoxamine was incorporated into the silica matrix of $Fe_3O_4/SiO_2$ material (material **3a**). The pre-synthesized maleimide linker (3-maleimide-propyltriethoxysilane) was anchored to a magnetite-based support, prior to reaction with deferoxamine, obtaining material **3b**. In the case of PMVEAMA−deferoxamine (material **1**) preparation, a suspension of PMVEAMA in toluene was added to a solution of deferoxamine in DMF at temperature of ∼110 °C, which led to a full opening of maleic rings in the polymer chain. Moreover, silica-based materials were synthesized by adding isocyanate- or maleimide-functionalized silica particles to deferoxamine solution in DMF at room temperature, yielding materials **2a** and **2b**, respectively.

**2.2. Characterization of the Deferoxamine-Modified Adsorbents.** Each synthesized adsorbent was characterized with FT-IR spectroscopy, which spectra are collected in Figure 2a. The successful incorporation of deferoxamine into the supports' surface is unambiguously proven by a band at 1051 $cm^{-1}$ ($\nu_1$), which is related to N−OH stretching, specific for DFO structure.[27] Such a signal is visible only in the spectrum of **1**, which is due to its overlapping by a broad band originating from Si−O−Si stretching of the silica matrix in each of the other materials. Nevertheless, signals at approximately 1570 and 1640 $cm^{-1}$ ($\nu_2$ and $\nu_3$, $N-H_{(amide)}$ and $C=O_{(amide)}$, respectively) undoubtedly prove the formation and incorporation of amide bonds, and thus the presence of deferoxamine domains. Moreover, two bands at around 2855 and 2930 $cm^{-1}$ ($\nu_5$ and $\nu_6$, respectively) are related to C−H stretching of methylene groups present in the deferoxamine structure. A signal at approximately 1705 $cm^{-1}$ ($\nu_4$) on the spectra of **1**, **2b**, and **3b** may be attributed to the remaining unmodified domains, such as C=O stretching of maleic anhydride of PMVEAMA or C=C stretching of the maleimide ring in materials **2b** and **3b**. Each of the materials was also characterized using thermogravimetric measurements (Figure 2b). The very first step at a temperature range between 70 and 130 °C is strictly connected with the evaporation of solvent residues. For all the curves, the main decomposition step starts at approximately 150 °C, which corresponds to the melting point of deferoxamine. The TG curves of the materials based on either $Fe_3O_4$ or $Fe_3O_4/SiO_2$ platforms exhibit this oxidation step with ∼7.5% loss of mass, corresponding to ∼0.135 mmol $g^{-1}$ loading of deferoxamine. However, the spectrum of material **1** presents much more intensified sample decomposition by ∼25%, indicating the higher deferoxamine loading to PMVEAMA chains. Further decomposition steps present in the spectrum are connected with the oxidation of organic residues remaining unmodified by deferoxamine. Also, elemental analysis in CHN mode was performed for the synthesized hybrid materials, which results are collected in Table 1. The most informative values are nitrogen percentages in the samples, since nitrogen atoms appear only in deferoxamine domains and the maleimide linker, in which grafting is known, and therefore eliminates any calculation disturbances. Using the obtained %N values, the loading of the Fe-chelator on the supports was determined, which is in good agreement with the results obtained during thermal analysis.

The results of XRD analysis of magnetite nanoparticle-based materials **3a** and **3b** are shown in Figure S2. The deferox-



https://doi.org/10.1021/acsomega.1c01411
ACS Omega 2021, 6, 15168−15181

**Table 1. Values of Nitrogen, Carbon, and Hydrogen Percentages in the Adsorbents Obtained in Elemental Analysis with an Indication of the Calculated Deferoxamine-Loading Values**

| | | elemental analysis | | | |
|---|---|---|---|---|---|
| | adsorbent | % N | % C | % H | loading [mmol $g^{-1}$] |
| **1** | PMVEAMA–DFO | 7.04 | 51.96 | 8.51 | 1:3[a] |
| **2a** | $SiO_2$–NCO–DFO | 2.01 | 7.84 | 1.97 | 0.226 |
| **2b** | $SiO_2$–maleimide–DFO | 1.31 | 8.29 | 1.72 | 0.134 |
| **3a** | $Fe_3O_4/SiO_2$–NCO–DFO | 1.34 | 4.27 | 1.38 | 0.137 |
| **3b** | $Fe_3O_4/SiO_2$–maleimide–DFO | 1.31 | 3.58 | 0.97 | 0.134 |

[a]For the polymer (PMVEAMA) functionalization, a ratio of modified to unmodified maleic anhydride domains was only calculated.

amine-modified materials' spectra show no significant changes with respect to the spectrum of pristine $Fe_3O_4$ nanoparticles. This is related to incorporating a thin layer of silica–deferoxamine on their surface, which does not influence the spectrum shape. However, the hybrid materials' spectra exhibit a broad peak of low intensity at around 21.1° related to the silica shell (even if shifted in relation to the theoretical pattern). Nevertheless, a signal at around 35.5° appears to be narrower in the **3a** and **3b** spectra than for bare $Fe_3O_4$, implying the material size increase. Signals at approximately 30.2° are slightly wider for the spectra of the functionalized hybrid materials, which is caused by the overlapping of $Fe_3O_4$ and $SiO_2$ reflexes, both appearing at around 30.2°. Moreover, the hybrid materials' spectra show a tiny reflex at around 36.4°, indicating the new organo-derivative XRD signal. On the basis of the positions of signals and their full width at half-maximum (FWHM) values, the mean size of the characterized materials $D_{hkl}$ was calculated using the Scherrer equation, which mathematical expression is given below, where $k$ is the Scherrer constant [−], $\lambda$ is the wavelength of X-ray irradiation [nm], $B$ is the FWHM value [rad], and $2\theta$ is the signal position [°]:

$$D_{hkl} = \frac{k \cdot \lambda}{B \cdot \cos 2\theta}$$

Accordingly, the calculated mean size of pristine $Fe_3O_4$ nanoparticles was 15.39 nm, while the mean sizes of materials **3a** and **3b** were 18.31 and 18.92 nm, respectively, which indicates a proper silyl–deferoxamine grafting, leading to the particles' size increase.

All the obtained deferoxamine-loaded hybrid materials were also subjected to visualization using the SEM technique (Figure 3A–E). For the polymer-based and $SiO_2$-based materials, the size of the particles is approximately 50 $\mu$m, which is connected with the polymeric character of the material's **1** support, as well as with the size of bare silica particles used for the preparation of materials **2a** and **2b**, which was between 40 and 63 $\mu$m. Therefore, the size of the silica particles after functionalization with DFO residues might have insignificantly increased. The obtained materials, which are not based on the magnetite core, were also characterized with EDX–SEM after their treatment with Fe(III) ions. The Fe-mapping is presented in Figure 3F–H, which undoubtedly

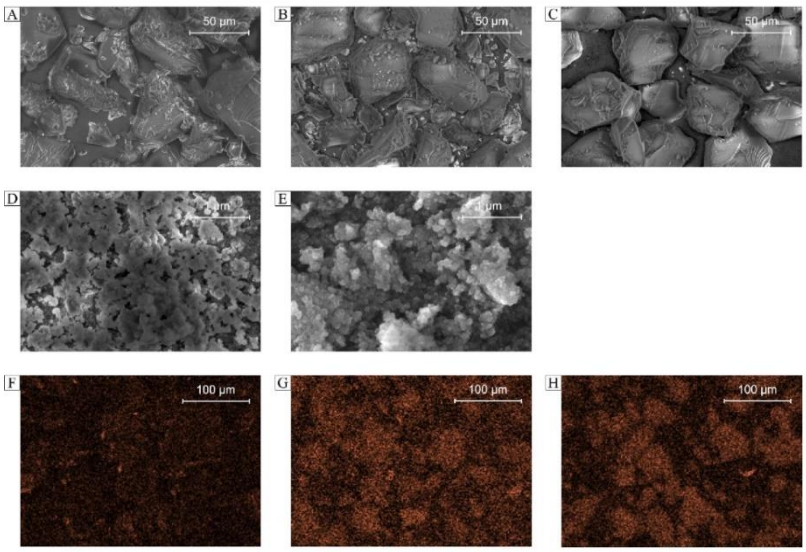


**Figure 3.** SEM images (A–C) and EDX–SEM mapping of Fe(III) ions (F–H) adsorbed to the hybrid materials: (A, F) PMVEAMA–DFO; (B, G) $SiO_2$–NCO–DFO; (C, H) $SiO_2$–maleimide–DFO). SEM images of magnetite-based hybrid materials: (D) $Fe_3O_4/SiO_2$–NCO–DFO; (E) $Fe_3O_4/SiO_2$–maleimide–DFO). Fe is visualized in orange.



https://doi.org/10.1021/acsomega.1c01411
ACS Omega 2021, 6, 15168−15181

indicates the complexation of ferric ions in a higher extent by silica-based materials than the polymeric material. Such a phenomenon may be connected with a fixed porosity of silica particles, enhancing the ions' adsorption efficiency. Moreover, Figure 3D,E presents the images of $Fe_3O_4$-based hybrid materials, which show the nanometric size of round-shaped particles of the deferoxamine-modified materials. The synthesized $Fe_3O_4$ nanoparticles of 15.39 nm as a magnetically active support did not significantly increase after encapsulation within the silica matrix and DFO conjugation, which is an important issue for nanomaterials applied as adsorbents.

The chelation of Fe(III) ions by deferoxamine domains may also influence the surface and the size of the pores of the materials. Thus, the most widely used techniques, which allow for assessment of structural features of solids – the BET (Brunauer, Emmett, and Teller) isotherm and the BJH (Barrett, Joyner, and Halenda) method – were implemented for material **3a**, as an example of the synthesized hybrid material. The used methods may highlight the differences between the porous features of the deferoxamine-loaded material before and after Fe adsorption. The molecular receptor chelates the cations by wrapping around them; therefore, it may influence the materials' pore sizes and surface area. The porous properties of both material **3a** and Fe-loaded material **3a** were determined using $N_2$ adsorption–desorption analysis, which is presented in Figure S3. The shapes of the isotherms for both bare and iron-loaded material **3a** can be classified as type IV, which postulates capillary condensation of the adsorbed gas in small pores at pressures below the saturation pressure of the gas. Therefore, based on the isotherms' shapes, the material meets the criteria of mesoporosity.[28] The material's mesoporosity was also proven by BJH calculation during adsorption and desorption of nitrogen, which responded in the pore sizes of **3a** and **3a–Fe(III)** of 11.370 and 11.407 nm, respectively, calculated based on the adsorption curves, and 13.186 and 13.174 nm, respectively, for the desorption curves. Moreover, the volume of pores was established with mean values of 0.234 $cm^3\ g^{-1}$ for material **3a** and 0.239 $cm^3\ g^{-1}$ for Fe-loaded material **3a**. The surface areas of both materials were established using the BJH method, which gave 68.3 $m^2\ g^{-1}$ for material **3a** and 66.7 $m^2\ g^{-1}$ for material **3a** with chelated Fe(III) ions. All the parameters calculated for the two types of materials are very similar, with no drastic differences, which indicates that the formed deferoxamine–Fe(III) complex on the material's surface has no significant impact on the porosity. Moreover, the second synthesized magnetite-based material (material **3b**) was characterized for its porous features using the same analytical methods. The material was described with its pore sizes of 11.402 and 13.079 nm calculated from the adsorption and desorption curves, respectively. Also, the surface area was calculated to be 68.3 $m^2\ g^{-1}$ and the mean pore volume was calculated to be 0.279 $cm^3\ g^{-1}$, which jointly indicate the similarity of both obtained materials containing the $Fe_3O_4$ core. Additionally, the pore size distributions established for the pristine magnetic materials and the one complexed with Fe(III) ions are presented in Figure S4. The distribution profiles obtained for materials **3a** and **3b** are almost overlapped, while the pore size distribution of the material **3a–Fe(III)** complex exhibits only insignificant change, which is consistent with the presented BET analysis.

All the materials were tested for their stability in para-physiological conditions of phosphate-buffered saline (PBS). After the incubation, the solutes were analyzed using ESI–MS in order to investigate whether deferoxamine dissociates from the materials under the conditions mimicking the biological environment. The spectra of the solutes showed no signals referring to the dissociated deferoxamine residue ($m/z$ 561.5), but only the signals corresponding to the components of the buffer used; therefore, the materials' stability can be concluded.

**2.3. Investigation of the Adsorptive Properties of the Fe-Chelating Materials.** The synthesized materials were designed as chelating systems dedicated to Fe(III) ions since surface-introduced deferoxamine exhibits high binding efficiency. The formation of the deferoxamine–Fe complex was proven by ESI–MS measurements, which spectra are presented in Figure S5. An aqueous solution of free deferoxamine mesylate gives a single monoprotonated signal at 561.5 $m/z$, which is a molecular peak of deferoxamine. The spectra of its complexes with either Fe(III) or Fe(II) ions are presented in Figure S5b,c, respectively. Two signals corresponding to mono- and diprotonated complexes are visible at 614.4 and 307.7 $m/z$, respectively. Moreover, the signal present at 561.5 $m/z$ related to free deferoxamine can be a result of electrospray ionization mode, which leads to easier fragmentation. Interestingly, the signal at 561.5 $m/z$ is significantly lower for Fe(III)-complex than for Fe(II)-complex, which highlights the higher affinity of ferric ions toward the formation of DFO–iron complexes. The choice of different supports for anchoring deferoxamine (polymeric chain, amorphous silica, and SPIONs) can also lead to conclusions on their influence on the final adsorptive properties. To fully characterize the materials' sorptive nature, several experiments were carried out, including isothermal, kinetic, and thermodynamic studies.

*2.3.1. Influence of pH on Fe(III) Adsorption.* Figure 4 shows the dependence between Fe(III) ions adsorption efficiency on the hybrid materials and the solution pH. The materials were subjected to adsorption of ferric ions in the pH ranging between 1 and 5, according to precipitation of $Fe(OH)_3$ in more basic conditions for 5 mM solution, as well as in 5 mM solution in distilled water, which was characterized to be of pH 2.45 (gray line in Figure 4). Below pH 6, the iron–

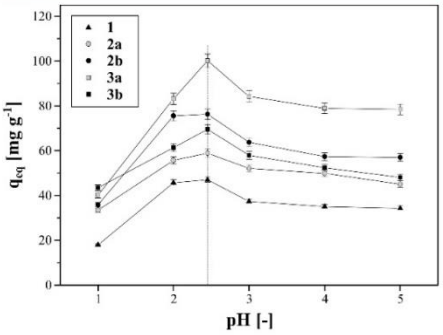


**Figure 4.** Influence of the solution pH on the amount of Fe(III) ions adsorbed on the deferoxamine-functionalized hybrid materials (gray dotted line corresponds to the pH of 5 mM aqueous solution of $Fe(ClO_4)_3$ – 2.45).



https://doi.org/10.1021/acsomega.1c01411
ACS Omega 2021, 6, 15168–15181

deferoxamine complexes can be classified as $[FeLH]^+$, where L is the ligand (deferoxamine), Fe is the ferric ion, and H is the proton.[29] Therefore, the adsorption may be limited only due to repulsive interactions between excessive $H^+$ and $Fe^{3+}$ ions visible at pH 1. At the most acidic environment studied, the adsorption rates reached 38−62% of the maximal adsorption capacity under the given conditions. The adsorption rates increased with increasing pH, reaching maxima at pH 2.45, which corresponds to Fe(III) solution in pure distilled water. Then, $q_{eq}$ values slightly decreased, primarily due to the use of sodium salts as buffers' ingredients, leading to the competitive binding of $Na^+$ ions. Nevertheless, the decrease is not drastic, ranging between 21.7 and 30.8%.

*2.3.2. Preparation of Adsorption Isotherms.* The experimental data obtained for adsorption isotherms were fitted to the Langmuir and the Freundlich models. The first model assumes a formation of the adsorbate monolayer on the adsorbent surface, which is due to the equal binding efficiency of all the binding sites and neglecting the interactions between adsorbed molecules, while the latter is mostly based on the assumption that adsorbate molecules may interact with each other via electrostatic, hydrogen, or $\pi-\pi$ interactions, forming the adsorbate multilayer.[30] Graphical representations of the Langmuir and the Freundlich isotherms are presented in Figure 5 and Figure S6, respectively, while the calculated parameters for both isothermal models are collected in Table 2.

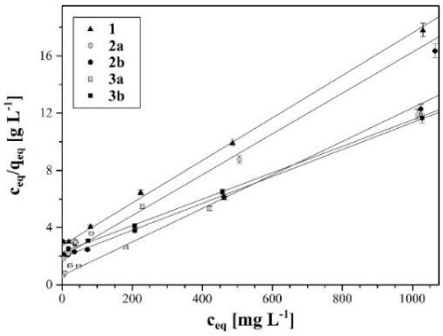


**Figure 5.** Fitting of the experimental data to the Langmuir isotherm model.

Undoubtedly, adsorption of Fe(III) ions on each hybrid material follows the Langmuir model, which is proven by the calculated $R^2$ value higher (≥0.997) and $\chi^2$ values lower (≤0.120) than those for the Freundlich model. This is consistent with the chemical nature of ferric ions, which hinders the intermolecular interactions, leading to the formation of the adsorbate monolayer. On the basis of the Langmuir fitting, the values of maximal adsorption capacity of the materials toward Fe(III) were established. The $q_{max}$ values varied between 87.41 and 140.65 mg g$^{-1}$, reaching the highest values for $SiO_2$ and $Fe_3O_4/SiO_2$ particles conjugated with deferoxamine through the maleimide linker. Such a phenomenon might be a result of additional iron ion trapping within a cyclic domain of maleimide. Nevertheless, satisfactory results were obtained for the other materials based on PMVEAMA and silica or SPIONs functionalized through the isocyanate linker. Although the experimental data are not described preferably with the Freundlich model, the values of $1/n$ constants connected with the intensity of the adsorption process and heterogeneity of the adsorbent's surface were calculated. The lower the $1/n$ value, the more intense the adsorption process. For all the materials, the values ranged between 0.56 and 0.79, indicating the efficiency of adsorption processes.

*2.3.3. Kinetic Studies of Fe(III) Adsorption.* The obtained experimental data for the kinetic studies of Fe(III) adsorption on the synthesized hybrid materials were fitted to pseudo−first−order and pseudo−second−order kinetics, intraparticle diffusion theory, and the Elovich model. The highest linear correlation of the experimental data was achieved for the pseudo−second−order kinetic model (Table 3), which plot is presented in Figure 6a. Comparing the calculated $R^2$ values for the pseudo−second−order kinetic model (Table 3) and the values calculated for the pseudo−first−order kinetic model presented in Figure S7a (Table S1), it is easily shown that the adsorption experiment follows the pseudo−second−order kinetic model. This result implies that the formation of various interactions between the adsorbent and analytes (including electron sharing, the formation of chemical bonds, or proton exchange) is the adsorption rate-limiting step.[31] Accordingly, the adsorption of Fe(III) ions on the hybrid materials is limited by their coordination by deferoxamine residues on the materials' surface. The modeling allowed for the calculation of the initial metal ion adsorption rate, which appeared to be the highest for magnetite-based particles and the lowest for silica-based particles. Thus, the time needed for half-adsorption should be opposite to $k_i$ values, which is proven by the lowest $t1/2$ values for materials **3a** and **3b**, while the highest for materials **2a** and **2b**. In order to verify the physical nature of the rate-limiting step, the intraparticle diffusion model was implemented to fit the experimental data, in which the plot $q_t$ vs ln $t$ may form a multilinear plot, as shown in Figure 6b. The theory introduced by Weber and Morris assumes the multilinearity of the plot when intraparticle diffusion is not the only step limiting the rate of adsorption.[32] The presented plots show two separate phases; thus, two factors limit the

**Table 2. Isothermal Parameters Calculated for Fe(III) Adsorption on the Hybrid Materials**

| | Langmuir isotherm | | | | Freundlich isotherm | | | |
|---|---|---|---|---|---|---|---|---|
| adsorbent | $q_{max}$ [mg g$^{-1}$] | $K_L$ [×10$^2$] [L mg$^{-1}$] | $R^2$ | $\chi^2$ | $1/n$ [−] | $K_F$ [mg g$^{-1}$ (L mg$^{-1}$)$^{1/n}$] | $R^2$ | $\chi^2$ |
| **1** | 87.41 ± 2.20 | 0.60 ± 0.03 | 0.9984 | 0.120 | 0.79 ± 0.01 | 0.64 ± 0.02 | 0.9709 | 0.328 |
| **2a** | 95.08 ± 2.87 | 0.84 ± 0.04 | 0.9980 | 0.063 | 0.61 ± 0.01 | 1.78 ± 0.07 | 0.9590 | 0.148 |
| **2b** | 137.93 ± 3.63 | 0.49 ± 0.02 | 0.9974 | 0.098 | 0.79 ± 0.01 | 0.99 ± 0.04 | 0.9713 | 0.651 |
| **3a** | 110.86 ± 1.94 | 2.92 ± 0.11 | 0.9985 | 0.077 | 0.56 ± 0.01 | 4.32 ± 0.18 | 0.9626 | 1.201 |
| **3b** | 140.65 ± 3.86 | 0.45 ± 0.02 | 0.9984 | 0.048 | 0.78 ± 0.01 | 0.93 ± 0.03 | 0.9864 | 0.311 |



https://doi.org/10.1021/acsomega.1c01411
ACS Omega 2021, 6, 15168−15181

Table 3. Kinetic Parameters Calculated for Pseudo−Second−Order and Intraparticle Diffusion Kinetic Models

| | pseudo-second-order | | | | intraparticle diffusion | | | |
|---|---|---|---|---|---|---|---|---|
| | | | | | $k_{id}$ [mg g$^{-1}$ h$^{-1/2}$] | | $R^2$ | |
| adsorbent | $k_2 \cdot 10^2$ [mg g$^{-1}$ h$^{-1}$] | $k_i$ [mg g$^{-1}$ h$^{-1}$] | $t_{1/2}$ [h] | $R^2$ | step 1 | step 2 | step 1 | step 2 |
| **1** | 0.48 ± 0.03 | 8.32 ± 1.26 | 4.98 ± 0.51 | 0.9969 | 12.5 ± 0.9 | 5.3 ± 0.6 | 0.9934 | 0.9941 |
| **2a** | 0.17 ± 0.01 | 6.12 ± 0.96 | 9.69 ± 0.93 | 0.9951 | 9.9 ± 0.4 | 8.9 ± 1.3 | 0.9965 | 0.9906 |
| **2b** | 0.14 ± 0.01 | 6.53 ± 1.07 | 10.30 ± 1.01 | 0.9983 | 11.6 ± 1.7 | 54.7 ± 9.1 | 0.9894 | 0.9251 |
| **3a** | 0.22 ± 0.01 | 17.58 ± 2.32 | 5.11 ± 0.43 | 0.9988 | 23.8 ± 0.3 | 58.5 ± 0.7 | 0.9950 | 0.9995 |
| **3b** | 0.20 ± 0.01 | 14.86 ± 2.04 | 5.77 ± 0.50 | 0.9980 | 23.3 ± 0.4 | 58.1 ± 0.8 | 0.9919 | 0.9977 |

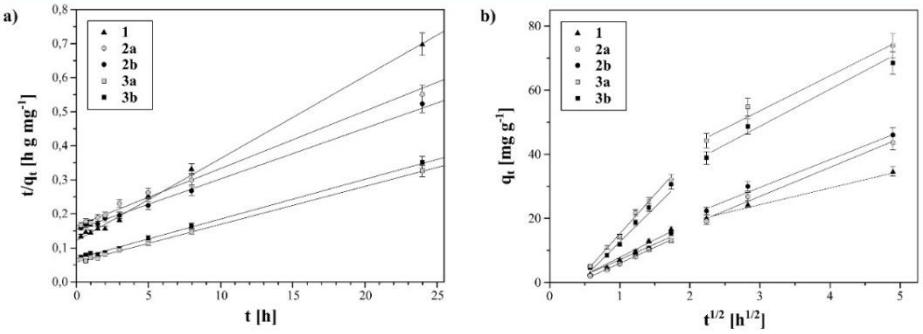


Figure 6. Experimental data fitting to kinetic models: (a) pseudo−second−order; (b) intraparticle diffusion.

adsorption rate within the adsorption progress. The first one is connected with an initial surface diffusion, while the second one is based on gradual adsorption limited by either intraparticle or pore diffusion. Moreover, the experimental kinetic data were fitted to the Elovich model (Figure S7b) in order to demonstrate whether adsorption of ferric ions on the hybrid materials may include the heterogeneous diffusion process as the rate-limiting step. However, due to the relatively low $R^2$ values calculated for this model (Table S1), such findings would be deniable.

*2.3.4. Thermodynamics of the Adsorption.* Thermodynamic studies involved measurements of the amounts of metal ions absorbed on the deferoxamine-functionalized particles in equilibrium states (after 24 h incubation) in three different temperatures: 298, 313, and 328 K. The obtained experimental data were fitted to the van't Hoff equation, which linear plots $\ln K_d$ vs $1/T$ are presented in Figure 7. Based on the calculated slopes and intercepts, three informative parameters were established, i.e., adsorption standard enthalpy ($\Delta H°$) and entropy ($\Delta S°$) and Gibbs free energy values ($\Delta G°$) for experiments conducted under the given thermal conditions. The parameters are collected in Table 4.

All the plots were characterized with high correlation coefficients $R^2$, which values were higher than 0.9870, and extremely low $\chi^2$ coefficients, indicating the good linearity of the plots. Adsorption of Fe(III) ions on the deferoxamine-loaded materials was found to be an endoenergetic process ($\Delta H°$ values are positive), which is more intense with the temperature increase − values of Gibbs free energies for higher temperature are more negative, and thus, the process is intensified. Interestingly, the established parameters are directly connected with the ones obtained during kinetic

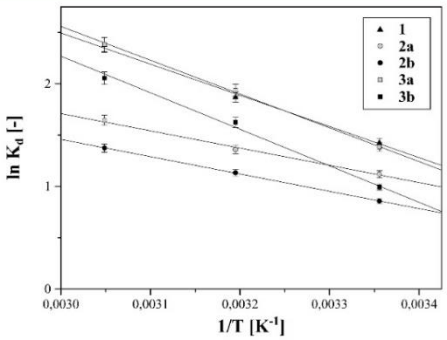


Figure 7. Plots of the van't Hoff equation fitted to the thermodynamic studies of ferric ion adsorption on the hybrid materials.

studies. The silica-based materials **2a** and **2b** can be described as the least influenced by the temperature increase and the ones that exhibit the lowest adsorption rate constants $k_2$ and $k_i$ and the highest values of time needed for adsorption of half-equilibrium adsorbate ($t_{1/2}$). Moreover, for all the materials, entropy values are relatively high, which suggest that an increased randomness mostly drives the metal ion adsorption at the solution−adsorbent interface related to solvation effects. Such conclusions are rather evident, considering that Fe(III) adsorption is based only on the formation of non-covalent coordination bonds between the receptor and analyte.



https://doi.org/10.1021/acsomega.1c01411
ACS Omega 2021, 6, 15168−15181

Table 4. Calculated Thermodynamic Parameters for Fe(III) Adsorption

| adsorbent | $\Delta H°$ [kJ mol$^{-1}$] | $\Delta S°$ [J mol$^{-1}$ K$^{-1}$] | $R^2$ | $\chi^2$·(×10$^2$) | $\Delta G°$ [kJ mol$^{-1}$] | | |
|---|---|---|---|---|---|---|---|
| | | | | | 298 K | 313 K | 328 K |
| **1** | 25.27 ± 2.14 | 96.59 ± 6.97 | 0.9904 | 0.118 | −3.53 | −4.86 | −6.48 |
| **2a** | 13.98 ± 1.57 | 56.14 ± 5.08 | 0.9873 | 0.064 | −2.77 | −3.54 | −4.49 |
| **2b** | 14.04 ± 1.26 | 54.23 ± 4.10 | 0.9997 | 0.001 | −2.12 | −2.95 | −3.74 |
| **3a** | 27.39 ± 2.13 | 103.46 ± 6.92 | 0.9979 | 0.032 | −3.42 | −5.04 | −6.50 |
| **3b** | 29.62 ± 1.71 | 107.74 ± 5.62 | 0.9896 | 0.242 | −2.46 | −4.23 | −5.60 |

*2.3.5. Effect of Coexisting Trivalent Ions.* The influence of an additional trivalent ion presence on the adsorption selectivity toward ferric ions has been assessed using exemplary silica-based materials **2a** and **2b**. The materials were incubated in three two- or three-component mixtures containing Fe(III), Al(III), and/or Cr(III) ions. The percentages of the metals adsorbed on the hybrid materials were determined using X-ray fluorescence (XRF) measurements (Figure S8) of the material−ion complexes, which are collected in Table 5.

Table 5. Percentages of the Ions Adsorbed on the Silica-Based Materials 2a and 2b Investigated by XRF Analyses

| adsorbent | ionic system | percentage of the ions adsorbed [%] | | |
|---|---|---|---|---|
| | | Fe | Al | Cr |
| material **2a** | Fe/Al | 93.5 | 6.5 | |
| | Fe/Cr | 91.4 | | 8.6 |
| | Fe/Al/Cr | 94.0 | 2.5 | 3.5 |
| material **2b** | Fe/Al | 97.4 | 2.6 | |
| | Fe/Cr | 95.7 | | 4.3 |
| | Fe/Al/Cr | 94.1 | 2.2 | 3.7 |

Each of the experiments showed that the materials are highly selective toward ferric ions (the percentages of Fe(III) ions are higher than 90%), which is driven by the highest stability constant of the DFO−Fe complex, compared to the complexes with other metal ions. The low, but detectable, contents of Al(III) or Cr(III) might be connected with their chelation by the free deferoxamine residues remaining after the complexation of Fe(III) ions.

**2.4. Chelation of Ferric Ions from the Biological Complex.** The synthesized hybrid materials contain biologically compatible platforms and exhibit very promising Fe-adsorptive properties; they can find application in the treatment of diseases caused by long-term or sudden burst release of iron ions in human organisms. The exemplary deferoxamine-loaded hybrid material **3a** was investigated for competitive complexation of Fe(III) ions from the protoporphyrin IX−Fe(III) complex named hemin. PPIX−Fe complex formation and its interaction with $Fe_3O_4$−$SiO_2$−NCO−DFO were monitored using electrospray-ionization mass spectrometry (ESI−MS) analysis in positive mode, and the corresponding spectra are presented in Figure 8. The formation of PPIX−Fe complex was undoubtedly proven by signals at 679.7 and 701.6 $m/z$ appearing in the spectrum in positive mode, which corresponds to the protonated $[(\text{PPIX} + \text{Fe}-2\text{H} + 2\text{Na} + \text{H}_2\text{O}) + \text{H}]^+$ form and its sodium adduct, respectively, as well as their bicharged forms at 340.4 and 351.4 $m/z$. Also, the signal at 359.4 $m/z$ is related to the bicharged protonated sodium adduct of the $[(\text{PPIX} + \text{Fe} + \text{Cl}-2\text{H} + 2\text{Na}) + \text{H} + \text{Na}]^{2+}$ form. The similar trend of the signals distances as for 340.4, 351.4, and 359.4 $m/z$ is visible for the signals at 453.5, 464.5, and 472.5 $m/z$, indicating PPIX−Fe complex adducts. Although the spectrum exhibits mono- and bicharged signals corresponding to free porphyrin domains not complexing Fe(III) ions ($m/z$ 282.5 $[\text{PPIX} + 2\text{H}]^{2+}$; 304.4 $[\text{PPIX} + 2\text{Na}]^{2+}$; 563.6 $[\text{PPIX} + \text{H}]^+$; 585.6 $[\text{PPIX} + \text{Na}]^+$), their intensity is relatively low, which proves high Fe(III)-complexing efficiency. The obtained PPIX−Fe complex treated with an excess of deferoxamine led to a complete transfer of Fe(III) ions to the DFO domain, which is proven by both the appearance of a signal at 614.4 $m/z$ $[\text{DFO}-2\text{H} + \text{Fe}]^+$ and the disappearance of signals corresponding to the PPIX + Fe complex in Figure 8b. Moreover, the spectrum shows two signals related to free PPIX at 563.5 and 585.5 $m/z$ and a signal of free deferoxamine at 561.5 $m/z$ caused by its excessive usage in the experiment, which proves the competitive extraction of iron ions by the studied siderophore. These results have prompted examining the hybrid materials' potential for competitive chelation of ferric ions, which was conducted using material **3a** as an exemplary scavenger. After a very short incubation of the material in the PPIX−Fe complex solution, the aqueous phase was analyzed, the spectrum of which is given in Figure 8c. The most intensive signal at 614.4 $m/z$ corresponds to DFO−Fe complex, which is a consequence of a nanosized character of the material used, not fully separable within the short time of magnetic separation, and thus getting to the ionization source. Nevertheless, it confirmed a very efficient competitive binding of Fe(III) ions within the deferoxamine-loaded material's matrix, leaving PPIX uncomplexed. Similar results were observed for the samples containing material **3a** incubated in a series of buffer solutions, which were citric acid/sodium hydrogen phosphate buffers of pH values ranging between 3 and 8, and phosphate-buffered saline (PBS) of pH 7.4. The choice of such conditions was triggered by the different pH of fluids in human organisms. The corresponding ESI−MS spectra presented the signals originating from the ingredients of buffers and the signal referring to the complex of DFO and Fe(III) ions, as a pending organic domain on the not fully separated adsorptive nanoparticles. Therefore, the exemplary material **3a** was proven for efficient ferric ion transfer from its PPIX complex in a wide range of aqueous environments.

Very satisfactory results of direct or competitive complexing of ferric ions may lead to the materials' further biological applications, especially the materials based on magnetically active $Fe_3O_4$ nanoparticles, which have already been proven as valuable targeted drug- or energy-transporting platforms. One of the reasons for their high *in vitro* and/or *in vivo* applicability is their nanosize allowing for an enhanced circulation within the bloodstream. Also, the paramagnetic character of $Fe_3O_4$ nanoparticles allows for targeted transport based on the three-dimensional concentration of the particles using an external point or rotating magnetic field.[33−36] Not only such features lead to a directed transport of drugs to target sites (such as tumors, organs, tissues, etc.), improving the selectivity of the



https://doi.org/10.1021/acsomega.1c01411
ACS Omega 2021, 6, 15168−15181

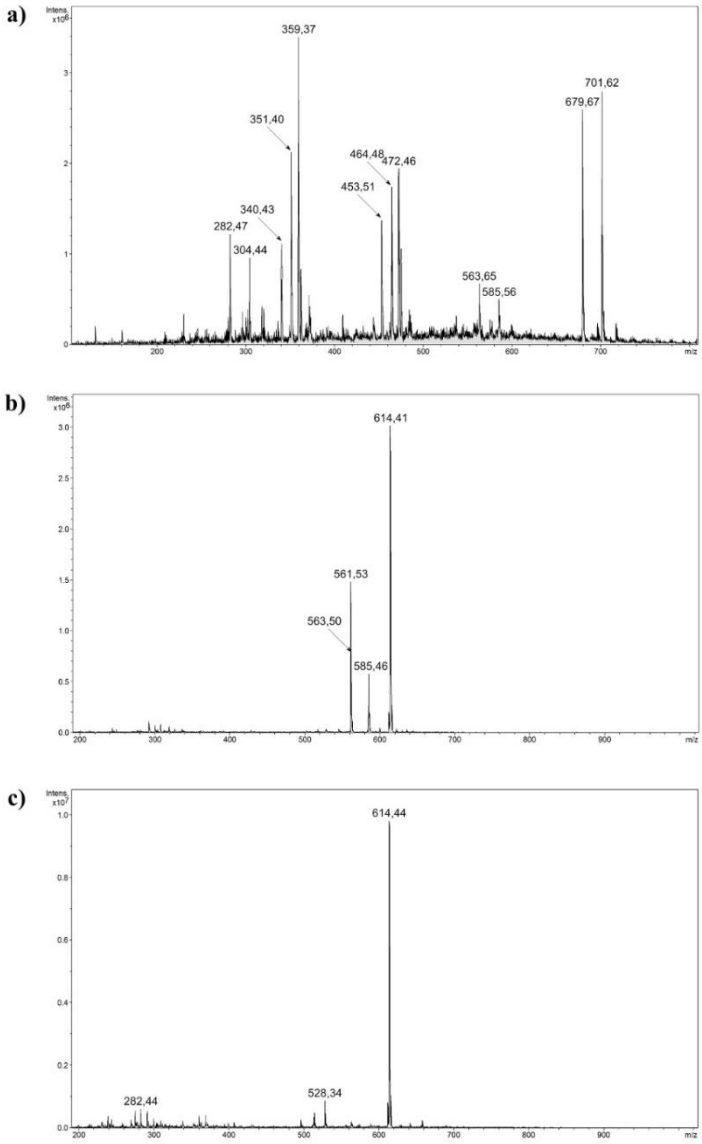


**Figure 8.** Positive ESI−MS spectra: (a) the formed PPIX−Fe complex; (b) PPIX−Fe complex interaction with pure deferoxamine; (c) PPIX−Fe complex interaction with deferoxamine-loaded $Fe_3O_4$-based hybrid material **3a**.

therapeutic effect, but also $Fe_3O_4$-based systems exhibit efficiency in hyperthermia treatment, thanks to the possibility of heat generation at the specific organism site.[37] The paramagnetic features of magnetite-based materials function-



https://doi.org/10.1021/acsomega.1c01411
ACS Omega 2021, 6, 15168−15181

alized with deferoxamine were examined using materials **3a** and **3b**. Figure S9 presents the concentration of the particles using a neodymium magnet in two different media (human serum and prepared phosphate-buffered saline), which afford physiological or paraphysiological conditions. The particles are easily concentrated with the magnet even at a distance between the magnet and the sample of 5 cm, which indicates the easy directing of the particles using the external magnetic field. Therefore, the magnetite-based materials can find application as iron ion scavengers at targeted organism sites.

## 3. CONCLUSIONS

The recent study presents the synthesis of deferoxamine-loaded hybrid materials using three different supports. The obtained materials were characterized with several analytical techniques, involving the characterization of raw hybrid materials and their complexes with Fe(III) ions. The materials were subjected to various adsorption studies, which responded in the comprehensive characterization of the materials' adsorptive potential toward ferric ions. All the materials showed high effectiveness in the adsorbate binding, reaching adsorption capacities of 87.41 to 140.65 mg $g^{-1}$, which correspond to 1.56 to 2.52 mmol $g^{-1}$. The highest values were obtained for magnetite-based materials **3a** and **3b**, which might be related to the use of a nanosized support. Moreover, material **3a**, as a magnetically active exemplary material, was studied for competitive binding of Fe(III) ions from their complex with PPIX, corresponding to hemin − an iron-containing porphyrin found in human blood. The material exhibited high effectiveness, which, jointly with its ability for being magnetically directed, may lead to further biological application in the treatment of hematologic diseases.

## 4. MATERIALS AND METHODS

**4.1. Chemicals.** The majority of the reagents were obtained from Sigma Aldrich (Saint Louis, USA) (deferoxamine mesylate salt ≥92.5%; poly(methyl vinyl ether-*alt*-maleic anhydride) of average $M_w$ ∼216,000 Da and $M_n$ ∼80,000 Da; tetraethyl orthosilicate ≥99.0%, 3-(triethoxysilyl)propyl isocyanate 95%; (3-aminopropyl)-triethoxysilane 97%; maleic anhydride 99%; 1,1,1,3,3,3-hexamethyldisilazane for synthesis ≥98%; $ZnCl_2$ ≥98%, anhydrous; $Fe(ClO_4)_3{\cdot}xH_2O$, low chloride; protoporphyrin IX (PPIX) ≥95%; human serum from human male AB plasma, USA origin, sterile-filtered). Silica modified with surface isocyanate and maleimide groups was obtained from SiliCycle Inc. (Quebec, Canada) and characterized as follows: $SiO_2$−maleimide (size: 40−63 μm, loading: 0.68 mmol $g^{-1}$) and $SiO_2$−isocyanate (size: 40−63 μm, loading: 1.41 mmol $g^{-1}$). The other substances were of purity grade p.a. and obtained from POCH (Gliwice, Poland) ($FeCl_3{\cdot}6H_2O$ ≥97%; $Na_2HPO_4{\cdot}2H_2O$ ≥99%; $NaH_2PO_4{\cdot}H_2O$ ≥99%; $Et_2O$ 99.5%; KCl 99.5%; anhydrous EtOH 99.8%; $NH_4OH$ 25%), Stanlab (Lublin, Poland) (HCl 35−38%; citric acid monohydrate; toluene), and EUROCHEM (Tarnów, Poland) (NaCl 99.5%; DMF, DCM). Moreover, $(NH_4)_2Fe(SO_4)_2{\cdot}6H_2O$ was supplied by Aktyn (Suchy Las, Poland), and DMSO was purchased from Merck (Darmstadt, Germany), which was dried over molecular sieves 4 Å prior to its use.

**4.2. Instruments.** Characterization of materials involved using several analytical techniques. The FT-IR spectra of deferoxamine-loaded hybrid materials were recorded on a Bruker IFS 66v/S (Bremen, Germany) spectroscope operating in the wavelength range between 400 and 4000 $cm^{-1}$ with a resolution of 2 $cm^{-1}$, using KBr pellets as the sample medium. The thermogravimetric measurements were performed using a Setaram Setsys 1200 analyzer (Caluire, France) operating between 20 and 1000 °C with a heating rate set for 5 °C $min^{-1}$. The samples were heated in an airstream. The quantities of C, H, and N contents in the hybrid materials were calculated based on the elemental analysis performed in an Elementar Vario EL III analyzer (Langenselbold, Germany). The obtained DFO-loaded materials were also visualized using an FEI Quanta FEG 250 (Hillsboro, OR, USA) scanning electron microscope (SEM) operating in a high vacuum condition of 70 Pa. The instrument used an accelerating voltage of 10 kV and a working distance varying between 9.9 and 10.4 mm. The SEM images were obtained with magnitudes of 2000× for materials **1**, **2a**, and **2b** and of 100,000× for $Fe_3O_4$-based materials **3a** and **3b**. Moreover, for non-magnetite-based materials, energy dispersive X-ray spectroscopic (EDX) imaging was performed. The magnetite, magnetite−silica, and magnetite-based hybrid materials were also characterized using a Bruker D8 Advance (Bremen, Germany) powder diffractometer (XRD). The apparatus used Cu K$\alpha$1 X-ray energy of wavelength $\lambda$ of 1.5406 Å (Johansson type) and worked in a high-angle mode in the $2\theta$ range between 6 and 60°. Also, magnetite-based materials **3a** and **3b** and the exemplary complex of material **3a** with adsorbed Fe(III) ions were characterized with the Brunauer−Emmet−Teller (BET) isotherm performed using a Quantachrome Autosorb iQ (Boynton Beach, USA). The samples were outgassed for 12 h at 100 °C prior to their analysis for nitrogen adsorption and desorption at a temperature of 77.35 K. According to the experimental data, the samples' surface areas were established using the BET and Barrett−Joyner−Halenda (BJH) methods. The range of relative pressure $p/p_0$ used for the measurements was from 0.0 to 1.0, where the applicability of the methods is from 0.05 to 0.3 and from 0.1 to 1.0 for the BET and BJH methods, respectively.

The progress of Fe(III) adsorption on the DFO-loaded hybrid materials was monitored by UV−Vis assays using an Agilent 8453 spectrophotometer (Santa Clara, USA), operating in the range of wavelengths between 200 and 1000 $cm^{-1}$ with a resolution of 1 $cm^{-1}$. The samples were placed in a poly(methyl methacrylate) (PMMA) cuvette (optical path length: 10 mm), and the spectra were recorded in triplicate in order to avoid any disturbances. The competitiveness in trivalent ion binding by materials **2a** and **2b** was monitored using a MiniPal2 X-ray spectrofluorometer (XRF) supplied by Malvern PANalytical B.V. (Almelo, Netherlands) equipped with a rhodium vacuum tube as a source of X-rays. The analyses were performed for 200 s with an X-ray tube voltage of 13 kV and automatically adopted current, which varied between 18 and 30 μA. Moreover, the measurements were conducted using a no element-excluding filter.

The materials' stability and the competitive binding of Fe(III) ions by the chosen material **3a** from a prepared PPIX−Fe (hemin) complex were monitored using an amaZon SL ion trap Bruker (Bremen, Germany) mass spectrometer with an electrospray ionization source (ESI−MS). The samples were injected into the ionization source at a flow rate of 10 μL $min^{-1}$ by a syringe pump. The spectrometer worked in a so-called "enhanced resolution mode" and a detection range between 100 and 1000 $m/z$. The desolvating gas ($N_2$) flowed



https://doi.org/10.1021/acsomega.1c01411
ACS Omega 2021, 6, 15168−15181

at a rate of 800 L $h^{-1}$, while the cone gas (He) flowed at a rate of 50 L $h^{-1}$. The voltages were set at −4.5 and −0.5 kV for the capillary and the endplate offset, respectively.

**4.3. Synthesis of the Deferoxamine-unctionalized Hybrid Materials.** *4.3.1. PMVEAMA-Based Material.* A solution of deferoxamine mesylate (0.84 g; 1.28 mmol) in 30 mL of DMF was placed in a three-neck round-bottom flask and charged with a reflux condenser. The solution was purged with inert gas ($N_2$) and heated to 110 °C. Under a nitrogen atmosphere, a solution of PMVEAMA (0.4 g) in 30 mL of toluene:DMF mixture (2:1; v:v) was added dropwise through a dropping funnel, with subsequent heating and mixing for 16 h. Afterward, a cooled solution was treated with $Et_2O$ to obtain the brown precipitate. The crude product was dissolved in EtOH and recrystallized with $Et_2O$, yielding 1.16 g (93.5%) of material **1**.

Material **1**: FT-IR (KBr) $cm^{-1}$: 3399 (broad, $\nu$ O−H, N−H stretch), 2930 ($\nu$ C−H asym stretch), 2859 ($\nu$ C−H sym stretch), 1769 ($\nu$ C═O anhydride ring stretch), 1700 ($\nu$ C═O carboxylic acid stretch), 1654 ($\nu$ C═O amide stretch), 1558 ($\nu$ N−H amide bend), 1438 ($\nu$ O−H bend), 1193 ($\nu$ C−O stretch), 1051 ($\nu$ N−OH stretch), 785 ($\nu$ N−H bend).

*4.3.2. Silica-Based Hybrid Materials.* The anchoring of deferoxamine on the silica modified with either isocyanate or maleimide groups was based on the same synthetic protocol. A solution of deferoxamine mesylate (0.52 g; 0.8 mmol) in 40 mL of DMF was heated to ∼75 °C and purged with nitrogen. Then, 2 g of isocyanate- or maleimide-modified was added in a few portions. Mixing under an inert atmosphere at elevated temperature was continued for 2 h for isocyanate-functionalized silica particles or 5 h for maleimide-functionalized silica particles, leading to material **2a** or material **2b**, respectively. Afterward, the warm mixture was filtered off, and the solid was washed with DMF (30 mL) and DCM (25 mL), obtaining white material **2a** and yellow material **2b**.

Material **2a**: FT-IR (KBr) $cm^{-1}$: 3427 (broad, $\nu$ O−H, N−H stretch), 2939 ($\nu$ C−H asym stretch), 2891 ($\nu$ C−H sym stretch), 1647 ($\nu$ C═O amide stretch), 1572 ($\nu$ N−H amide bend), 1092 (broad, $\nu$ Si−O−Si sym stretch), 805 ($\nu$ Si−O−Si asym stretch), 467 ($\nu$ Si−O−Si bend).

Material **2b**: FT-IR (KBr) $cm^{-1}$: 3447 (broad, $\nu$ O−H, N−H stretch), 2926 ($\nu$ C−H asym stretch), 2854 ($\nu$ C−H sym stretch), 1709 ($\nu$ C═C maleimide stretch), 1655 ($\nu$ C═O amide stretch), 1414 ($\nu$ O−H bend), 1094 (broad, $\nu$ Si−O−Si sym stretch), 958 ($\nu$ Si−OH bend), 803 ($\nu$ Si−O−Si asym stretch), 698 ($\nu$ = C−H maleimide bend), 467 ($\nu$ Si−O−Si bend).

*4.3.3. Magnetite-Based Hybrid Materials. 4.3.3.1. Synthesis of the $Fe_3O_4$–$SiO_2$ Platform.* Magnetic iron oxide (II,III) was obtained using the standard coprecipitation method. An aqueous solution of $FeCl_3{\cdot}6H_2O$ (10.81 g; 0.04 mol) and $(NH_4)_2Fe(SO_4)_2{\cdot}6H_2O$ (7.84 g; 0.02 mol) in 400 mL of distilled water in a three-neck round-bottom flask was purged with $N_2$. During mixing and constant purging with the inert gas, a solution of 30 mL of $NH_4OH$ in 20 mL of distilled water was added dropwise with immediate precipitation of magnetite. After ammonia was added, the mixture was stirred for 1 h. The precipitate was collected using an external neodymium magnet, then washed two times with distilled water (50 mL) and two times with ethanol (50 mL), and dried under vacuum at 50 °C for 8 h, yielding magnetic nanoparticles (4.52 g; 97.6%). The obtained $Fe_3O_4$ nanoparticles were further encapsulated within the silica matrix using the standard Stöber method. The dried magnetite nanoparticles were dispersed in 300 mL of $H_2O$:EtOH mixture (2:1; v:v) on an ultrasound bath at room temperature. Next, 30 mL of ammonia was added. During continuous stirring, a solution of TEOS (490 μL; 2.25 mmol) in 20 mL of EtOH was added dropwise. The mixture stayed in the ultrasound bath for 3 h, obtaining dark brown particles. Afterward, the solid was separated using the magnet, washed two times with distilled water (50 mL) and two times with ethanol (50 mL), and dried under vacuum at 50 °C for 8 h, yielding $Fe_3O_4$–$SiO_2$ platform.

*4.3.3.2. Synthesis of $Fe_3O_4$–$SiO_2$–NCO–Deferoxamine.* To a solution of deferoxamine mesylate (0.79 g; 1.2 mmol) in 50 mL of anhydrous DMSO placed in the ultrasound bath, (3-isocyanatopropyl)triethoxysilane (297 μL; 1.2 mmol) was added. After mixture stirring for 2 h under an inert gas atmosphere, 2.4 g of $Fe_3O_4$–$SiO_2$ particles was added in a few portions. The silyl-derivative incorporation into the silica matrix covering the magnetite core was carried out for 16 h at room temperature under an inert gas atmosphere ($N_2$). The resulting deferoxamine-modified magnetite-based hybrid material was separated with a magnet, washed two times with EtOH (20 mL) and two times with DCM (20 mL), and then dried under vacuum at 50 °C for 8 h. The resulting dark brown particles were assigned as material **3a**.

Material **3a**: FT-IR (KBr) $cm^{-1}$: 3384 (broad, $\nu$ O−H, N−H stretch), 2918 ($\nu$ C−H asym stretch), 2855 ($\nu$ C−H sym stretch), 1634 ($\nu$ C═O amide stretch), 1435 ($\nu$ O−H bend), 1018 ($\nu$ Si−O−Si sym stretch), 953 ($\nu$ Si−OH bend), 795 ($\nu$ Si−O−Si asym stretch), 582 ($\nu$ Fe−O stretch).

*4.3.3.3. Synthesis of $Fe_3O_4$–$SiO_2$–Maleimide–Deferoxamine.* Synthesis of deferoxamine-functionalized magnetic particles through the maleimide linker was based on a synthesis of 3-maleimide-propyltriethoxysilane, with its further anchoring to $Fe_3O_4$–$SiO_2$ surface, which then underwent functionalization with deferoxamine. The maleimide-derivative was obtained in a three-step process: (1) To a solution of maleic anhydride (0.35 g; 3.6 mmol) in 60 mL of anhydrous DMSO, 3-aminopropyltriethoxysilane (842 μL; 3.6 mmol) was added. The ring-opening process was handled under continuous stirring for 2 h at room temperature. (2) Then, the mixture was heated to 80 °C in an oil bath, and a solution of hexamethyldisilazane (755 μL; 3.6 mmol) in a DMSO:toluene mixture (2:1; v:v) and $ZnCl_2$ (0.49 g; 3.6 mmol) were added. The reaction mixture was further stirred for 5 h at 80 °C. (3) Afterward, the mixture was cooled to room temperature, and then the unreacted reagents were extracted with cold $Et_2O$ (3 × 75 mL). The obtained DMSO solution of the silane maleimide-derivative was poured to $Fe_3O_4$–$SiO_2$ (2.4 g) suspension dispersed in 40 mL of anhydrous DMSO. The silane binding to the surface silica matrix was continued for 16 h under a nitrogen atmosphere at room temperature. The obtained $Fe_3O_4$–$SiO_2$–maleimide particles were separated, washed one time with DMSO and three times with EtOH, and then dried under vacuum at 50 °C. The dried particles were then poured into a solution of deferoxamine mesylate (0.79 g; 1.2 mmol) in 50 mL of anhydrous DMSO. The reaction of deferoxamine functionalization in the ultrasound bath was carried out for 24 h at room temperature, under a nitrogen atmosphere. The resulting dark brown particles were separated, washed with fresh solvents (1 × 10 mL DMSO, 3 × 20 mL EtOH), and dried under vacuum (50 °C), obtaining material **3b**.



https://doi.org/10.1021/acsomega.1c01411
ACS Omega 2021, 6, 15168−15181

Material **3b**: FT-IR (KBr) $cm^{-1}$: 3396 (broad, $\nu$ O−H, N−H stretch), 2930 ($\nu$ C−H asym stretch), 2855 ($\nu$ C−H sym stretch), 1700 ($\nu$ C═C maleimide stretch), 1630 ($\nu$ C═O amide stretch), 1577 ($\nu$ N−H amide bend), 1404 ($\nu$ O−H bend), 1050 ($\nu$ Si−O−Si sym stretch), 797 ($\nu$ Si−O−Si asym stretch), 582 ($\nu$ Fe−O stretch).

**4.4. Stability of Deferoxamine-Functionalized Materials.** The materials' stability in biological conditions was investigated by incubation of 15 mg samples of each material in 20 mL of preprepared phosphate-buffered saline (PBS), which affords paraphysiological conditions. The incubation was handled at 37 °C for 24 h with constant shaking. Afterward, the solids were centrifuged, and the solutes were injected for ESI−MS analysis.

**4.5. Fe(III) Adsorption Experiments.** *4.5.1. The Influence of pH on Adsorption Processes.* Adsorption processes in different aqueous environments were performed using 5 mM solutions of $Fe(ClO_4)_3{\cdot}6H_2O$ buffered in prepared solutions of pH 1 and 2 (hydrochloric acid/potassium chloride buffer), pH 3, 4, and 5 (citric acid/disodium hydrogen phosphate), and pure distilled water. Each experiment involved using 10 mg of sample of each hybrid material, which was poured into 10 mL of Fe(III) ion solution buffered in a particular medium. Each sample was shaken for 24 h at room temperature. Afterward, the solids were separated by filtration using a Schott funnel, centrifugation, or using a magnet, depending on the type of material used. The solutions were then investigated for the amount of remaining metal ions, established using UV−Vis spectrophotometric measurements ($\lambda_{max}$ = 297 nm). The amount of Fe(III) absorbed $q_{eq}$ on the hybrid material was calculated using the below equation, where $c_0$ and $c_{eq}$ are the initial and the equilibrium concentrations of the metal used, respectively [mM], $V$ is the volume of the solution used [mL], $m$ is the sample mass [mg], and $M$ is the molar mass of the adsorbate [g $mol^{-1}$].

$$q_{eq} = \frac{(c_0 - c_{eq})\cdot V}{m}\cdot M$$

*4.5.2. Adsorption Isotherms.* Isothermal studies involved adsorption of Fe(III) ions from their perchlorate salt aqueous solution in distilled water at different concentrations: 0.1, 0.5, 1, 2, 5, 10, and 20 mM. The experimental protocol and the quantification of the metal adsorbed on the materials were similar to those described in Section 4.5.1. The obtained experimental data were then fitted to two widely used isothermal models: the Langmuir and the Freundlich models, which are presented below, respectively

$$\frac{c_{eq}}{q_{eq}} = \frac{1}{q_{max}}c_{eq} + \frac{1}{q_{max}K_L}$$

$$\log q_{eq} = \frac{1}{n}\log c_{eq} + \log K_F$$

where $q_{max}$ is the maximal adsorption capacity of the material toward the studied analyte [mg $g^{-1}$], $K_L$ is the Langmuir adsorption constant related to the analyte affinity to the adsorption binding sites [L $mg^{-1}$], $1/n$ is the empirical constant indicating the heterogeneity of the adsorbent, and $K_F$ is the Freundlich adsorption constant characteristic at a given temperature [mg $g^{-1}$ (L $mg^{-1})^{1/n}$].

*4.5.3. Adsorption Kinetics.* The performing of kinetic studies was based on the quantification of the metal uptake from its aqueous solution depending on the contact time. Thus, 15 mg of sample of each hybrid material was added to 20 mL of 5 mM solution of Fe(III) ions in distilled water. The solute was collected in preset time intervals (0.25, 0.5, 0.75, 1, 2, 3, 5, 8, and 24 h), in order to calculate the collective amount of metal absorbed $q_t$ at time $t$, using the below equation (analogical to the equation adopted to the equilibrium state), where $c_t$ is the concentration of the metal at time $t$ [mM]:

$$q_t = \frac{(c_0 - c_t)\cdot V}{m}\cdot M$$

The obtained experimental data were subsequently fitted to several kinetic models, leading to the decent characterization of the adsorption processes. The models used were the pseudo−first−order kinetic model, the pseudo−second−order kinetic model, the intraparticle diffusion model, and the Elovich model, in which linear plots are given below in appropriate order

$$\log(q_{eq} - q_t) = -\frac{k_1}{2.303}t + \log q_e$$

$$\frac{t}{q_t} = \frac{1}{q_e}\cdot t + \frac{1}{k_2 q_e^{\,2}}$$

$$q_t = k_{id}\sqrt{t} + C_{id}$$

$$q_t = \beta\ln t + \beta\ln(\alpha\beta)$$

where $q_e$ is the calculated equilibrium amount of metal absorbed [mg $g^{-1}$], $k_1$ is the pseudo-first-order kinetics constant [$h^{-1}$], $k_2$ is the pseudo-second-order kinetics constant [g $mg^{-1}$ $h^{-1}$], $k_{id}$ is the intraparticle diffusion constant [mg $g^{-1}$ $h^{-1/2}$], $C_{id}$ is the intraparticle diffusion plot intercept [mg $g^{-1}$], $\alpha$ is the Elovich constant [mg $g^{-1}$ $min^{-1}$], and $\beta$ is the Elovich exponent [mg $g^{-1}$]. Moreover, based on the pseudo-first- and pseudo-second-order kinetic fitting, initial adsorption rate constants $k_i$ [mg $g^{-1}$ $h^{-1}$] were calculated, respectively

$$k_i = k_1 q_e$$

$$k_i = k_2 q_e^{\,2}$$

Linear fitting of the experimental data to the pseudo−second−order kinetic model also allowed for establishing the half-adsorption time $t_{1/2}$ [h], which is equal to the time needed for adsorption of the half amount of analyte adsorbed in equilibrium:

$$t_{1/2} = \frac{1}{k_2 q_e}$$

*4.5.4. Adsorption Thermodynamics.* Thermodynamic studies were based on the reaching Fe(III) adsorption equilibrium state at three different incubation temperatures: 298, 313, and 328 K. To 5 mL of ferric perchlorate aqueous solution in distilled water of concentration 5 mM, 10 mg of sample of the hybrid material was introduced. Each mixture was incubated in 298, 313, or 328 K for 24 h. Afterward, the amount of metal adsorbed on the hybrid material was calculated using the same protocol as given in Section 4.5.1. The obtained data were fitted to the van't Hoff equation, which is given below



https://doi.org/10.1021/acsomega.1c01411
ACS Omega 2021, 6, 15168−15181

$$\ln K_d = -\frac{\Delta H^\circ}{R}\frac{1}{T} + \frac{\Delta S^\circ}{R}$$

where $K_d$ is the distribution coefficient [L $g^{-1}$] calculated as $q_{eq}/c_{eq}$, $R$ is the ideal gas constant (8.314 J $mol^{-1}$ $K^{-1}$), and $\Delta H^\circ$ and $\Delta S^\circ$ are the standard enthalpy [J $mol^{-1}$] and entropy [J $mol^{-1}$ $K^{-1}$], respectively, of Fe(III) adsorption on the particular hybrid material. Moreover, values of Gibbs free energies $\Delta G^\circ$ [J $mol^{-1}$ $K^{-1}$] in particular conditions were calculated:

$$\Delta G^\circ = -RT \ln K_d$$

**4.6. Competitive Binding of Trivalent Ions.** A series of 50 mg samples of silica-based materials **2a** and **2b** were incubated for 24 h with 10 mL samples of three different Fe-containing mixtures of trivalent ions (Fe/Cr/Al, Fe/Cr, or Fe/Al systems). The mixtures, which contained $Fe(ClO_4)_3$, $Cr(ClO_4)_3$, and/or $Al(ClO_4)_3$ at their final concentration of 5 mM, were prepared using distilled water as a solvent. After the incubation time, the solids were centrifuged, the solutes were separated, and the material−ion complexes were dried under vacuum in the desiccator at room temperature. The dried samples were subjected to XRF analysis.

**4.7. Chelation of Ferric Ions from the Biological Complex.** In order to investigate the competitiveness of the materials in binding Fe(III) ions, the exemplary material **3a** was studied using a complex of protoporphyrin IX (PPIX) and Fe(III) ions. The complex was obtained by mixing 5 mL of a 0.1 mM solution of PPIX in methanol with 5 mL of a 0.1 mM solution of Fe(III) ions in distilled water for 24 h at room temperature. Afterward, 2.5 mL of the obtained PPIX−Fe complex was diluted with 2.5 mL of $H_2O$:MeOH (1:1) mixture, leading to the final complex concentration of 0.025 mM, and 10 mg of **3a** was purged into the solution. The mixture was shaken for 1 min, and then the material was separated using an external magnetic field. The formation of PPIX−Fe and the progress of Fe-binding within the adsorptive material were monitored using ESI−MS analysis. Moreover, the competitiveness studies were also performed using pre-prepared citric acid/sodium hydrogen phosphate buffers of pH 3, 4, 5, 6, 7, and 8 and phosphate-buffered saline (PBS). Briefly, 0.5 mL of a 0.5 mM solution of PPIX−Fe in a mixture of $H_2O$:MeOH (1:1) was added to 9.5 mL of the buffers, and then 10 mg samples of **3a** were added. The incubation and analysis conditions were the same as described above.

## ■ ASSOCIATED CONTENT

### Supporting Information

The Supporting Information is available free of charge at https://pubs.acs.org/doi/10.1021/acsomega.1c01411.

A presentation of the synthetic protocols for obtaining the DFO-loaded hybrid materials; the XRD spectra of magnetite-based materials; the BET isotherms and the pore size distribution profiles of $Fe_3O_4$-cored materials **3a**, **3a−Fe(III)**, and **3b**; the ESI−MS spectra of free deferoxamine and its complexes with Fe(III) and Fe(II) ions; additional plots and coefficients calculated for the adsorption experiments; the XRF spectra of materials **2a** and **2b** complexed with other co-existing trivalent ions; the images of the magnetite-based materials concentrated using a neodymium magnet (PDF)

## ■ AUTHOR INFORMATION


### Corresponding Author

**Mateusz Pawlaczyk** − *Faculty of Chemistry, Adam Mickiewicz University, Poznań 61-614, Poland*; orcid.org/0000-0002-2340-1363; Phone: +48 61 829 17 97; Email: mateusz.pawlaczyk@amu.edu.pl

### Author

**Grzegorz Schroeder** − *Faculty of Chemistry, Adam Mickiewicz University, Poznań 61-614, Poland*

Complete contact information is available at: https://pubs.acs.org/10.1021/acsomega.1c01411


### Notes

The authors declare no competing financial interest.

## ■ ACKNOWLEDGMENTS

The work was supported by grant no. POWR.03.02.00-00-I026/16 cofinanced by the European Union through the European Social Fund under the Operational Program Knowledge Education Development.

## ■ REFERENCES


(1) Rassu, G.; Salis, A.; Porcu, E. P.; Giunchedi, P.; Roldo, M.; Gavini, E. Composite chitosan/alginate hydrogel for controlled release of deferoxamine: A system to potentially treat iron dysregulation diseases. *Carbohydrate Polym.* **2016**, *136*, 1338−1347.

(2) Li, Y.; Yang, H.; Ni, W.; Gu, Y. Effects of deferoxamine on blood−brain barrier disruption after subarachnoid hemorrhage. *PLoS One* **2017**, *12*, No. e0172784.

(3) Lane, D. J.; Mills, T. M.; Shafie, N. H.; Merlot, A. M.; Moussa, R. S.; Kalinowski, D. S.; Kovacevic, Z.; Pichardson, D. R. Expanding horizons in iron chelation and the treatment of cancer: role of iron in the regulation of ER stress and the epithelial − mesenchymal transition. *Biochem. Biophys. Acta* **2014**, *1845*, 166−181.

(4) Hider, R. C.; Zhou, T. The design of orally active iron chelators. *Ann. N. Y. Acad. Sci.* **2005**, *1054*, 141−154.

(5) Cozar, O.; Leopold, N.; Jelic, C.; Chis, V.; David, L.; Mocanu, A.; Tomoaia−Cotis, M. IR, Raman and surface−enhanced Raman study of desferrioxamine B and its Fe(III) complex, ferrioxamine B. *J. Mol. Structure* **2006**, *788*, 1−6.

(6) Larcher, G.; Dias, M.; Razafimandimby, B.; Bomal, D.; Bouchara, J. P. Siderophore Production by Pathogenic Mucorales and Uptake of Deferoxamine B. *Mycopathologia* **2013**, *176*, 319−328.

(7) Hatcher, H. C.; Singh, R. N.; Torti, F. M.; Torti, S. V. Synthetic and natural iron chelators: therapeutic potential and clinical use. *Future Med. Chem.* **2009**, *1*, 1643−1670.

(8) Schnellmann, J. G.; Pumford, N. R.; Kusewitt, D. F.; Bucci, T. J.; Hinson, J. A. Deferoxamine delays the development of the hepatotoxicity of acetaminophen in mice. *Toxicol. Lett.* **1999**, *106*, 79−88.

(9) Chen, J.; Marks, E.; Lai, B.; Zhang, Z.; Duce, J. A.; Lam, L. Q.; Volitakis, I.; Bush, A. I.; Hersch, S.; Fox, J. H. Iron Accumulates in Huntington's Disease Neurons: Protection by Deferoxamine. *PLoS One* **2013**, *8*, No. e77023.

(10) Darwish, S. F.; El−Bakly, W. M.; El−Naga, E. M.; Awad, A. S.; El−Demerdash, E. Antifibrotic mechanism of deferoxamine in concanavalin A induced−liver fibrosis: Impact on interferon therapy. *Biochem. Pharmacol.* **2015**, *98*, 231−242.

(11) Yang, Y.; Xu, Y.; Su, A.; Yang, D.; Zhang, X. Effects of Deferoxamine on Leukemia In Vitro and Its Related Mechanism. *Medical Sci. Monit.* **2018**, *24*, 6735−6741.

(12) Tada, M.; Niwano, Y.; Kohno, M. Generation Mechanism of Deferoxamine Radical by Tyrosine−Tyrosinase Reaction. *Anal. Sci.* **2015**, *31*, 911−916.

(13) Liu, J.; Obando, D.; Schipanski, L. G.; Groebler, L. K.; Witting, P. K.; Kalinowski, D. S.; Richardson, D. R.; Codd, R. Conjugates of Desferrioxamine B (DFOB) with Derivatives of Adamantane or with Orally Available Chelators as Potential Agents for Treating Iron Overload. *J. Med. Chem.* **2010**, *53*, 1370−1382.
(14) Wang, Y.; Liu, Z.; Lin, T. M.; Chanana, S.; Xiong, M. P. Nanogel−DFO conjugates as a model to investigate pharmacokinetics, biodistribution, and iron chelation in vivo. *Int. J. Pharm.* **2018**, *538*, 79−86.
(15) Ran, Q.; Yu, Y.; Chen, W.; Shen, X.; Mu, C.; Yuan, Z.; Tao, B.; Hu, Y.; Yang, W.; Cai, K. Deferoxamine loaded titania nanotubes substrates regulate osteogenic and angiogenic differentiation of MSCs via activation of HIF−1α signaling. *Mater. Sci. Eng. C* **2018**, *91*, 44−54.
(16) Li, H.; Luo, B.; Wen, W.; Zhou, C.; Tian, L.; Ramakrishna, S. Deferoxamine immobilized poly(D,L−lactide) membrane via polydopamine adhesive coating: The influence on mouse embryo osteoblast precursor cells and human umbilical vein endothelial cells. *Mater. Sci. Eng. C* **2017**, *70*, 701−709.
(17) Park, J. Y.; Park, S.; Lee, T. S.; Hwang, Y. H.; Kim, J. Y.; Kan, W. J.; Key, J. Biodegradable micro−sized discoidal polymeric particles for lung−targeted delivery system. *Biomaterials* **2019**, *218*, 119331.
(18) Gao, F.; Ieritano, C.; Chen, K. T.; Dias, G. M.; Rousseau, J.; Bénard, F.; Seimbille, Y. Two bifunctional desferrioxamine chelators for bioorthogonal labeling of biovectors with zirconium−89. *Org. Biomol. Chem.* **2018**, *16*, 5102−5106.
(19) Biesuz, R.; Emma, G.; Milanese, C.; Dacarro, G.; Taglietti, A.; Nurchi, V. M.; Alberti, G. Novel DFO−SAM on mesoporous silica for iron sensing. Part I. Synthesis optimization and characterization of the material. *Analyst* **2014**, *139*, 3932−3939.
(20) Alberti, G.; Emma, G.; Colleoni, R.; Pesavento, M.; Nurchi, V. M.; Biesuz, R.; Biesuz, R. Novel DFO−functionalized mesoporous silica for iron sensing. Part 2. Experimental detection of free iron concentration (pFe) in urine Samales. *Analyst* **2014**, *139*, 3940−3948.
(21) Yehuda, Z.; Hadar, Y.; Chen, Y. Immobilization of Fe Chelators on Sepharose Gel and Its Effect on Their Chemical Properties. *J. Agric. Food Chem.* **2003**, *51*, 5996−6005.
(22) Alberti, G.; Quattrini, F.; Colleoni, R.; Nurchi, V. M.; Biesuz, R. Deferoxamine−paper for iron(III) and vanadium(V) sensing. *Chem. Papers* **2015**, *69*, 1024−1032.
(23) Yan, F.; Shrestha, Y. K.; Spurgeon, C. L. Determination of ferric ions using surface−enhanced Raman scattering based on desferrioxamine−functionalized silver nanoparticles. *Chem. Commun.* **2013**, *49*, 7962−7964.
(24) Galinetto, P.; Taglietti, A.; Pasotti, L.; Pallavicini, P.; Dacarro, G.; Giulotto, E.; Grandi, M. S. Sers Activity of Silver Nanoparticles Functionalized With a Desferrioxamine B Derived Ligand For Fe(III) Binding and Sensing. *J. Appl. Spectroscopy* **2016**, *82*, 1052−1059.
(25) Roy, E. G.; Jiang, C.; Wells, M. L.; Tripp, C. Determining Subnanomolar Iron Concentrations in Oceanic Seawater Using a Siderophore−Modified Film Analyzed by Infrared Spectroscopy. *Anal. Chem.* **2008**, *80*, 4689−4695.
(26) Xi, Z.; Zheng, B.; Wang, C. Synthesis, Surface Modification, and Biolabeling with Aptamer of $Fe_3O_4$@$SiO_2$ Magnetic Nanoparticles. *Nanosci. Nanotech. Lett.* **2016**, *8*, 1061−1066.
(27) Umemura, M.; Kim, J. H.; Aoyama, H.; Hoshino, Y.; Fukumura, H.; Nakakaji, R.; Sato, I.; Ohtake, M.; Akimoto, T.; Narikawa, M.; Tanaka, R.; Fujita, T.; Yokoyama, U.; Taguri, M.; Okumura, S.; Sato, M.; Eguchi, H.; Ishikawa, Y. The iron chelating agent, deferoxamine detoxifies Fe(Salen)−induced cytotoxicity. *J. Pharm. Sci.* **2017**, *134*, 203−210.
(28) Sing, K. S. W.; Everett, D. H.; Haul, R. A. W.; Moscou, L.; Pierotti, R. A.; Rouquerol, J.; Siemieniewska, T. Reporting Physisorption Data for Gas/Solid Systems with Special Reference to the Determination of Surface Area and Porosity. *Pure Appl. Chem.* **1985**, *57*, 603−619.
(29) Crisponi, G.; Nurchi, V. M.; Crespo−Alonso, M.; Sanna, G.; Zoroddu, M. A.; Alberti, G.; Biesuz, R. A Speciation Study on the Perturbing Effects of Iron Chelators on the Homeostasis of Essential Metal Ions. *PLoS One* **2015**, *10*, No. e0133050.
(30) Pawlaczyk, M.; Schroeder, G. Efficient Removal of Ni(II) and Co(II) Ions from Aqueous Solutions Using Silica−based Hybrid Materials Functionalized with PAMAM Dendrimers. *Solvent Extr. Ion Exch.* **2020**, *38*, 496−521.
(31) Chen, S.; Qin, C.; Wang, T.; Chen, F.; Li, X.; Hou, H.; Zhou, M. Study on the adsorption of dyestuffs with different properties by sludge−rice husk biochar: Adsorption capacity, isotherm, kinetic, thermodynamics and mechanism. *J. Mol. Liq.* **2019**, *285*, 62−74.
(32) Tan, K. L.; Hameed, B. H. Insight into the adsorption kinetics models for the removal of contaminants from aqueous solutions. *J. Taiwan Inst. Chem. Eng.* **2017**, *74*, 25−48.
(33) Nigam, S.; Bahadur, D. Doxorubicin−loaded dendritic−$Fe_3O_4$ supramolecular nanoparticles for magnetic drug targeting and tumor regression in spheroid murine melanoma model. *Nanomedicine: NBM* **2018**, *14*, 759−768.
(34) Zhao, S.; Yu, X.; Qian, Y.; Chen, W.; Shen, J. Multifunctional magnetic iron oxide nanoparticles: an advanced platform for cancer theranostics. *Theranostics* **2020**, *10*, 6278−6309.
(35) Krzyminiewski, R.; Dobosz, B.; Schroeder, G.; Kurczewska, J. The principles of a new method, MNF−3D, for concentration of magnetic particles in three−dimensional space. *Measurements* **2017**, *112*, 137−140.
(36) Krzyminiewski, R.; Dobosz, B.; Schroeder, G.; Kurczewska, J. Focusing of $Fe_3O_4$ nanoparticles using a rotating magnetic field in various environments. *Phys. Lett. A* **2018**, *382*, 3192−3196.
(37) Perigo, E. A.; Hemery, G.; Sandre, O.; Ortega, D.; Garaio, E.; Plazaola, F.; Teran, F. J. Fundamentals and advances in magnetic hyperthermia. *Appl. Phys. Rev.* **2015**, *2*, No. 041302.



https://doi.org/10.1021/acsomega.1c01411
*ACS Omega* 2021, 6, 15168−15181

## Supporting Information

# Deferoxamine–Modified Hybrid Materials for Direct Chelation of Fe(III) Ions from Aqueous Solutions and Indication of the Competitiveness of *In Vitro* Complexing toward a Biological System

Mateusz Pawlaczyk*, Grzegorz Schroeder

Faculty of Chemistry, Adam Mickiewicz University in Poznań, Uniwersytetu Poznańskiego 8, 61–614 Poznań, Poland

* Corresponding author: Mateusz Pawlaczyk, mateusz.pawlaczyk@amu.edu.pl, tel: +48 61 829 17 97

## Figure captions:

**Figure S1.** Synthetic routes for obtaining the deferoxamine–functionalized hybrid materials

**Figure S2.** Top: XRD spectra of the synthesized bare $Fe_3O_4$ and $Fe_3O_4$–$SiO_2$–NCO–DEF (**3a**) and $Fe_3O_4$–$SiO_2$–maleimide–deferoxamine (**3b**) hybrid materials; Bottom: a representation of theoretical XRD pattern of $Fe_3O_4$ (blue) and $SiO_2$ (red) (JCPDS card no. 01–088–0315)

**Figure S3**. BET isotherms obtained for material **3a** before and after the complexation of Fe(III) ions, and for material **3b**. The red line refers to the nitrogen adsorption, while the blue line to the desorption step

**Figure S4.** The pore size distribution of materials **3a** (green), **3b** (blue), and the complex material **3a**–Fe(III) (red)

**Figure S5**. The ESI–MS spectra in positive mode of aqueous solutions: a) pure deferoxamine mesylate; b) deferoxamine–Fe(III) complex using $FeCl_3$; c) deferoxamine–Fe(II) complex using Mohr's salt ($(NH_4)_2Fe(SO_4)_2$)

**Figure S6.** The experimental data fitting to the Freundlich isothermal model

**Figure S7.** The kinetic experimental data fitted to: a) the pseudo–first–order kinetic model; b) the Elovich model

**Figure S8**. The XRF spectra of the complexes of materials **2a** and **2b** with trivalent metal cations. The materials were incubated with three different systems, containing Fe(III), Al(III), and/or Cr(III) cations

**Figure S9**. Concentrating of material **3a** (a, b) and **3b** (c, d) by neodymium magnet in: PBS buffer (a, c) and human serum (b, d). The distances between magnet and sample are 0 cm (left) and 5 cm (right)

## Table heading:

**Table S1.** Additional kinetic parameters calculated for Fe(III) adsorption kinetics fitted to the pseudo–first–order and the Elovich models

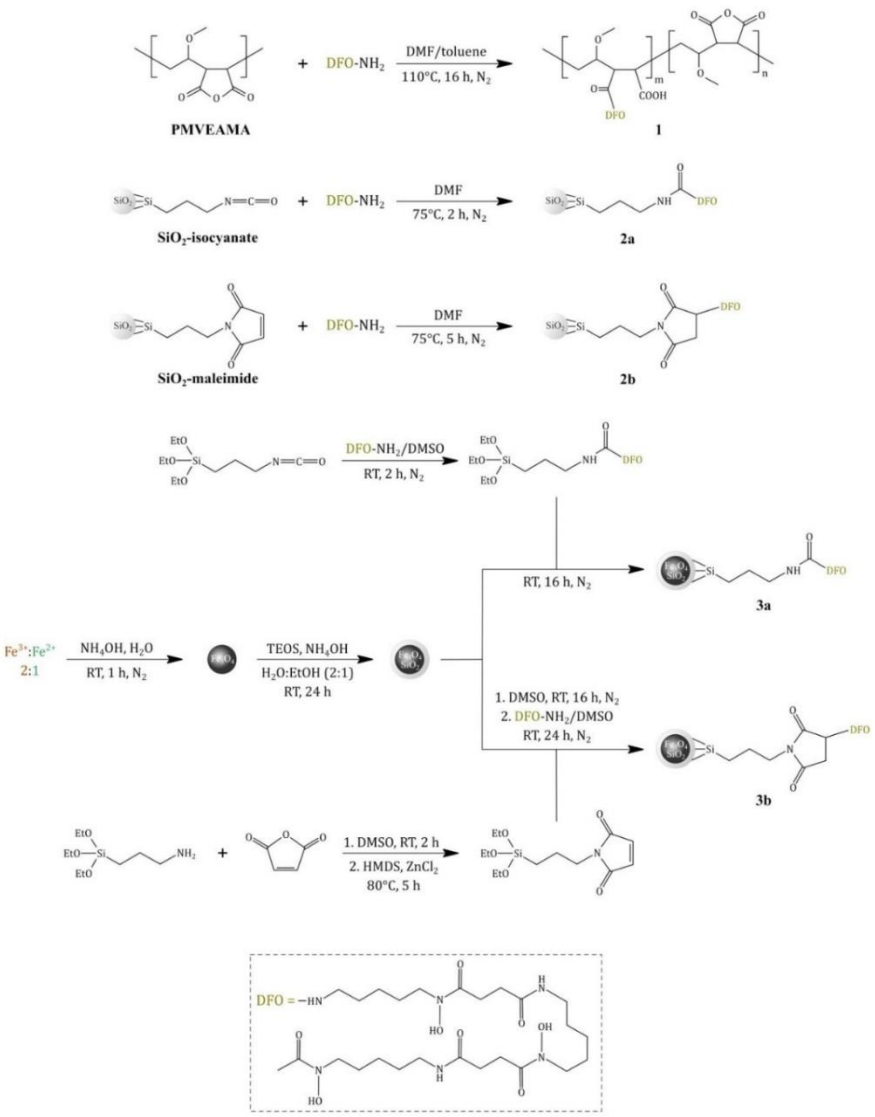


**Figure S1.** Synthetic routes for obtaining the deferoxamine–functionalized hybrid materials

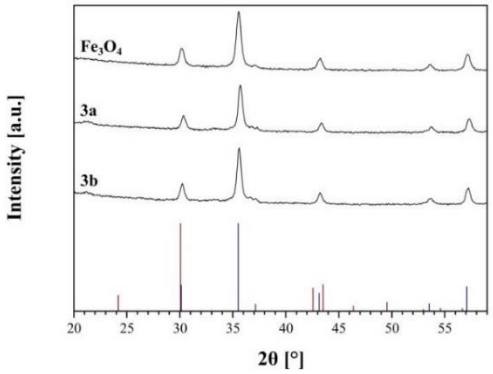


**Figure S2.** Top: XRD spectra of the synthesized bare $Fe_3O_4$ and $Fe_3O_4$–$SiO_2$–NCO–DEF (**3a**) and $Fe_3O_4$–$SiO_2$–maleimide–deferoxamine (**3b**) hybrid materials; Bottom: a representation of theoretical XRD pattern of $Fe_3O_4$ (blue) and $SiO_2$ (red) (JCPDS card no. 01–088–0315)

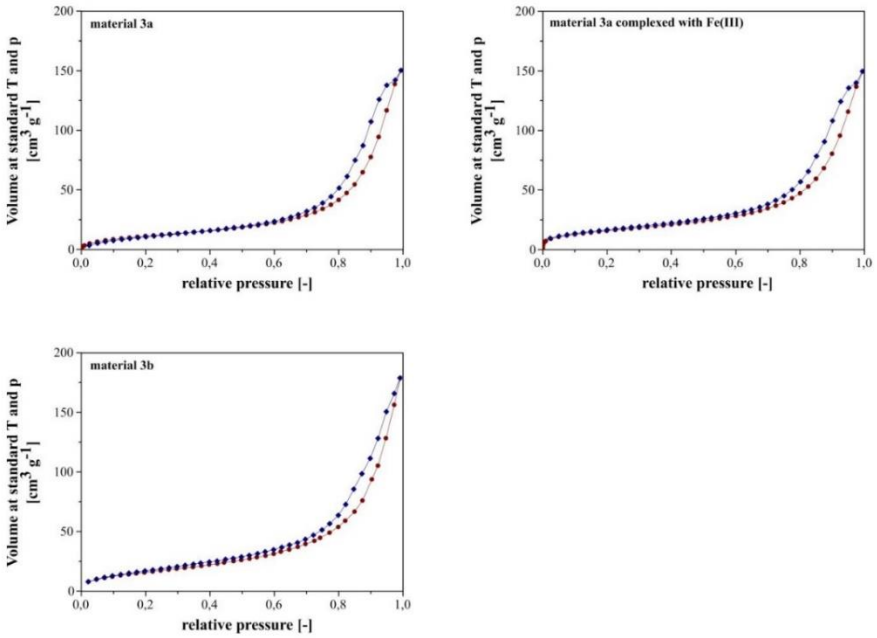


**Figure S3**. BET isotherms obtained for material **3a** before and after the complexation of Fe(III) ions, and for material **3b**. The red line refers to the nitrogen adsorption, while the blue line to the desorption step

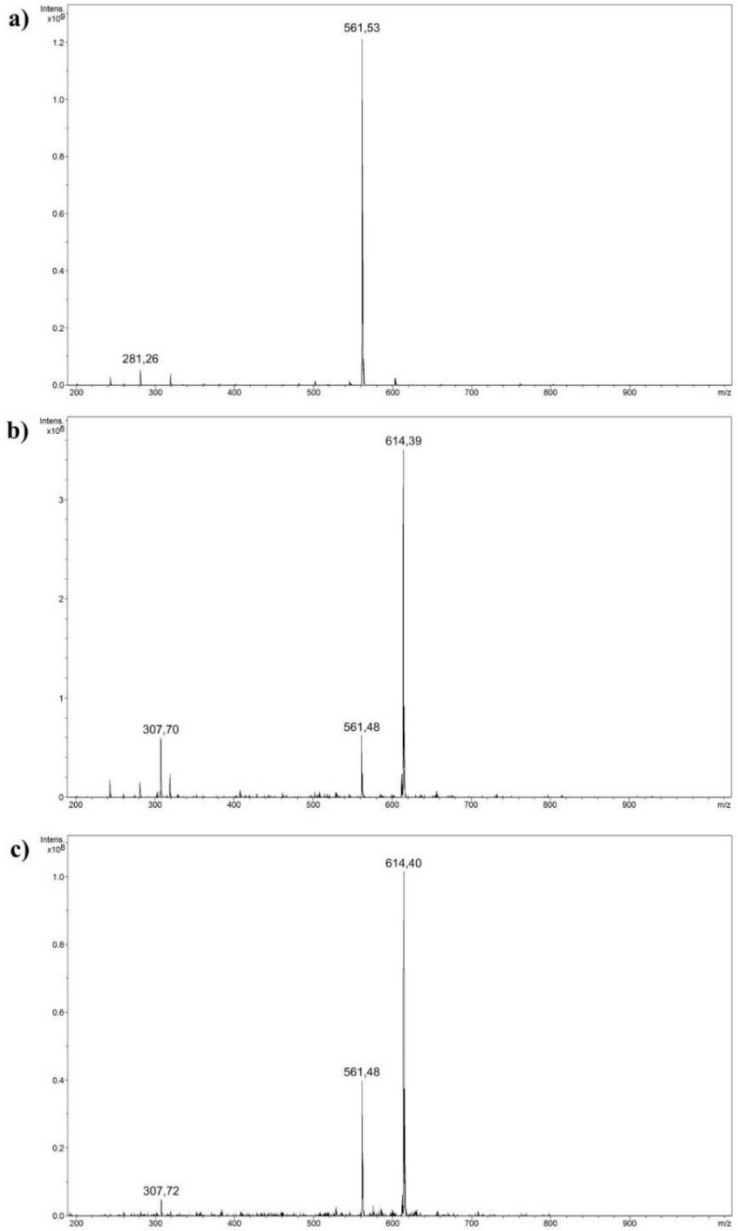


**Figure S5**. The ESI–MS spectra in positive mode of aqueous solutions: a) pure deferoxamine mesylate; b) deferoxamine–Fe(III) complex using $FeCl_3$; c) deferoxamine–Fe(II) complex using Mohr's salt ($(NH_4)_2Fe(SO_4)_2$)

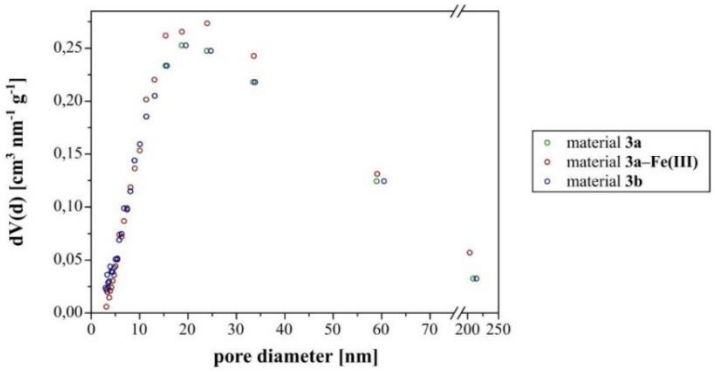


**Figure S4.** The pore size distribution of materials **3a** (green), **3b** (blue), and the complex material **3a**–Fe(III) (red)

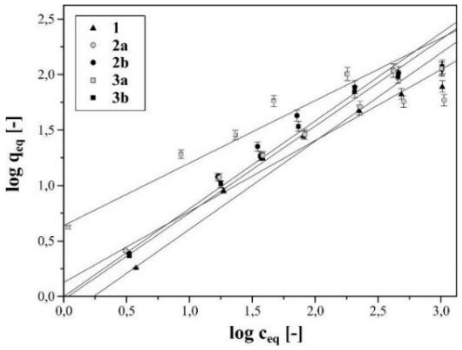


**Figure S6.** The experimental data fitting to the Freundlich isothermal model

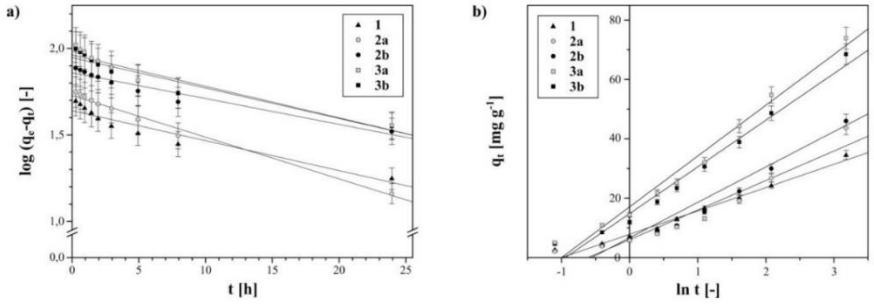


**Figure S7.** The kinetic experimental data fitted to: a) the pseudo–first–order kinetic model; b) the Elovich model

**Table S1.** Additional kinetic parameters calculated for Fe(III) adsorption kinetics fitted to the pseudo–first–order and the Elovich models

| Material | Pseudo–first–order | | | Elovich model | | |
|---|---|---|---|---|---|---|
| | $k_1 \cdot 10$ [$h^{-1}$] | $k_i$ [mg $g^{-1}$ $h^{-1}$] | $R^2$ | α [mg $g^{-1}$ $min^{-1}$] | β [mg $g^{-1}$] | $R^2$ |
| **1** | 0.40 ± 0.07 | 1.75 ± 0.45 | 0.9189 | 0.37 ± 0.02 | 0.129 ± 0.007 | 0.9809 |
| **2a** | 0.56 ± 0.07 | 2.99 ± 0.60 | 0.9875 | 0.32 ± 0.08 | 0.103 ± 0.011 | 0.9162 |
| **2b** | 0.34 ± 0.09 | 2.50 ± 0.84 | 0.9467 | 0.35 ± 0.07 | 0.095 ± 0.009 | 0.9339 |
| **3a** | 0.42 ± 0.09 | 3.86 ± 1.17 | 0.9044 | 0.78 ± 0.08 | 0.059 ± 0.004 | 0.9760 |
| **3b** | 0.41 ± 0.09 | 3.60 ± 1.11 | 0.9179 | 0.68 ± 0.08 | 0.064 ± 0.003 | 0.9747 |

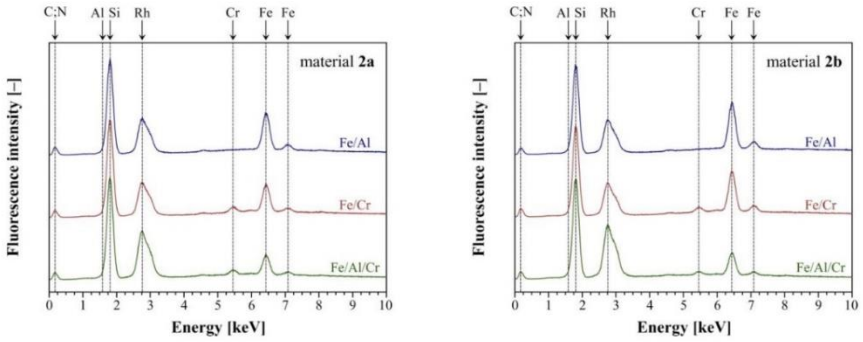


**Figure S8**. The XRF spectra of the complexes of materials **2a** and **2b** with trivalent metal cations. The materials were incubated with three different systems, containing Fe(III), Al(III), and/or Cr(III) cations

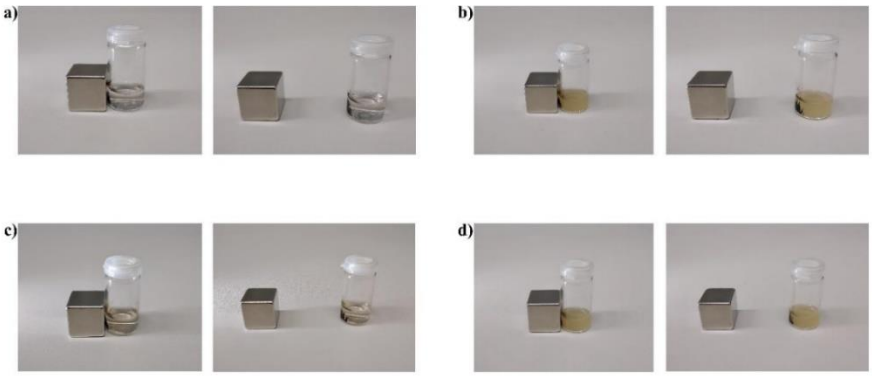


**Figure S9**. Concentrating of material **3a** (a, b) and **3b** (c, d) by neodymium magnet in: PBS buffer (a, c) and human serum (b, d). The distances between magnet and sample are 0 cm (left) and 5 cm (right)

# Appendix B – the declaration of co-author

UNIWERSYTET IM. ADAMA MICKIEWICZA W POZNANIU

**Wydział Chemii**

Prof. dr hab. Grzegorz Schroeder

Poznań, 06.09.2021 r.

**Declaration of the publication co-author**

I declare that in the publications:

1. M. Pawlaczyk, G. Schroeder, Adsorption studies of Cu(II) ions on dendrimer-grafted silica-based materials, Journal of Molecular Liquids 281 (2019), 176-185; DOI: 10.1016/j.molliq.2019.02.043
2. M. Pawlaczyk, G. Schroeder, Efficient Removal of Ni(II) and Co(II) Ions from Aqueous Solutions Using Silica-based Hybrid Materials Functionalized with PAMAM Dendrimers, Solvent Extraction and Ion Exchange 38(5) (2020), 496-521; DOI: 10.1080/07366299.2020.1766742
3. M. Pawlaczyk, G. Schroeder, Dendrimer-Functionalized Hybrid Materials Based on Silica as Novel Carriers of Bioactive Acids, Molecules 25(11) (2020), 2660-2680; DOI: 10.3390/molecules25112660
4. M. Pawlaczyk, G. Schroeder, Dual-Polymeric Resin Based on Poly(methyl vinyl ether-alt-maleic anhydride) and PAMAM Dendrimer as a Versatile Supramolecular Adsorbent, ACS Applied Polymer Materials 3(2) (2021), 956-967; DOI: 10.1021/acsapm.0c01254

Collegium Chemicum, ul. Uniwersytetu Poznańskiego 8, 61-614 Poznań
NIP 777 00 06 350, REGON 000001293
tel. +48 61 829 15 53, +48 61 829 15 98, +48 61 829 1601

**www.chemia.amu.edu.pl**

5. M. Pawlaczyk, G. Schroeder, Deferoxamine-Modified Hybrid Materials for Direct Chelation of Fe(III) Ions from Aqueous Solutions and Indication of the Competitiveness of In Vitro Complexing toward a Biological System, ACS Omega 6(23) (2021), 15168-15181;
   DOI: 10.1021/acsomega.1c01411

my substantive contribution, as the supervisor of the doctoral dissertation of mgr inż. Mateusz Pawlaczyk in the preparation, conducting, analysis, and development of research, and their further presentation in the form of publications, were:

- The conceptualization, organization, and managing of the researches described in the publications;
- The discussion and co-analysis of the research results;
- The revision and editing of the final manuscripts of the publications.

At the same time, I solely agree for the appending of the above-presented articles, as a coherent collection of scientific reports published in international JCR-reported journals, of mgr inż. Mateusz Pawlaczyk into the doctoral dissertation.

Prof. dr. hab. Grzegorz Schroeder